

**Modelling Thermal Comfort and Energy Saving
Enhancements in an Office Room Served by Stratified Air
Distribution Systems**

Thesis submitted for the degree of

Doctor of Philosophy

at the University of Leicester

by

Ahmed Qasim Ahmed



Engineering Department

University of Leicester

November 2017

Ahmed Qasim Ahmed

Modelling Thermal Comfort and Energy Saving Enhancements in an Office
Room Served by Stratified Air Distribution Systems

Abstract

A numerical study is performed into the effects of the location of exhaust diffusers in relation to the room heat sources on thermal comfort and energy saving. A new concept of the combination of indoor heat sources and the exhaust outlet was also employed in this investigation. The results showed that the indoor thermal environment and energy saving were greatly improved by combining the exhaust outlets with some of the room's heat sources. For further improvement, this concept was also used along with a novel local exhaust ventilation system in the modelled office room. This system was adopted and developed for use in office spaces, where the exhaust opening was combined with the office workstation into a single unit. The main aim was to help extract the warmed and contaminated air locally before it could disperse across the room. Three different amounts of recirculated air and three different heights of the combined system were analysed. The results showed a significant improvement in energy savings and inhaled air quality in the room using the new ventilation system. It was also found that the performance of this system was greatly influenced by the height factor. In addition, in this research, the LES method was employed to investigate the complex characteristics of airflow and temperature distribution in the office room which used the concept of combining the exhaust outlet with room heat sources. The results revealed that the airflow and temperature distribution were highly unsteady and unstable, particularly in the regions where buoyancy works effectively to cause a high number of perturbations. The developed CFD models were thoroughly validated.

Acknowledgements

Firstly, I would like to express my deep and sincere gratitude to my supervisor, Dr Shian Gao, for his assistance, support, understanding, encouragement and personal guidance with this thesis. Also, I would like to thank my second supervisor, Dr Andrew McMullan. Special thanks also goes to Dr Aldo Rona for his useful feedback and valuable suggestions. My appreciation goes to my colleagues in the engineering department – Thermo Fluid Group – for their help and their support during my research. Also, I would like to thank the Ministry of Higher Education and Scientific Research of Iraq for the financial support of the project.

To my father, mother, sisters and brothers I would like to say: "Thank you for the help, thank you for the support, and thank you for everything".

I would like to express my deep thanks to my family my wife and my son, particularly my wife, for her love, encouragement, and patience, which was always given to me to help complete this long and difficult journey.

Ahmed Qasim Ahmed

Contents

Abstract.....	I
Acknowledgements	II
Contents.....	III
List of Figures.....	VII
List of Tables.....	XII
Nomenclatures	XIII
Chapter 1 Introduction.....	1
1.1 Background.....	1
1.2 Ventilation strategies.....	2
1.2.1 Mixing ventilation (MV)	2
1.2.2 Under-floor air distribution (UFAD) system	3
1.2.3 Displacement ventilation (DV) system	3
1.2.4 Personalised ventilation (PV) system	5
1.2.5 Local exhaust ventilation (LEV) system.....	6
1.3 Evaluation indexes for ventilation systems.....	7
1.3.1 Thermal comfort	8
1.3.2 Energy saving.....	8
1.3.3 Indoor air quality (IAQ)	9
1.4 Computational Fluid Dynamics (CFD) for indoor air simulation.....	9
1.5 Aims and Objectives	10
1.6 Thesis outline	11
Chapter 2 Literature Review.....	13
2.1 Introduction	13
2.2 The influence of the layout of exhaust and return openings.....	14
2.3 Local exhaust ventilation and personalised ventilation system	23
2.4 Using LES for the indoor environment prediction.....	36

Chapter 3 Numerical Methods.....	40
3.1 Introduction	40
3.2 Governing equations	41
3.3 Discretization	43
3.4 Turbulence computation.....	46
3.4.1 RNG k- ϵ modelling	47
3.4.2 Large Eddy Simulation (LES) method	47
3.5 Numerical schemes.....	49
3.5.1 Pressure-velocity coupling.....	49
3.5.2 SIMPLE algorithm.....	50
3.5.3 Under-relaxation factor	52
Chapter 4 Influence of Exhaust Locations on Energy Consumption and on the Indoor Thermal Environment.....	53
4.1 Introduction	53
4.2 Case description	54
4.3 Computational model	56
4.3.1 Air flow modelling	56
4.3.2 Discrete phase model.....	58
4.4 Validation of the CFD algorithm	61
4.4.1 Validation of fluid flow.....	61
4.4.2 Particle transport validation	65
4.5 Grid independence.....	66
4.6 Results and discussion	69
4.6.1 Thermal comfort evaluation	69
4.6.2 Local thermal discomfort	78
4.6.3 Energy saving.....	81
4.6.4 The quality of the indoor air evaluation.....	83

Chapter 5 Development of a Novel Local Exhaust Ventilation System for Office Rooms.....	87
5.1 Introduction	87
5.2 Methods	88
5.3 Mesh generation	92
5.4 Results and discussion	95
5.4.1 Indoor thermal comfort	95
5.4.2 Temperature distribution in the vertical direction	99
5.4.3 Energy saving evaluation	109
5.4.4 The quality of the indoor air in the breathing and in the inhaled zones.	110
Chapter 6 Height Impact of the New Local Exhaust System.....	114
6.1 Introduction	114
6.2 Background to the investigated case	115
6.3 Mesh generation and independence test	116
6.4 Results and discussion	117
6.4.1 Temperature distribution near the foot zone	117
6.4.2 Occupants thermal discomfort evaluation.....	120
6.4.3 Draught risk evaluation.....	124
6.4.4 Energy saving evaluation	126
6.4.5 The quality of the indoor air in the breathing and inhaled zones .	127
Chapter 7 The Air Turbulence and Flow Behaviours for the Combined System Using RANS Modelling and LES	130
7.1 Introduction	130
7.2 Background to the investigated case	131
7.3 Mesh design for the LES method.....	132
7.4 Validation work for the LES method	135
7.5 Convergence evaluation of the LES method.....	136

7.5.1	Monitoring points	137
7.5.2	Discrete Fourier Transform.....	140
7.6	Results and discussion	142
7.6.1	Temperature distribution.....	142
7.6.2	Velocity distribution.....	149
Chapter 8 Conclusion and Future Work		156
8.1	Conclusion	156
8.2	Future work	160
Appendices		161
Appendix 1 Publication List.....		161
References.....		162

List of Figures

Figure 1-1: Mixing ventilation [3].	2
Figure 1-2: Underfloor Air Distribution system [5].	3
Figure 1-3: (a) Stratification level with a DV system and (b) DV system in an office room [9, 10].	4
Figure 1-4: Types of personalised ventilation system [15].	6
Figure 1-5: Local exhaust ventilation (LEV) [20].	7
Figure 2-1: Schematic diagram of various combinations of UFAD system [35].	15
Figure 2-2: Experimental climate chamber (a): arrangement of the climate chamber; (b): real climate chamber [39].	16
Figure 2-3: Schematic diagram of the experimental room [23].	17
Figure 2-4: Simulated room arrangement [43].	18
Figure 2-5: Four different layouts of supply and exhausts opening in the investigated room [50].	19
Figure 2-6: (a): Average temperature for the lower and upper zone; (b): cooling load evaluation with heat source height [54].	20
Figure 2-7: Schematic diagram of the investigated room [57].	22
Figure 2-8: Schematic diagram of the task ventilation system in the experimental chamber [62].	23
Figure 2-9: Schematic diagram of the PV system combined with the chair [12].	24
Figure 2-10: Experimental setup of the investigated room [67].	25
Figure 2-11: Walking scenarios in the investigated office room	26
Figure 2-12: Experimental setup of the tested ventilation system[70]	27
Figure 2-13: Schematic diagram of the experimental ductless PV system of [54]; (1) the air terminal device, (2) heat sources, (3) table, (4) fan, (5) duct system, (6) intake source of the DPV system, and (7) floor level [54].	28
Figure 2-14 Experimental chamber for the investigated room.	29
Figure 2-15: Schematic diagram of the tested room with DV/PV system [75].	30
Figure 2-16: Experimental chamber setup [79], (a) top view; (b) side view.	32
Figure 2-17: Schematic diagram of the investigated chamber.	33
Figure 2-18: Experimental setup for the investigated room [84].	35
Figure 2-19: Computational room domain [113].	38

Figure 2-20: Simulated room domain [116].	39
Figure 3-1: Discretization of the computational domain into finite volumes in three- and two-dimensional views.	44
Figure 3-2: Two-dimensional exploded view for the discrete points in the control volume and its neighbouring cells.	46
Figure 3-3: The iterative procedure behind the SIMPLE algorithm.	51
Figure 4-1: (a) The configuration of the simulated room; 1- occupant_1; 2- occupant_2; 3- PC case; 4- PC monitor; 5- ceiling lamps; 6- displacement ventilation (DV) inlet; 7- return inlet; 8- exhaust inlet; 9- external wall; 10- contaminant source (line source) at door; 11- contaminant source at window (line source), and (b) the arrangement of the equipment of the simulated office (top view).	55
Figure 4-2: Schematic diagram of the validation room model [69].	61
Figure 4-3: The measured locations in the experimental chamber; (a) side view and (b) top view.	62
Figure 4-4: Comparison between the simulated and experimental temperature and velocity profiles at five vertical poles; (a) temperature distribution (square symbol: experimental results [69]; dashed line: simulated results); (b) velocity magnitude distribution (circle symbol: experimental results [69]; dashed line: simulated results).	65
Figure 4-5: Schematic diagram of the ventilated chamber of the validation case for Lagrangian particle-tracking [151].	65
Figure 4-6: Comparison between the simulated and experimental normalized particle concentration at different locations at $x = 0.2$ m, 0.4 m and 0.6 m (triangle symbols: experimental data [151]; dashed line: simulated results).	66
Figure 4-7: Inflation boundary layer around the human body.	67
Figure 4-8: Mesh independence test for; (a) temperature profile °C, (b) velocity profile (m/sec).	68
Figure 4-9: Indoor thermal comfort in each case study for both occupants; (a) PMV index; (b) PPD index.	72
Figure 4-10: Temperature (°C) and velocity distribution (m/s) at the central plane $x=2$ m and $y =1.75$ m for all case studies: (case 1) exhaust located at the centre of ceiling between the two heat sources; (case 2) exhaust located at the ceiling	

level, at the external wall; (case 3) exhaust combined with the light slots; (case 4) exhaust located at the ceiling level above the DV supply opening; (case 5) exhaust combined with the return opening.....	78
Figure 4-11: Monitoring points for each case study.....	78
Figure 4-12: Temperature difference in °C in the vertical direction for each case study; (a) for occupant -1 and (b) for occupant -2.	79
Figure 4-13: Temperature distribution in the vertical direction at four different locations for each case study.	81
Figure 4-14: Inhaled area around the occupants, 0.5 m cube (microenvironment).	85
Figure 4-15: Comparison of the particle concentration for each case study; (a) for the inhaled area of each occupant; (b) for the breathing level.	86
Figure 5-1: (a) LEVO system: 1- lamps, 2 - air suction part, 3 - exhaust inlet and 4 - table; (b) LEVO system combined with the office heat sources and suction airflow direction.	89
Figure 5-2: (a) Configuration of the simulated room: 1 - occupant 1, 2 - occupant 2, 3 - PC case, 4 - PC monitor, 5 - DV inlet, 6 - return inlet, 7 - contaminant source 1 and 8 - contaminant source 2; (b) The equipment arrangement on the simulated office.	90
Figure 5-3: Inflation boundary layer around the human body.	92
Figure 5-4: y^+ value for the occupant zone.	93
Figure 5-5: Mesh independence test for; (a) temperature profile °C, (b) velocity profile (m/sec).	94
Figure 5-6: The predicted PMV values in the reference case and LEVO case for (a) occupant -1 and (b) occupant -2.....	96
Figure 5-7: The predicted PDD values in the reference case and LEVO case for (a) occupant -1 and (b) occupant -2.....	97
Figure 5-8: Temperature distribution (°C) of the near foot zone at three monitoring points, point 1, 2 and 3, for each case study and for both occupants.....	99
Figure 5-9: (a) Monitoring points; (b), (c) and (d) Temperature difference $\Delta T_{head - foot}$ (°C) in the vertical direction for each case study.	102
Figure 5-10: Temperature distribution °C and the airflow pattern at the mid plane ($x=2m$) for each case study (a) with LEVO and (b) without LEVO.	105

Figure 5-11: Temperature gradients in the vertical direction for each case study at four different locations, pole 1, 2, 3 and 4 respectively.	108
Figure 5-12: Comparison of the quality of indoor air for each case study; (a) contaminant concentration at breathing level; (b) and (c) the inhaled air quality for occupant_1 and occupant_2 respectively.	113
Figure 6-1: The LEVO system operation and flow direction at three investigated heights.	116
Figure 6-2: Inflation boundary layer around the human body.	117
Figure 6-3: (a) Three monitoring points, points 1, 2 and 3, for each case study and (b) and (c) temperature distribution (°C) of the near foot zone for occupant_1 and occupant_2 respectively.	119
Figure 6-4: (a) Monitoring points; (b) Temperature difference in the vertical direction for each case study at four poles.	121
Figure 6-5: Temperature distributions and the airflow pattern in the middle plane (x = 2 m) for each case study.	123
Figure 6-6: Comparison of the PD values for both occupants in each case study.	125
Figure 6-7: Comparison of the quality of indoor air for each case study; (a) contaminant concentration at the breathing level; (b) the inhaled air quality for both occupants.	129
Figure 7-1: (a) The configuration of the simulated room: 1 – occupant_1; 2 – occupant_2; 3 – PC case; 4 – PC monitor; 5 – displacement ventilation (DV) inlet; 6 – return inlet; 7 – external wall; 8 – combined system-1 (exhaust inlet and ceiling lamps); 9 – combined system-2; 10 – zone-1; 11 – zone-2; and (b) the arrangement of the equipment within the simulated office.	132
Figure 7-2: Mesh distribution in the investigated room domain.	134
Figure 7-3: Boundary layers inflation (a) around the occupants, and (b) near the external wall.	134
Figure 7-4: Comparison of measured and simulated air velocity magnitude (m/sec) at poles 3 and 4.	135
Figure 7-5: Comparison of measured and simulated air temperature (°C) at poles 3 and 4.	136

Figure 7-6: RMS convergence test (m/s) for different flow times at the pole located in the room centre.	137
Figure 7-7: (a) Monitoring points; (b), (c) and (d) instantaneous velocity components at monitoring points 1, 2 and 3, respectively.....	139
Figure 7-8: Graphs (a), (b) and (c) show the FFT analyses for velocity components v_x , v_y and v_z , respectively, at three monitoring points.....	142
Figure 7-9: The RANS predictions of the temperature distribution.	144
Figure 7-10: The instantaneous temperature contours derived from the LES.	148
Figure 7-11: The mean temperature distribution contour derived from the LES.	148
Figure 7-12: RANS predictions of velocity magnitude (m/s).	150
Figure 7-13: Instantaneous velocity magnitude colour iso-levels from the LES predictions.....	154
Figure 7-14: Mean velocity magnitude colour iso-levels from the LES.....	154
Figure 7-15: The instantaneous iso-surfaces of the velocity magnitude at $t = 100$ sec.	155

List of Tables

Table 4-1: Cooling load for the simulated office room.	55
Table 4-2: Case studies description.	56
Table 4-3: Numerical methods and boundary condition details.	57
Table 4-4: Mesh independence test.	67
Table 4-5: The relation between PMV and thermal sensation.	70
Table 4-6: Energy saving for cooling coil.	83
Table 5-1: Case studies.	91
Table 5-2: Cooling load for the simulated office room.	91
Table 5-3: Mesh independence test.	93
Table 5-4: Energy saving for cooling coil for each case study.	110
Table 6-1: Case studies	115
Table 6-2: Energy saving for the cooling coil for each case study.	126

Nomenclatures

Abbreviations

DV	Displacement ventilation
HVAC	Heating, ventilation and air conditioning system
IAQ	Indoor air quality
LEV	Local Exhaust Ventilation
LEVO	Local Exhaust Ventilation for Office
MV	Mixing ventilation
PD	Percentage Dissatisfied people
PV	Personal velocity
PMV	Predicted mean vote
PPD	Predicted percentage of dissatisfied
STRAD	Stratified air distribution system
UFAD	Underfloor air distribution system

Variables

C	Mean particle concentration (kg/m^3)
$C_{1\varepsilon}, C_{2\varepsilon}$	Model constants in the term ε of the turbulence model
C_n	Normalised concentration.
C_p	Contaminant concentration in a specific region (kg/m^3)
C_e	Concentration at exhaust (kg/m^3)
C_μ	Model constant of the turbulence model
c_p	Specific heat of air ($\text{J}/(\text{kg K})$)
d_p	Particle diameter (m)
dt	Particle residence time (s)
F_D	Inverse of relaxation time (1/s)
\vec{F}_a	Force acting on particle (N)
\vec{F}_b	Brownian force (N)
\vec{F}_s	Saffman's lift forces (N)

\vec{F}_{thermal}	Thermophoretic Force (N)
\vec{g}	Gravitational acceleration (m/s ²)
i	Trajectory index
j	Cell index
k	Turbulent kinetic energy per unit mass (J/kg)
\dot{m}	Mass flow rate associated with each trajectory (kg/s)
\dot{m}_e	Exhaust mass flow rate (kg/s)
n	Trajectory number
P_k	Additional term in the turbulence model
$Q_{\text{coil-STRAD}}$	Cooling coil load for the STRAD system (W)
Q_{space}	Cooling coil load of space (W)
Q_{vent}	Ventilation load (W)
$Q_{\text{coil-MV}}$	Cooling coil load for the mixing ventilation system (W)
S	Mean strain rate tensor magnitude (1/s)
S_{ij}	Strain rate tensor (1/s)
T	Air temperature (°C)
TU	Turbulence intensity
T_e	Exhaust temperature (°C)
T_{set}	Room set temperature (°C)
t	Time (s)
\vec{u}_p	Particle velocity vector (m/s)
u	Fluid velocity (m/s)
u'_i	Fluctuating velocity (m/s)
V_j	Volume associated with i trajectory and cell j (m ³)

Greek letters

β	Coefficient of thermal expansion (1/K)
ε	Turbulent dissipation rate (m ² /s ³)
λ	Molecular mean free path (m)
μ	Dynamic viscosity (kg/(m s))
ξ_i	Normally distributed random number
ρ	Fluid density (kg/m ³)

ρ_p	Particle density (kg/m ³)
σ_k	Model constant for k equation of the turbulence model
σ_ε	Model constant for ε equation of the turbulence model

Chapter 1 Introduction

1.1 Background

The main aim of a Heating, Ventilation and Air Conditioning (HVAC) system is to create a healthy and comfortable environment for the occupants of a building. Many people spend a great deal of their time inside buildings; indeed, according to a recent study, most people spend around 70-90% of their time indoors [1]. Furthermore, the productivity and satisfaction of a building's occupants depend on the comfort level inside that building. Therefore, a well-designed HVAC system is required to provide a healthy environment and acceptable thermal conditions in order to enhance human thermal comfort and indoor air quality (IAQ). Recently, global warming and the energy crisis have become huge issues around the world, especially in the industrialised countries. HVAC systems play a key role in these issues. The heating, ventilation and air conditioning applications in commercial buildings demand a large amount of energy to provide a comfortable indoor environment [2]. Many strategies are used to reduce the energy consumption in HVAC systems. Using insulation within buildings will help to reduce the heat transfer through walls. Furthermore, decreasing ventilation flow rate can help to reduce the demand for energy. However, these strategies may cause thermal discomfort and eventually have an influence on human health and productivity. Therefore, special attention should be paid to the design of any ventilation system.

1.2 Ventilation strategies

In recent years, many strategies for the design of ventilation systems, such as displacement ventilation (DV) systems, mixing ventilation (MV), underfloor air distribution (UFDA), personal ventilation (PV) systems and local exhaust ventilation (LEV), have been widely used to provide an acceptable thermal environment in inhabited buildings and to enhance the IAQ while reducing the energy consumption. In heating ventilation and air conditioning applications, there are many types of ventilation system that are widely used around the world, as described in sections 1.2.1 - 1.2.5.

1.2.1 Mixing ventilation (MV)

A mixing ventilation (MV) system is one of the main types of ventilation systems used in the majority of heating ventilation and air conditioning systems in the residential sector. The system involves mixing a fresh air supply with the indoor air in the room, which leads to a complete dilution of the polluted room air with the supply of fresh air in order to reduce the concentration of contaminants in the occupied zone [3]. With this kind of ventilation system, a uniform air quality can be achieved in a given room. However, using an MV system can reduce the quality of inhaled air. Figure 1-1 shows the principle of the MV system in an office room.

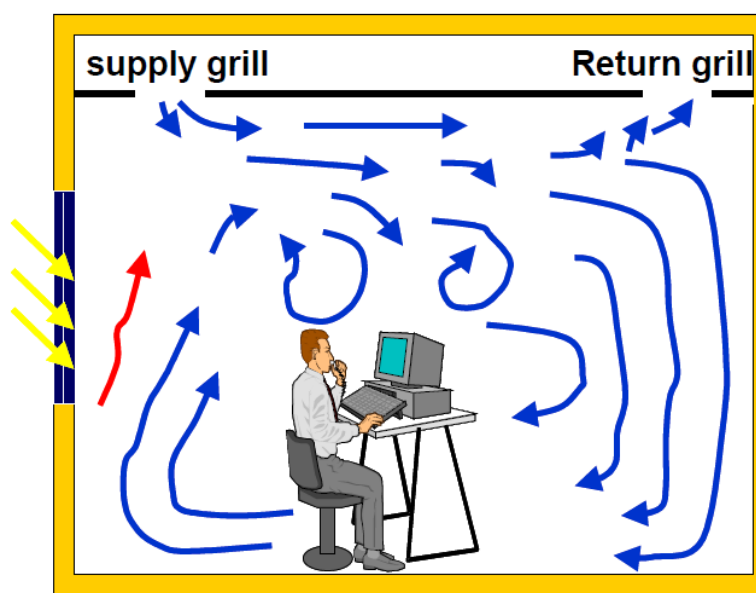


Figure 1-1: Mixing ventilation [3].

1.2.2 Under-floor air distribution (UFAD) system

With an underfloor air distribution (UFAD) system, fresh air flows from the floor in the occupied area towards the ceiling, as shown in Figure 1-2. Using this method of ventilation helps increase the flexibility of the room space subdivision and creates thermal stratification, which is a significant issue in terms of energy saving [4]. However, draft discomfort and cold feet are considered to be the main drawbacks of this system.

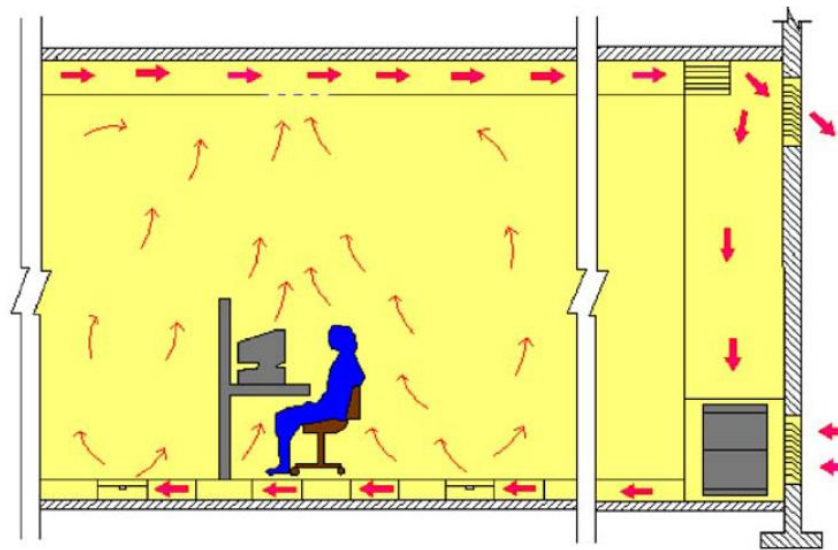
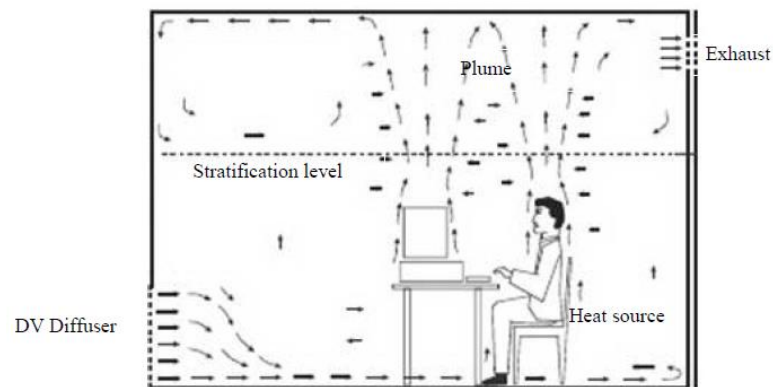


Figure 1-2: Underfloor Air Distribution system [5].

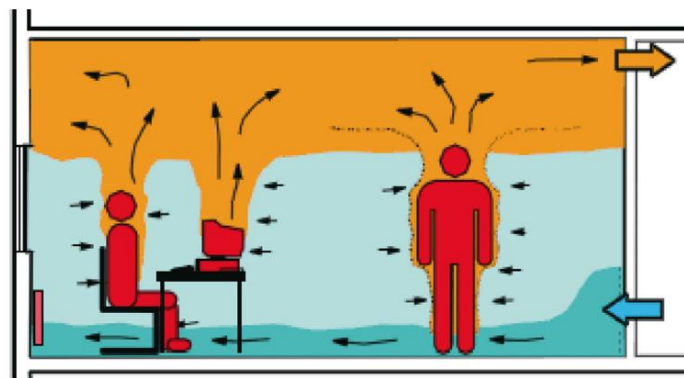
1.2.3 Displacement ventilation (DV) system

With a displacement ventilation (DV) system, the fresh and cool air is normally supplied at, or close to, floor level at low velocity and air is extracted at ceiling level, as shown in Figure 1-3. This system has been widely used in Scandinavian countries in recent years [6]. In this system, the warm air moves up (thermal plumes) towards the ceiling by natural convection, where it is warmed by contacting room heat sources such as people, equipment and lights. Stratification of temperatures and contaminant concentration forms in the room, and the horizontal temperature profile is uniform except for the regions near the DV supply and heat sources.

In this system, the room is divided into two zones: the breathing zone from floor to head level, and the contamination zone from head level to the ceiling. Recently, DV system has attracted more attention worldwide, due to its ability to improve the IAQ and provide a comfortable environment in a room [7]. Moreover, the energy consumption of the DV system is 33% less than that of an equivalent MV system [8]. However, a draft risk due to temperature differences between head and foot levels, as well as the movement contaminant distribution are considered to be the main drawbacks of this type of ventilation system.



(a)



(b)

Figure 1-3: (a) Stratification level with a DV system and (b) DV system in an office room [9, 10].

1.2.4 Personalised ventilation (PV) system

In recent years, thermal comfort, in conjunction with energy saving, has become a main concern for researchers. Ventilation systems play a significant role in achieving these. As previously mentioned, the different types of ventilation systems, those of DV, UFAD and MV, have a number of limitations in terms of thermal comfort and energy saving. Therefore, a considerable number of studies have been undertaken in recent years that seek to improve ventilation systems and energy consumption.

The personalised ventilation (PV) system is a new concept, as introduced by Fanger [11]. As shown in Figure 1-4, there are different types of PV systems depending on location. The main aim of this system is to supply fresh and cool air directly to the breathing zone of room occupants, where airflow and direction may be individually controlled by occupants. Using a PV system can help to improve the thermal environment around room occupants and enhance the quality of the inhaled air. Furthermore, the PV system can save energy compared to an equivalent MV systems. Numerous studies have been undertaken on improving the PV system effectiveness and its performance. Different kinds of air terminal devices for the PV system, exhaust locations, as well as their use in combination with DV, UFAD and MV systems, have been examined to consider their ability to enhance IAQ and energy savings. It was found that PV systems have the ability to improve the thermal microenvironment around the occupants by directing fresh and cool air towards the breathing zone and the potential for energy savings and thermal comfort is increased [12, 13] and [14].

Despite all these positive characteristics of PV systems, there are some drawbacks. The flexibility of air terminal devices is limited, especially when occupants move around an office, and also the manual control of the air flow rate can be problematic, especially with some types of air terminal device. Furthermore, most types of PV system direct fresh air towards the upper body of the seated person, which leads to an increased risk of thermal discomfort due to the temperature difference between the upper and lower parts of their body.

Therefore, more attention should be paid to enhance the PV system by reducing the temperature difference between the head and foot levels in order to improve the thermal comfort and increase the potential for energy savings.

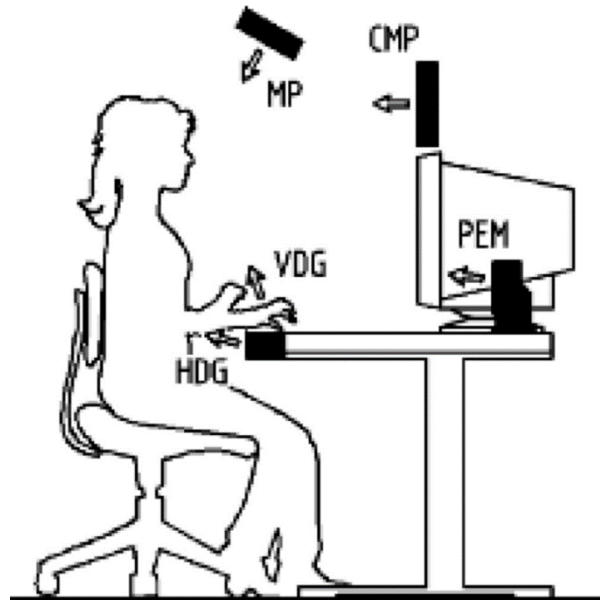


Figure 1-4: Types of personalised ventilation system [15].

1.2.5 Local exhaust ventilation (LEV) system

Local Exhaust Ventilation (LEV) systems are considered one of the most important types of ventilation system; they are widely used in industrial applications and are not a new method of ventilation. This system aims to provide a suitable working environment by reducing the contaminant concentration, particularly in the working zone, and also to control the contaminant transmission in occupied areas [16-19] (see Figure 1-5). In LEV systems, contaminated air is extracted locally before contaminants can disperse into the working area, as this helps to significantly reduce the contaminant concentration in the inhaled area and provide a healthy and comfortable environment for workers.

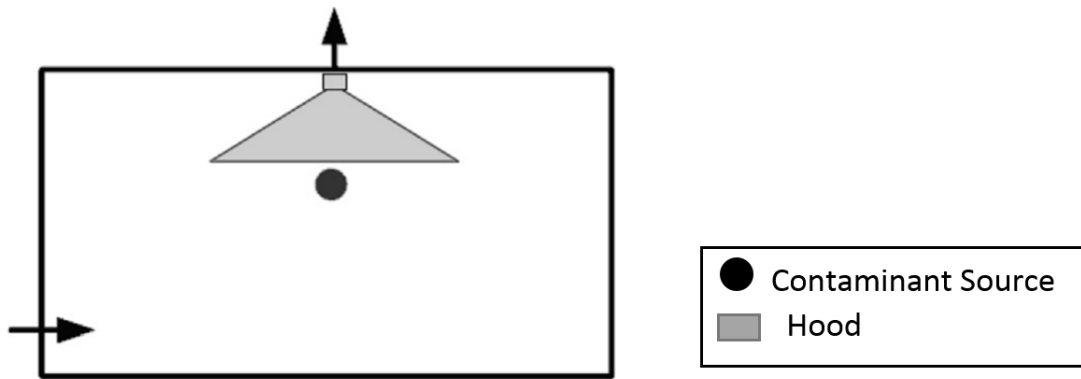


Figure 1-5: Local exhaust ventilation (LEV) [20].

1.3 Evaluation indexes for ventilation systems

HVAC systems are considered one of the most important parts of modern buildings. These systems have developed rapidly in recent years. The main role of this type of system is to provide a suitable environment to occupants in terms of indoor thermal comfort and air quality. This requires the consumption of energy. Recently, global warming and carbon emission have become huge issues around the world, the approach to which requires realistic solutions from researchers. Regarding the HVAC system, reducing energy demand without improving the systems may create a thermally uncomfortable environment and reduce the quality of the inhaled air. This will influence the occupants' productivity and cause significant issues in terms of health, all of which may ultimately result in significant economic loss. Therefore, in any ventilation system design, many evaluation indexes should be carefully considered. A careful balance should be found by researchers between the different evaluation indexes, depending on a building's type, size, occupations, applications and other factors to provide a healthy and comfortable indoor thermal environment with an acceptable degree of energy saving. Thermal comfort, energy saving and indoor air quality are considered the most important indexes and these are widely used by researchers to evaluate and develop ventilation systems.

1.3.1 Thermal comfort

The vertical temperature gradient is one of the major factors in evaluating indoor thermal comfort in the Stratified Air Distribution system (STRAD) system. As recommended by the American Society of Heating, Refrigerating and Air-Conditioning Engineers (ASHRAE) standard [21], the temperature difference between head level and foot level should not exceed 3 °C. In addition, the indoor thermal environment can also be evaluated using Fanger's comfort equations [22]. In this thermal comfort model, the thermal balance for the whole human body is expressed by two indexes, the predicted mean vote (PMV) and the predicted percentage of dissatisfied (PPD).

1.3.2 Energy saving

The heating, ventilation and air conditioning applications in commercial buildings consume about 43% of their total energy requirements [2].

In HVAC systems, many strategies are employed to enhance energy savings in buildings. Reducing heat transfer in building walls by using insulation and decreasing ventilation flow rates can help to enhance energy savings. However, reducing ventilation flow rates can also lead to increased pollutant concentrations and temperatures in the occupied zone, which can cause thermal discomfort and will eventually have an impact on human health. Therefore, great consideration should be given to the ventilation system design. For the STRAD system, only the occupied zone is required to be thermally comfortable, which enhances the potential to increase energy savings. In addition, many strategies should be used to employ the STRAD system benefits to provide a healthy and comfortable environment that only requires a low energy consumption.

1.3.3 Indoor air quality (IAQ)

The main impulse to develop or enhance any ventilation system is to improve the indoor air quality. Reducing contaminant concentrations in buildings requires increasing attention. The occupants' productivity is greatly influenced by the quality of the indoor air. In addition, providing good air quality may help to create a healthy and comfortable environment for occupants and may help to increase productivity and reduce the risk of transmission of infectious diseases. For these reasons, the evaluation of indoor air quality has received greater attention from researchers. Many strategies are used to assess the quality of indoor air, such as the air change effectiveness, the number of air changes, the air age, the effectiveness of contaminant removal and the ventilation effectiveness. All these strategies have been used to successfully evaluate indoor air quality for different applications within buildings.

1.4 Computational Fluid Dynamics (CFD) for indoor air simulation

The computational fluid dynamics (CFD) approach has become a powerful tool for modelling indoor air flow. It can provide detailed information on temperature, air distribution and pollutant distribution inside buildings. Furthermore, a CFD model has the ability to simulate a wide range of flow problems for different configurations at high levels of accuracy and low cost when compared to similar experimental work. Therefore, accurate CFD predictions can help to improve the design of the HVAC system, which would consequently provide a healthy and comfortable environment with acceptable thermal conditions.

1.5 Aims and Objectives

In order to improve the knowledge of air distribution in office ventilation systems, this research uses and develops different techniques and methods to reduce the energy consumption and create a healthy and comfortable indoor environment for occupants. The objectives of this research are:

- 1) To study the effects of the location of exhaust diffusers in relation to the room heat sources in terms of thermal comfort and energy savings in an office served by a DV system.
- 2) To develop a new ventilation system using local exhaust ventilation systems for office rooms, named the LEVO system, and to enhance the indoor thermal comfort of the environment, the inhaled air quality and achieving energy savings.
- 3) To study the impact of the exhaust opening height for the novel LEVO system on the indoor thermal environment and energy savings.
- 4) Using LES, to provide a better understanding of the complex characteristics of airflow and temperature distribution in an equipped office room, using a combined system, and to help designers to make further improvements.

1.6 Thesis outline

This thesis is structured into eight chapters, which can be summarised as follows:

Chapter One: Provides a general background to, and the aims of, this research.

Chapter Two: Reviews the different techniques developed by researchers to create healthy and comfortable indoor environments with acceptable ranges of energy consumption. In the first part of this chapter, the influences of the opening layout on the indoor environment and energy savings are briefly reviewed. The second part of this chapter introduces the concept of the LEV system and its impact on the indoor thermal environment and energy savings. Finally, this chapter introduces several research efforts that have used LES to simulate airflows and temperature distributions indoors.

Chapter Three: Introduces the numerical methods used in this research.

Chapter Four: Presents a numerical investigation of the influences of the positions of exhaust openings where the warm and contaminated air is extracted, and their relation to room heat sources in terms of the indoor thermal environment and energy savings.

Chapter Five: Develops the concept of the LEV system for use in office spaces. In this chapter, a novel local exhaust ventilation system for offices (LEVO) is combined with an office workstation in one unit. Energy savings, thermal comfort and inhaled air quality are used to evaluate the performance of the new system.

Chapter Six: The impact of the exhaust opening height for the proposed LEVO system are investigated numerically to show the effects on the indoor thermal environment and energy savings. The performance of the new system is assessed for three different heights for the exhaust opening.

Chapter Seven: Discusses the LES methods used to investigate the complex characteristics of airflow and temperature distribution in an office room using the concept of combining the ceiling lamps with exhaust opening.

Chapter Eight: Gives the conclusions of the present study and describes some recommendations for future work.

Chapter 2 Literature Review

2.1 Introduction

In recent years, indoor thermal comfort, quality of indoor air and energy efficiency have been attracting increasing attention worldwide because of their influence on human safety, health, and work productivity. In order to achieve the requirements of indoor thermal comfort and energy efficiency in designing or selecting any ventilation system, certain parameters need to be carefully considered. The various different types of ventilation strategies and air distribution systems which have been developed for different types of buildings will be presented briefly in this chapter. Also, the roles of the different types of ventilation systems in providing the required indoor thermal comfort levels and energy savings are outlined and discussed in detail in this chapter. In the first part of this chapter, the impact of the opening layout on the indoor thermal environment and energy efficiency is presented, followed by a description of the concept of the LEV system and PV system and its impact on energy savings, thermal comfort, and inhaled air quality. Finally, the turbulence characteristics of the indoor airflow and temperature fields that can be determined using LES are briefly discussed.

2.2 The influence of the layout of exhaust and return openings

An efficient HVAC system design requires the proper placement of the supply inlet and exhaust outlet with respect to a room's geometric configuration, distribution of indoor heat sources and indoor thermal conditions [23-26]. With the increase in energy used for improving the quality of the indoor environment [27-29], it is necessary to use effective ventilation strategies [30-32] while maintaining an acceptable indoor thermal environment. In most air distribution systems, the ventilation performance and energy savings are greatly influenced by the arrangements of the supply, return, and of the exhaust diffuser positions.

An initial investigation that studied the relationship between the opening position and energy consumption was performed by Bagheri and Gorton [33]. They investigated the relationship between the return outlet location and cooling coil load. They concluded that extra energy saving can be achieved by positioning the return vent in the cooled zone near the floor. Their contributions were extended by Filler [34], who reported that energy saving can be improved by placing the return vent near the perimeter walls of the room where the convective heat flux will be extracted directly by means of the return vent before mixing with the air in the occupied zone. In line with Bagheri and Gorton [33] and Filler [34], Hongtao et al. [35] found that extra energy saving can be achieved by separating the exhaust and return vents in two different elevations, as shown in Figure 2-1. Awad et al. [36] conducted further experiments to investigate airflow patterns and the velocity distribution using different exhaust diffuser locations. Their results indicated that the exhaust diffuser's position had a great impact on the level of the thermal stratification layers which consequently affected the cooling coil load.

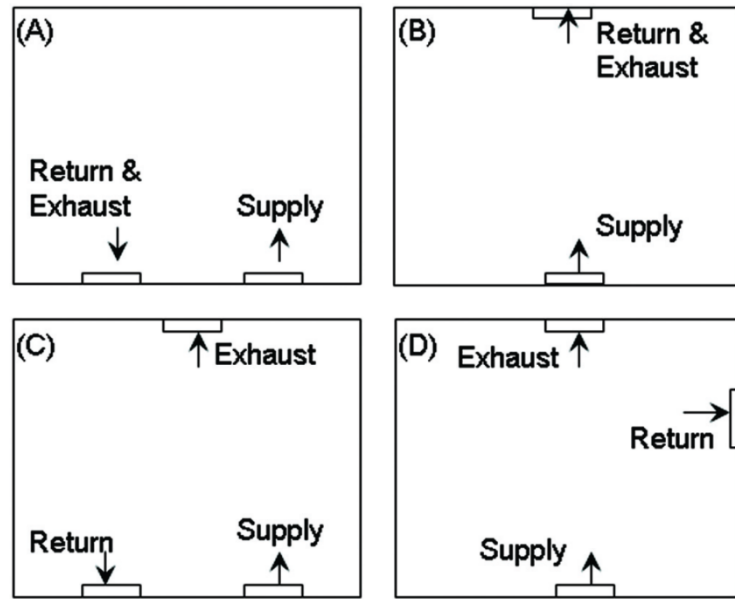


Figure 2-1: Schematic diagram of various combinations of UFAD system [35].

Another study by Awad et al. [37] discussed the stratified flow distribution indoors in two scenarios, along and across the inlet flow, using different parameters. They found that many factors have an impact on flow stratification. One of these factors is the input flow locations. A few years later, the energy saving evaluation for different locations of the supply opening was performed by Cheng et al. [38]. They reported that a 20.8% energy saving is achieved when the supply inlet is located at the floor level and the return outlet is located at the occupied level. They also found that the energy saving and indoor thermal comfort were improved by distributing the supply diffuser in the occupied zone. An extended study by Cheng et al. [39] investigated the impact of separating the return and exhaust locations on human thermal comfort and energy saving. A validated CFD model was used to simulate the airflow and temperature distribution inside an equipped office room with different heights of the return opening (see Figure 2-2). A cooling coil load calculation method was used in this study to calculate the cooling load; a significant reduction in the cooling coil load was predicted by reducing the height of the exhaust in an office room. Also it was found that thermal comfort and extra energy saving can be achieved by locating the exhaust grille close to the external wall at ceiling level.

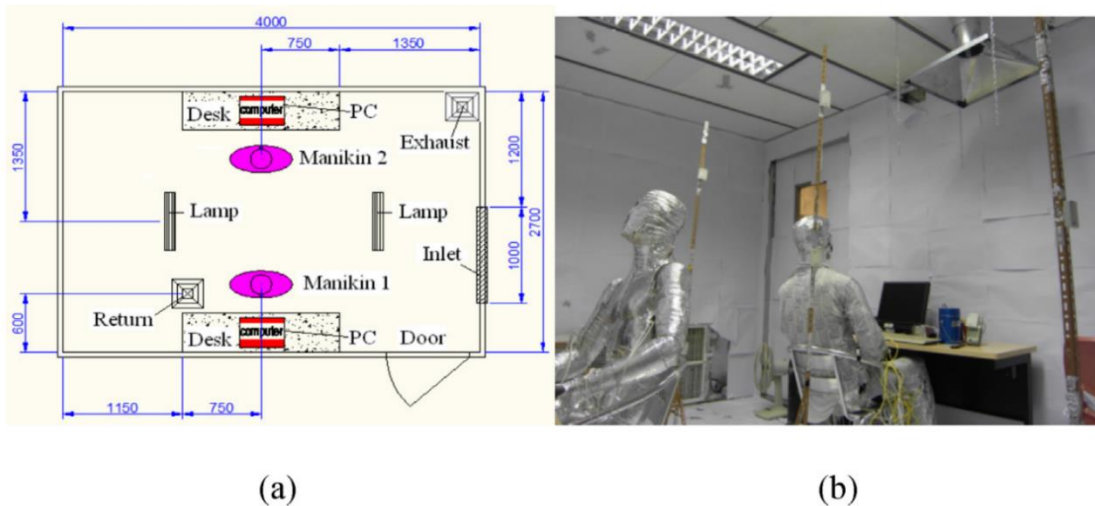


Figure 2-2: Experimental climate chamber (a): arrangement of the climate chamber; (b): real climate chamber [39].

Fong et al. [26] performed an experimental study using three different ventilation systems with six different exhaust configurations to investigate the impact of these systems on the indoor thermal environment and energy consumption. Their results show that significant improvements in thermal comfort and reductions energy consumption were achieved when the exhaust opening was located at the ceiling level (rear-middle-level). Such methods were also used by Kuo and Chung [40] to investigate the impact of the supply and of the outlet diffuser positions on indoor thermal comfort in the occupied zone using different ventilation strategies. Based on their simulation results, they found that the longer the supply air throw in the occupied region is, the better the indoor thermal comfort achieved. A few years later, He et al. [23] reported that the exhaust vent position may not greatly influence the pattern of airflow, but it can significantly affect the indoor exposure level (see Figure 2-3).

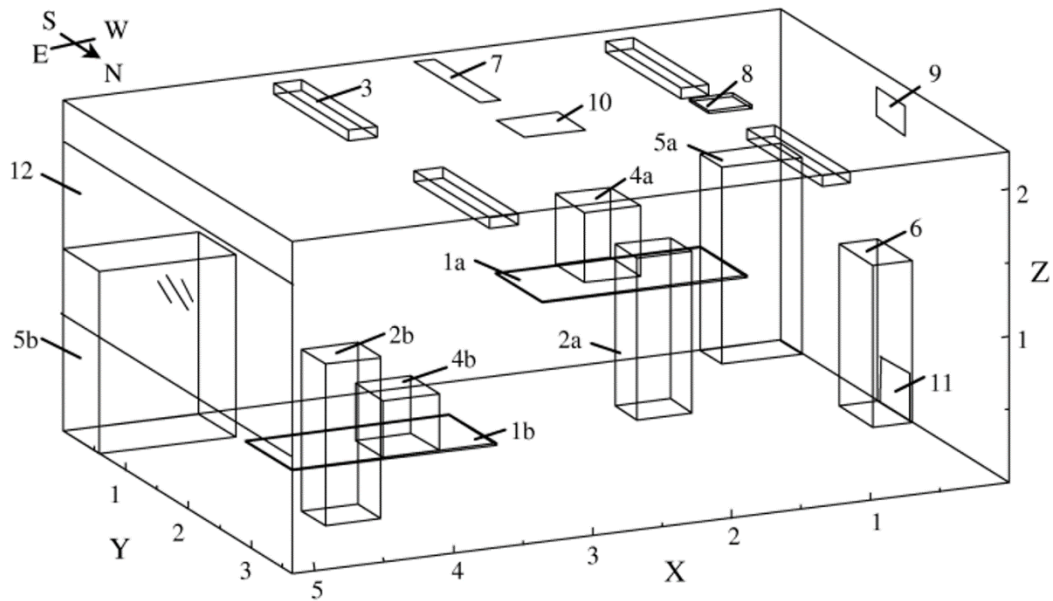


Figure 2-3: Schematic diagram of the experimental room [23].

Lin et al. [41] extended the investigation of the Kuo and Chung [40] and studied the impact of the position of the supply diffusers on the DV system performance. They revealed that for a better indoor environment the supply opening should be located close to the room centre. More investigations of the outlet layout impact on the indoor environment were performed by Espinosa and Glicksman [42]. They performed a numerical study in an office room to show the influences of the heat source density, inlet positions and geometry on the indoor temperature distribution. They found that the inlet location has a significant impact on the temperature distribution indoors. They also found that, by locating the inlet opening in the lower part of the investigated room near the return opening, the indoor air temperature will be far more uniformly distributed. Similar to that, Heidarinejad et al. [43] looked into the influence of the return opening heights on thermal comfort, energy savings and indoor air quality in a room served by an underfloor air distribution UFAD system (see Figure 2-4). They found that reducing the height of the return opening to 1.3 m above floor level will help to improve energy savings by up to 15.3% for the same level of thermal comfort. Fitzgerald and Woods [44] found that the height of the exhaust opening has a significant impact on the indoor air stratification.

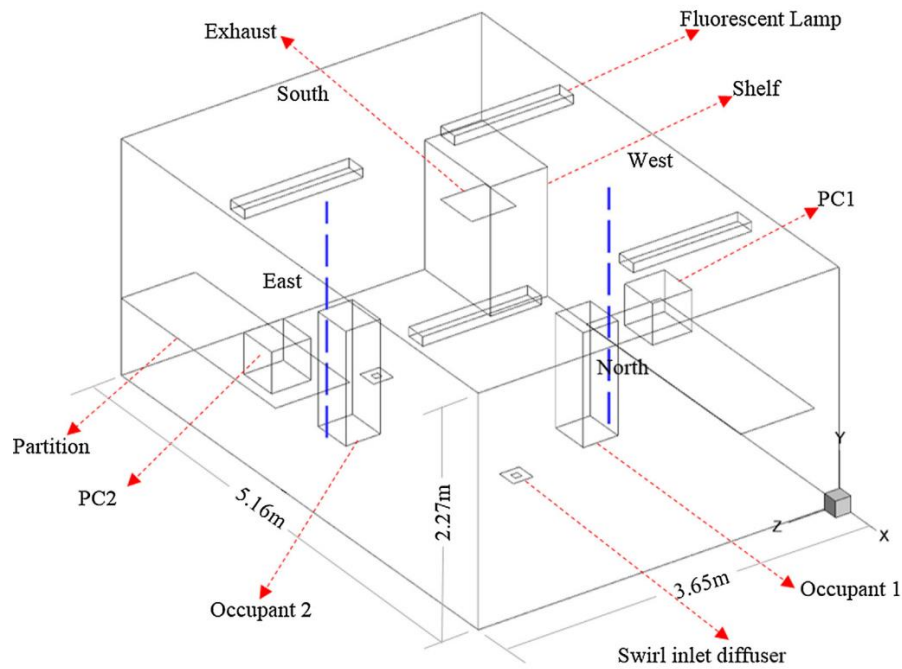


Figure 2-4: Simulated room arrangement [43].

Regarding the quality of indoor air, Thool and Sinha reported that cleaner air environmental conditions can be achieved in terms of contaminant distribution when using the exhaust vent at the upper part and the supply diffuser at the low part of the room [45]. The influences of the supply and exhaust locations of diffusers were numerically investigated by Khan et al. [46]. Their results showed that a better IAQ was achieved by locating the exhaust opening near the ceiling level. Similar to that, Cheong and Phua [47] examined the performance of contaminant removal using different strategies of ventilation systems in hospital rooms. They found that the best performance in contaminant removal occurred by situating the supply and exhaust diffuser on the wall behind the patient's bed. In line with Cheong and Phua [47], Neilsen et al. [48] studied the risk of cross-contamination in a hospital room using a downward ventilation system. They revealed that the position of the return openings played a significant role in the transmission of exhaled contaminants in the room. Ho et al. [49] further performed a numerical study to investigate the impact of the supply and exhaust openings for a surgery room's indoor thermal environment and the quality of the indoor air. The results showed a significant enhancement of the indoor thermal environment by installing the supply opening on the centre line of the room's vertical wall. Another study by Qian et al. [50] considered the pollutant transmission in a

hospital ward using a downward ventilation system. They found that the fine particle removal efficiency was improved by using an exhaust at a high level, while locating the exhaust at a low level improved the particle removal efficiency for large-size particles (see Figure 2-5).

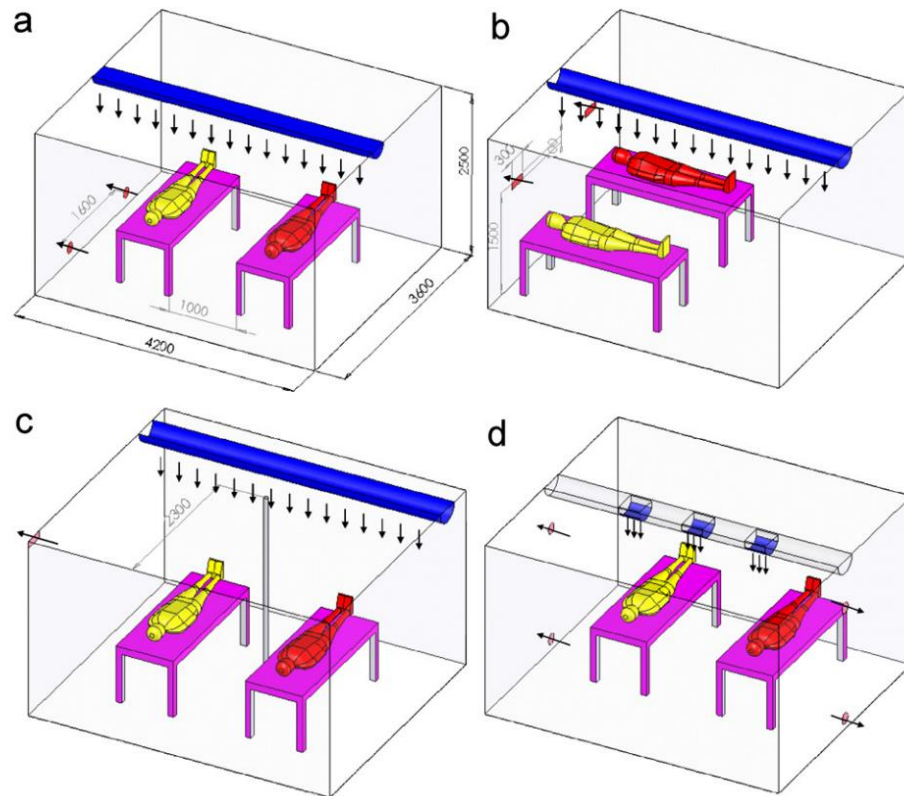
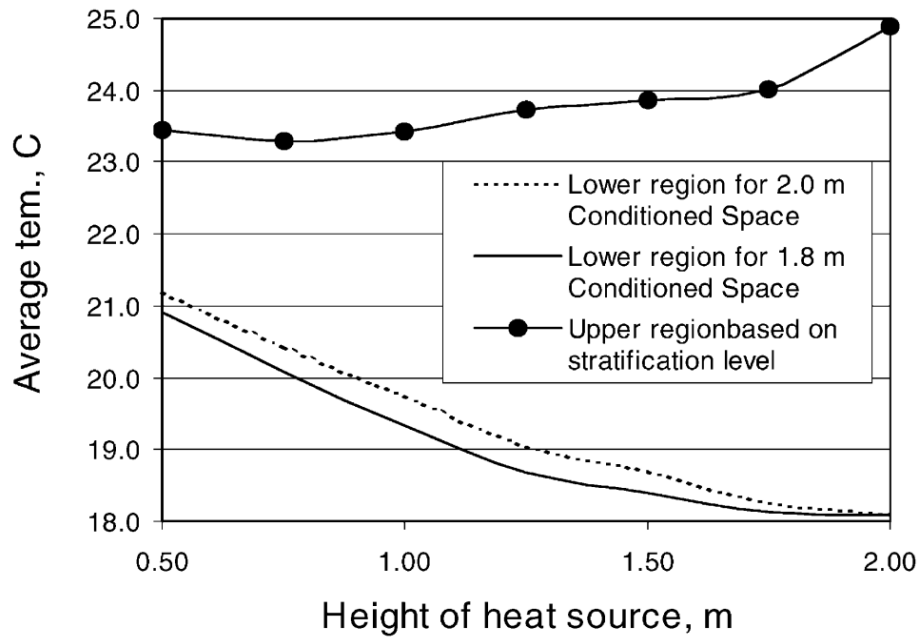


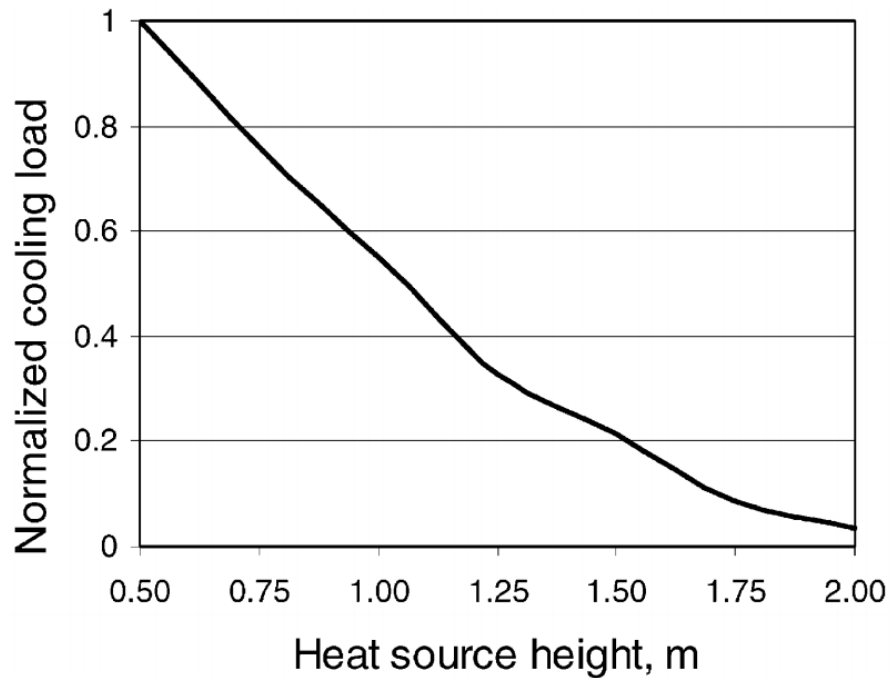
Figure 2-5: Four different layouts of supply and exhausts opening in the investigated room [50].

Thermal plumes generated from occupants and indoor heat sources play a significant role in increasing the exposure level for the occupants in the breathing zone by transporting the particles from floor level towards the upper part of the room, passing through the occupant inhaled area [34, 51, 52]. Therefore, the arrangement of the heat sources in a room may play an important role in the room's air flow pattern, thermal comfort, contaminant distribution and energy saving [53]. An initial study related to this concept was performed by Park and Holland [54]. They investigated the effect of heat source positions on the thermal stratification in a room served by a DV system. Their results showed that the indoor thermal environment and the energy consumption, as shown in Figure 2-6, are significantly influenced by changing the positions of the room's heat

sources, and they also found that by increasing the height of heat source location, the convective heat becomes less significant.



(a)



(b)

Figure 2-6: (a): Average temperature for the lower and upper zone; (b): cooling load evaluation with heat source height [54].

Another study was performed by Gan [55] to calculate the local thermal discomfort. It was found that the optimum supply velocity and temperature, considering the distance between the occupant, heat source, and the supply diffuser, have a significant impact on improving the thermal comfort and perceived temperature of the occupants. Also, the performance of the DV system with a floor supply system was investigated by Kobayashi and Chen [56]. The study was conducted in a full scale office room served by a floor supply DV system. It was found that the acceptable thermal environment can be achieved by using a suitable air change rate for a high cooling load.

More information was given by Ho et al. [57], who conducted a comparative study between two types of air distribution system, underfloor air distribution system and overhead air distribution system (see Figure 2-7). The thermal comfort and the indoor air quality in an equipped office room were evaluated for each system. Different parameters of thermal environment inside the room with different locations and angles for supply air terminal device were simulated in this study. Previous experimental results were used to validate the CFD model. The results showed that in terms of thermal comfort, indoor air quality and energy saving, the underfloor air distribution system seems better than the overhead air distribution system.

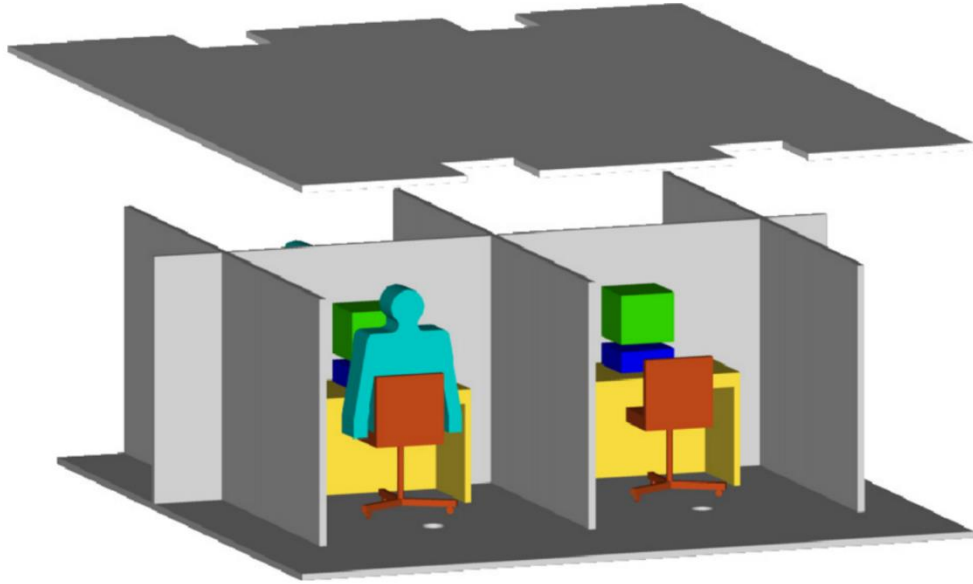


Figure 2-7: Schematic diagram of the investigated room [57].

Thus, the Indoor thermal comfort, indoor air quality and energy savings are affected by many parameters in any ventilation system. One of the main affecting factors is the locations of the inlet and outlet openings. Furthermore, an optimal selection of the return and of the exhaust opening positions have a considerable impact on the indoor thermal environment and on the energy saving [38, 39, 43].

Most previous studies have investigated the effects of the supply and return diffuser locations on the performance of the ventilation system, thermal comfort, IAQ and energy savings. But limited research has been performed to investigate the relationship between the location of the exhaust outlet diffuser and the heat sources in a room. The effects of the location of exhaust diffusers where the warm and contaminant air is extracted and their relation to room heat sources on thermal comfort and energy saving need more investigation.

2.3 Local exhaust ventilation and personalised ventilation system

In recent decades, various ventilation methods and devices have been developed to provide comfortable thermal environments for occupants and to reduce the demand for energy [58-61]. One of the most important strategies is to use a LEV system, also called the Personalised Exhaust (PE) system. In this system, warm and contaminated air is extracted locally before it reaches the occupied area, which consequently enhances the quality of the inhaled air. Furthermore, the PV system is considered to be one of the most important systems which is investigated extensively by researchers to provide a comfortable indoor environment and reduced energy consumption.

Faulkner et al. [62] investigated the task ventilation system for its thermal comfort and ventilation effectiveness. An air supply nozzle under a desk edge (see Figure 2-8) was used to direct air towards the occupant with different flow rates and different angles. This study showed that an enhancement of the ventilation rate in the breathing zone and in the thermal comfort condition as well as a reduction in energy consumption can be achieved by using a task ventilation system technique.

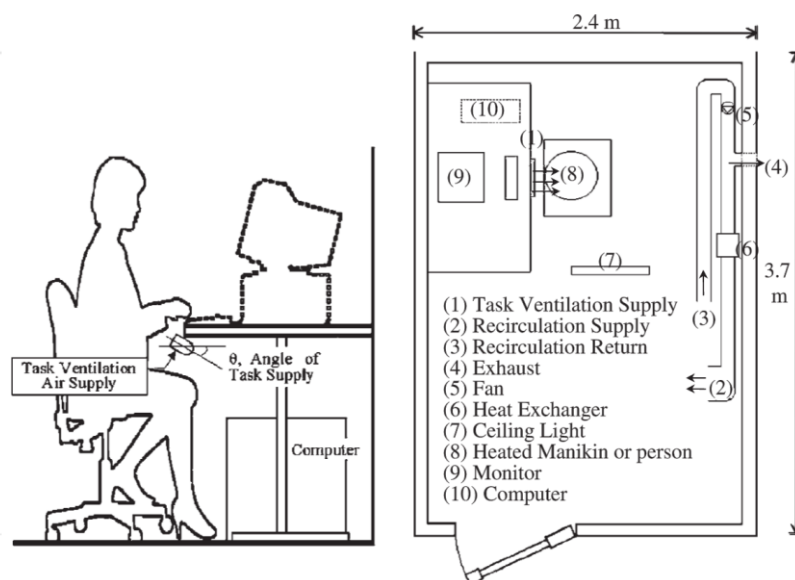


Figure 2-8: Schematic diagram of the task ventilation system in the experimental chamber [62].

This line of work was extended by Gao and Niu [63] who studied the micro-thermal environment around the occupants with and without a PV system. The air quality around the human body as well as the personal ventilation efficiency were used to determine the performance of using the personalised ventilation system. It was found that enhanced air quality can be achieved by using a 0.8 l/s air flow rate PV system. The performance of the PV system using a chair-based personalized ventilation system of Figure 2-9, and the occupant's response to this system were investigated by Niu et al. [12]. The thermal comfort, the IAQ and the human response were studied in these experiments. By using eight different air terminal devices (ATD), it was found that an enhancement of the inhaled air quality can be achieved by using a supply flow rate of personalised ventilation under 0.3 l/s. It was also found that the thermal comfort with the PV system can be better than with a MV system when the supply temperature of the PV system is below room temperature.

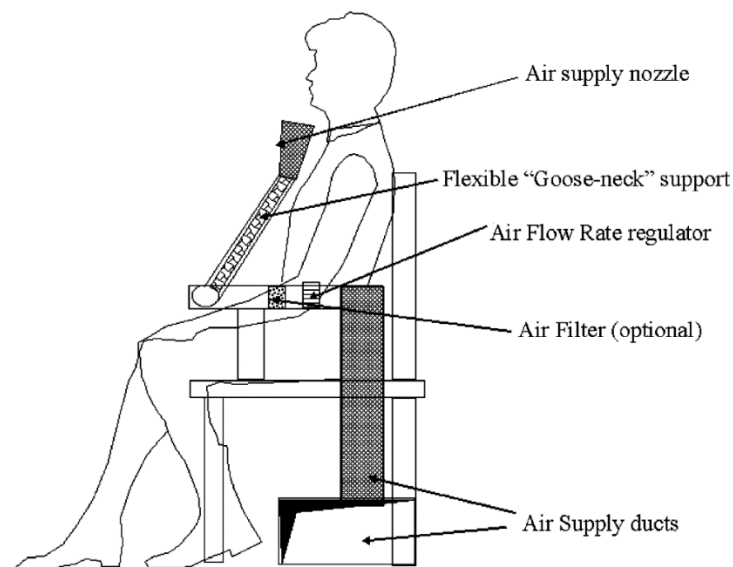


Figure 2-9: Schematic diagram of the PV system combined with the chair [12].

A further investigation was performed by Li, Niu [64] who used two types of personalised ventilation system a chair-based PV and a desk-mounted PV system to investigate the thermal comfort and air quality in terms of carbon dioxide (CO₂) concentration around the occupant in a room with different types of ventilation system, by using numerical modelling. DV and MV were used in this study as the main system of ventilation. It was found that better inhaled air quality can be achieved by using a combined system of DV and PV, to direct fresh air

towards the occupant. Recently, an extended study was performed by Kong et al. [65]. They investigated three different kinds of air terminal devices (ATDs) to show their effectiveness in removing the local heat generated from the occupants in the microenvironment area. The results show that the selected ATD, type I, was the best among the three types tested because of its ability to remove a satisfactory amount of generated heat from the occupant area for the same energy consumption as the other two ATD types. Another recent study was carried out by Habchi et al. [66], who enhanced the quality of the inhaled air in an office space by using a new ventilation system that was a combination of the a ceiling ventilation system with a fan installed on the desk near the occupant. In line with that, Bivolarova et al. [67] combined the concept of the LEV system with the bed shown in Figure 2-10 in order to reduce pollutants in the occupant area that may be generated by the human body and others causes. The results show that by using the concept of the LEV in this proposed system, the quality of the indoor air and inhaled air was improved significantly.

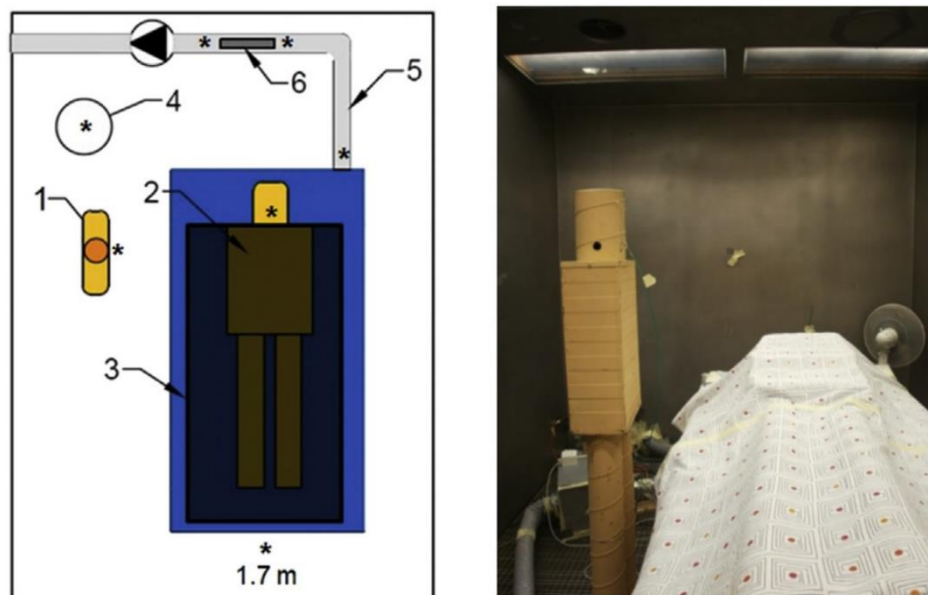


Figure 2-10: Experimental setup of the investigated room [67].

A further investigation was performed by Halvoňová and Melikov [68], who compared the performance of a DV system in an office room with and without ductless personalised ventilation systems, also considering the disturbance due to walking persons close to supply opening (see Figure 2-11). Two seated thermal manikins with two workstations were used in a full scale test room. The results showed that walking persons, as well as the manner of walking, have a significant contribution to reducing the quality of inhaled air as a result of mixing clean and cold air at floor level with the contaminated and warm air at a high level. It was also found that the performance of combining a personal ventilation with DV was better than that of a DV system alone.

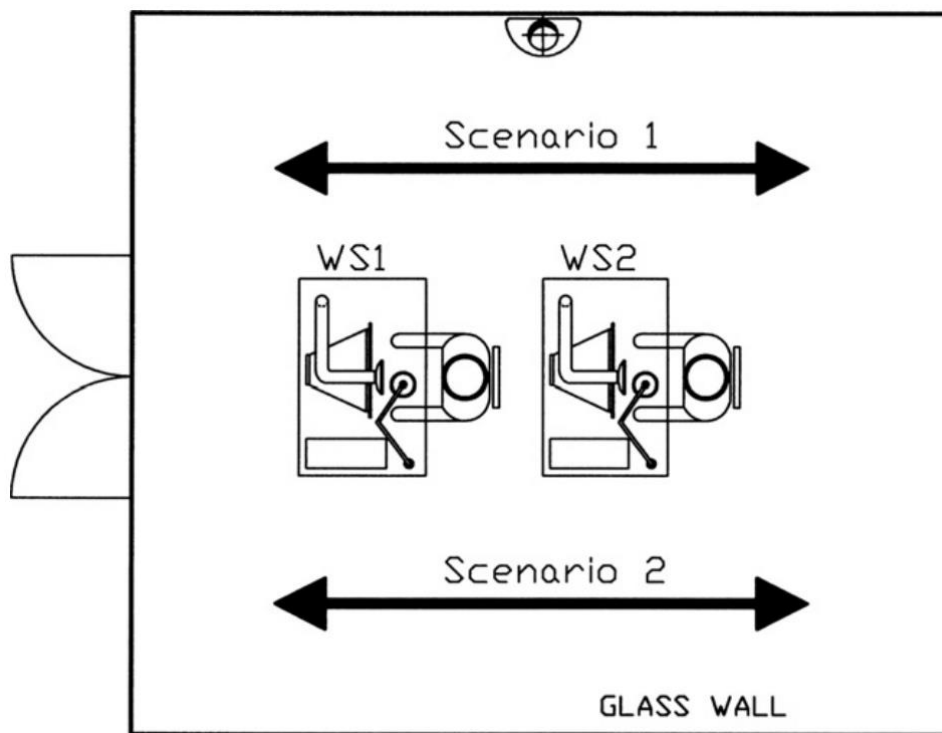


Figure 2-11: Walking scenarios in the investigated office room

Similar to that, an experimental study and a CFD simulation were used by Xu et al. [69] to investigate the performance of personal displacement ventilation PDV in a full scale test chamber with different locations of contaminant sources. A validated CFD model was used to simulate the indoor air distribution and the contaminant transport in the chamber. It was revealed that this technique of PDV needs design improvements. Specifically, the airflow of the air-conditioned environment needs to be more active to enhance the thermal microenvironment

around the human in terms of air velocity, temperature distribution and contaminant transport. Similar to Xu et al. [69], Conceição et al. [70] evaluated the thermal comfort level and IAQ around the occupant by using two PV systems mounted on the classroom desk and located in a slightly hot climate (see Figure 2-12). This study used a thermal manikin, two analysers for indoor environment, a numerical model for thermal comfort and a CFD model. The results showed that this system achieved acceptable levels of human thermal comfort and IAQ as well as delivering energy saving.

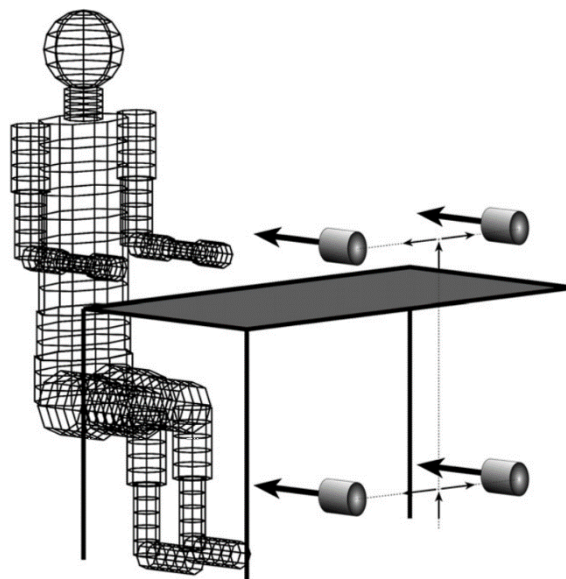


Figure 2-12: Experimental setup of the tested ventilation system[70]

An extensive study by Tham and Pantelic [71] was performed to investigate the performance of a combined system of the desk based personalised ventilation air terminal device (DPV ATD) with a desk mounted fan (DMF) in a test room. The Manikin-based equivalent temperature (T_{equ}) was used to evaluate the cooling effect for each part of the human occupant. Furthermore, the effectiveness of ventilation system was evaluated based on the personalised exposure effectiveness (PEE). Four different locations of (DPV ATD) were examined in this study. The results showed that a uniform distribution of temperature across the manikin and thermal comfort can be achieved by using the (DPV ATD) coupled with (DMF) system. Halvonová and Melikov [72] performed an extended investigation to study the performance of a ductless personalised ventilation (PCV) system in conjunction with a DV system in a full scale room with different

layouts of workstation and partitions (see Figure 2-13). Two thermal manikins and two tracer gases were used to simulate the seated occupants and the air pollution respectively. It was shown that the room which uses the PCV in conjunction with the DV system can provide a good quality of inhaled air in comparison with the room served by the DV system alone. It was also shown that the PVC system had the potential to enhance the thermal comfort and the IAQ around the occupant.

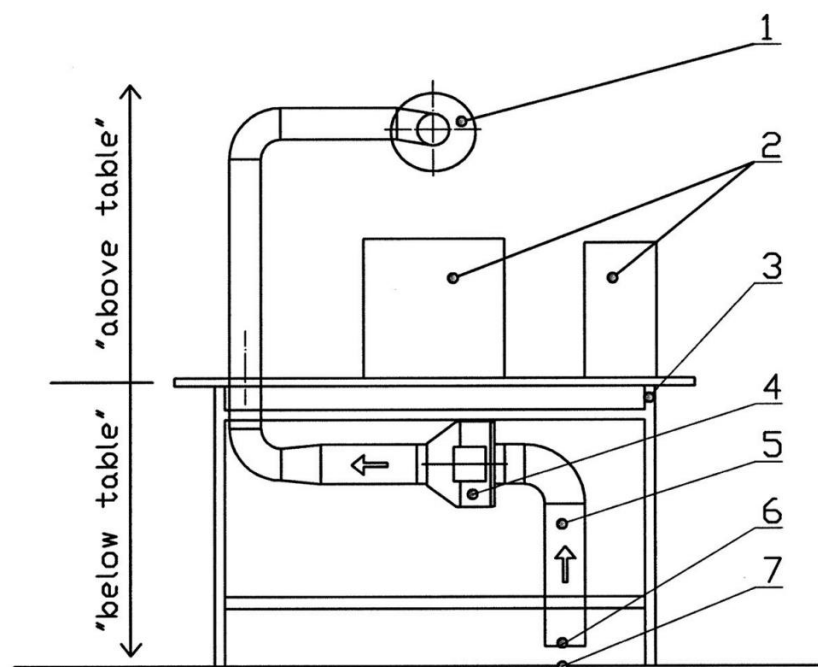


Figure 2-13: Schematic diagram of the experimental ductless PV system of [54]; (1) the air terminal device, (2) heat sources, (3) table, (4) fan, (5) duct system, (6) intake source of the DPV system, and (7) floor level [54].

Schiavon and Melikov [73] studied the energy conservation in a room located in a cold climate and served by a PV system by controlling the supply air temperature. The results showed that the supply air temperature of the PV system played a significant role in the energy saving strategy and it was also found that the optimum energy saving can be achieved with an air supply temperature at 20 °C. Another study by Li et al. [74] investigated the potential of enhancing the thermal comfort for occupants by using a coupled system of a PV system with a UFAD system (see Figure 2-14). It was found that the thermal environment around the occupant and the thermal comfort could be improved by supplying circulated warm air at foot level by means of a UFAD system and directing fresh air towards the breathing zone by using a PV system. The results also revealed that the thermal comfort and the IAQ with the combined system of PV-UFAD were much better than those with the UFAD alone or with MV with a ceiling air supply.



Figure 2-14 Experimental chamber for the investigated room.

Kanaan et al. [75] investigated the performance of the combined system of DV and PV system in an office room (see Figure 2-15). The flow rates of DV, PV and exhalation, as well as the thermal plume from occupants, were used to investigate the CO₂ concentration and transport in the room space. It was found that in DV system with a supply temperature at 18 °C and in the PV system with a supply temperature range from 18 to 22 °C and a PV flow rate range from 4 L/s to 10 L/s improved the quality of inhaled air by more than 20% in the breathing zone.

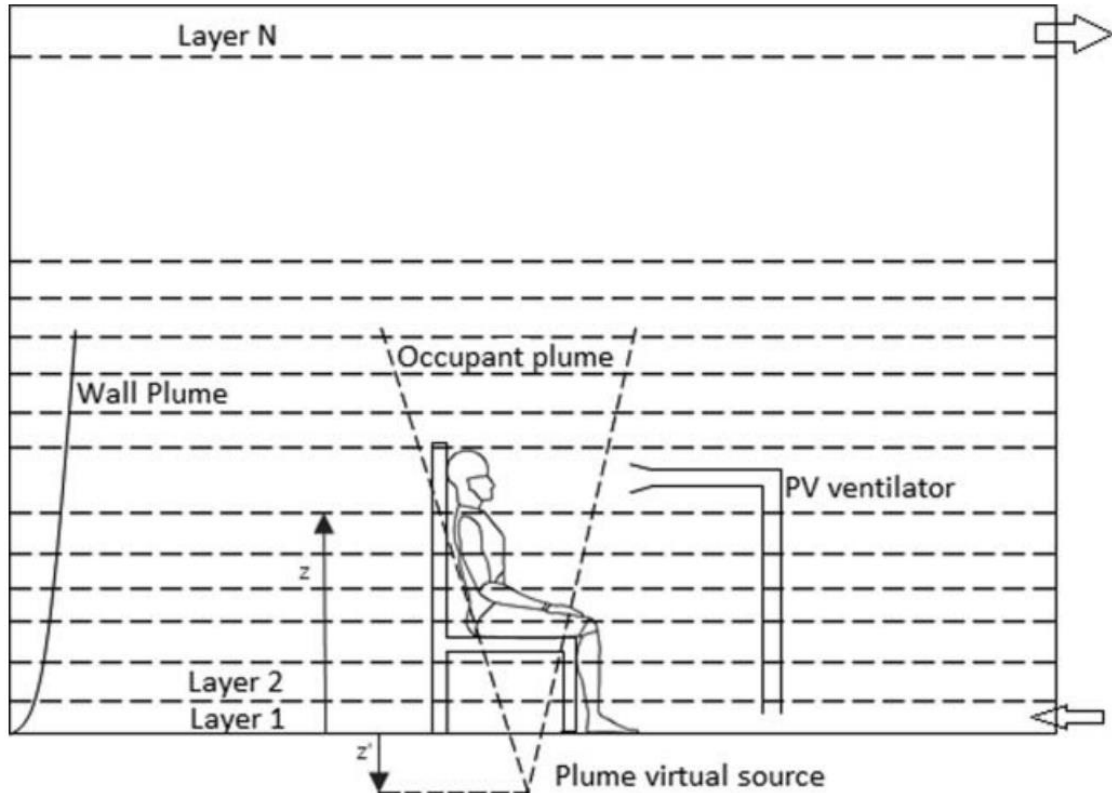


Figure 2-15: Schematic diagram of the tested room with DV/PV system [75].

Another investigation was performed by Yang et al. [76], who investigated the potential of saving energy by using a combined system of a ceiling mounted PV system and a MV system in an office room located in a warm and humid climate, compared to using MV alone and to using a MV system with a PV desk mounted controlled by a seated occupant. Different airflow rates with different numbers of outlets for PV system were used in this study. The results showed that energy saving in the cooling mode can be achieved by adding a ceiling mounted personalised ventilation system in a room served by MV system. It was also found that the energy used to moving air was increased but the total energy consumption was decreased.

This study was followed by Metzger [77] who evaluated the performance of a PV system by using a Taguchi-method-based approach with a limited simulations of computational fluid dynamic. This technique was used to determine the optimised indoor thermal environment. It was found that the supplied air velocity and temperature have a significant impact on the IAQ and on the human thermal comfort, as well as on the energy saving. It was also found that the flow rate has a significant impact on the IAQ and a minor impact on the thermal comfort and on the energy consumption. A recent study by Makhoul et al. [13] investigated the impact of a ceiling mounted PV system assist with a small fan mounted on a desk for improving the thermal environment around a seated human in an office room. It was found that the thermal comfort and a good air quality around the occupant can be achieved by using this coupled system of a desk fan with the ceiling mounted PV system. It was also found that the coupled system was achieved up to 13% of energy saving compared with the conventional ventilation system. The impact of the coupled system of a DV system with a personalised ventilation system on the human thermal comfort and energy saving was examined by another study of Makhoul et al. [78]. In their study, a transient thermal space model was developed and coupled with a bioheat model to predict the skin and core temperature for each segment of human body in order to evaluate the overall thermal comfort. A typical layout of an office room with six occupants was used to evaluate the energy saving with and without a personalised ventilation system for the same level of thermal comfort. It was found that for the nineteen - hour daily operation, the combined system of DV and PV used around 27% less energy consumption than the DV system alone for the same level of thermal comfort. It was also found that, when the temperature in the occupied zone exceeds 26 °C, energy saving was not achievable. Makhoul et al. [79] also studied the contaminant transport between office stations by using PV system coupled with a peripheral diffuser mounted on the ceiling (see Figure 2-16). The results showed that the canopy which is formed by a peripheral diffuser plays a significant role in reducing the concentration of contaminants moving towards the microenvironment around the human and enhancing the air quality around the occupant as well as energy saving.

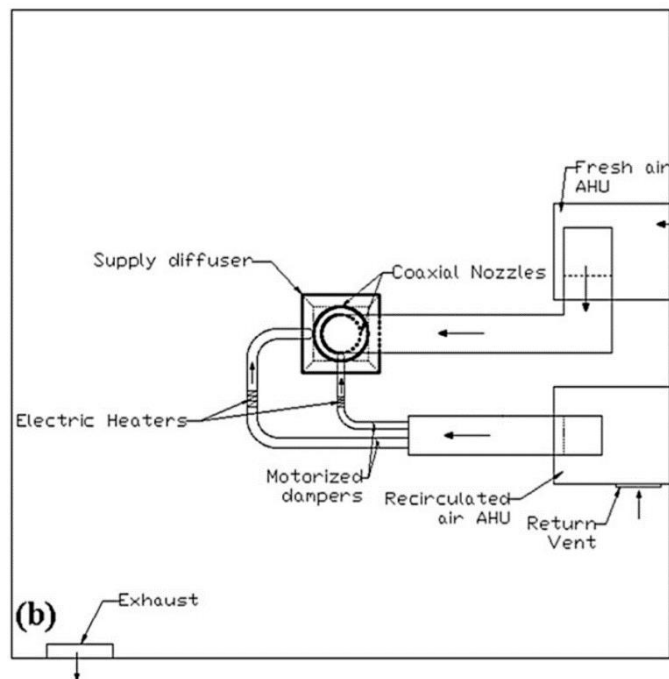
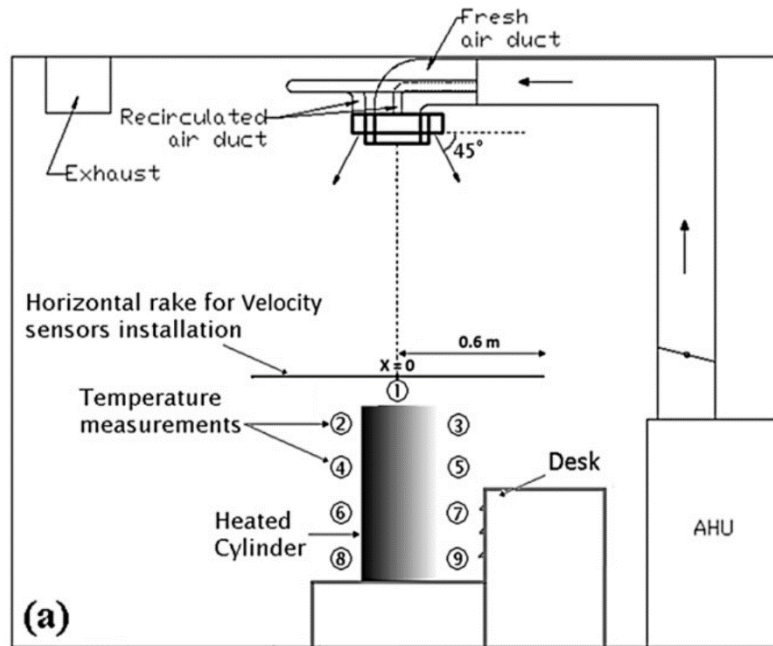


Figure 2-16: Experimental chamber setup [79], (a) top view; (b) side view.

Makhoul et al. [14] extended their research to investigate the performance of a combination system made up by a diffuser mounted on the ceiling and a coaxial nozzle personalised ventilation, which was directing the fresh air towards the breathing zone. The results showed that, at the same level of thermal comfort, up to 34% of energy saving can be achieved, compared with a MV system, by directing fresh air towards the breathing zone. In line with that, Magnier et al. [80] performed an experimental study in a full - scale room served by a DV system aided by a PV system (see Figure 2-18). It was found that, by using this coupled system, a higher temperature in the occupied zone was acceptable and energy savings were achieved.

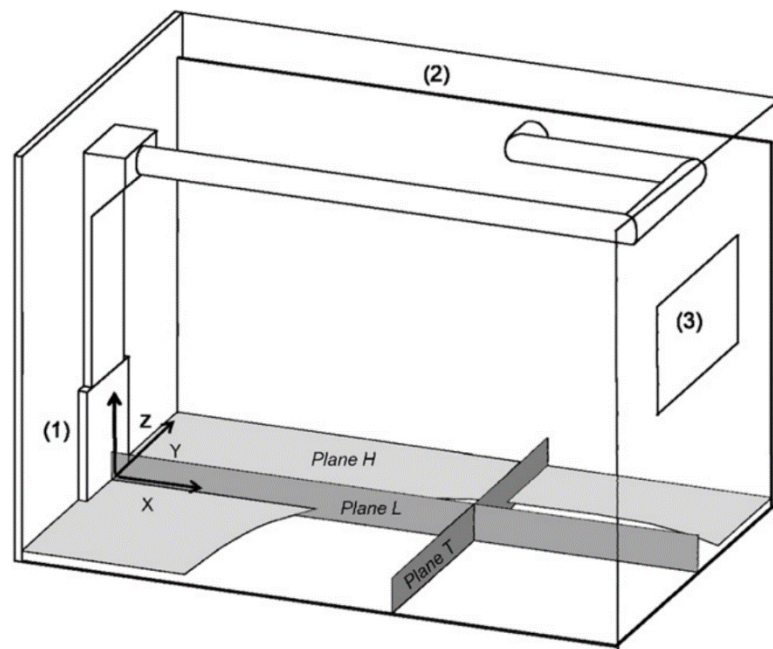


Figure 2-17: Schematic diagram of the investigated chamber.

Zhou and Kim [81] studied the impact of a PV system on the contaminant particles emitted from the carpet and the distribution of temperature in the microenvironment around the occupant seated in an office room. An experimental study was used to validate the CFD model. It was found that the control of the air flow rate of the PV system plays the main role in increasing the effectiveness of the ventilation. It was also found that the PV system has a significant impact on the pollutant concentration and on the temperature distribution in the area around the occupant. A further investigation was performed by Kang et al. [82] to study the performance of a PDV system in a full - scale chamber by using different

locations of pollutant sources. Experimental results were used to validate the CFD model which was used to predict the air movement, the temperature distribution and the pollutant transport inside the room. It was found that this type of PDV system cannot generate an acceptable thermal environment around occupants and would need more investigation to make this kind of ventilation system acceptable. A few years later, Dygert and Dang [17] proposed to use a local exhaust suction device in an airplane. Their results showed that up to a 90% reduction of exposure to contamination coming from other passengers is achieved. Furthermore, they concluded that this type of LEV is suited to a high density occupation. Another study by Zitek et al. [19] investigated the thermal environment and the air quality around the occupants in an aircraft using a separate airflow supply and a separate local exhaust. Their results showed that using this system protected the occupants from the possible dispersion of diseases in an aircraft environment. A further investigation was performed by Yang et al. [83] who researched the performance of three different kinds of personal exhaust (PE) device. They found that the quality of the inhaled air was enhanced by using a PE just above the occupant's shoulder level. In the same line of work, Junjing et al. [84] studied the performance of a PV system coupled with a PE system in a room served by a DV system (see Figure 2-18). The PE system was developed to introduce fresh air towards the breathing zone of occupants and to exhaust some of exhaled air from the microenvironment around the occupants. Two exhaust devices combined with a chair were located close to the shoulder level of a thermal manikin. Twelve different locations of seated occupants were used to simulate the occupants' position in an office room environment. The results showed that, compared with a PV system alone, a good quality of inhaled air can be achieved by using a coupled system of PE-PV.

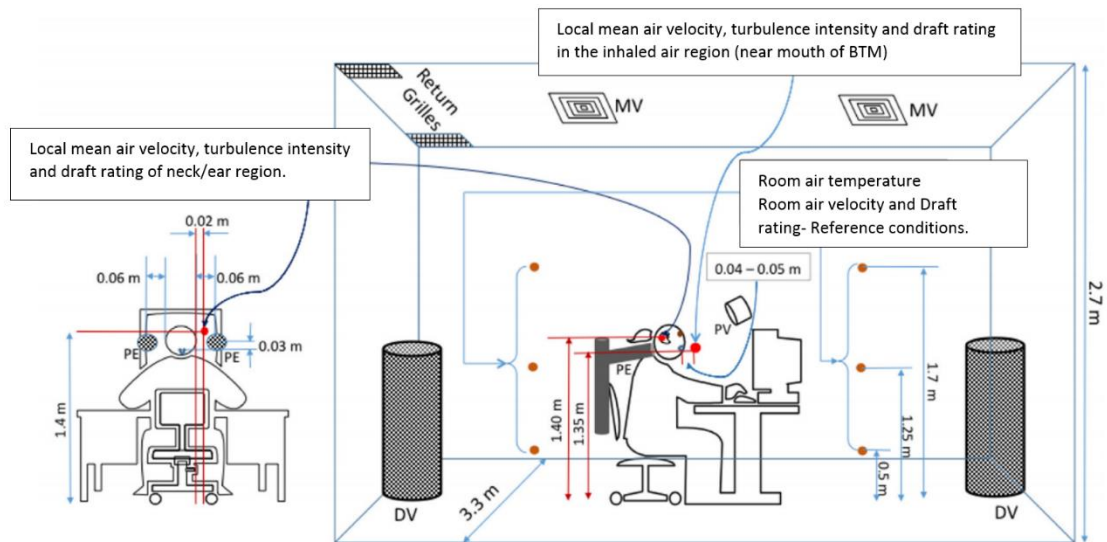


Figure 2-18: Experimental setup for the investigated room [84].

In line with Junjing et al. [84], Melikov et al. [85] used a LEV concept to develop the thermal environment around a hospital bed and investigated the reduction of the exposure to contaminants for the doctor and the patient with and without the LEV system. They found that with the LEV system the contaminants exposure level was reduced significantly for people who sat close to the patient. This study was extended by Bolashikov et al. [86] who explored the thermal environment around the occupant by combining the local exhaust with a local supply using a PV unit incorporated with seat. They found that using this system enabled them to enhance the quality of the inhaled air.

The previous studies focused on using the LEV system in hospitals rooms, airplanes and on some industrial applications to improve the quality of the inhaled air and to provide a healthy and comfortable environment for the occupants. However, very limited studies have considered the LEV system as a ventilation system in an office space [83, 86], and have a great impact on the energy consumption.

2.4 Using LES for the indoor environment prediction

For an optimum design, detailed information as to the turbulence characteristics of the air flow and temperature distribution are of particular importance [87]. One of the main difficulties with an experimental approach is the provision of a detailed prediction as to the turbulence characteristics of airflow and the temperature at any given point in the domain, requiring a considerable experimental effort and, consequently, a high cost. The advantages of computational techniques such as CFD are that they can provide accurate information through the domains whilst significantly reducing time and cost compared to the experiment. CFD has become a powerful technique in the simulation of, and solving the majority of problems associated with, indoor air flow, as it can provide detailed information regarding the temperature, the air distribution and the pollutant distribution inside buildings [63, 71, 88, 89]. Furthermore, a CFD model has the ability to simulate a wide range of flow problems that might be associated with different configurations to high levels of accuracy when compared with experimental work. Therefore, accurate CFD predictions can help improve the design of HVAC systems, which consequently can provide healthy and comfortable environments with acceptable thermal conditions [90-93]. For the accurate prediction of airflow and temperature distributions indoors, a suitable turbulence model should be selected [94]. Turbulence models have evolved rapidly over the years and many approaches have been developed to improve the accuracy of the predictions.

The Reynolds Averaged Navier-Stokes (RANS), Large Eddy Simulation (LES) and Direct Numerical Simulation (DNS) represent the three most popular turbulent flow modelling approaches [95]. Among these CFD turbulence models, RANS predictions have been widely used for indoors air flow simulation in order to understand the average temperature and velocity distributions. The RANS models work well with boundary layer and incur in manageable computational times and resources. The RANS models in general, and the Renormalisation Group (RNG) $k-\epsilon$ model in particular, have seen widespread use in the prediction of the airflow and temperature distributions in the indoor environment, some of the numerical results of which have provided acceptable time-average air flow distributions [96-99]. However, this method only has the ability to resolve the mean flow and cannot resolve the instantaneous airflow field. In most indoor

environments, the flow field is unsteady and unstable [100, 101]. In order to realise an efficient design and provide a suitable analysis of the indoor thermal environment, more detailed information regarding the instantaneous nature of the flow and of its temperature distribution is required; to this end, either a DNS or LES approach is required to resolve the turbulent fluctuations associated with the flow. DNS predictions are more accurate than RANS and LES in terms of the airflow and of the temperature distributions. However, DNS requires significant computational resources and time, particularly when dealing with complex geometries. In LES, all large scale eddies are resolved by using a low-pass filter on the Navier-Stokes equations, while the small eddies are modelled using a sub-grid scale (SGS) model. The computational resources and time required for a LES are significantly less than those required by the equivalent DNS, but they are greater than those required by the RANS. In comparison with the RANS approach, the LES method has shown very good agreement with experimental results when a fine grid is generated in the wall region, and that this method is widely used to predict the characteristics of indoor thermal environments [102-106].

Lin et al. [104] and Ebrahimi [107] used a simple room geometry to compare experimental results with LES predictions, finding that the indoor air movement was unsteady and unstable. In their study, the main unsteady flow features were the thermal plumes generated by occupants sitting in the region, and the effects of such perturbations were well predicted by the LES model. Similar to that, Zhu et al. [108] revealed that the occupants' thermal comfort is influenced by the dynamic characteristic of the airflows. LES were also used by Zhang and Chen [109]. They performed LES simulations within a simple room geometry to predict the indoor thermal environment using the proposed filtered dynamic SGS model in conjunction with the LES method. They found that LES was able to predict the indoor air simulation accurately. McGrattan [110] and Musser and McGrattan [111] conducted numerical studies using LES to predict the indoor thermal environment within an isothermal room. They revealed that the LES method provided a detailed description of, and accurate results for, the associated indoor airflow. Jiang and Chen [112] reported on the ability of LES model to predict the velocity and temperature distribution in a building ventilated purely through

natural ventilation concepts. This study was extended by Karadimou and Markatos [113], who investigated indoor airflow and particle concentration distributions, as shown in Figure 2-19, using LES. The results of their study showed that LES are capable of providing high accuracy results, especially in regions where the airflow is highly unstable, with strong recirculation's.

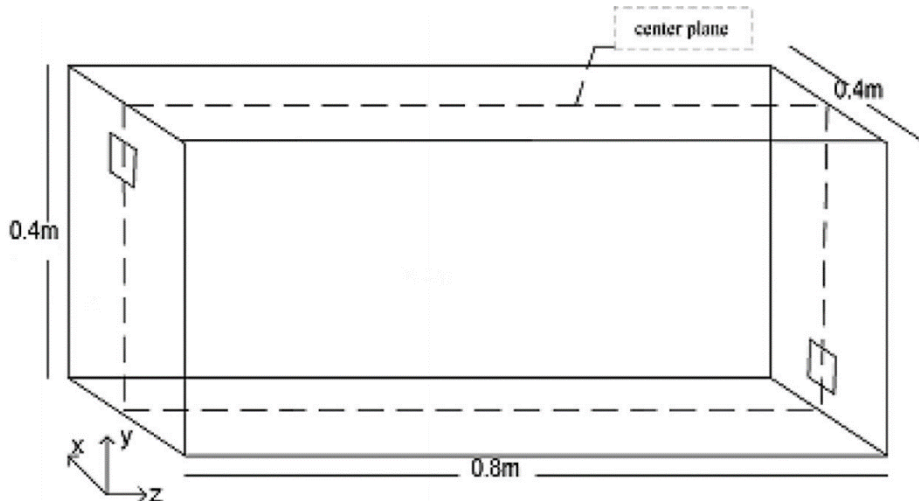


Figure 2-19: Computational room domain [113].

Davidson and Nielsen [114] studied the airflow distribution in a ventilated small room using LES. The Smagorinsky SGS model and a dynamic SGS model were used in this investigation. The results showed that both models provided highly accurate indoor airflow predictions. However, the dynamic SGS model was in slightly better agreement with the experimental data compared with the Smagorinsky model. Another study was performed by Emmerith and McGrattan [115] to investigate the performance of LES in a ventilated room. The results showed that LES gives accurate predictions of indoor airflow and are in good agreement with the experimental and simulated data reported in the reference [114] for all room domains, except in the regions near the floor and the ceiling. Tian et al. [116] revealed that the LES method was the best amongst various turbulence models. It was found that this method was in good agreement with experimental results of indoor contaminant concentration distributions (see Figure 2-20). Overall, it can be concluded that LES can overcome the predictive and computational drawbacks and limitations of both the RANS and the DNS approaches.

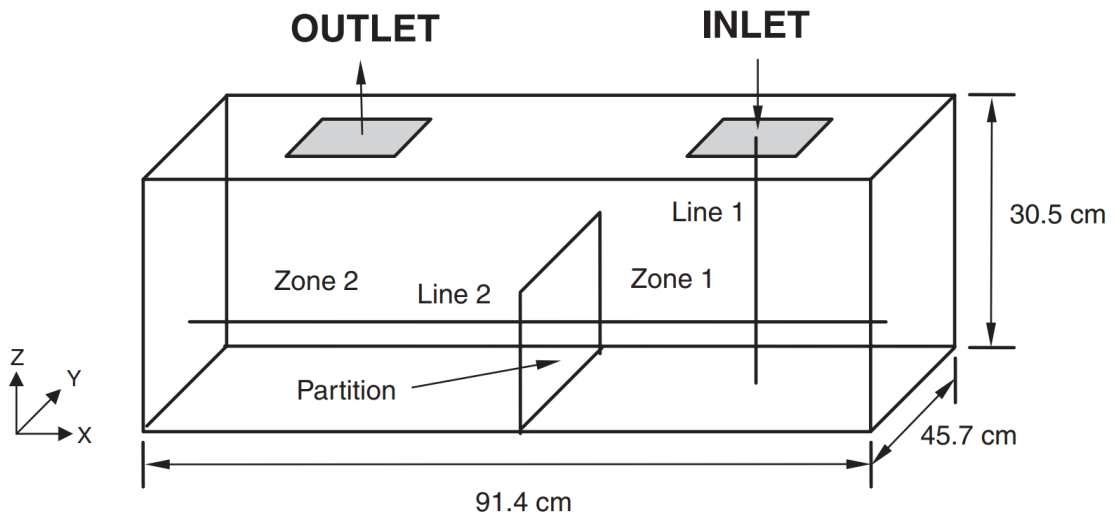


Figure 2-20: Simulated room domain [116].

Although LES modelling requires relatively high computational resources and needs more time in comparison with RANS modelling [117-123], a considerable number of researchers have shown the superiority of the LES method in predicting the characteristics of the flow field, temperature distributions, and of the indoor contaminant concentration distributions. Most previous researchers have employed the LES method to predict the indoor thermal environments for very simple room geometry; indeed, some of these researchers have studied only simple air flow in a clear room. The LES analysis of the behaviour of the complicated nature of instantaneous airflow and temperature distributions in realistic office environments containing complex equipment might thus be regarded as being very limited, or even insufficient. Thus, in this study, the LES method has been employed to predict detailed information regarding the turbulence flow behaviour and temperature distribution in a realistic office room which uses the concept of the incorporation of exhaust openings into ceiling lamps in a combined system.

Chapter 3 Numerical Methods

3.1 Introduction

CFD has become key to solving the many complex indoor air flow problems. It provides detailed information on temperature, air distribution and of the pollutant distribution inside buildings. Furthermore, CFD has the ability to simulate a wide range of flow problems for different configurations with high levels of accuracy and low cost compared with experimental work. To solve the flow governing equations, an appropriate turbulence models, discretisation techniques, as well as methods of grid generation are used. CFD can help to provide detailed information on indoor thermal environments and on the contaminant transport inside buildings, which may be used to solve ventilation problems by predicting the thermal comfort and the energy consumption. For a good prediction of the indoor air movement, many factors need to be taken into account, such as the temperature gradient, the room shape and the furniture distribution, as well as the inlet and the extraction terminal locations. As a large room has many obstacles and heat sources, such as occupants and room equipment, the indoor flow is assumed to be turbulent. The CFD method has the ability to provide accurate predictions of air temperature distributions, air velocity, air pressure, and relative humidity of air, contaminant concentrations and the turbulence characteristics for airflow both indoors and outdoors. This ability is obtained by solving the partial differential equations for the continuity equation, the momentum equation, the energy equation, the chemical species concentrations, and for other turbulence parameters. A brief description of the governing equations is given in the first part of this chapter, followed by the discretization method. Finally, the turbulence model and the numerical scheme are explained in more detail.

3.2 Governing equations

In indoor airflow problems about ventilation and air conditioning, flow governing equations are used to describe the airflow characteristics inside buildings. The combination of the continuity equation, the momentum equation, the energy equation as well as the scalar transport equation can describe the airflow and pollutant transport inside a given room. A wide range of fluid flow problems impose the conservation of momentum through the Navier-Stokes equations [124, 125]. For this study, the incompressible three-dimensional form of the continuity, momentum and energy equations are expressed as [126]:

- Conservation of mass (continuity equation)

$$\frac{\partial \rho}{\partial t} + \frac{\partial(\rho u_i)}{\partial x_i} = 0 \quad (3-1)$$

where

$$\mathbf{u} = [u, v, w]$$

Equation 3-1 represents the time dependant three-dimensional continuity equation for a compressible fluid. For an incompressible flow, the density (ρ) is assumed to be constant, and hence there is no change of the density with time. Therefore, equation (3-1) becomes:

$$\frac{\partial(u_i)}{\partial x_i} = 0 \quad (3-2)$$

- Conservation of momentum (momentum equation)

$$\frac{\partial(\rho u_i)}{\partial t} + \frac{\partial(\rho u_i)}{\partial x_i} + \frac{\partial(\rho u_j u_i)}{\partial x_j} = -\frac{\partial p}{\partial x_i} + \frac{\partial \tau_{ij}}{\partial x_i} + \rho g_i + F \quad (3-3)$$

where p and τ are the static pressure and the viscous stress tensor, respectively, while ρg and F represent the forces due to gravity and external body force, respectively.

- Conservation of energy (energy equation)

$$\rho \frac{De}{Dt} = [-\nabla(pu)] + \left[\frac{\partial(u\tau_{xx})}{\partial x} + \frac{\partial(u\tau_{yx})}{\partial y} + \frac{\partial(u\tau_{zx})}{\partial z} + \frac{\partial(v\tau_{xy})}{\partial x} + \frac{\partial(v\tau_{yy})}{\partial y} + \frac{\partial(v\tau_{zy})}{\partial z} + \frac{\partial(w\tau_{xz})}{\partial x} + \frac{\partial(w\tau_{yz})}{\partial y} + \frac{\partial(w\tau_{zz})}{\partial z} \right] + \nabla \cdot (k\nabla T) \quad (3-4)$$

The governing equations (3-1), (3-2) and (3-4) can be expressed in the general transport equation form as follows:

$$\frac{\partial(\rho\phi)}{\partial t} + \frac{\partial(\rho\mathbf{u}_j\phi)}{\partial x_j} = \frac{\partial}{\partial x_j} \left(\Gamma \frac{\partial\phi}{\partial x_j} \right) + S_\phi \quad (3-5)$$

where

$\frac{\partial(\rho\phi)}{\partial t}$ represents the rate of change of an intensive variable ϕ in a control volume with respect to time. $\frac{\partial(\rho\mathbf{u}_j\phi)}{\partial x_j}$ represents the convective term used to describe the net rate of the flow for variable ϕ caused by velocity \mathbf{u} .

$\frac{\partial}{\partial x_j} \left(\Gamma \frac{\partial\phi}{\partial x_j} \right)$ represents the diffusion term used to describe the diffusion of ϕ within the control volume, and

S_ϕ is the source term.

For all fluid flow, the general transport equation can be expressed by:

Rate of change + Convection = Diffusion + Source.

The Navier-Stokes equations are used to accurately describe fluid flow in the domain. In these equations, the fluid is assumed to behave as a continuum. An analytical solution to the Navier-Stokes equations is not possible for the majority of engineering flow problems, with the exception of very simple flow problems that use the Direct Numerical Simulation (DNS) approach. This DNS approach can compute turbulent flow by solving the Navier-Stokes equations directly and without approximations. However, the DNS approach requires considerable computational time and resources. Therefore, another method, RANS, is used to solve the complex flow problem at only low computational cost yet with good accuracy of predictions. This method computes averaged (Reynolds-averaged) variables for steady and unsteady flow. In addition, it can also be used to simulate the effect of turbulence fluctuation on the mean air flow using different turbulence models. This method is the most popular for indoor air flow simulations due to its low computational cost and its ability to provide reasonably accurate predictions for indoor environments.

3.3 Discretization

Analytical and numerical methods are usually used to solve partial differential equations. Although the exact solution can be found analytically for simple problems, this method cannot be used with complex flow problems. In essence, the governing equations as discussed in section 3.2 are used to describe the air motion and the thermal distribution within a room. However, these equations are non-linear, strongly coupled and are difficult to solve analytically. Therefore, numerical methods are used as an alternative approach to solve such complex system of equations. Numerical solutions can be of various types, such as the finite difference method (FDM), the finite element method (FEM) and the finite volume method (FVM). In this study, the FVM was chosen to solve the governing equations of the fluid flow problem. This method starts from the integral form of the general transport equations over an arbitrarily small control volume (CV).

Therefore, the generalised transport equation (3-5) can be written in the integral form as follows:

$$\int_{CV} \frac{\partial(\rho\phi)}{\partial t} dV + \int_{CV} \nabla \cdot (\rho \mathbf{u}\phi) dV = \int_{CV} \nabla \cdot (\Gamma \nabla \phi) dV + \int_{CV} S_{\phi} dV \quad (3-6)$$

where

Γ : the diffusion coefficient

S: general source term

ϕ : variable property

$$\nabla : \frac{\partial}{\partial x} i + \frac{\partial}{\partial y} j + \frac{\partial}{\partial z} k$$

At steady state, the rate of change of $\rho\phi$ is equal to zero, and equation (3-6) becomes:

$$\int_{CV} \nabla \cdot (\rho \mathbf{u}\phi) dV = \int_{CV} \nabla \cdot (\Gamma \nabla \phi) dV + \int_{CV} S_{\phi} dV \quad (3-7)$$

With the FVM method, the domain is divided into a finite number of control volumes using a computational mesh and the pressure, temperature and velocities are predicted as cell-averaged values, as shown in Figure 3-1. The variable, ϕ , in the integral form of the general transport equation (3-7) is taken as being located at the centre of the control volume.

Interpolation schemes are used in order to interpolate the face value of the variable ϕ_f between cells.

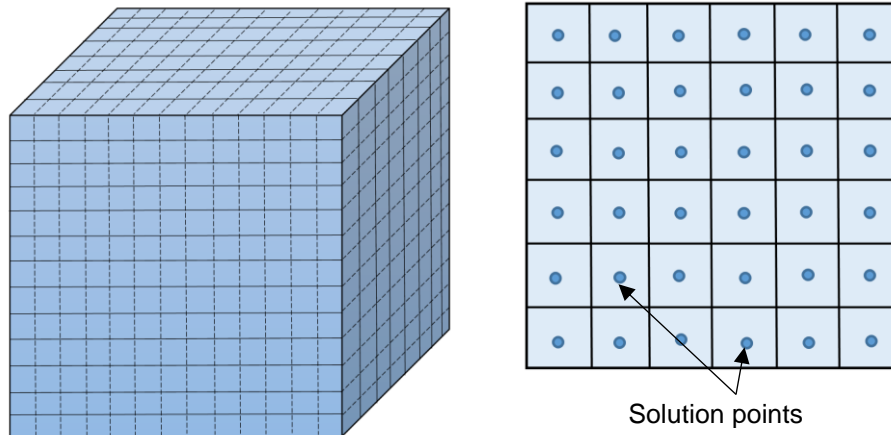


Figure 3-1: Discretization of the computational domain into finite volumes in three- and two-dimensional views.

Various numerical schemes can be used depending on the flow being modelled:

- The first-order upwind scheme is considered one of the simplest numerical schemes that are capable of providing accurate and stable calculations and it is usually used at the starting point of the calculation procedure.
- The second-order upwind scheme is considered more accurate but less stable than the first-order upwind scheme. However, the results of the face value can fall outside the cell average values of two neighbouring cells. Therefore, it is very important to use limiters for the face value predictions.
- The power-law scheme stems from the use of an analytical solution to the convection and diffusion equations in one dimension. In this scheme, an exponential profile through the cell-averaged values is used to determine the face value. Compared with the first-order upwind scheme, this scheme gives an accurate solution for low Reynolds numbers (Re), $Re < 5$.
- The QUICK scheme, or the quadratic upwind interpolation for convective kinetics scheme, is widely used with quadrilateral and hexahedral meshes. However, in high-gradient regions, this scheme gives unstable calculations of low accuracy.

- The central-differencing scheme provides better accuracy of solutions compared with the first-order upwind scheme, and also works well with the LES method due to its lower numerical diffusion. However, with a high Peclet number (Pe), $Pe > 2$, this scheme may give oscillating solutions and provide unstable calculations.

By applying the Gauss divergence theorem to the integral form of the general transport equation:

$$\sum_f^{N_{faces}} \rho_f \phi_f U_f \cdot A_f = \sum_f^{N_{faces}} \Gamma_\phi (\nabla \phi)_n \cdot A_f + S_\phi \Delta V \quad (3-8)$$

In order to compute the gradient of the scalar field, the Green-Gauss node-based method is used in this study because of its accuracy compared with other types of gradient estimators. For the cell centre, P, as shown in Figure 3-2, the gradient computation for the scalar, ϕ , can be written as follows:

$$(\nabla \phi)_P = \frac{1}{V} \sum_f \phi_f \cdot A_f \quad (3-9)$$

Based on Figure 3-2, the general transport equation is discretized, and becomes:

$$\begin{aligned} & [(\rho u \Delta A) \phi]_e - [(\rho u \Delta A) \phi]_w + [(\rho v \Delta A) \phi]_n - [(\rho v \Delta A) \phi]_s + [(\rho w \Delta A) \phi]_h - \\ & [(\rho w \Delta A) \phi]_l = \left[\left(\Gamma \frac{\partial \phi}{\partial y} \right) \Delta A \right]_n - \left[\left(\Gamma \frac{\partial \phi}{\partial y} \right) \Delta A \right]_s + \left[\left(\Gamma \frac{\partial \phi}{\partial x} \right) \Delta A \right]_e - \left[\left(\Gamma \frac{\partial \phi}{\partial x} \right) \Delta A \right]_w + \\ & \left[\left(\Gamma \frac{\partial \phi}{\partial z} \right) \Delta A \right]_h - \left[\left(\Gamma \frac{\partial \phi}{\partial z} \right) \Delta A \right]_l + [S_\phi \Delta V] \end{aligned} \quad (3-10)$$

Rearranging the discretized form of the general transport equation, one obtains:

$$a_P \phi_P = a_W \phi_W + a_N \phi_N + a_E \phi_E + a_S \phi_S + a_H \phi_H + a_L \phi_L + b \quad (3-11)$$

The general form for the linearized transport equation can be expressed as:

$$a_P \phi_P = \sum_{nb} a_{nb} \phi_{nb} + b \quad (3-12)$$

The Algebraic Multigrid Scheme (AMG) is used to iteratively solve for the linearized form of the transport equation for all cells in the domain.

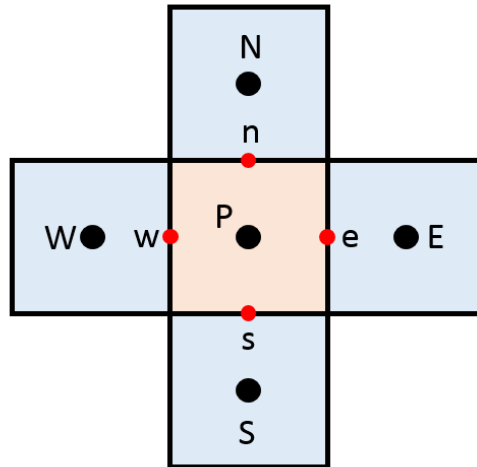


Figure 3-2: Two-dimensional exploded view for the discrete points in the control volume and its neighbouring cells.

3.4 Turbulence computation

Turbulent flow occurs when the Reynolds (Re) number for air flow is high. The airflow in buildings is affected by several variables. Room configurations, equipment, occupants, locations of supply and extraction openings, as well as the distribution of heat sources, all have a significant impact on determining the airflow pattern in the domain. Basically, most indoor airflows can be assumed to be turbulent. For most practical airflow problems, an analytical solution to the Navier-Stokes equations is not available. Therefore, the mean flow is an approximation that is used to model a turbulent airflow problem. Turbulence models have evolved rapidly over the years and many approaches, such as LES and turbulence transport models, have been developed to improve the predicted results. Turbulence transport models can be classified into two types: the Reynolds stress model and the eddy viscosity model. The eddy viscosity model can be divided into three categories: the zero-equation model, one-equation model and two-equation model, where the two-equation model is the most popular turbulence model used for HVAC applications. In this study, two types of turbulence modelling, the RNG $k-\varepsilon$ model and the LES method, are used to predict air velocities and air temperature distributions indoors.

3.4.1 RNG k- ε modelling

For a good prediction of the indoor air movement and of the contaminant dispersion, an appropriate turbulence model was selected from various existing models. The two–equation renormalized group RNG k – ε turbulence model was used to predict the turbulent airflow. This model can produce an accurate prediction of indoor air flow, temperature and contaminant distribution [127-130]. The RNG k – ε form, similar to that of the standard k – ε turbulence model, can be expressed as [131]:

$$\frac{\partial(\rho k)}{\partial t} + \frac{\partial(\rho k u_i)}{\partial x_i} = \frac{\partial}{\partial x_j} \left[\left(\mu + \frac{\mu_t}{\sigma_k} \right) \frac{\partial k}{\partial x_j} \right] + P_k + \rho \varepsilon \quad (3-13)$$

$$\frac{\partial(\rho \varepsilon)}{\partial t} + \frac{\partial(\rho \varepsilon u_i)}{\partial x_i} = \frac{\partial}{\partial x_j} \left[\left(\mu + \frac{\mu_t}{\sigma_\varepsilon} \right) \frac{\partial \varepsilon}{\partial x_j} \right] + C_{1\varepsilon} \frac{\varepsilon}{k} P_k + C_{2\varepsilon}^* \rho \frac{\varepsilon^2}{k} \quad (3-14)$$

where

$$C_{2\varepsilon}^* = C_{2\varepsilon} + \left(C_\mu \eta^3 (1 - \eta/\eta_0) \right) / (1 + \beta \eta^3) \text{ with } \eta = (Sk/\varepsilon) \text{ and } S = \sqrt{2S_{ij}S_{ij}},$$

The values of the constant in RNG k – ε turbulence model are:

$$C_\mu = 0.0845, \sigma_k = 0.7194, \sigma_\varepsilon = 0.7194, C_{\varepsilon 1} = 1.42, C_{\varepsilon 2} = 1.68, \eta_0 = 4.38 \text{ and } \beta = 0.012.$$

3.4.2 Large Eddy Simulation (LES) method

For the LES, the large-scale eddies are solved directly by the Navier–Stokes equations, while small eddies are modelled by using a sub-grid scale (SGS) model. The large and small eddies are separated using a spatial filtering operation. Based on the resolved scale of motion, the Smagorinsky (SGS) model constant (C_s) is dynamically calculated [132, 133].

In the LES, the effect of density changes on the resolved large scale is taken into account, as explained in the following equations. Equation (3-15) details the SMG stress tensor:

$$T_{ij} = \overline{\rho u_i u_j} - (\overline{\rho u_i} \overline{\rho u_j} / \overline{\rho}) \quad (3-15)$$

where T_{ij} and τ_{ij} are calculated using the Smagorinsky-Lilly model:

$$\tau_{ij} = -2 C_\rho \bar{\rho} \Delta^2 \tilde{S} \left(\tilde{S}_{ij} - \frac{1}{3} \tilde{S}_{kk} \delta_{ij} \right) \quad (3-16)$$

$$T_{ij} = -2 C \hat{\rho} \hat{\Delta}^2 \left| \hat{S} \right| \left(\hat{S}_{ij} - \frac{1}{3} \hat{S}_{kk} \delta_{ij} \right) \quad (3-17)$$

where Δ is the grid filter width, and the test filter width, $\hat{\Delta} = 2\Delta$. The coefficient, C , is the same for both equations (equation 3-16 and equation 3-17). \hat{S}_{ij} is to the strain rate tensor, whilst the term τ_{ij} refers to the convective momentum transport due to interactions between eddies (which are not resolved).

The grid and test filtered SGS are related as follows [133]:

$$L_{ij} = T_{ij} - \hat{\tau}_{ij} = \bar{\rho} \tilde{u}_i \tilde{u}_j - \frac{1}{\bar{\rho}} \left(\bar{\rho} \tilde{u}_i \bar{\rho} \tilde{u}_j \right) \quad (3-18)$$

where \tilde{u}_i and \bar{p} represent the filtered velocity and pressure, respectively, and L_{ij} is calculated from the large eddy field. From equation 3-17 and equation 3-18, the C coefficient can be calculated as follows:

$$C = \frac{(L_{ij} - L_{kk} \delta_{ij} / 3)}{M_{ij} M_{ij}} \quad (3-19)$$

where

$$M_{ij} = -2 \left(\hat{\Delta}^2 \hat{\rho} \left| \hat{S} \right| \hat{S}_{ij} - \Delta^2 \bar{\rho} \left| \hat{S} \right| \tilde{S}_{ij} \right) \quad (3-20)$$

M_{ij} is the resolved stress tensor, with the over-bar referring to the spatial filtering operation, and \tilde{u}_i and \bar{p} represent the filtered velocity and pressure, respectively. In LES, the time step setting (Δt) is extremely sensitive. Using a suitable time step will improve the simulation accuracy by resolving the temporal dynamics for the smallest resolved eddies. Depending on the simulation accuracy and the Courant–Friedrichs–Lewy (CFL) requirement, using a small time step is highly recommended to avoid an unstable simulation, particularly during the start-up period where the expected variation in temperature and velocity are typically high [134].

3.5 Numerical schemes

In ANSYS FLUENT [135], two types of solvers are available: a pressure-based solver and a density-based solver. In this study, the air motion and heat flow within the room are considered as low-speed, incompressible flow and therefore a pressure-based solver was chosen as being the most suitable for this study, whereas the density-based solver is not suitable for indoor air flow because this solver is usually used for high-speed compressible flow applications. However, the pressure-based solver in Ansys Fluent has the ability to solve various problems related to the compressible flow.

The force due to gravity has a significant impact on indoor thermal environments and flow behaviour. The heat fluxes generated by the room heat sources can cause localised differences in the indoor air density (buoyancy effect) and this may be too significant to ignore. Therefore, the Boussinesq assumption is used when the changes in density are small and relatively insignificant; and it is for this reason that the Boussinesq assumption is used in this study. Here, the thermal expansion coefficient can be defined as [136]:

$$\beta = -\frac{1}{\rho} \left(\frac{\partial \rho}{\partial T} \right)_p \approx -\frac{1}{\rho} \frac{\rho_o - \rho}{T_o - T} \quad (3-21)$$

where the subscript o represents a reference value. By rearranging the above equation, the Boussinesq approximation can be written as:

$$(\rho_o - \rho) \approx \rho \beta (T - T_o) \quad (3-22)$$

3.5.1 Pressure-velocity coupling

Four types of the pressure-velocity algorithms are available in FLUENT [135]: The SIMPLE, SIMPLEC, PISO and Coupled. Among these algorithms, SIMPLE and SIMPLEC are widely used for steady-state flow problems, while PISO is usually used for the time-dependent flow problems. In this study, the semi-implicit method for pressure-linked equations (SIMPLE) algorithm is used for pressure-velocity coupling.

3.5.2 SIMPLE algorithm

The SIMPLE algorithm concept is one of the numerical procedures used to solve the Navier-Stokes equations, as developed by Patankar and Spalding [137]. For an incompressible flow, the density is taken as constant and not itself linked to the pressure. In this method, the estimated pressure (p^*) is used to calculate the velocity (u^*) in the momentum equation, with the pressure then corrected as depending on the velocities to satisfy the continuity equation. Figure 3-3 shows the procedures behind this concept. The corrected pressure and the pressure correction term can be expressed as:

$$p' = p - p^* \quad (3-23)$$

Since the velocity field depends on the estimated pressure, the velocity correction term can be written as:

$$u' = u - u^* \quad , \quad v' = v - v^* \quad \text{and} \quad w' = w - w^* \quad (3-24)$$

By using the SIMPLE algorithm, the relationship between pressure and velocity can be written as:

$$u'_e = \frac{A_e}{a_p - \sum a_{nb}} (P_p - P_e) \quad (3-25)$$

where a_p is given in equation (3-12) and $\sum a_{nb}$ is the summation of the neighbouring coefficients.

In order to express the pressure-correction equation in its general transport form, the continuity equation is stated as a function of the velocity correction, u' . Then substituting $P_p - P_e$ for u' as per eq. (3-25).

$$a_p p'_p = \sum a_{nb} p'_{nb} + S_c \quad (3-26)$$

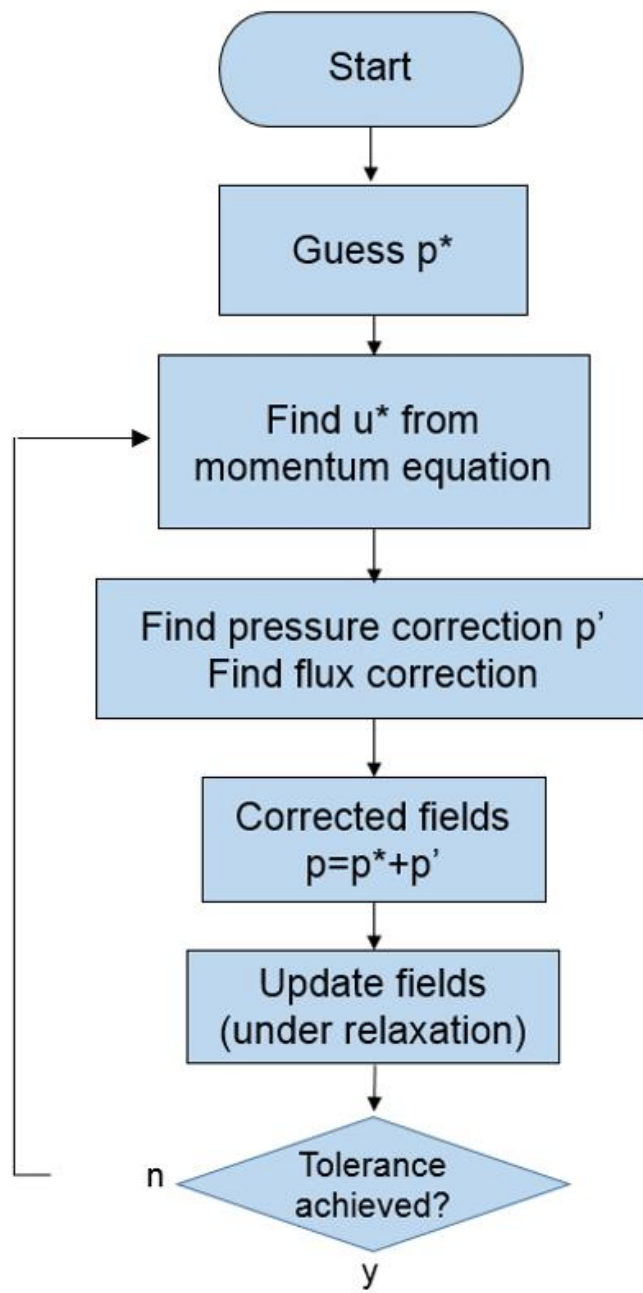


Figure 3-3: The iterative procedure behind the SIMPLE algorithm.

3.5.3 Under-relaxation factor

For the first iteration, unsteady versions of the pressure and temperature transport equations are used to approximate the velocity field in order to solve the pressure correction equation and the momentum equation. These values are updated for each iteration until certain convergence criteria are achieved for the pressure and velocity. An under-relaxation factor is used to reduce the numerical solution change in each iteration. This accelerates the convergence and improves the stability of the calculations. With under-relaxation, the new value of ϕ depends on the old value of ϕ , the change $\Delta\phi$, and the under-relaxation value, α .

$$\phi = \phi_{old} + \alpha \Delta\phi \quad (3-27)$$

where $0 < \alpha < 1$.

Chapter 4 Influence of Exhaust Locations on Energy Consumption and on the Indoor Thermal Environment

4.1 Introduction

In this chapter, the effects of the location of exhaust diffusers where the warm and contaminant air is extracted and their relation to room heat sources on the thermal comfort and the energy consumption are investigated numerically for an office served by a DV system. The investigated room is briefly described in the first part of this chapter. Then, the details of the CFD model and of the boundary conditions that are used for room air flow modelling are presented. The computational mesh dependence of the CFD predictions is tested in this chapter. Finally, the amount of energy consumption, the indoor thermal comfort, and the indoor air quality for various exhaust locations is evaluated and discussed in details.

4.2 Case description

In an office room, many factors affect the pattern of airflow, the thermal comfort, the indoor air quality, and the energy consumption. The locations of the supply and exhaust opening diffuser are considered one of the most important factors that influence the indoor airflow behaviour and consequently affect the energy consumption and indoor the thermal environment.

The aim of this study is to investigate various locations of the exhaust outlet diffuser in relation to the heat sources in a room and determine their impact on the indoor thermal environment and on the energy consumption. This study used a typical small office with the dimensions of 4.0 m long, 3.5 m wide, and 2.7 m high. Heat sources in the office include two occupants, two computer cases, two monitors, two ceiling lamps and the heat gain from the external wall. The other boundary walls, the ceiling and the floor are modelled an adiabatic. The heat rate emitted from each heat source is listed in Table 4-1. Based on the average environment in Iraq, the heat emitted from the external walls were selected to be in accord with these criteria. Two sources of contaminant are used in this study to simulate the contaminants coming from outside and entering the domain through the window and the door frame (line sources). Contaminants were modelled with a 0.7 μm particle size and with a density of 912 kg/m^3 . This particle size belongs to particles in the accumulation mode (0.1-2 μm), such as those found in building dust and smoke. With the DV system, fresh and cool air is normally supplied at or close to the floor level with low velocity. A stratification of temperatures and contaminant concentration is typically formed in the room and the horizontal temperature profile is typically uniform except for the region near the DV supply and heat sources. Therefore, in this study, the supply DV inlet (1.0 m \times 0.6 m) is located at the floor level of the side wall and the return opening (1.2 m \times 0.2 m) is located at the upper boundary of the occupied zone, 1.3 m from the floor level, as recommended by Cheng et al. [39]. Figure 4-1 shows the arrangement of the heat source and of the contaminant source locations in the simulated room. The set room temperature in the occupied zone is 24°C. Eighty percent of the supplied air is recirculated from a return opening and the rest of the air is extracted from the exhaust opening at five different locations, as listed

in Table 4-2. The total supply airflow rate is 94 L/ sec, which is equal to 9 ACH (air changes per hour). The indoor air quality and the occupant productivity can be improved by increasing the ventilation rate [138], hence a high ventilation rate is used in this study. The supply air temperature is 19 °C.

Table 4-1: Cooling load for the simulated office room.

Internal heat sources	Cooling load (W)
Occupants	80 × 2
PC_case	50 × 2
PC_monitor	65 × 2
Ceiling lamps	60 × 2
External wall	502
Total	1012
Heat density	72 W/m ²

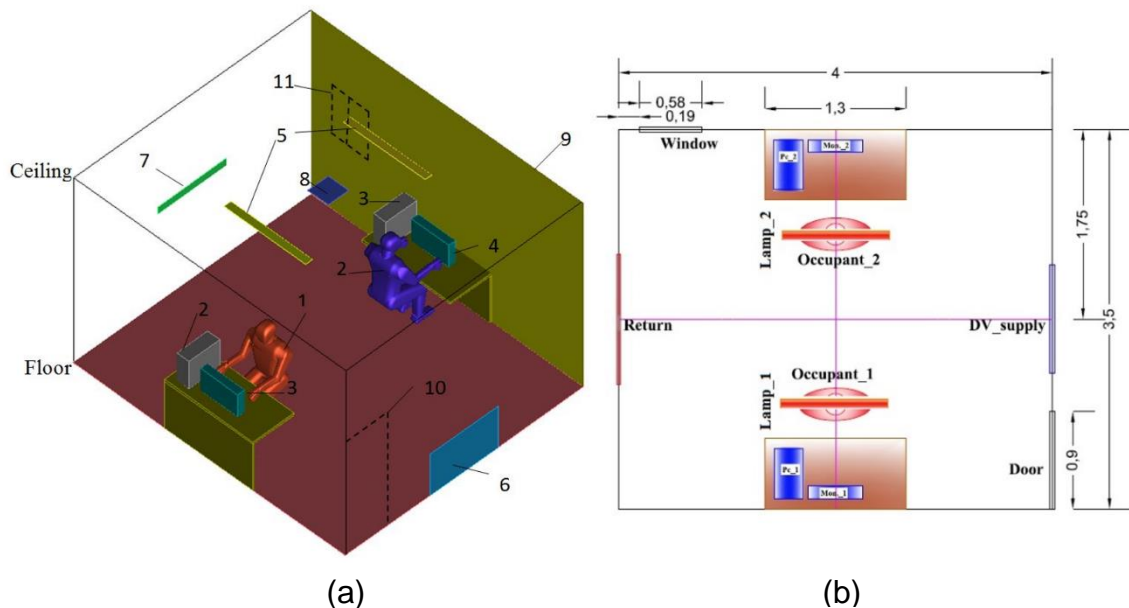


Figure 4-1: (a) The configuration of the simulated room; 1- occupant_1; 2- occupant_2; 3- PC case; 4- PC monitor; 5- ceiling lamps; 6- displacement ventilation (DV) inlet; 7- return inlet; 8- exhaust inlet; 9- external wall; 10- contaminant source (line source) at door; 11- contaminant source at window (line source), and (b) the arrangement of the equipment of the simulated office (top view).

Table 4-2: Case studies description.

Case study	Exhaust location
Case 1	Centre of the ceiling between two heat sources (ceiling lamps).
Case 2	Ceiling level, at the external wall.
Case 3	Combined with the light slots.
Case 4	Ceiling level above the DV supply opening (slightly away from the heat sources).
Case 5	Combined with the return opening.

4.3 Computational model

4.3.1 Air flow modelling

To obtain time - averaged predictions of the airflow inside a room, the two–equation renormalized group (RNG) model is used as the turbulence model. This model is one of the most popular turbulence models and it is widely used in room airflow predictions. This model can give satisfactory predictions in regions with swirling flows and also gives good predictions for rapidly strained flows. Therefore, this model is used in the present work to obtain time-averaged predictions. More details on this model are presented in section 3.4.1. For this study, the CFD program ANSYS FLUENT was used to solve the RANS equations and calculate the Lagrangian trajectories in a 3D computational model of the investigated office. The enhanced wall treatment with reasonable values of y^+ , $0.7 \leq y^+ \leq 4.5$, was applied to the near wall cells.

The Boussinesq assumption was employed to calculate the change in air density due to variations of temperature. The semi-implicit method for pressure-linked equations (SIMPLE) algorithm was chosen for pressure and velocity field coupling, and the second order upwind discretization scheme was chosen to solve all the variables in the simulation cases except for pressure, which was solved by a staggered scheme named pressure staggering option (PRESTO!). In the present study, the discrete ordinates (DO) model [139] was adopted to

simulate the radiation heat transfer emitted from internal heat objects. The details of the numerical methods and boundary conditions are summarized in Table 4-3.

Table 4-3: Numerical methods and boundary condition details.

Turbulence model	Renormalized group RNG $k - \epsilon$ turbulence model
Radiation model	Discrete ordinates (DO) radiation model
Numerical schemes	For pressure, Staggered third order scheme PRESTO!; for other terms, upwind second order; SIMPLE algorithm
Ceiling, floor, tables and bounded walls	Adiabatic wall
Supply air	Velocity inlet (94 L/sec , 19 °C)
Return air	Velocity inlet in negative direction (75.2 L/sec)
Exhaust	Pressure –outlet
Occupants	Uniform heat flux, with heat rate of 80 W × 2
PC_case	Uniform heat flux, with heat rate of 50 W × 2
PC_monitor	Uniform heat flux, with heat rate of 65 W × 2
Ceiling lamps	Uniform heat flux, with heat rate of 60 W × 2
External wall	Uniform heat flux, with heat rate of 502 W

4.3.2 Discrete phase model

The particle concentration distribution can be predicted using either the Eulerian-Eulerian or the Eulerian-Lagrangian method for a steady state particle concentration in the domain [140]. In this study, an Eulerian-Lagrangian model, known as the discrete phase model (DPM), was applied to track the particles through the fluid phase. The Eulerian approach was used to simulate the continuous phase (air flow field), while the Lagrangian approach was used to simulate the discrete phase (airborne particles). The continuous phase was treated as a continuum and solved using the RANS equations, while the discrete phase was solved by tracking individual particles through the calculated airflow field.

As the particle volume fraction was sufficiently small, the interaction between the two phases was assumed to be a one-way coupling; i.e. the particles were influenced by the drag and turbulence of airflow field but there was no influence of the particles on the continuous phase [141]. Particle size is classified into three modes: ultrafine (< 0.1 μm); accumulation (0.1-2 μm) and coarse (> 2 μm) [142]. In order to simulate the contaminant distribution coming from outside and entering the domain, this study employed the accumulation mode to predict the contaminant concentration distribution in the breathing zone and the quality of the inhaled air for each case.

4.3.2.1 Particle tracking equations

The Lagrangian approach is used to calculate the individual trajectories of each particle by solving the momentum equation. By equating the particle inertia to the external forces, the momentum equation can be expressed as:

$$\frac{d\vec{u}_p}{dt} = F_D(\vec{u} - \vec{u}_p) + \frac{\vec{g}(\rho_p - \rho)}{\rho_p} + \vec{F}_a \quad (4-1)$$

where the inertial force per unit mass m / sec^2 is represented on the left-hand side of equation (4-1), and the drag forces per unit mass are expressed in the first term of the right hand side. The gravitational and buoyancy forces are represented in the second term; \vec{F}_a is used to add any additional forces (per unit mass) which may have an impact on particle motion.

In the present work, the drag force is the most important force acting on the particles and it follows the Stokes drag law:

$$\vec{F}_{\text{drag}} = F_D(\vec{u} - \vec{u}_p) = \frac{18\mu}{\rho_p d_p^2 C_c} (\vec{u} - \vec{u}_p) \quad (4-2)$$

where C_c is the Cunningham correction factor which is calculated from:

$$C_c = 1 + \frac{2\lambda}{d_p} (1.257 + 0.4e^{-(1.1d_p/2\lambda)}) \quad (4-3)$$

In this study, the Basset history, pressure gradient and virtual mass were negligible or had no influence compared to the drag force [143]. For ventilated rooms, the Brownian motion, thermophoretic and Saffman's lift are two orders of magnitude smaller than the Stokes drag force and occasionally these forces become compatible with Stokesian drag force when fine size particles are used in fluid flow field [144]. The Brownian motion and Saffman lift forces may become considerable and influence the particle motion, especially in the turbulent boundary layer near the walls [145]. In addition, these forces may play a significant role in the deposition process [146-148], therefore, they were taken into consideration in this study. Therefore, the following form of equation 4-3 was used.

$$\frac{d\vec{u}_p}{dt} = F_D(\vec{u} - \vec{u}_p) + \frac{\vec{g}(\rho_p - \rho)}{\rho_p} + \vec{F}_b + \vec{F}_{\text{thermal}} + \vec{F}_s \quad (4-4)$$

In turbulent flow, the path of particles is significantly affected by the local turbulence intensity. In order to simulate the stochastic velocity fluctuations in airflow, the discrete random walk (DRW) approach was used in this study [143]. The airflow instantaneous velocity is represented by the sum of the time-averaged velocity \bar{u}_i and of the airflow fluctuating velocity u'_i .

The airflow fluctuating velocity components are modelled as:

$$u'_i = \xi_i \sqrt{\bar{u}_i'^2} = \xi_i \sqrt{2k/3} \quad (4-5)$$

As a result of the assumption of the one-way coupling between the airflow and the solid particles, the air flow field is solved first, and subsequently the particles are injected [149].

As mentioned previously, the airflow equations and the Lagrangian trajectories were calculated using ANSYS Fluent software. However, the Lagrangian approach does not directly calculate the concentration of the particles in the domain. Therefore, this study used a user-defined function (UDF) to calculate the concentration distribution of the particles from the trajectories. In order to calculate the particles concentration in the computational domain, it is required to compute the concentration on each computational cell in the domain. This can be achieved using the particle source in-cell (PSI-C) scheme based on the following equation:

$$C = \frac{\dot{m} \sum_{i=1}^n dt(i, j)}{V_j} \quad (4-6)$$

The accuracy and the stability of simulations based on the Lagrangian model were investigated by Zhang and Chen [140] and, based on their studies, the concentrations calculated are found to be statically stable when a sufficient number of trajectories are tracked in the domain. Therefore, numerical experiments were undertaken in this study to determine a sufficient number of tracked trajectory.

4.3.2.2 Boundary conditions

Particles escape the room and their trajectories terminate when they reach the inlets and exhaust outlets in the domain. When particles reach solid objects, they may attach to or rebound from the surface of these objects. In a ventilated room, particles are most likely to attach to the rigid body surface because they do not have enough energy to rebound to overcome adhesion [150]. When the mesh at the walls is not fine enough, the results will over predict the viscous sub-layer kinetic energy and the fluctuating velocity will increase in these regions which will increase the collision of particles with the walls. In this study, the inflation boundary layer was used near the walls with enough mesh refinement. Therefore, the particle collisions in these regions (near walls) were predicted accurately and the trap boundary condition was applied.

4.4 Validation of the CFD algorithm

4.4.1 Validation of fluid flow

An experimental study on the air velocity distribution and temperature distribution in a room environment was performed by Xu et al. [69]. This work was chosen to validate the accuracy of the current RANS model in the prediction of the indoor thermal environment. Figure 4-2 shows the schematic diagram of the experimental chamber. The simulation was performed in a typical small room with the dimensions of 6.0 m long, 3.9 m wide, and 2.35 m high, and with two heat sources, including one occupant (76 W) seating in front of the table and one computer (40 W) located on the table (see Figure 4-2). Five poles, pole 1, 2, 3, 4 and 5, were used in this validation to predict the temperature and velocity distribution (see Figure 4-3 a and b). The supply and exhaust diffuser dimensions were (0.4 m × 0.15 m) and (0.34 × 0.14 m) respectively. The supply air flow rate was 43 m³/h, which is equal to 0.79 ACH (air changes per hour). The supply air temperature was 19°C. Different wall temperatures were used for the boundary walls, ceiling and floor. Figure 4-4 a and b show a good agreement between the measured and the simulated results. Further details on this experiment can be found in Xu et al. [69].

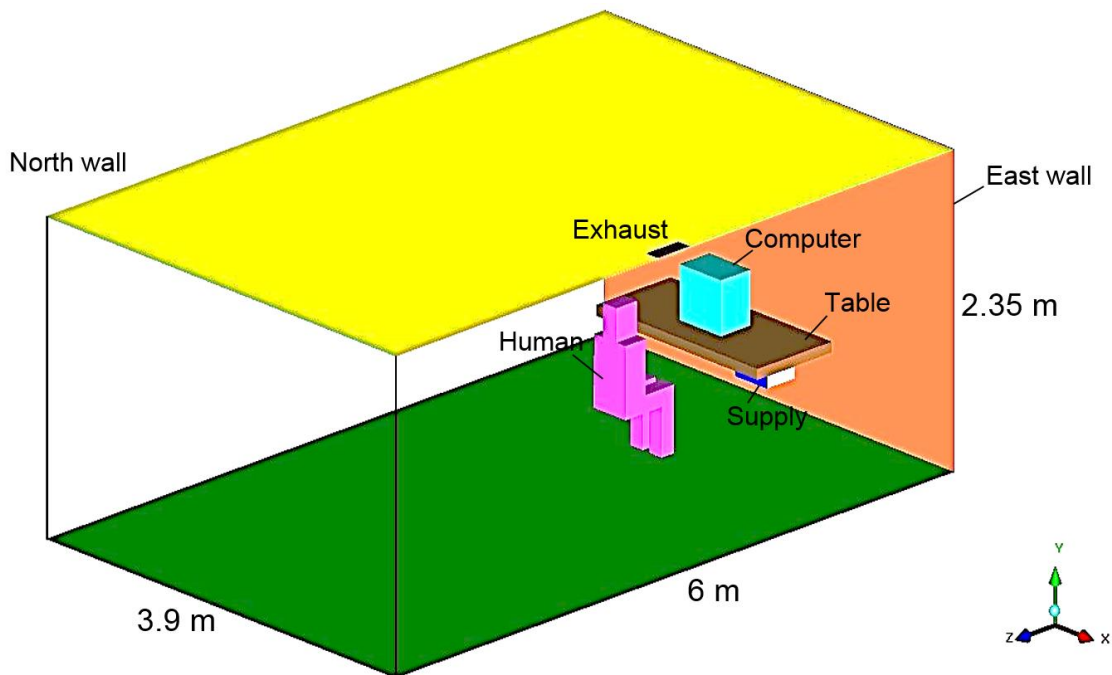
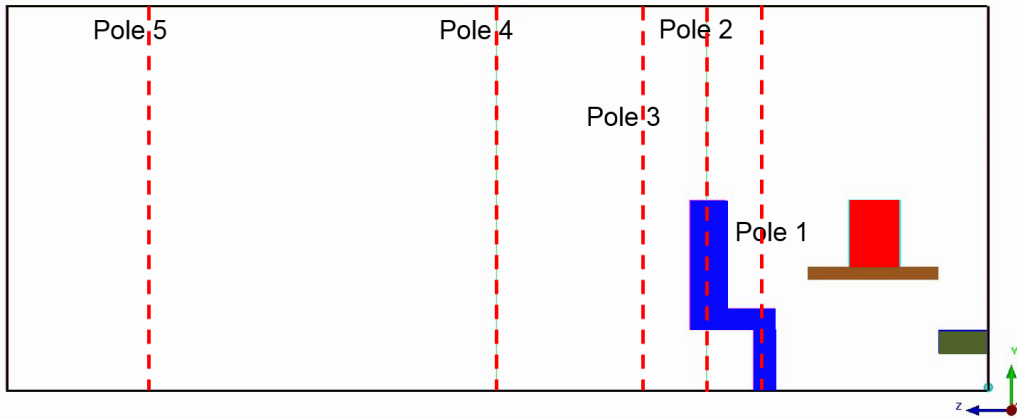
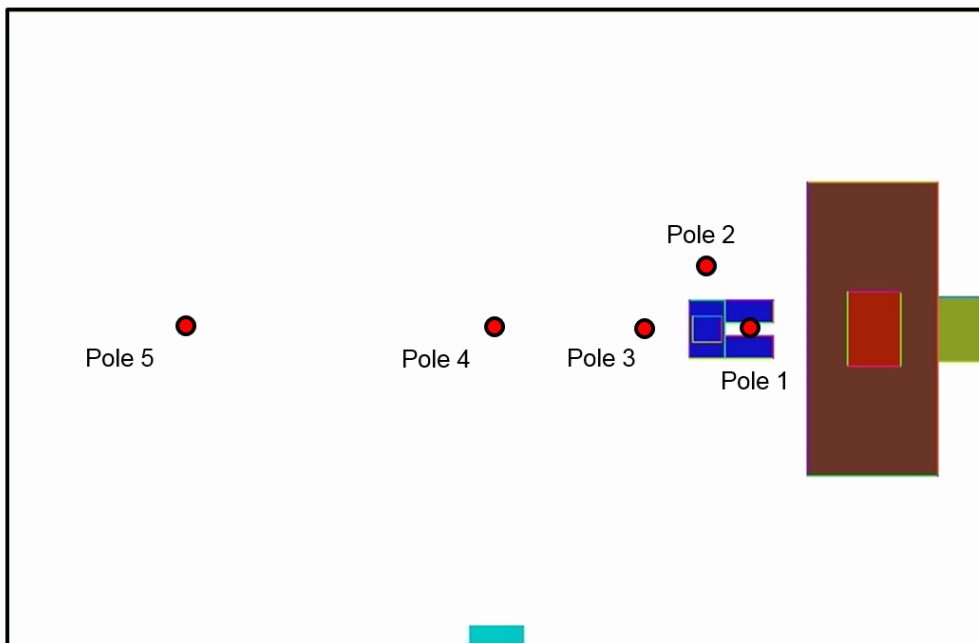


Figure 4-2: Schematic diagram of the validation room model [69].

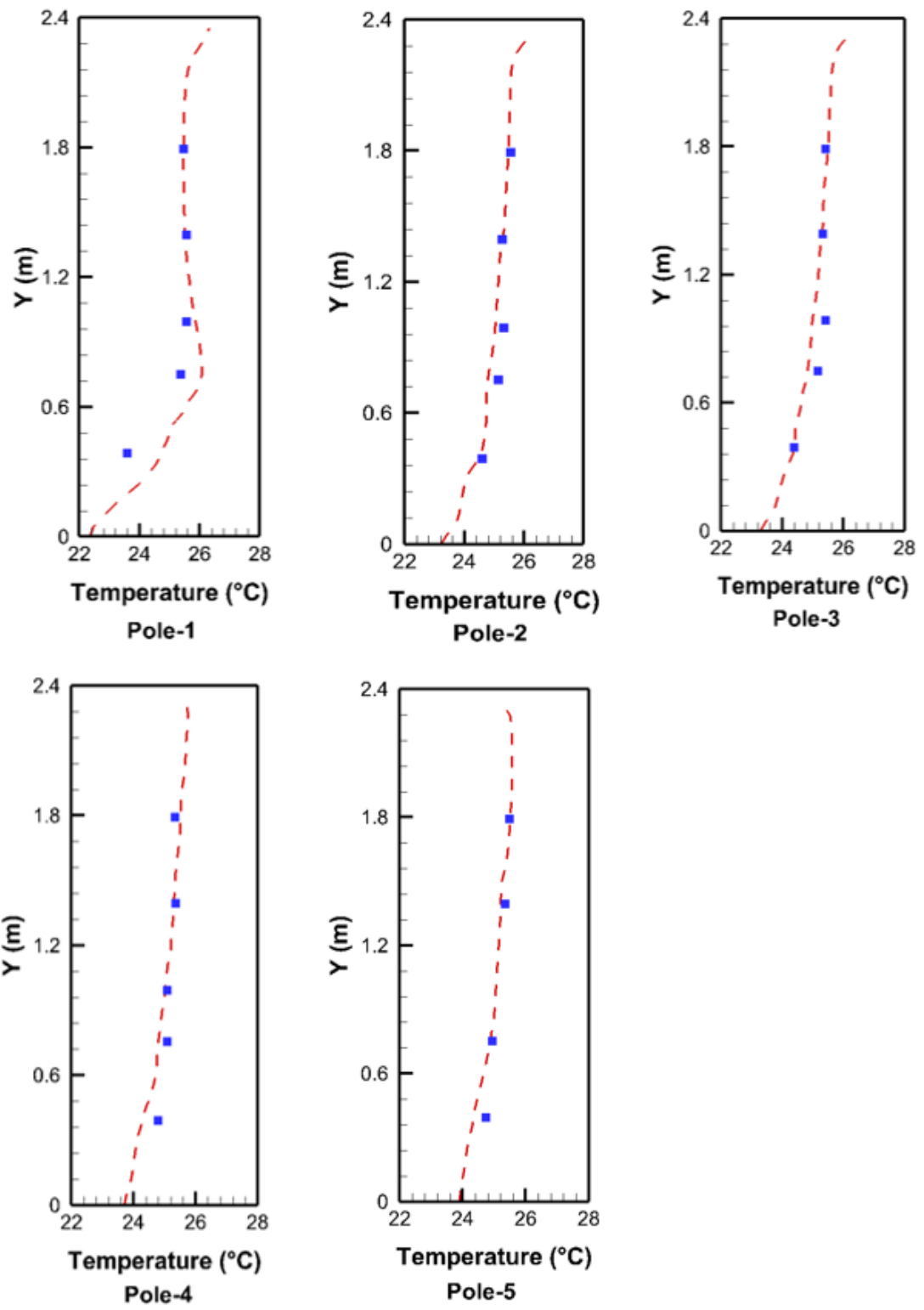


(a)

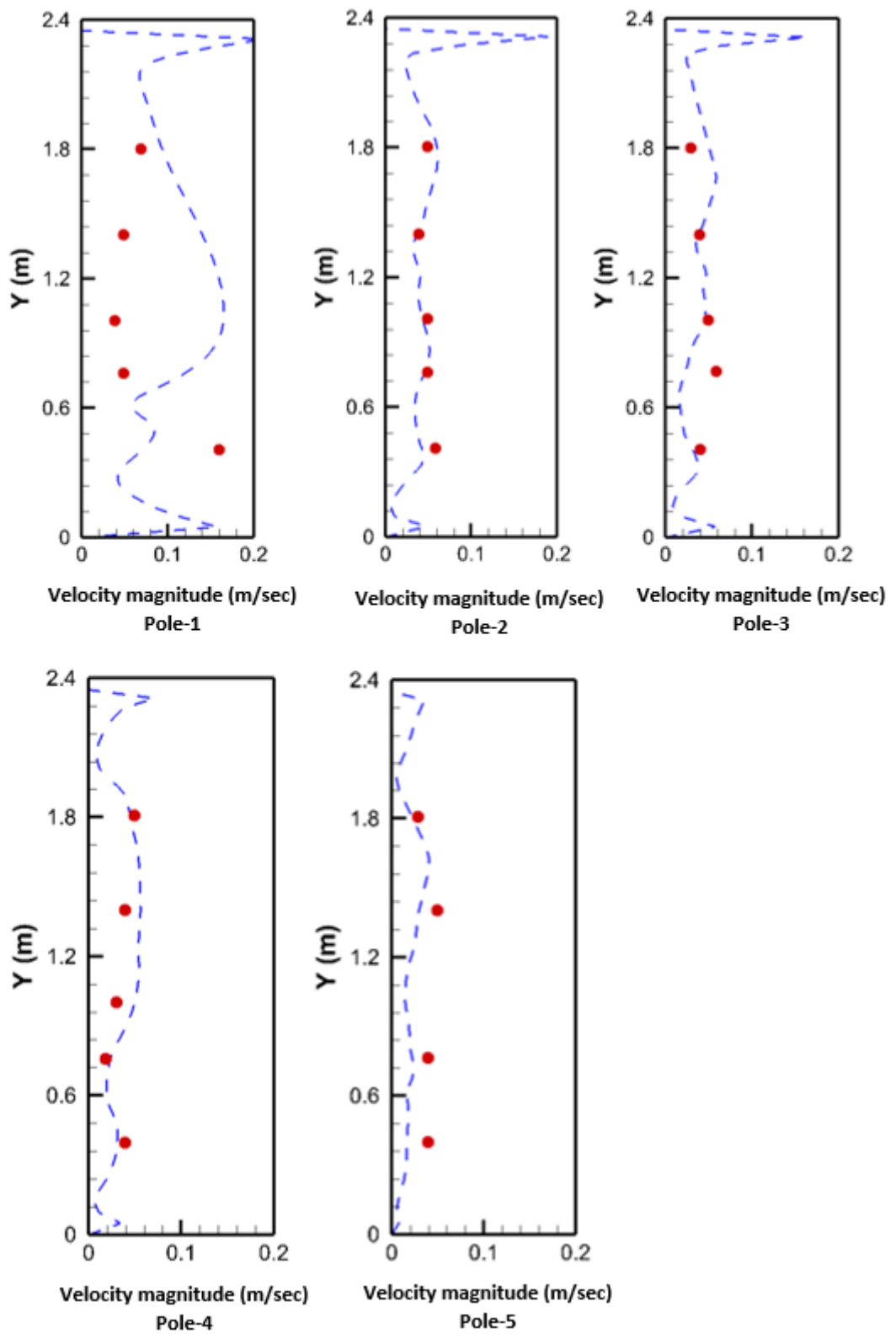


(b)

Figure 4-3: The measured locations in the experimental chamber; (a) side view and (b) top view.



(a)



(b)

Figure 4-4: Comparison between the simulated and experimental temperature and velocity profiles at five vertical poles; (a) temperature distribution (square symbol: experimental results [69]; dashed line: simulated results); (b) velocity magnitude distribution (circle symbol: experimental results [69]; dashed line: simulated results).

4.4.2 Particle transport validation

To validate the Lagrangian particle-tracking model, the experimental results of Chen et al. [151] are used to show the accuracy of this model. As shown in Figure 4-5, the dimensions of the room were 0.8 m × 0.4 m × 0.4 m. The inlet and the outlet had the same dimensions (0.04 m × 0.04 m) and were located in the centre of the test chamber. The supply velocity was 0.225 m/sec and the particle diameter was 10 μm with a density of 1400 kg/m³ (for the particles were supplied in the inlet). The particle concentration was normalised by the inlet concentration. Figure 4-6 illustrates the comparison between the simulated and experimental normalised concentration data at three different locations. A reasonable agreement between the predicted and experimental results can be seen from these graphs. Further details about the experiment found in Chen et al. [151].

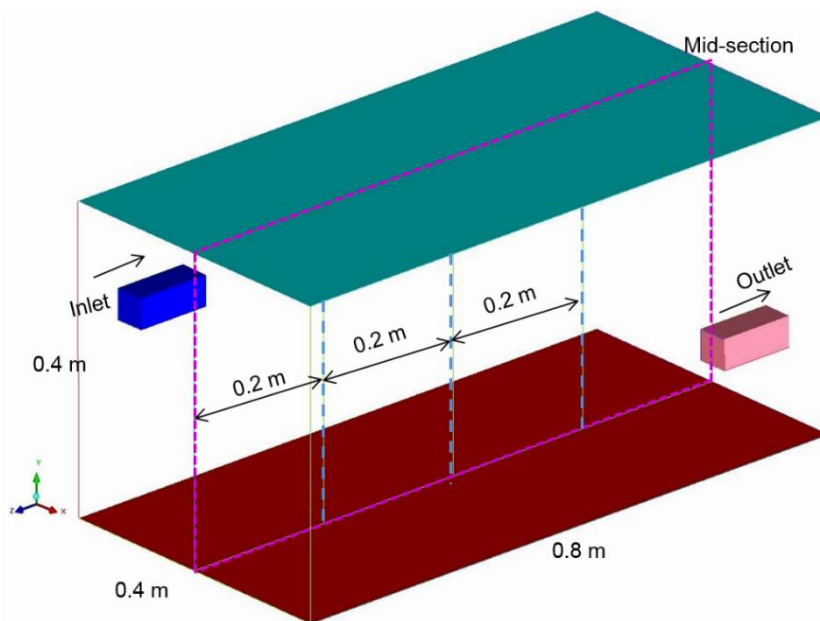


Figure 4-5: Schematic diagram of the ventilated chamber of the validation case for Lagrangian particle-tracking [151].

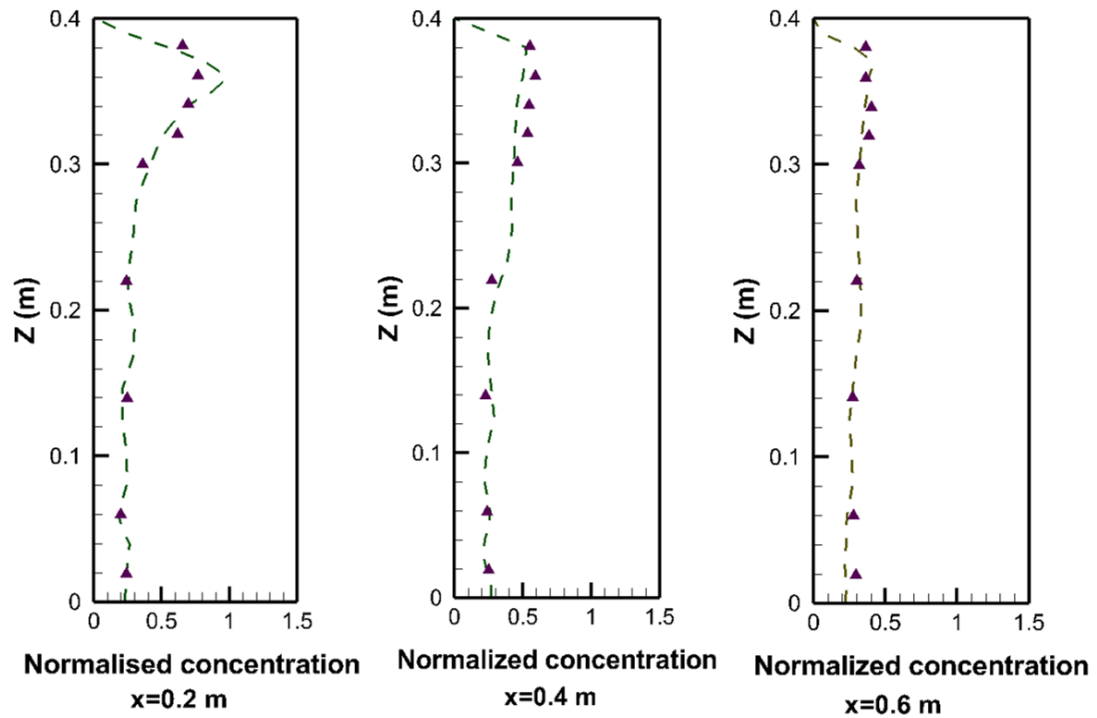


Figure 4-6: Comparison between the simulated and experimental normalized particle concentration at different locations at $x = 0.2$ m, 0.4 m and 0.6 m (triangle symbols: experimental data [151]; dashed line: simulated results).

4.5 Grid independence

As a result of the room and equipment complexity, ANSYS ICEM CFD software was used in this study to generate a tetrahedral unstructured mesh with an inflation boundary layer around the occupants and different element sizes. The grid around the occupants and other heat objects were designed to be fine enough to solve the boundary layer and capture the thermal environment behaviour. The surface grid was generated for the occupants, computers and monitors with 1 cm of element size, and 5 mm for the ceiling lamps. The mesh was clustered in regions that have high gradients of temperature and velocity, such as the boundary walls, the ceiling, the floor, and the table. For the mesh independence test, in order to control the total number of cells, only the element size in the domain was changed without changing the surface grid size for the internal heat sources and walls.

In order to resolve the boundary layer around the occupants, an inflation boundary layer was generated with the first layer thickness of 1.5 mm, and 4 layers with a growth rate of 1.2 (Figure 4-7). This generated y^+ values ranging between $0.7 \leq y^+ \leq 4.5$ for the first node adjacent to the solid surface. The Mesh independence test plays a significant role in the CFD simulation regarding results accuracy and prediction cost. In the current study, the grid size was selected by comparing the simulation results for three different sizes of grid as listed in Table 4-4. As shown in Figure 4-8 a and b, by comparing the simulation results for the temperature and velocity distribution for each grid size, there is no significant change in temperature and velocity distribution with increasing the grid cells from mesh_2 to mesh_3, Therefore, mesh 2 was selected to be the grid size for the rest of the study.

Table 4-4: Mesh independence test.

Mesh types.	Cells number
Mesh_1	865,235
Mesh_2	1,705,689
Mesh_3	2,415,523

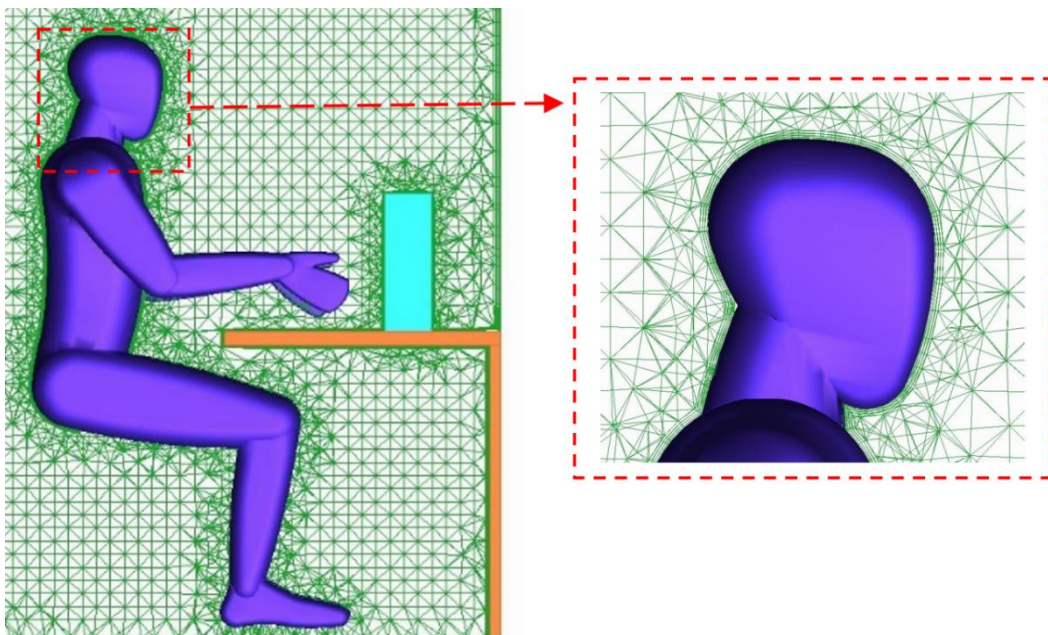
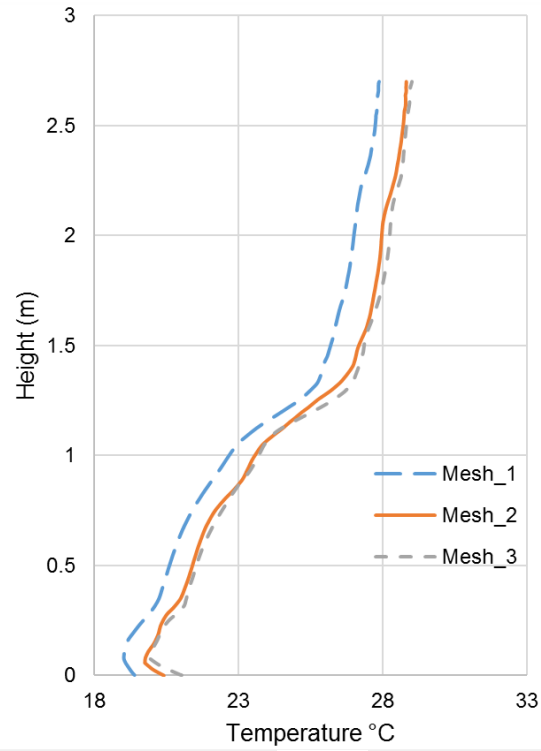
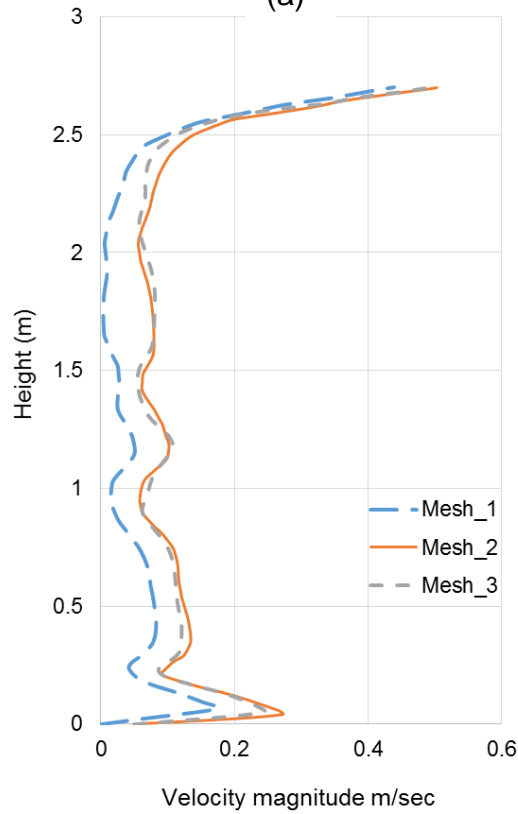


Figure 4-7: Inflation boundary layer around the human body.



(a)



(b)

Figure 4-8: Mesh independence test for; (a) temperature profile °C, (b) velocity profile (m/sec).

4.6 Results and discussion

4.6.1 Thermal comfort evaluation

The indoor human thermal comfort indices are evaluated using Fanger's comfort equations [22]. In this thermal comfort model, the thermal balance for the whole human body is expressed by two indices, the predicted mean vote (PMV) and the predicted percentage of dissatisfied (PPD). The PMV parameter refers to the mean value of the votes of people in the same thermal environment on a seven-point thermal sensation scale as shown in Table 4-5. In this index, the four physical variables (air temperature, mean radiant temperature, air velocity and relative humidity) and two personal variables (clothing and people activity) are used to predict the human thermal comfort conditions in the occupied zone. The PPD is an index which refers to the percentage of people in a large group who are prone to be thermally dissatisfied under specific thermal conditions. This is calculated from the PMV value. For the indoor human thermal comfort requirement, suitable PMV and PPD values are in the range of $-0.5 < \text{PMV} < 0.5$ and $\text{PPD} < 15$ percent respectively [152].

For a good indoor human thermal comfort, small PPD and PMV values are highly recommended. The PMV and PPD indices are calculated from the following equations [22]:

$$\begin{aligned} \text{PMV} = & (0.03e^{-0.036M} + 0.028)\{(M - W) - 3.05 \times 10^{-3} \\ & \times [5733 - 6.99(M - W) - p_a] - 0.42 \times [(M - W) - 58.15] \\ & - 1.7 \times 10^{-5}M(5867 - p_a) - 0.0014M(34 - t_a) - 3.96 \\ & \times 10^{-8}f_{cl} \times [(t_{cl} + 273)^4 - (\bar{t}_r + 273)^4] - f_{cl}h_c(t_{cl} \\ & - t_a)\} \end{aligned} \quad (4-7)$$

with

$$\begin{aligned} t_{cl} = & 35.7 - 0.028(M - W) \\ & - c_{cl} \{3.96 \times 10^8 f_{cl} \times [(t_{cl} + 273)^4 - (\bar{t}_r + 273)^4] \\ & + f_{cl}h_c(t_{cl} - t_a)\} \end{aligned} \quad (4-8)$$

$$\text{and } f_{cl} \begin{cases} 1+1.290 I_{cl} \\ 1.05+0.645 I_{cl} \end{cases} \quad \text{for } \begin{cases} I_{cl} \leq 0.078 \quad (\text{m}^2\text{°C/W}) \\ I_{cl} > 0.078 \quad (\text{m}^2\text{°C/W}) \end{cases} \quad (4-9)$$

$$\text{and } h_c \begin{cases} 2.38(t_{cl}-t_a)^{0.25} \\ 12.2\sqrt{v_{ar}} \end{cases} \quad \text{for } \begin{cases} 2.38(t_{cl}-t_a)^{0.25} > 12.1\sqrt{v_{ar}} \\ 2.38(t_{cl}-t_a)^{0.25} < 12.1\sqrt{v_{ar}} \end{cases} \quad (4-10)$$

where M and W are the metabolic rate and external work (W/m^2) respectively. p_a represents the partial water vapour pressure (Pa) and f_{cl} represents the ratio of the surface area for the clothed body over surface area for the naked body. t_a , t_{cl} and \bar{t}_r are the air temperature ($^{\circ}\text{C}$), the surface temperature for clothing ($^{\circ}\text{C}$) and the mean radiant temperature ($^{\circ}\text{C}$) respectively. c_{cl} is the clothing thermal insulation. v_{ar} refers to the relative air velocity, h_c and I_{cl} are the convective heat transfer coefficient ($\text{W/m}^2 \cdot ^{\circ}\text{C}$) and clothing thermal resistance ($\text{m}^2\text{°C/W}$) respectively.

The PPD index can be calculated by:

$$\text{PPD} = 100 - 95 \times e^{-(0.03353 \times \text{PMV}^4 + 0.2179 \times \text{PMV}^2)} \quad (4-11)$$

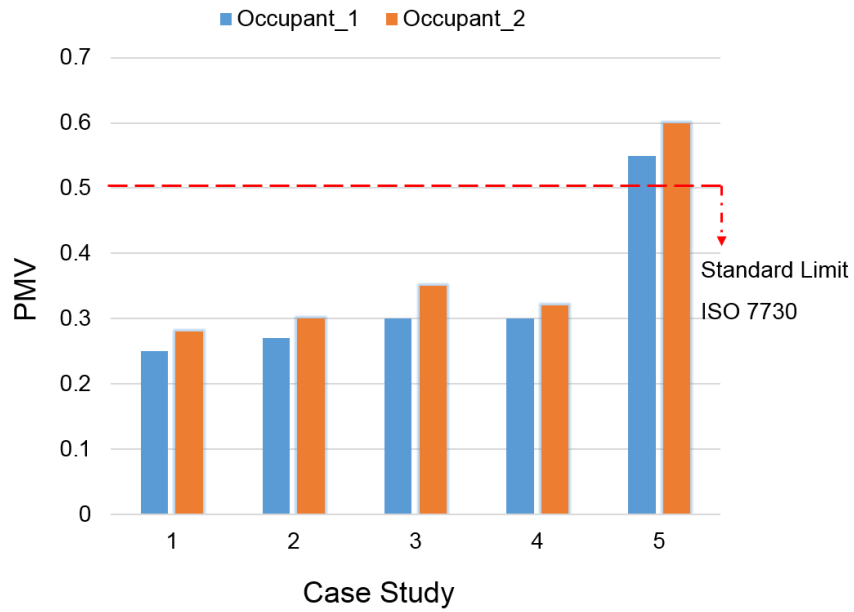
Table 4-5: The relation between PMV and thermal sensation.

PMV	Thermal sensation
+3	Hot
+2	Warm
+1	Slightly warm
0	Neutral
-1	Slightly cool
-2	Cool
-3	Cold

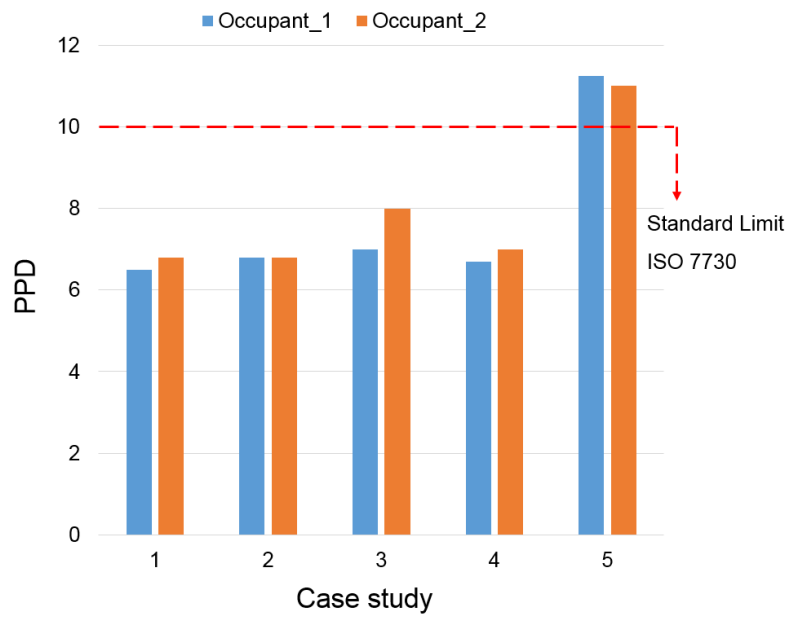
The PMV and PPD indices were used to evaluate the thermal comfort condition in each case study of Table 4-2. Figure 4-9 presents the PMV and PPD results for both occupants for each case. The PMV and PPD indices for each occupant were approximately the same with only a slight difference between them; this was due to the fact that the thermal environment around the occupants in the area near the external wall was mainly influenced by the heat flux of the external wall which subsequently affected the thermal comfort of the occupants in this region. Similar findings were reported by Horikiri et al. [153].

The values of the PPD and PMV indices values were in the acceptance range (i.e. below 10% for PPD and between 0.36 and 0.26 to for PMV) for out of the five cases, cases 1, 2, 3 and 4 (Figure 4-9 a and b). In order to explain this variation of the PPD and PMV indices, the temperature and velocity distribution were plotted for all five test cases. These predictions, reported in Figure 4-10, show that by locating the exhaust diffuser at the ceiling level, near or combined with the heat sources, the room air temperature and velocity distributions can be improved and tend to provide a more uniform distribution in most of the room's domains, which would produce a more comfortable thermal environment around the occupants.

On the other hand, when the exhaust diffuser was combined with the return outlet in one unit away from the room's heat sources, as in case 5, the occupants were predicted to become thermally unsatisfied and the thermal environment was predicted to be uncomfortable in most of the room's domains, compared with the other cases. This was due to the large amount of relatively fresh air coming by the supply diffuser being extracted directly from the combined unit diffuser in the occupied zone before mixing with the rest of the air in the room. In addition, the thermal plumes generated from the room's heat sources led to predicted increase in the temperature in the upper part of the room and the supply conditioned air does not effectively mix with warm air in the upper part of the room. All these factors created a non-homogeneous distribution of temperature, of velocity and an uncomfortable environment around the occupants as shown in Figure 4-10 (case 5). There was no significant influence of the velocity field on the PPD and PMV calculations, as most velocity magnitudes measured at the calculation points was very small (below 0.05 m/sec).



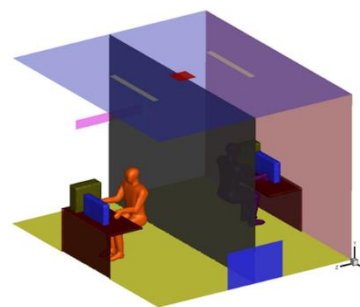
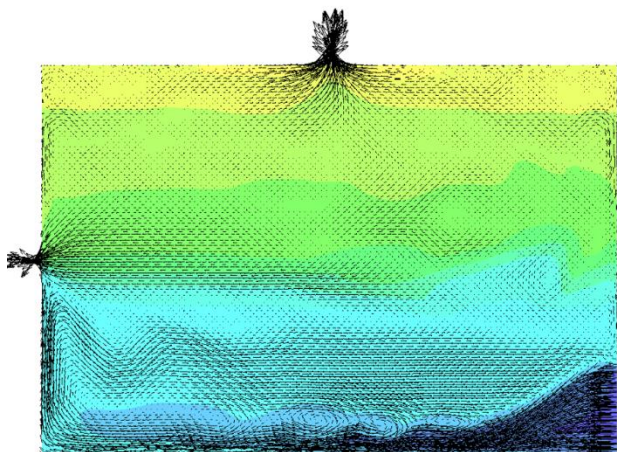
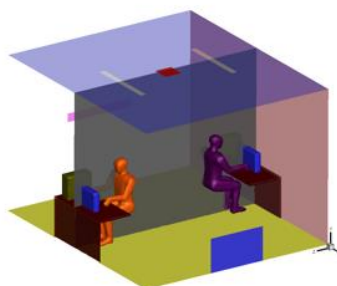
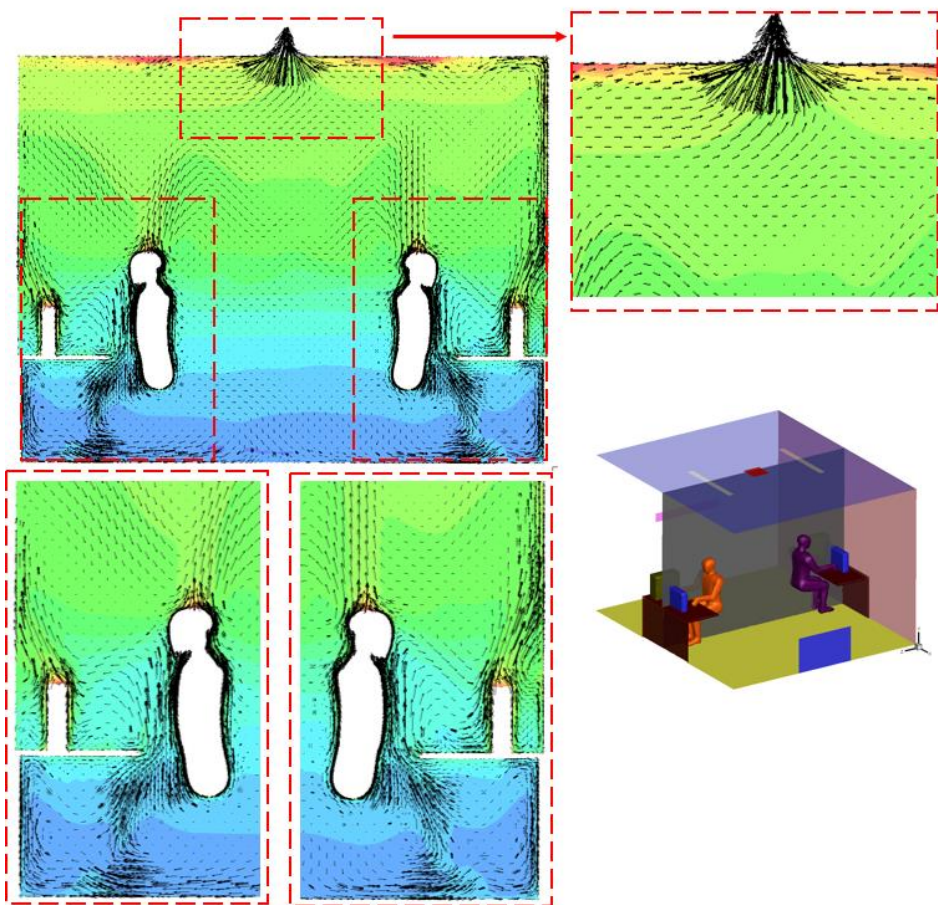
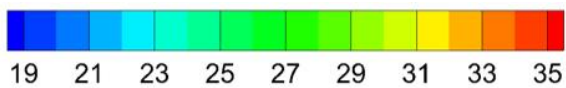
(a)



(b)

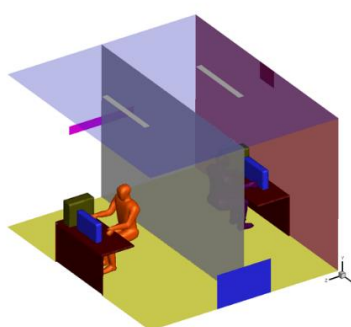
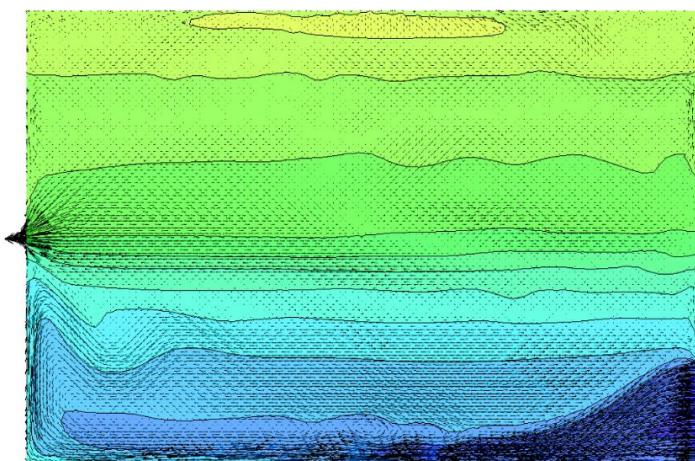
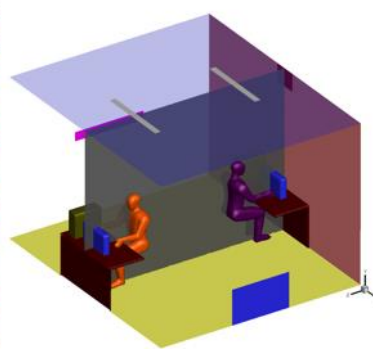
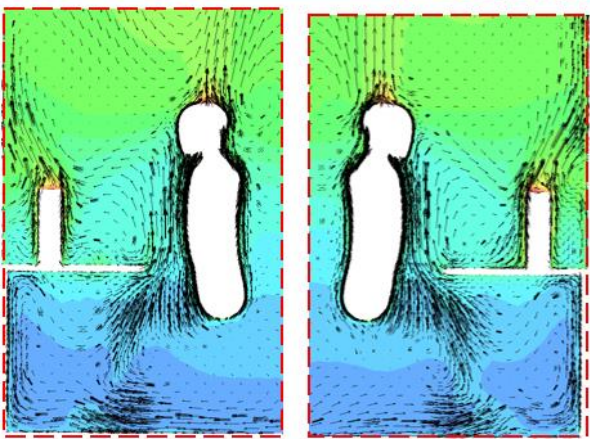
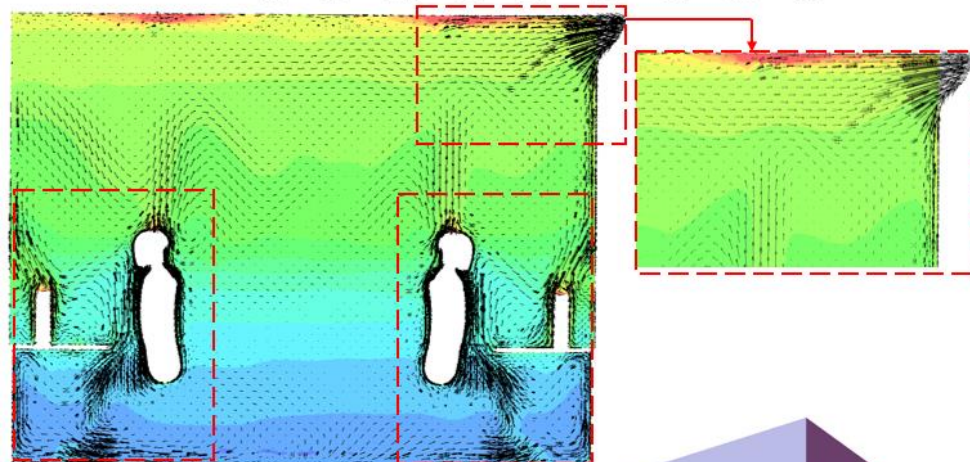
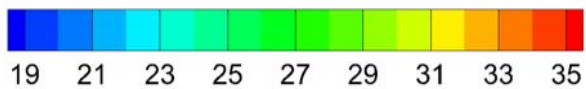
Figure 4-9: Indoor thermal comfort in each case study for both occupants; (a) PMV index; (b) PPD index.

Temperature °C

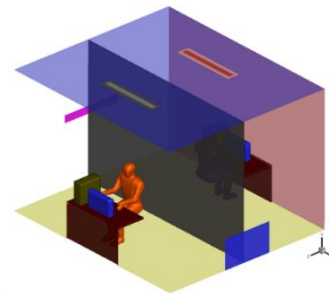
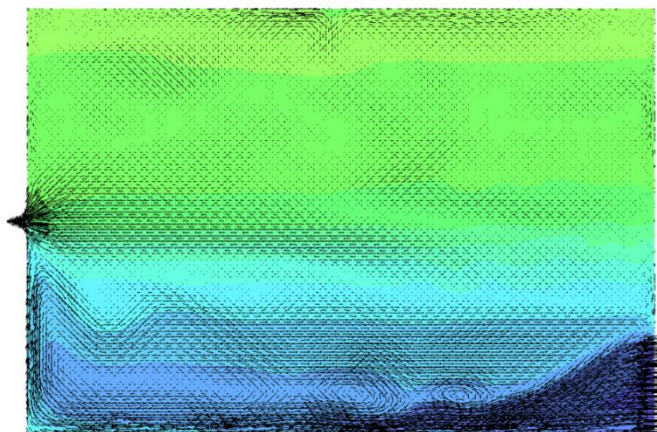
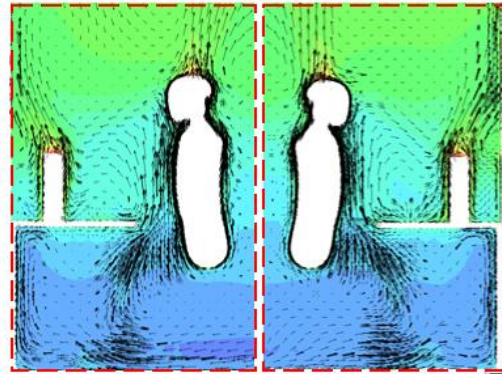
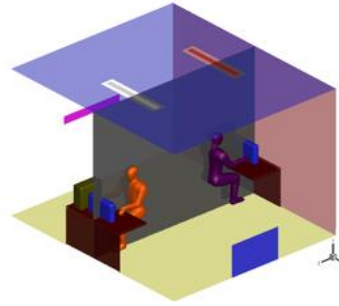
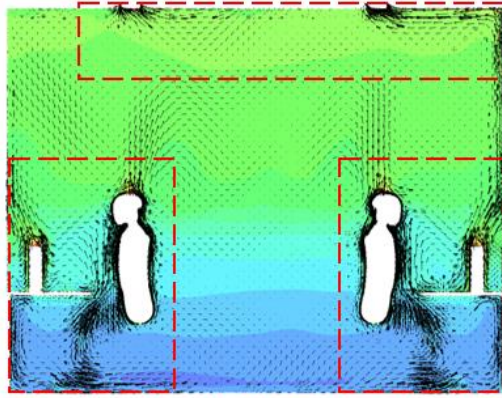
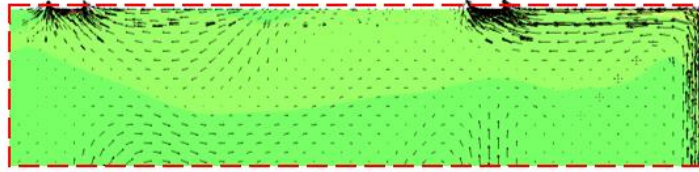
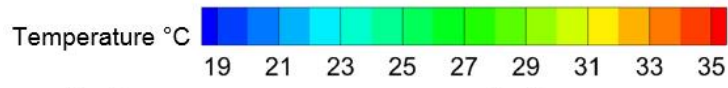


Case -1

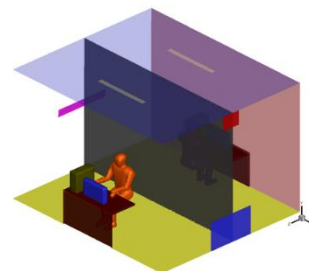
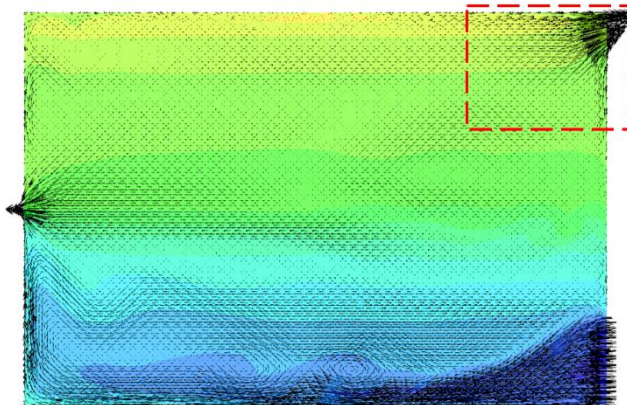
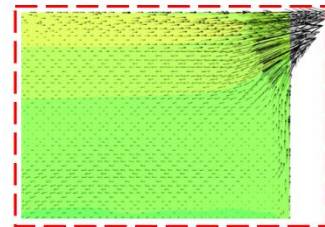
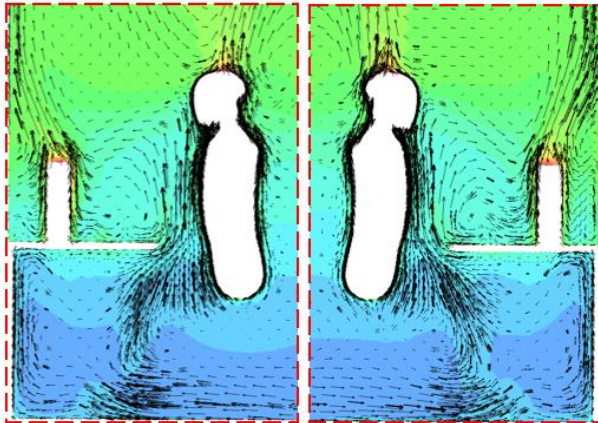
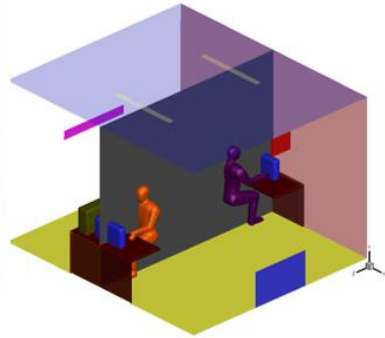
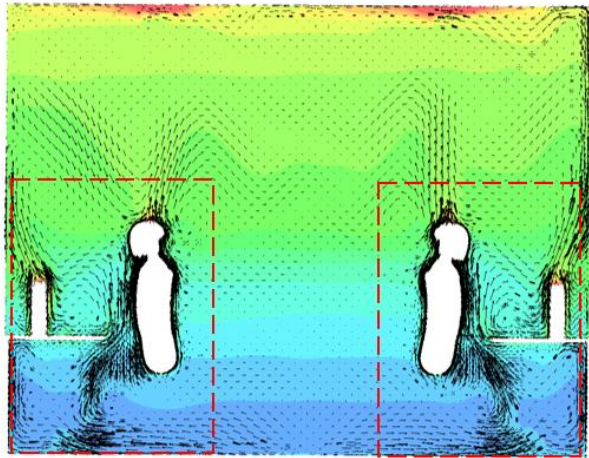
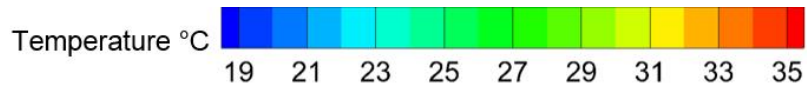
Temperature °C



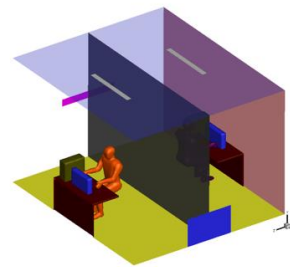
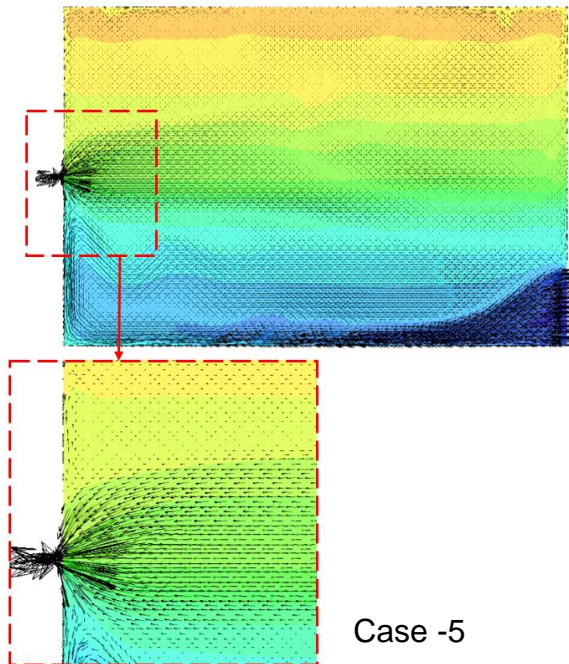
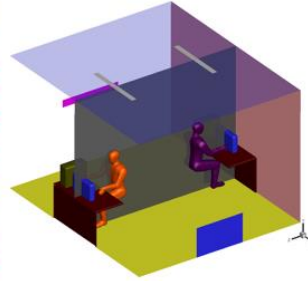
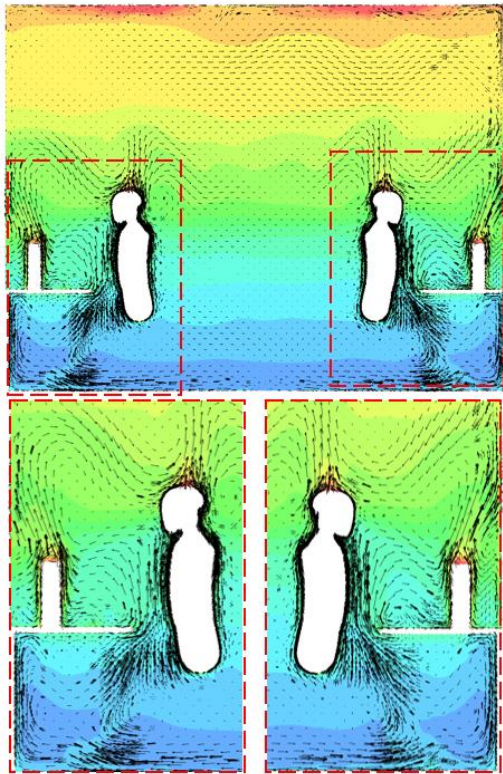
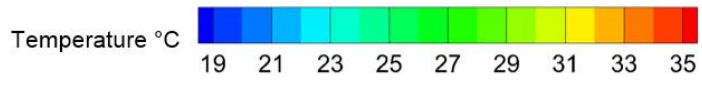
Case -2



Case -3



Case -4



Case -5

Figure 4-10: Temperature ($^{\circ}\text{C}$) and velocity distribution (m/s) at the central plane $x=2\text{ m}$ and $y =1.75\text{ m}$ for all case studies: (case 1) exhaust located at the centre of ceiling between the two heat sources; (case 2) exhaust located at the ceiling level, at the external wall; (case 3) exhaust combined with the light slots; (case 4) exhaust located at the ceiling level above the DV supply opening; (case 5) exhaust combined with the return opening.

4.6.2 Local thermal discomfort

The vertical temperature difference is one of the main factors in assessing the indoor thermal comfort in a STRAD system. According to the ISO7730 [152], the temperature difference between the head and foot level ($\Delta T_{\text{head-foot}}$) should not exceed $3\text{ }^{\circ}\text{C}$. The local thermal discomfort index was computed from the vertical temperature difference in the region around the occupants. Four positions (points I, II, III and IV), two points for each occupant, were used in this study to assess the thermal discomfort in each case (see Figure 4-11). As shown in Figure 4-12, the $\Delta T_{\text{head-foot}}$ values for cases 1, 2, 3 and 4 were in the accepted range for most locations and slightly higher at point I; the reason is that the location of this point was close to the supply inlet diffuser. Similar findings were reported by Lian and Wang [154].

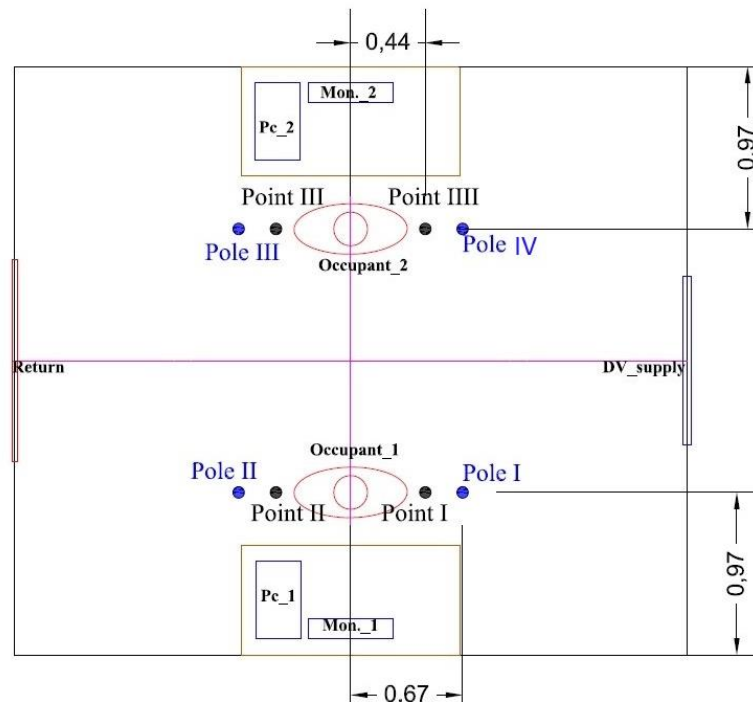
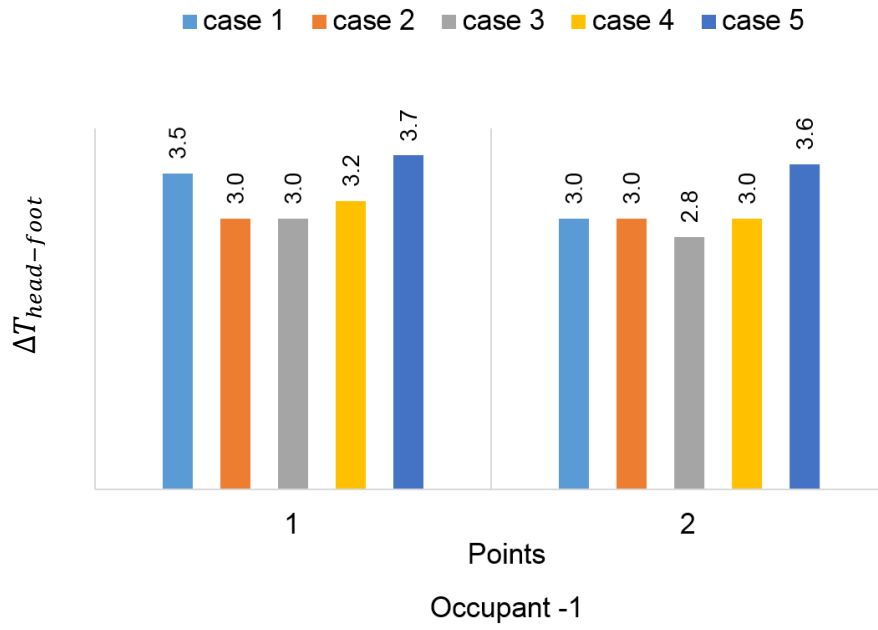
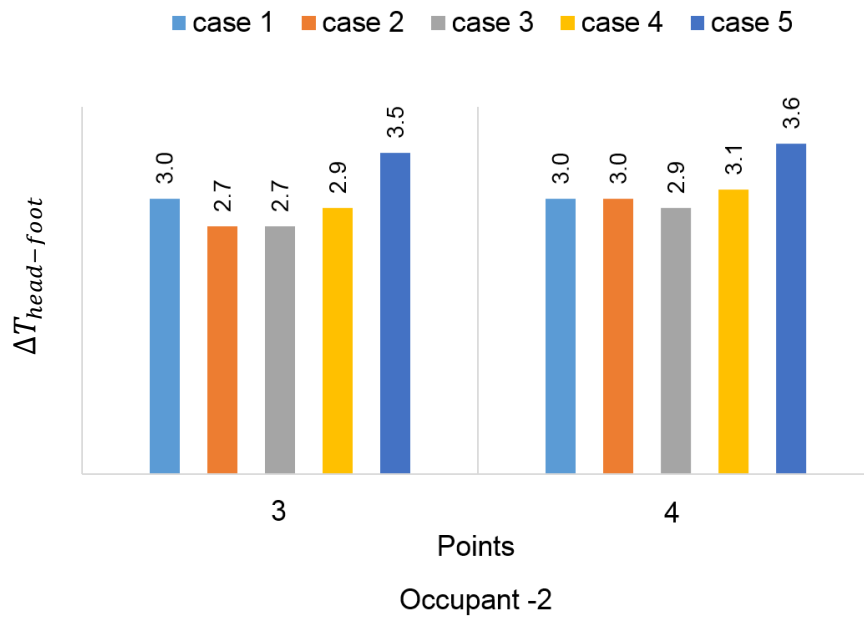


Figure 4-11: Monitoring points for each case study.



(a)



(b)

Figure 4-12: Temperature difference in °C in the vertical direction for each case study; (a) for occupant -1 and (b) for occupant -2.

For a detailed explanation of the temperature distribution in the vertical direction, Figure 4-13 shows the vertical temperature distribution along poles I, II, III and IV, in each case study. In cases 2 and 3, for which the exhaust outlets are combined with the heat sources (lamps and external wall) the $\Delta T_{\text{head-foot}}$ values were in the acceptance range at all points. The reason is that most of the heat flux emitted from these sources was extracted directly from the exhaust outlet diffuser before mix the warmed up air with the air in the occupied zone. This led to the temperature difference between the upper and lower parts being with the limits of ISO7730 [152] as shown in Figure 4-13, while for case 5, for which the exhaust is combined with the return outlet, the temperature difference was large and not with the limits of ISO7730 [152] for all the monitoring points. This is because part of the supply of fresh air was directly extracted from the combined outlet (return with exhaust) before it mixed with the warm air in the occupied area. The temperature difference between the upper and lower parts of the room was relatively high compared to the other case studies (see Figure 4-13 case 5) because a small amount of cold and fresh air was induced by the thermal plumes and reached the upper part of the room [155], causing an increase in the room air temperature in this area.

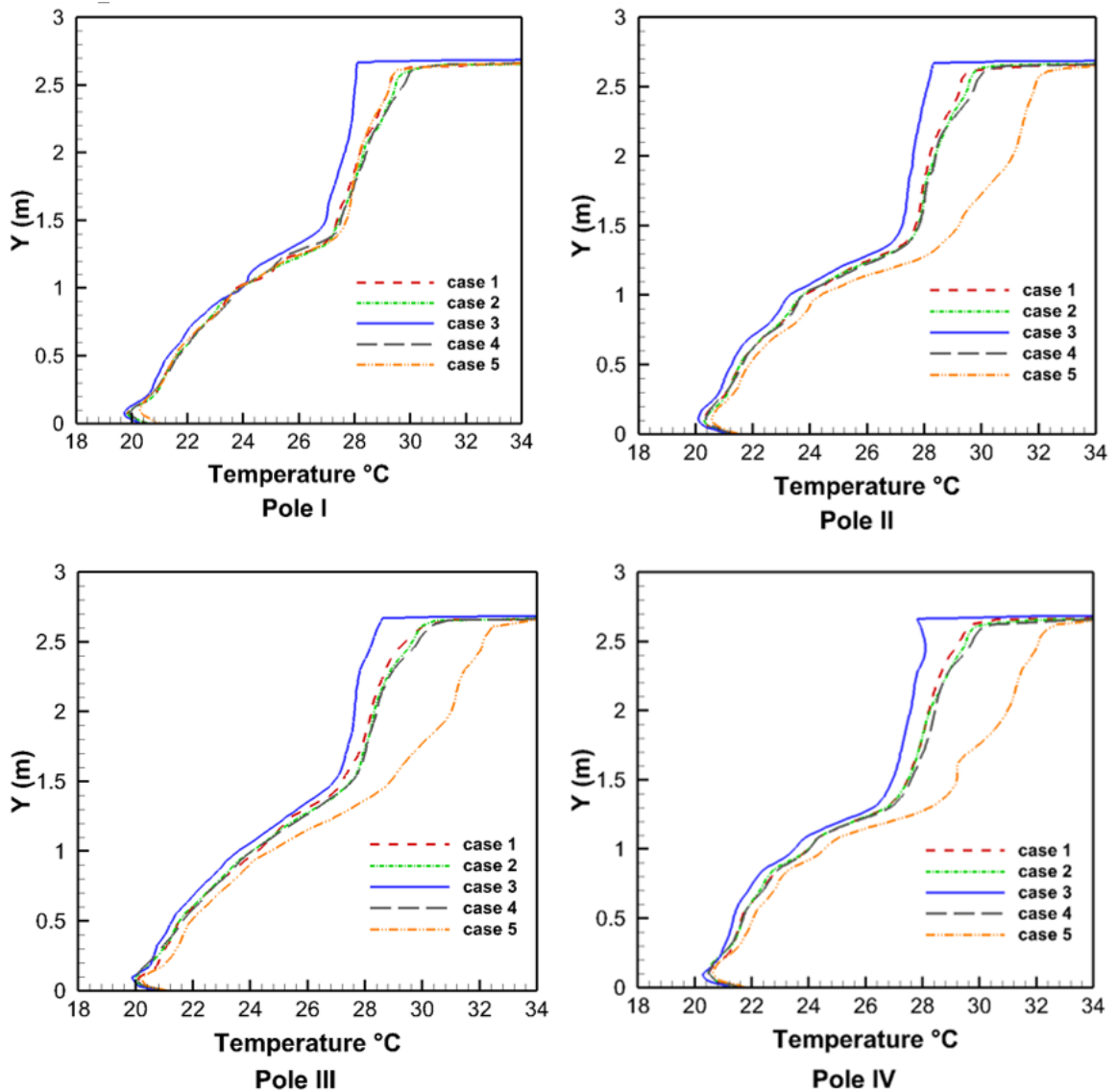


Figure 4-13: Temperature distribution in the vertical direction at four different locations for each case study.

4.6.3 Energy saving

In the STRAD system, only the area in the occupied zone is required to be thermally comfortable. This provides the means to reduce the energy consumption for the air-conditioning. In this system, the fresh air moves up by thermal plumes towards the ceiling by natural convection where it warms up by contact with internal room heat sources. Stratification of temperatures is formed in the room and the horizontal temperature profile is uniform except for the region near the supply diffuser and near the heat sources.

The energy savings were evaluated for each case study to show the impact of the exhaust location on the energy saving. Based on the CFD simulation results, Cheng et al. [39] developed a method for calculating the reduction in the cooling coil load in a room using the STRAD system. For the same set room temperature (T_{set}), the calculation of the cooling coil load in the STRAD system is different from that in the MV system:

$$\dot{Q}_{coil-STRAD} = \dot{Q}_{coil-MV} - c_p \times \dot{m}_e \times (T_e - T_{set}) \quad (4-12)$$

$$\dot{Q}_{coil-MV} = \dot{Q}_{space} + \dot{Q}_{vent} \quad (4-13)$$

where $\dot{Q}_{coil-STRAD}$ and $\dot{Q}_{coil-MV}$ represent the cooling coil load for the STRAD system and MV system respectively; \dot{Q}_{space} and \dot{Q}_{vent} are the cooling coil loads of the space and the ventilation load respectively and T_{set} is the room set temperature, which was 24°C for all case studies.

The term $c_p \times \dot{m}_e \times (T_e - T_{set})$ refers to the amount of cooling coil load reduction which is widely used to evaluate the energy saving in the STRAD system [38, 39, 43, 156]. This term was used in the present work to calculate the amount of energy saving for each case of Table 4-2. The direct extraction of the heat generated by the internal heat sources results in an increased exhaust temperature, and provides a thermally comfortable environment. This extraction will keep the indoor air temperature within an acceptable range, and consequently reduce the demand on the cooling coil to provide a greater supply of cold air, which subsequently helps to reduce energy consumption.

Table 4-6 contains that the reduction in the cooling coil load is proportional to the exhaust temperature in each case which is consist with equation 4-12. In cases 1 and 3 the energy efficiency $\Delta\dot{Q}_{coil}/\Delta\dot{Q}_{space}$ was better than for cases 2, 4 and 5 as in cases 1 and 3 the exhaust outlet diffuser was combined or located near the heat sources (lamps and external wall). This is because the direct extraction of the heat flux from these heat sources contributed to an increase in the exhaust temperature, consequently improving the potential for energy saving.

In addition, due to the reduction in air temperature in all domains of the room (see Figure 4-13), the less warm air in the occupant boundary entered the return grill which contributed to a reduction in the coil load. In contrast, in case 5 when the exhaust outlet was located away from room heat sources and combined with the return outlet, the relatively high warm air (see Figure 4-13, case 5) was recirculated and entered the return grill, causing increased energy consumption. Thus, energy saving was significantly increased to 25.0%, 13.8% and 12.65 % in cases 3, 1 and 2 respectively. From these results it can be concluded that the amount of energy saving depends on the distance between the exhaust diffuser and the heat sources as well as the combination of heat sources with the exhaust opening, i.e. extra energy saving can be achieved by locating the exhaust diffuser close to the heat object. In order to select the appropriate locations for exhaust diffusers, other factors such as the thermal comfort indices, the vertical temperature difference and the contaminants concentration distribution should be considered carefully.

Table 4-6: Energy saving for cooling coil.

Case study	T_e (°C)	T_r (°C)	$\Delta Q_{coil} = C_p \times m_e \times (T_e - T_{set})$ (W).	$\Delta Q_{coil} / \Delta Q_{space}$ (%)
Case_1	30.0	26.6	139.6	13.8
Case_2	29.5	26.7	128.0	12.65
Case_3	34.0	26.0	250.0	25.0
Case_4	29.3	26.7	123.0	12.18
Case_5	27.6	27.6	85.0	8.4

4.6.4 The quality of the indoor air evaluation

The quality of the indoor air plays a significant role in the evaluation of the indoor air distribution system performance, particularly in terms of the distribution and concentration of contaminants. The most important factors that affect the particle concentration distribution in a room are the location of the exhaust diffusers and that of the contaminant sources [157]. In the current work, the contaminant sources were located at the door and window frames to simulate contaminants

coming from outside and entering the domain from these frames with the same particle diameter as shown in Figure 4-1. The quality of the occupants' inhaled air (Figure 4-14) and the air quality in the breathing zone were used to evaluate the air quality for each case. The normalised contaminant concentration normalisation is defined as follows:

$$C_n = \frac{C_p}{C_e} \quad (4-14)$$

where C_n is the normalised concentration and C_p and C_e are the contaminant concentrations in a specific region and the concentration at the exhaust respectively.

Let the inhaled zone be a 0.5 m cube centred around each occupant's head, as shown in Figure 4-13. Figure 4-15 a and b compare the normalised particle concentration for each case study between the inhaled and the breathing zones. The particle concentration for occupant 1 was larger than the concentration for occupant 2 in all cases except for case 3. The reason for this is that the position of occupant 1 was very close to the door, which was one of the modelled contaminant sources. This is consistent with the findings reported by Licina et al. [158]. In addition, occupant 2 was located near the external wall, where the contaminant transport was greatly influenced by the convective heat flux that contributed to bringing a large amount of contaminants from the occupant zone towards the extractor outlet at the ceiling level, which consequently improved the inhaled air for occupant 2. Furthermore, in cases 1, 2, 3 and 4 the air in the inhaled area and the breathing zone showed better quality for both occupants compared to case 5 (see Figure 4-15 a and b). This is because the contaminants transported by the thermal heat plumes from heat sources in the lower part of the room were extracted at the ceiling level which consequently reduced the contaminant concentration at both the inhaled air and the breathing levels.

On the other hand, in case 5, due to there being no extractor opening at the ceiling level, the contaminants in the upper part of the room recirculated more and their concentration increase in all the room's domains, including the inhaled air and breathing level. The best air quality for the inhaled zone and breathing zone were achieved in case 3, as the combination of the exhaust and lamp

extracted a large amount of contaminants which led to a reduction in the contaminant concentration in both the inhaled and the breathing zones compared with the other case studies. From these results, it is clear that a satisfactory air quality can be achieved by locating the exhaust close to the room's heat sources. Similar findings were also reported by Serrano-Arellano et al. [159]. This is because the contaminants are mostly carried by the thermal plumes [160] of the heat source and extracted directly from the exhaust outlet which contributes to reducing the contaminant concentration in the room.

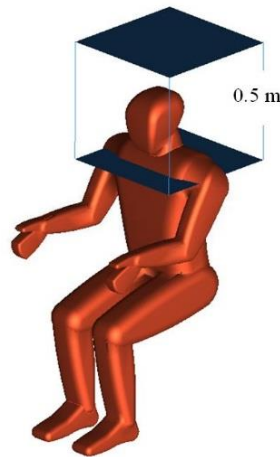
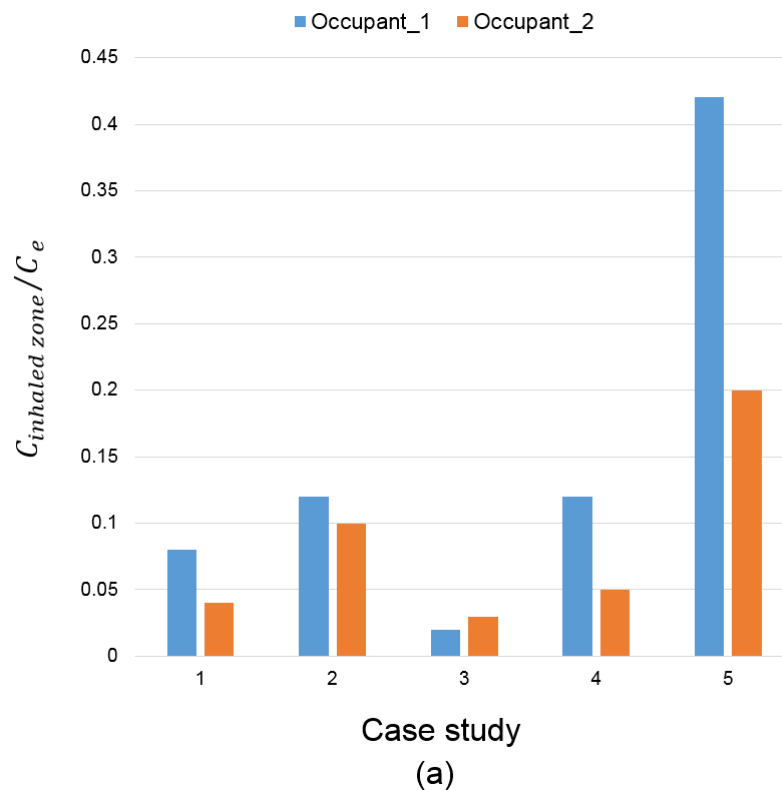


Figure 4-14: Inhaled area around the occupants, 0.5 m cube (microenvironment).



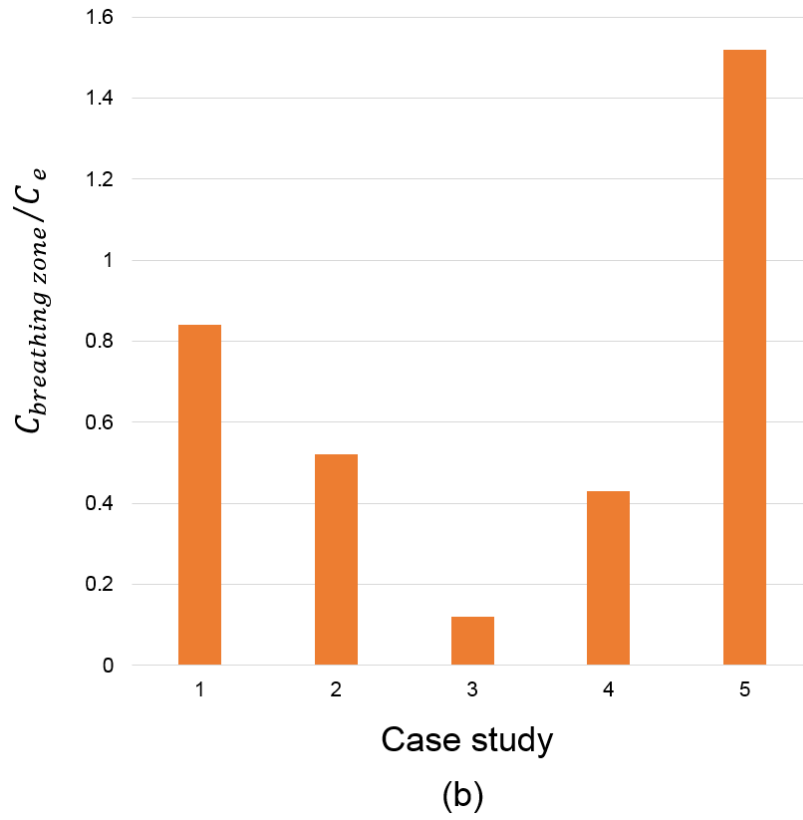


Figure 4-15: Comparison of the particle concentration for each case study; (a) for the inhaled area of each occupant; (b) for the breathing level.

Chapter 5 Development of a Novel Local Exhaust Ventilation System for Office Rooms

5.1 Introduction

In this chapter, the concept of the local exhaust ventilation system was developed for use in an office. A novel local exhaust ventilation system for offices was combined with an office workstation in one unit. The energy saving, the thermal comfort and the inhaled air quality were used to evaluate the performance of the new system. The concept of combining the room heat sources with the exhaust opening, which was presented in Chapter 4, has been further improved and used in this chapter along with the local exhaust ventilation system concept to extract a large amount of the generated heat flux and consequently improve the indoor thermal environment and obtain some energy savings. The performance of the new system for three different amounts of recirculated air was investigated numerically in an office room and compared with a conventional HVAC system with and without using the new system to show its impact on the indoor thermal environment and on the inhaled air quality. The CFD method, which was validated in Chapter 4, is used in this chapter to predict the indoor thermal environment and the contaminant concentration. The boundary conditions for the CFD model are kept the same for all case studies. The detailed information regarding the novel local exhaust ventilation system is presented in the first part of this chapter. Then, a grid independence test is performed to ensure that this study uses an appropriate mesh size. Finally, the impact of using the local exhaust ventilation concept in an office space to control the indoor thermal comfort, the energy consumption and the inhaled air quality is discussed in details in the last part of the chapter.

5.2 Methods

As discussed in Chapter 4, a brief investigation was performed of the combination between the room heat sources with the exhaust opening and on its impact on the indoor thermal environment and on the energy consumption. The results revealed that a good indoor environment at a lower with extra energy consumption can be achieved in rooms that combine the exhaust with the lamps into one unit [161]. In this chapter, the concept of combining concept between the room heat sources with exhaust opening has been further improved to extract a larger amount of the generated heat flux from the room heat sources. In addition, this concept is employed along with the local exhaust ventilation system in the current study for the investigated office room.

The local exhaust ventilation system, which aims to control the dispersion of contaminant and to extract contaminated air locally, is widely used in industrial applications. In this chapter, this concept is employed and further developed to be used in an office space. The main objectives of the proposed LEVO system are to improve the energy saving and provide a healthy and comfortable local environment around the occupants by controlling the heat convection resulting from the room heat sources, i.e. the thermal plumes generated by the occupants and by the other heat sources. Figure 5-1 shows schematic diagrams of the LEVO system combined with the office workstation and the air flow direction around the occupants in an office room.

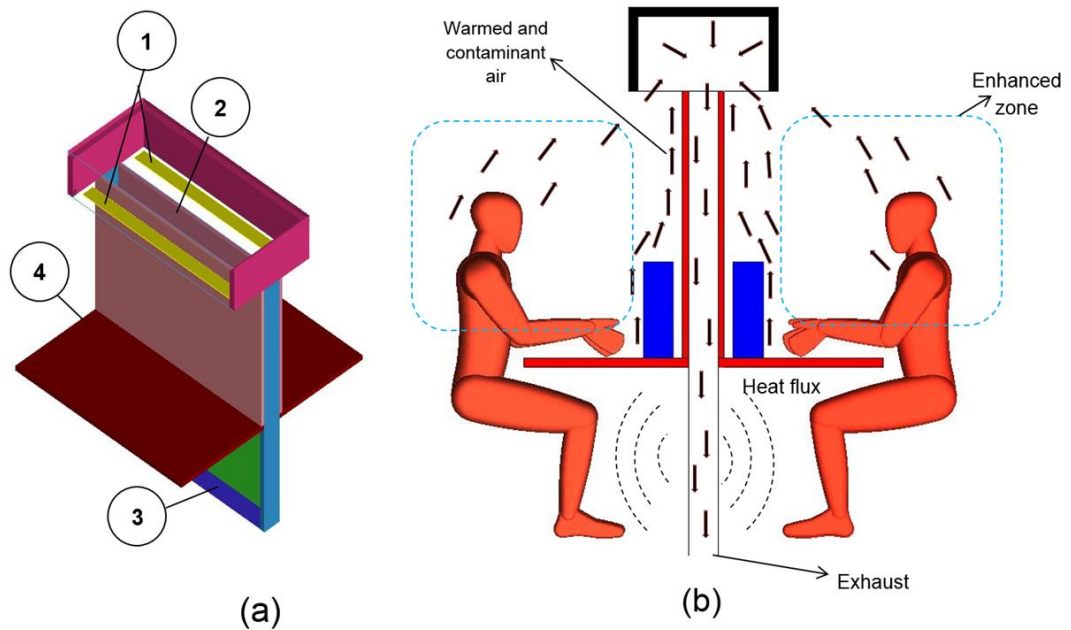


Figure 5-1: (a) LEVO system: 1- lamps, 2 - air suction part, 3 - exhaust inlet and 4 - table; (b) LEVO system combined with the office heat sources and suction airflow direction.

Two sources of contaminants were used in this study to simulate the contaminants generated by the office equipment and by office work activities. Particles of $0.7 \mu\text{m}$ in size with a density of 912 kg/m^3 were generated for each case study. This type of particles belongs to particles in the accumulation mode ($0.1\text{-}2 \mu\text{m}$), such as those found in building dust and smoke. A DV system was employed in this study as the main air distribution system. As mentioned previously, with the DV system, fresh and cool air is normally supplied at or close to the floor level with low velocity [162]. In this study, a supply DV diffuser ($1.0 \text{ m} \times 0.6 \text{ m}$) was located at floor level on the side wall and the return opening ($0.08 \text{ m} \times 1.0 \text{ m}$) was located at the upper boundary of the occupied area, 1.3 m from the floor level (see Figure 5-2), as recommended by Cheng et al. [39]. The set room temperature in the occupied zone was 24°C for all case studies. The total supply air velocity was 0.14 m/s and its temperature was 19°C .

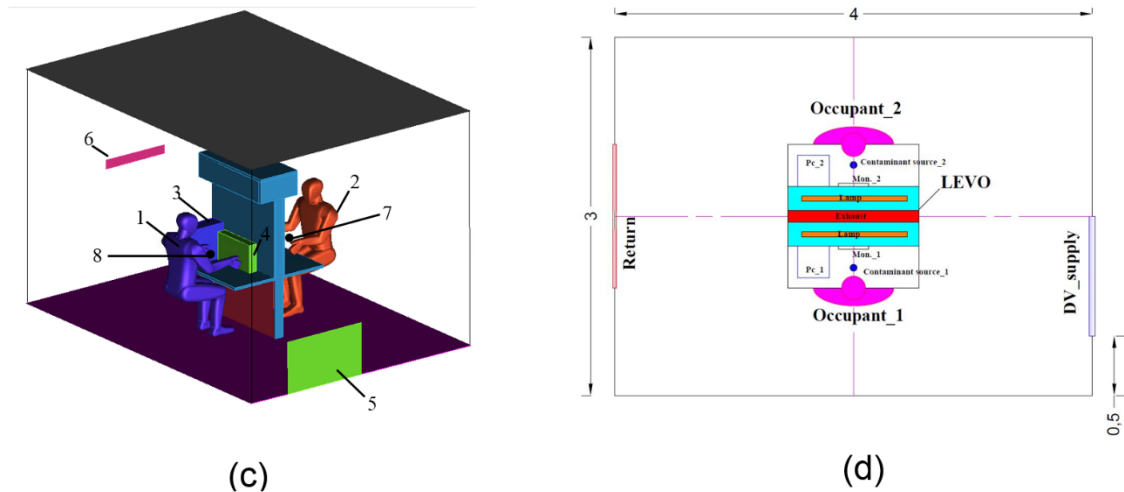


Figure 5-2: (a) Configuration of the simulated room: 1 - occupant 1, 2 - occupant 2, 3 - PC case, 4 - PC monitor, 5 - DV inlet, 6 - return inlet, 7 - contaminant source 1 and 8 - contaminant source 2; (b) The equipment arrangement on the simulated office.

In the LEVO system, the reading lamps and exhaust outlet are combined in one unit and are located above the heat sources of the workstation such as the monitors, computers, and occupants, at 1.6 m from the floor level (see Figure 5-1). In this system, the warm and contaminated air generated by the occupants and by the office activities is extracted locally before it mixes with the rest of the air in the room. In order to improve the temperature distribution in the vertical direction and reduce the temperature difference between the foot and head levels, the extracted warm air was directed towards the foot level. A small amount of the extracted heat is transferred into the area near the feet (see Figure 5-1b). This reduces the vertical temperature difference. This creates a healthy and comfortable work environment, especially in the area around the occupant's workstation, and causes the exhaust air temperature to increase, which leads to some energy saving.

In this chapter, a detailed 3D numerical simulation is performed using the commercial software ANSYS FLUENT to assess the performance of the LEVO system in providing localized thermal comfort and in enhancing the air quality in the inhaled area, as well as in reducing the energy consumption of the system. For an accurate prediction of the temperature, velocity and of the particle

concentration distribution, the numerical results were validated against the experimental results from the published work [69] and [151]. This was presented in Chapter 4. In order to determine the best performance of the LEVO system in the office, three different amounts of the return air were examined using the validated numerical model (see Table 5-1).

Table 5-1: Case studies.

Case study	Return air percentage
Case 1	35% (return velocity = 0.35 m/s).
Case 2	50% (return velocity = 0.50 m/s).
Case 3	65% (return velocity = 0.68 m/s).

Since this investigation targeted at the energy saving and the indoor thermal comfort in an office space, especially in the area around the occupants, a full-scale computational domain representing a typical office with dimensions of 4 m long, 3 m wide and 2.7 m high was used in the simulation. The office heat sources include two occupants, two computer cases, two monitors, and two lamps. The office bounded walls, ceiling and floor were modelled as adiabatic. Table 5-2 lists the heat rate emitted from each heat source.

Table 5-2: Cooling load for the simulated office room.

Internal heat sources	Cooling load
Occupants	60×2 W
PC case	60×2 W
PC monitor	70×2 W
Lamps	24×2 W
Total	428 W
Heat flux density based on the floor surface area	35.67 W/m ²

5.3 Mesh generation

As stated in the previous chapter, the grid independence test plays an important role in a CFD simulation towards demonstration the accuracy and cost of the predictions. As in Chapter 4, a tetrahedral unstructured mesh with inflation boundary layers around the occupants was generated using ANSYS ICEM CFD software to cope with geometrical complexity of the human bodies and of the office equipment. The meshes in areas of interest, which are the areas around the occupants and the occupied zone, were refined to capture the heat convection behaviour and to resolve the y^+ near the wall boundary layers (see Figure 5-3). The mesh was clustered in regions that have high temperature and velocity gradients such as at walls, equipment, and around the table. To resolve the boundary layer around the occupants, an inflation boundary layer of 5 layers was generated with a growth rate of 1.2 and the first layer thickness was 1.5 mm. As shown in Figure 5-4, the y^+ values of $0.7 \leq y^+ \leq 4.5$ was achieved. In the current study, the grid size was selected by comparing the simulation results from three different sizes of mesh as listed in Table 5-3. By increasing the grid cells from mesh_2 to mesh_3, there is no significant change in the predicted temperature and velocity distributions (see Figure 5-5). Therefore, mesh_2 with 2,753,932 cells was selected to be an adequate mesh for the rest of the simulations of Chapter 5.

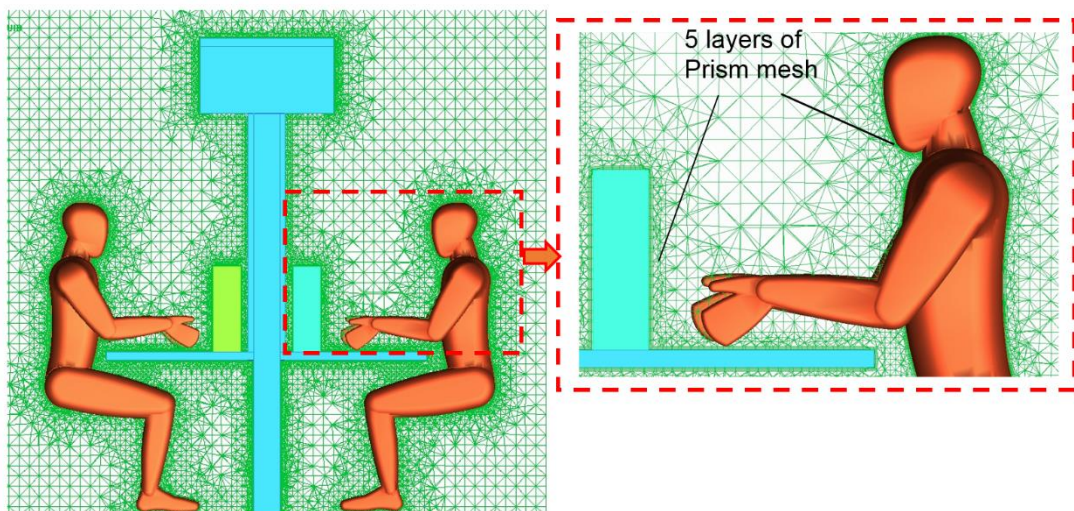


Figure 5-3: Inflation boundary layer around the human body.

Table 5-3: Mesh independence test.

Mesh types	Cells number
mesh_1	1,518,077
mesh_2	2,753,932
mesh_3	3,493,875

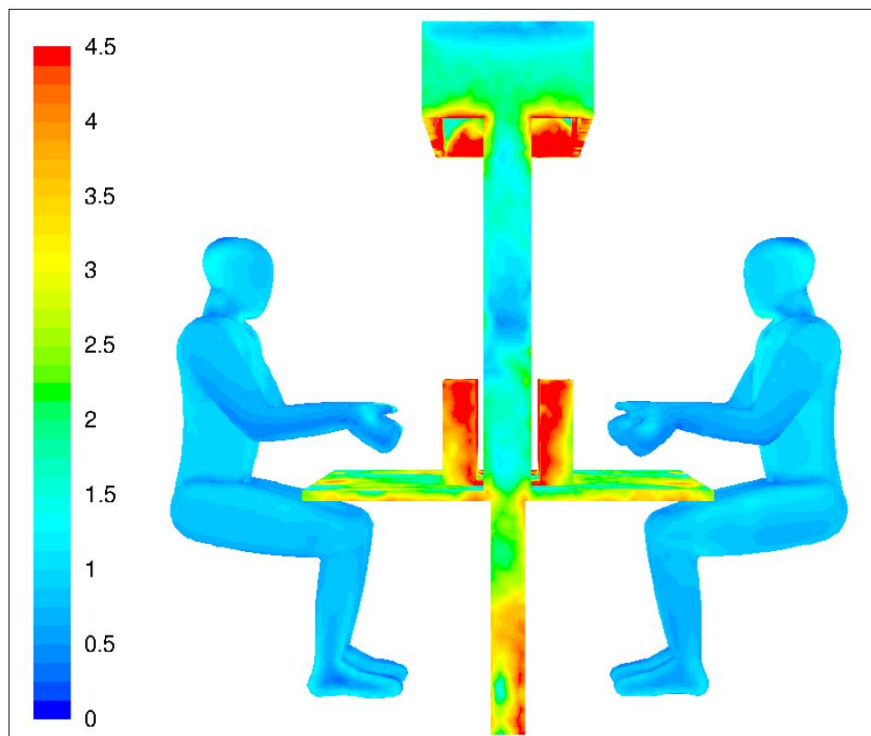
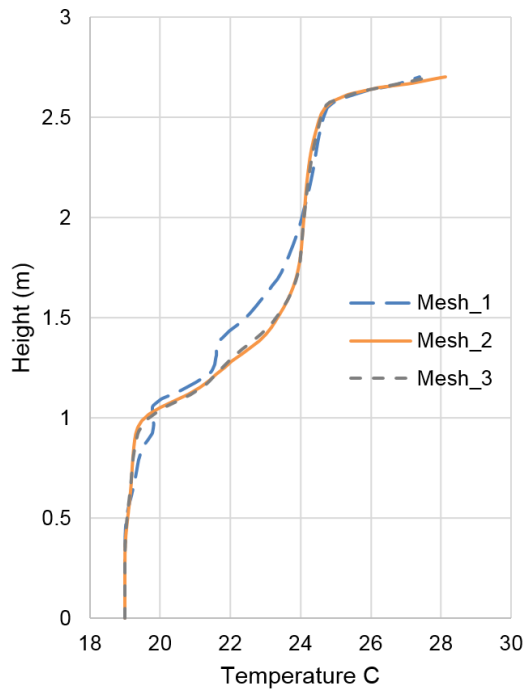
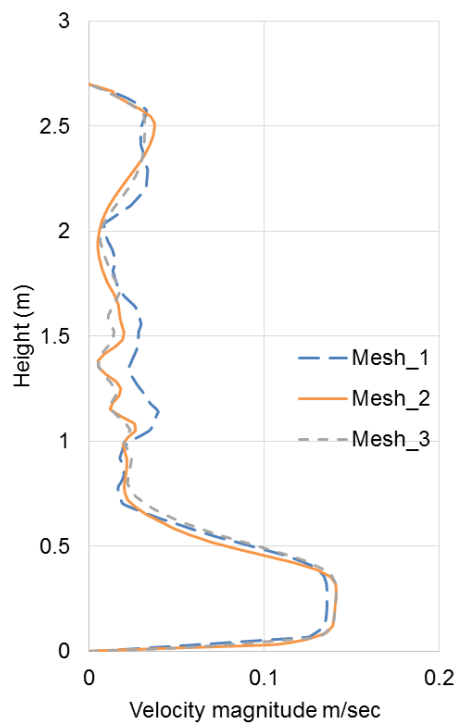


Figure 5-4: y^+ value for the occupant zone.



(a)



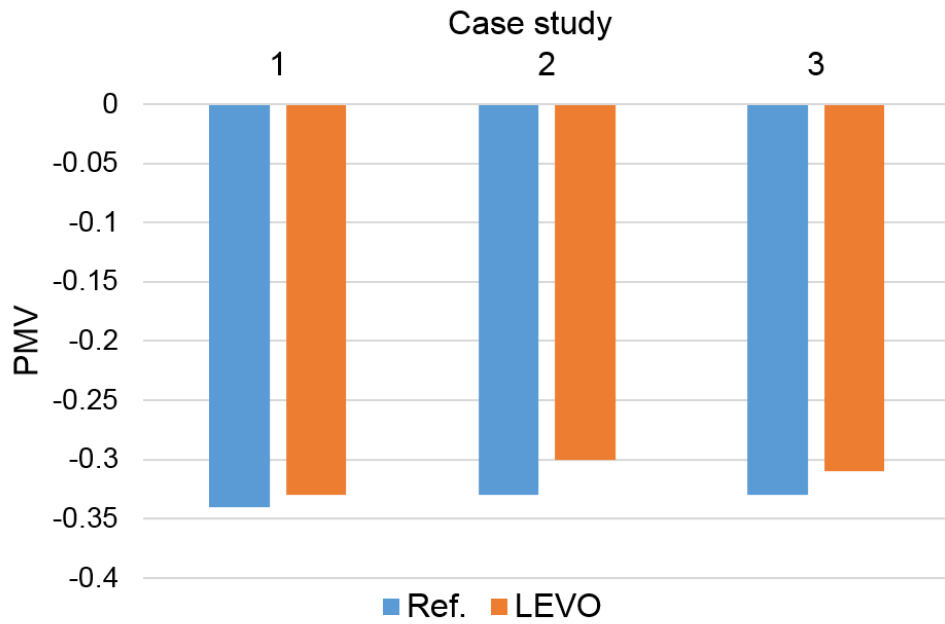
(b)

Figure 5-5: Mesh independence test for; (a) temperature profile °C, (b) velocity profile (m/sec).

5.4 Results and discussion

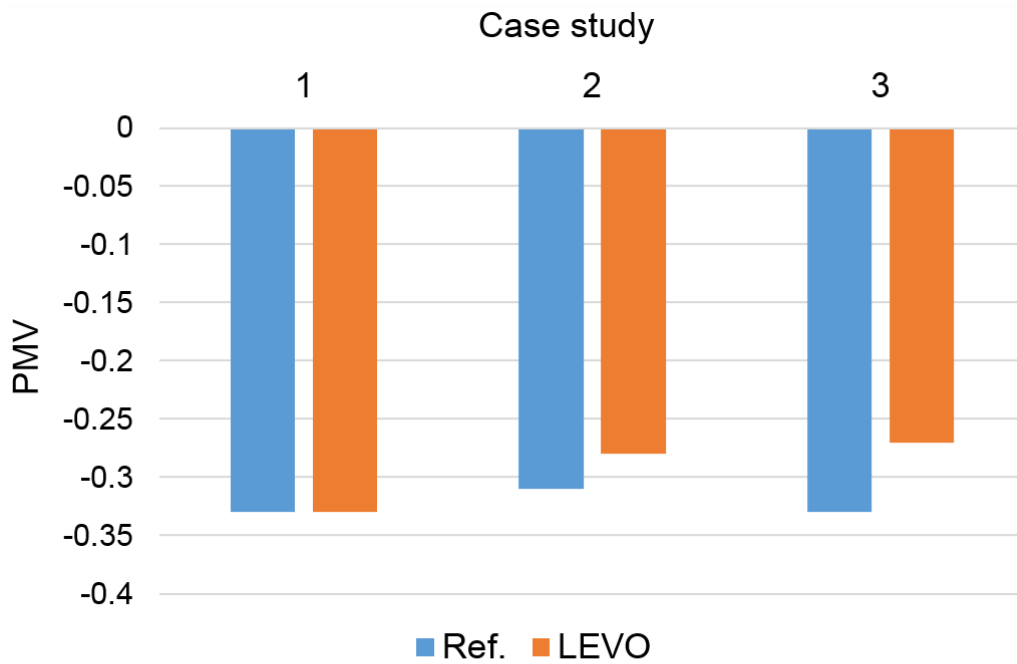
5.4.1 Indoor thermal comfort

As presented in Chapter 4, the thermal comfort for humans can be expressed by two indices, the PMV and the PPD. These indices are used to assess the human thermal comfort in each case study in this chapter. Figure 5-6 and Figure 5-7 compares the PMV and PPD predictions with and without the LEVO system for both occupants in the investigated room. Three different amounts of recirculated air were examined (see Table 5-1). In cases 1, 2 and 3, the PMV and PPD indices for the room with and without the LEVO system (reference case) were approximately the same with only a slight difference among them; this was due to the fact that the air temperature and velocity in the area near the feet, as shown in Figure 5-8, were slightly increased compared with the room without the LEVO system, which subsequently affected the thermal environment in these regions. Similar findings were reported by Horikiri et al. [153]. For all cases, the thermal comfort indices for occupant 2 were slightly better than those for occupant 1. This was because the position of occupant 2 was slightly further away from the inlet supply diffuser which provides a cold air draught. The above results show that the LEVO delivers no significant improvement of the indoor thermal environment based on the PPD and the PVM predictions. However, the other results show that with the LEVO, a significant improvement with an acceptable thermal comfort was achieved regarding the other evaluation parameters, such as the vertical temperature distribution, the air quality in the occupied zone as well as the energy saving.



Occupant -1

(a)



Occupant -2

(b)

Figure 5-6: The predicted PMV values in the reference case and LEVO case for (a) occupant -1 and (b) occupant -2.

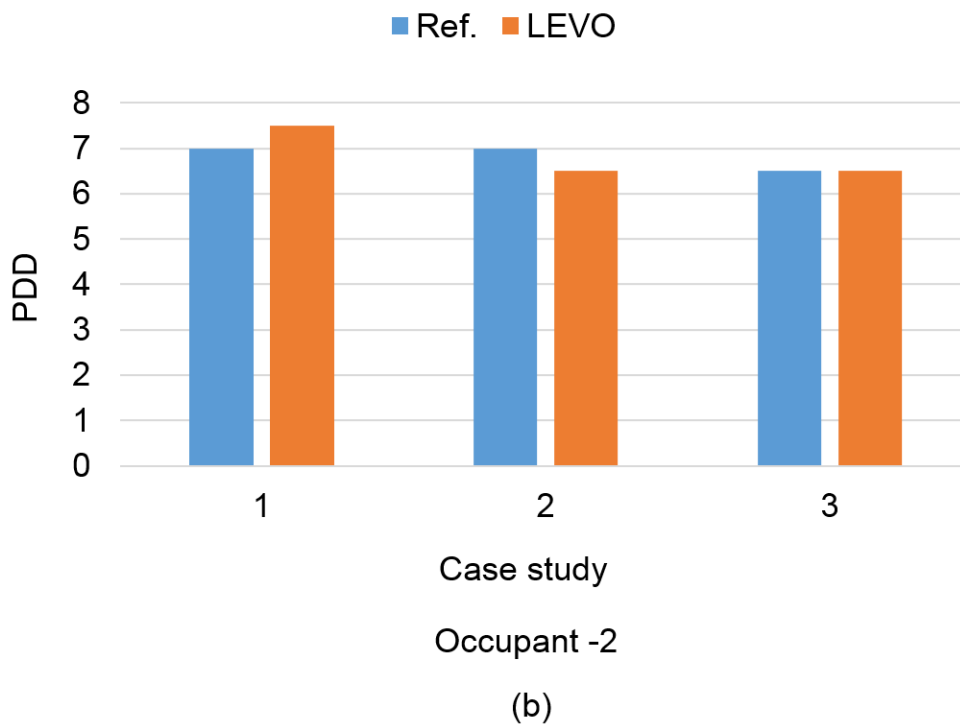
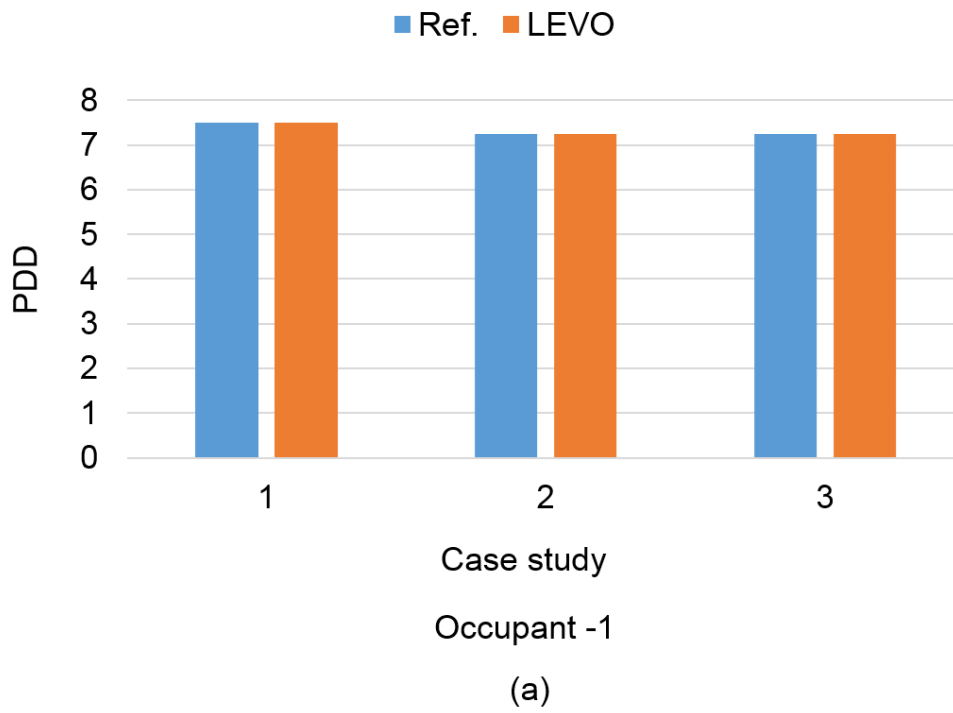
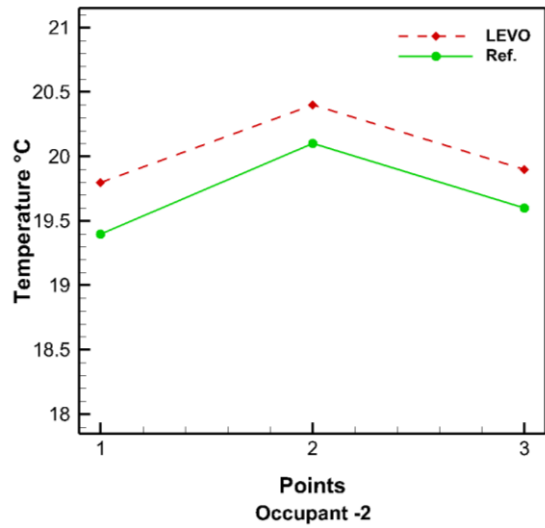
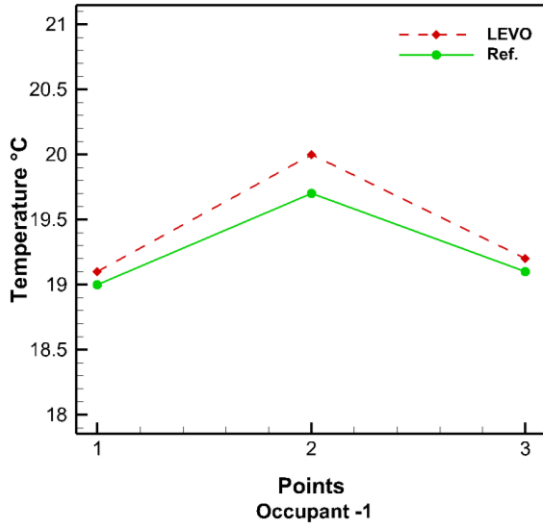
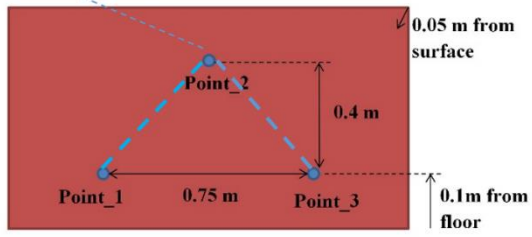
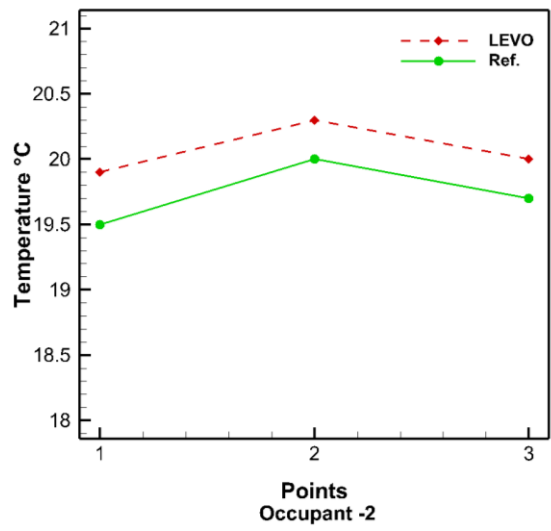
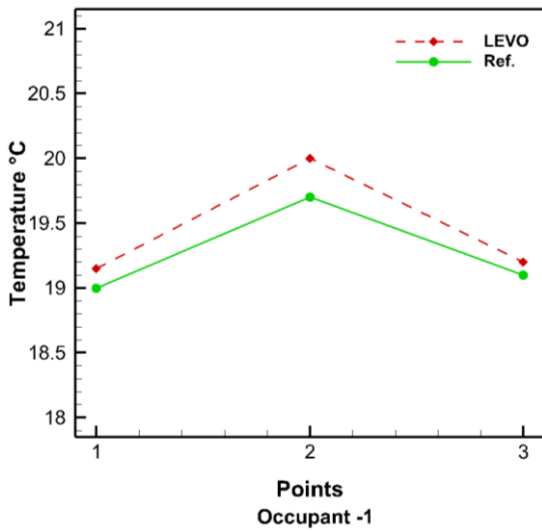


Figure 5-7: The predicted PDD values in the reference case and LEVO case for (a) occupant -1 and (b) occupant -2.

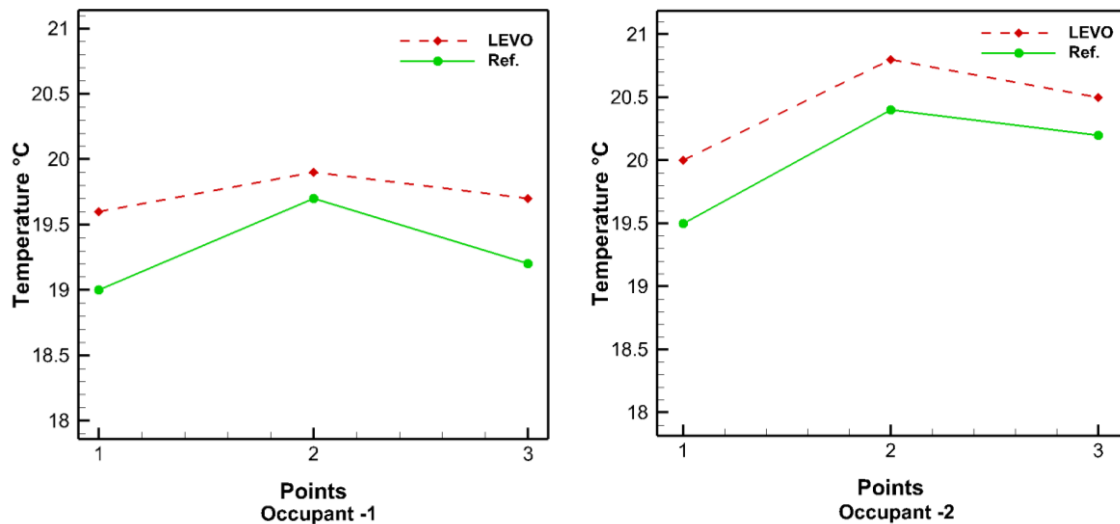
Monitoring points



Case -1



Case -2



Case -3

Figure 5-8: Temperature distribution (°C) of the near foot zone at three monitoring points, point 1, 2 and 3, for each case study and for both occupants.

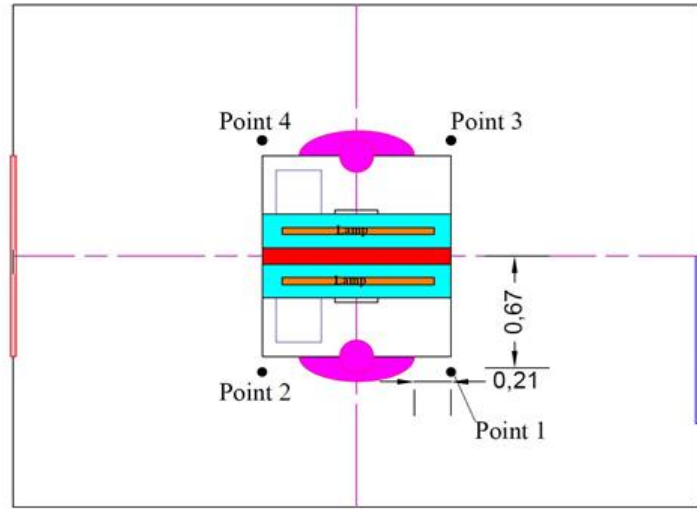
It is thus concluded that the impact of the heated area near the foot level on the thermal comfort around the seated occupants is not very significant, other than a slight enhancement of the PVM and of the PPD indices (see Figure 5-6 and Figure 5-7). In addition, for all data the PMV index was between -0.26 and -0.34, while the value of the PPD index was between 6.5 and 7.5. These indicate that the room was observed to be between neutral and slightly cool (see Table 4-1) and still within the thermal comfort range.

5.4.2 Temperature distribution in the vertical direction

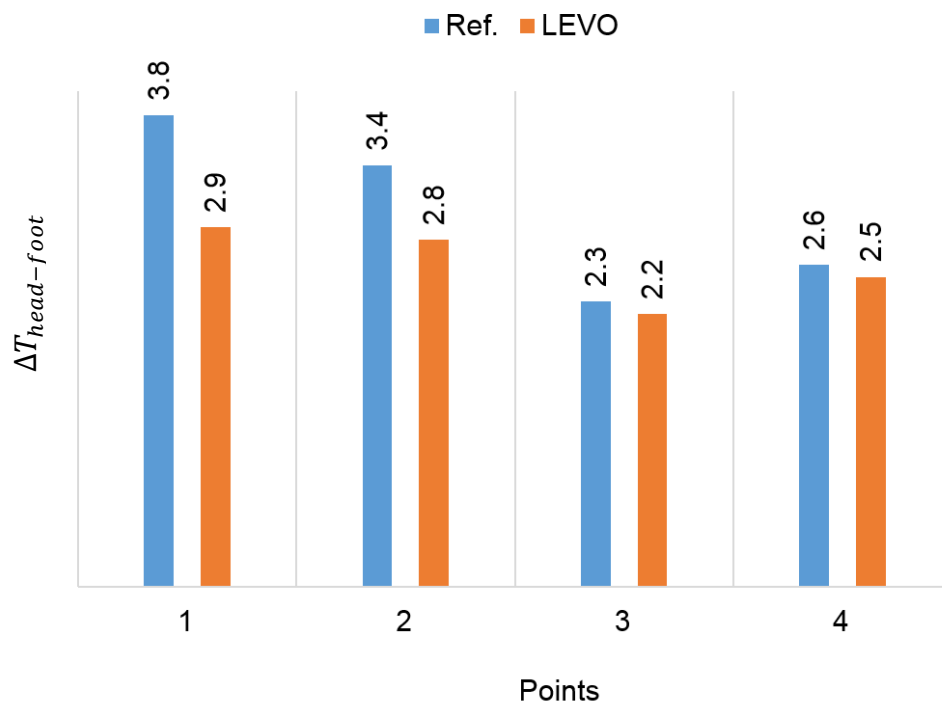
As quoted in Chapter 4, the temperature gradient in a vertical direction is one of the major factors in evaluating the indoor thermal comfort of a STRAD system. In this chapter, the local thermal discomfort index ($\Delta T_{head-foot}$) was evaluated in the region around the occupants. As shown in Figure 5-9 (a), four positions (points 1, 2, 3 and 4), two points at each occupant, were used in the current study to assess the thermal discomfort in each case. In cases 1, 2 and 3, Figure 5-9 b, c and d shows that using the LEVO system reduced the temperature difference between the head and feet in all locations compared with the room in which the system was not used. This is because the LEVO system works to extract the warm air in the vicinity of the occupants and directs it towards their feet. This process leads to a reduction in the air temperature at the head zone and to a

slightly increased air temperature at the foot level which reduced the temperature difference, $\Delta T_{head-foot}$, and improved human thermal comfort. The temperature difference, $\Delta T_{head-foot}$, at points 1 and 2 was slightly higher than at point 3 and 4. The reason for this is that the positions of points 1 and 2 were close to the supply inlet diffuser. Similar findings were reported by Lian and Wang [154]. It can be concluded that an enhancement to the human thermal comfort can be achieved by locally extracting the warm air generated by the room heat sources using the new LEVO system. Figure 5-10 shows the temperature and the qualitative velocity distribution for using the LEVO system and (b) for the reference case (without using the LEVO system). From these figures it can be seen that the local extraction of the heat generated by the room heat sources using the LEVO system improved the temperature differences between the upper and lower parts of the room. This will improve the temperature distribution inside the room domain and consequently improve the indoor thermal environment and energy saving.

A clearer representation of the temperature distribution in the vertical direction, is given in Figure 5-11 along four vertical poles passing through the monitoring points, 1, 2, 3 and 4 (see Figure 5-9 a). From this figure, it is possible to note that the temperature difference between the upper and lower parts of the room was reduced by using the LEVO system. This was due to the fact that the LEVO system extracted the warm air generated by the room heat sources locally at the work station before mixing with the rest of the room air. Similar findings were reported in Chapter 4. This process contributed to reducing the temperature differences between the upper and the lower parts of the room, which subsequently created a more homogenous distribution of the temperature in the room (see Figure 5-10).



(a)



(b)

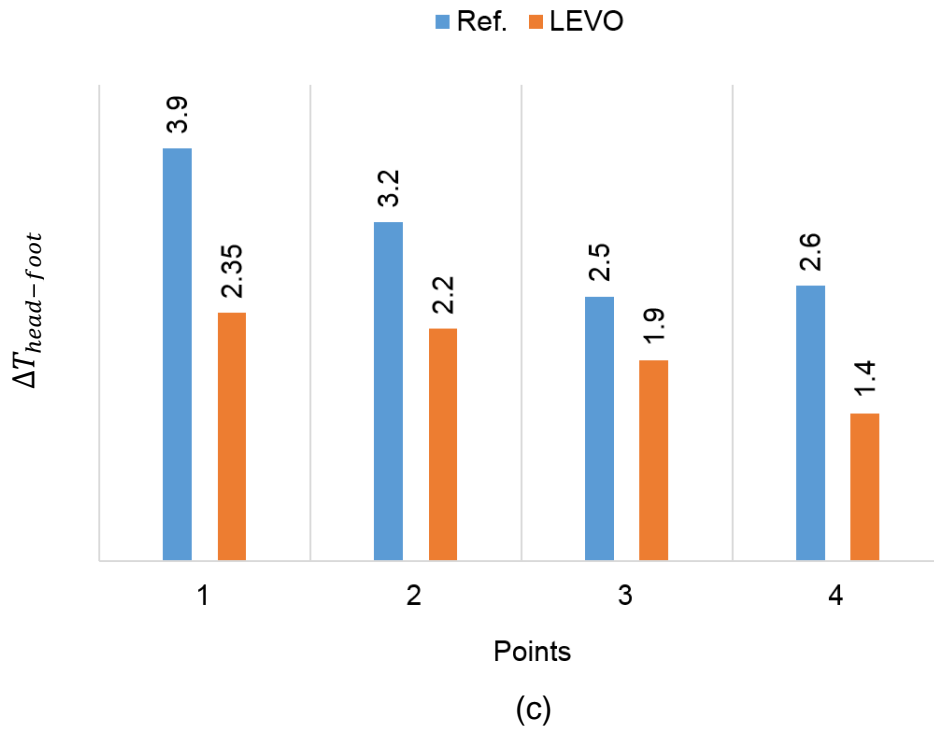
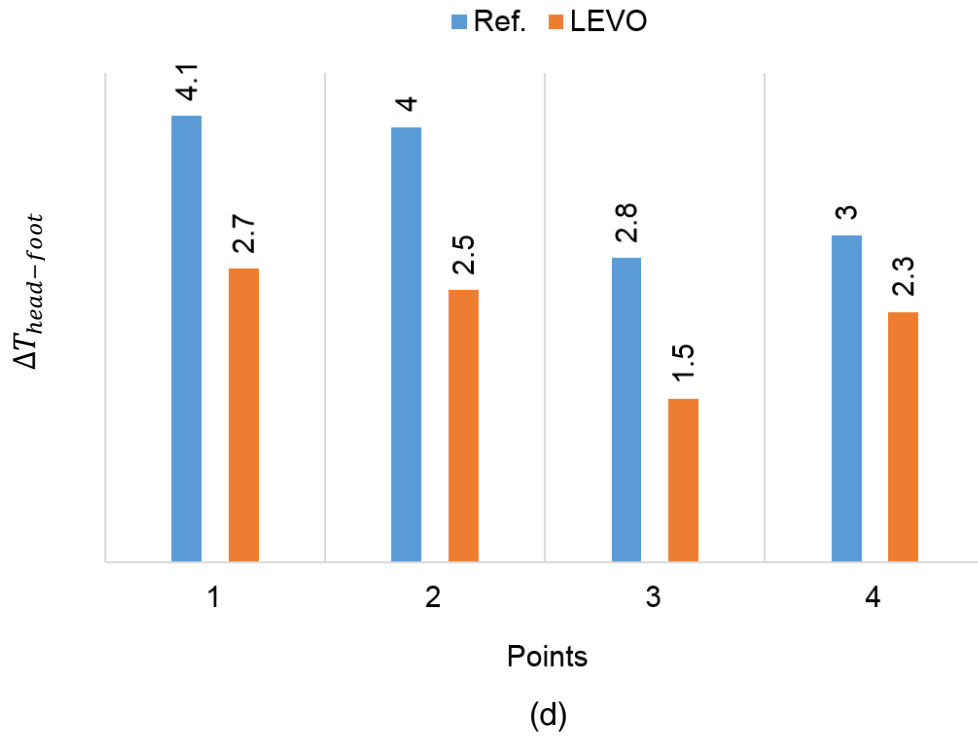
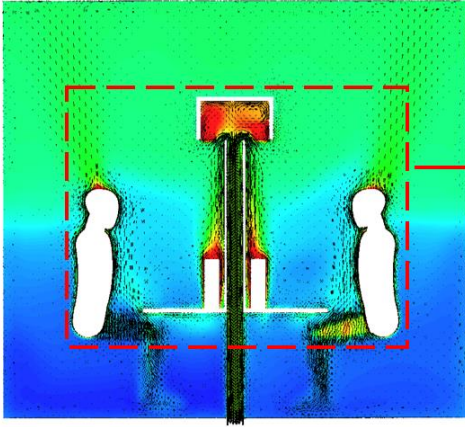
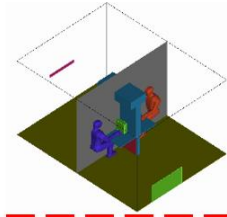
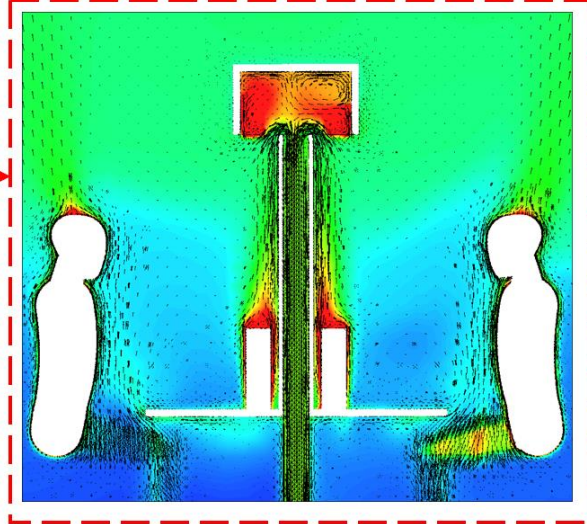


Figure 5-9: (a) Monitoring points; (b), (c) and (d) Temperature difference $\Delta T_{head-foot}$ (°C) in the vertical direction for each case study.

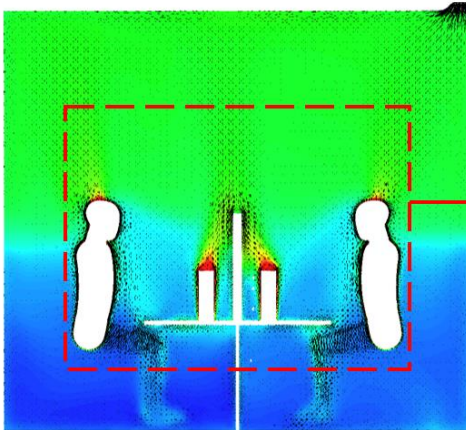
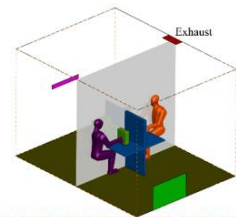
Temperature °C



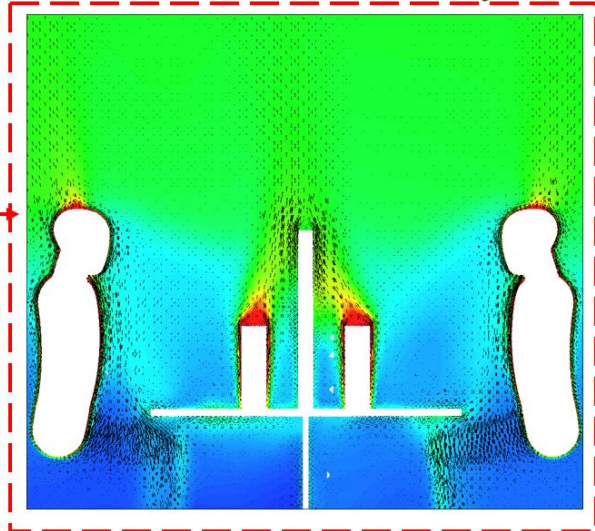
(a)



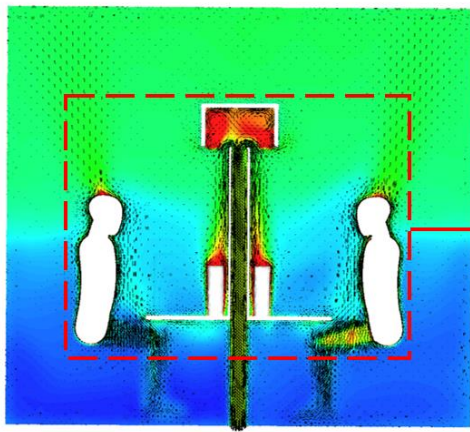
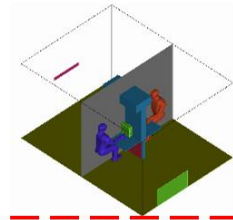
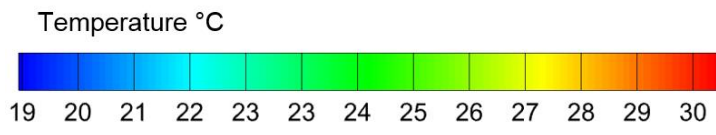
Temperature °C



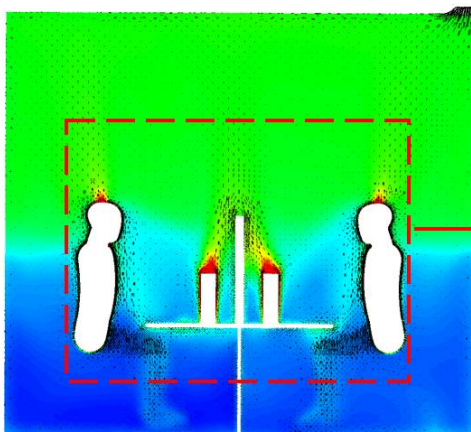
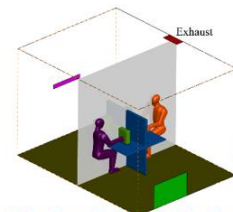
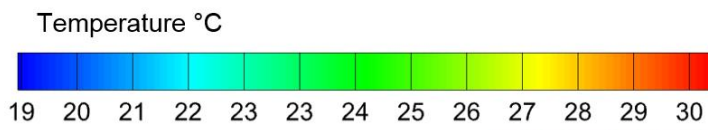
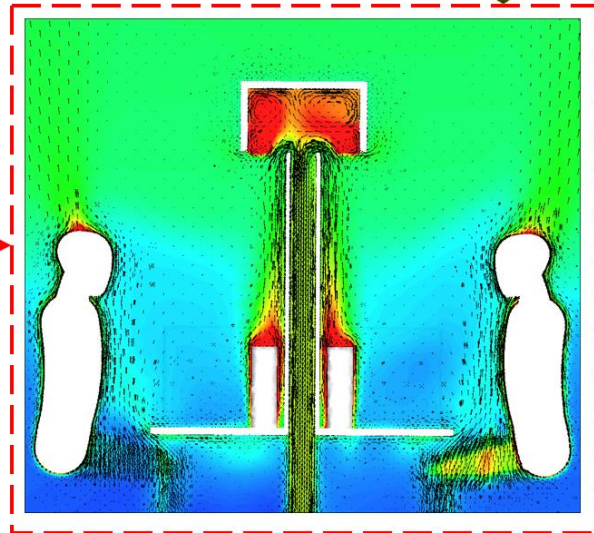
(b)



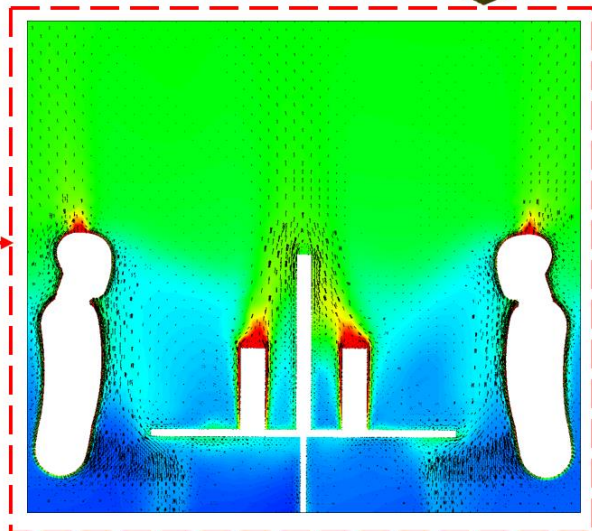
Case -1



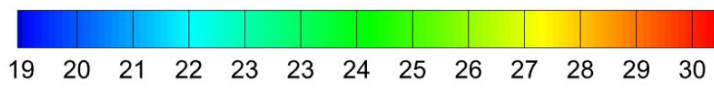
(a)



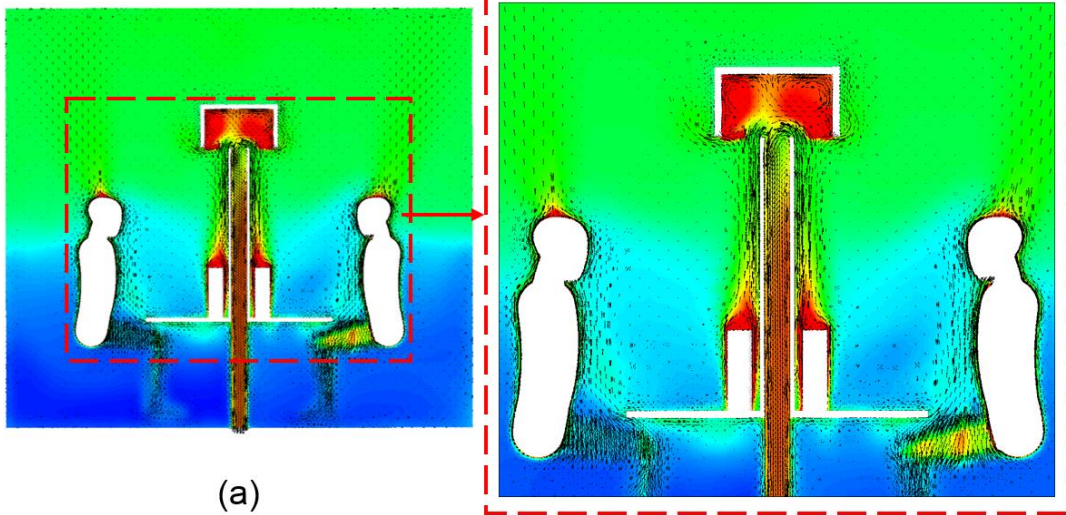
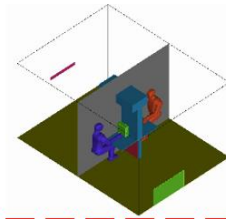
(b)



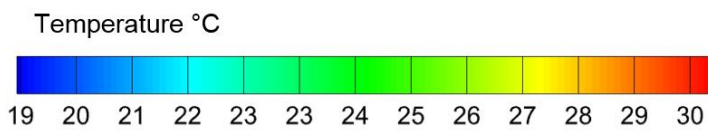
Case -2



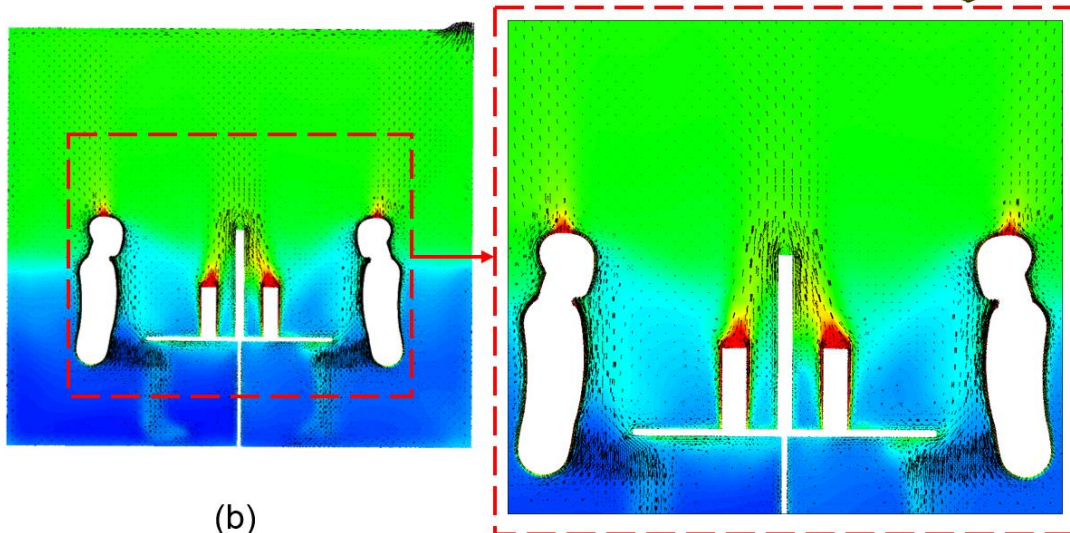
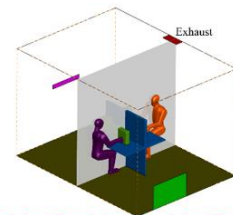
Temperature °C



(a)



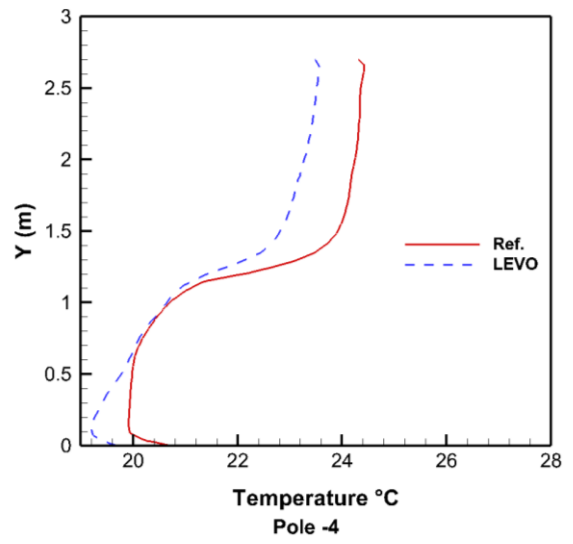
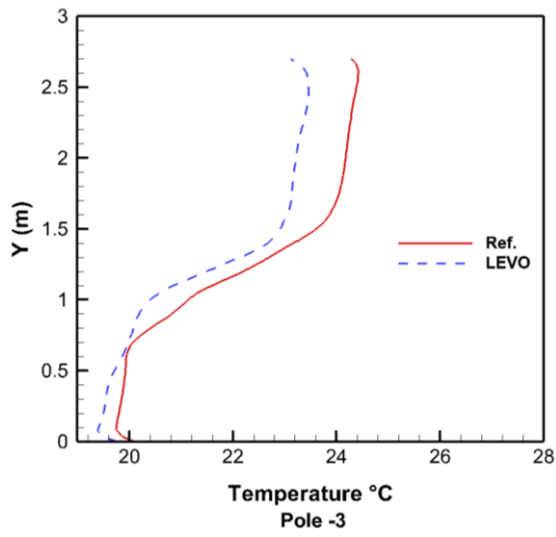
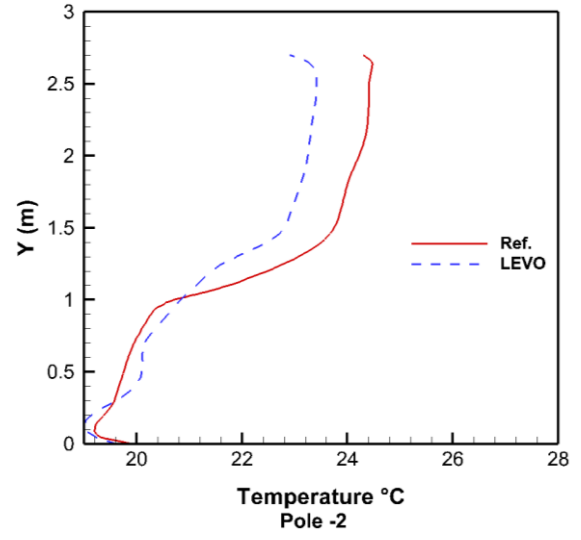
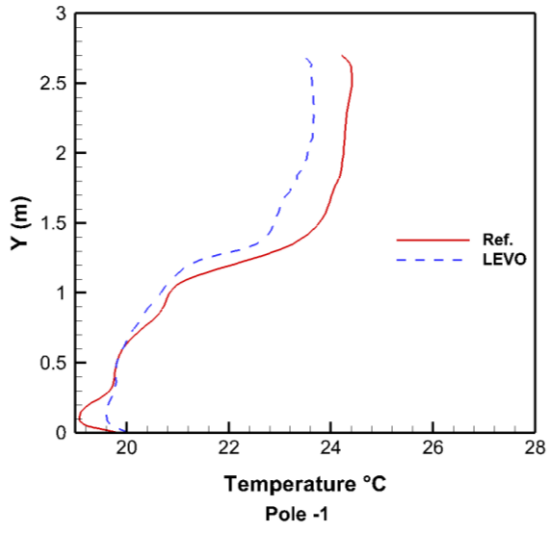
Temperature °C



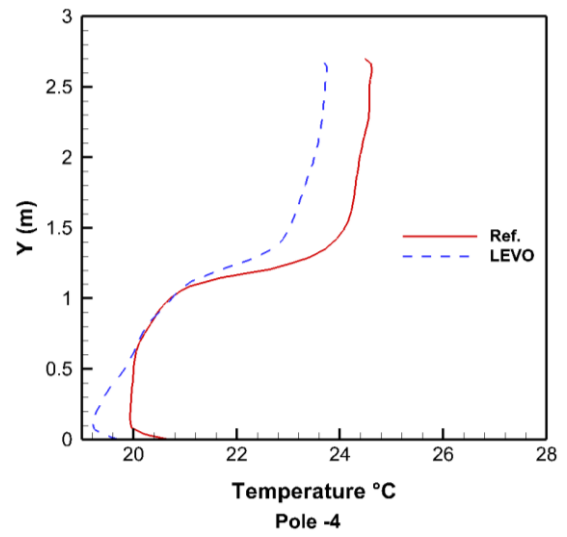
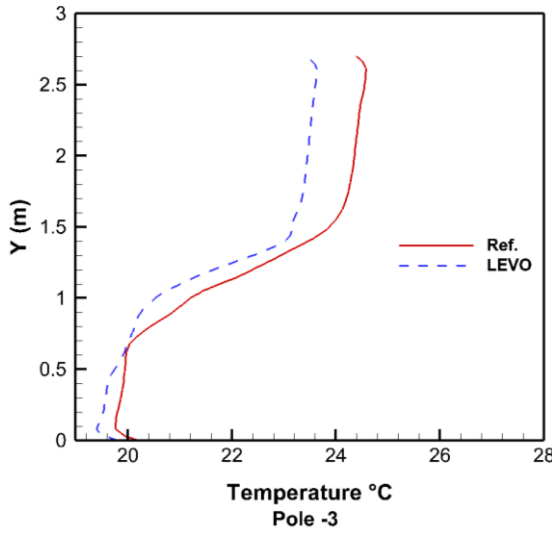
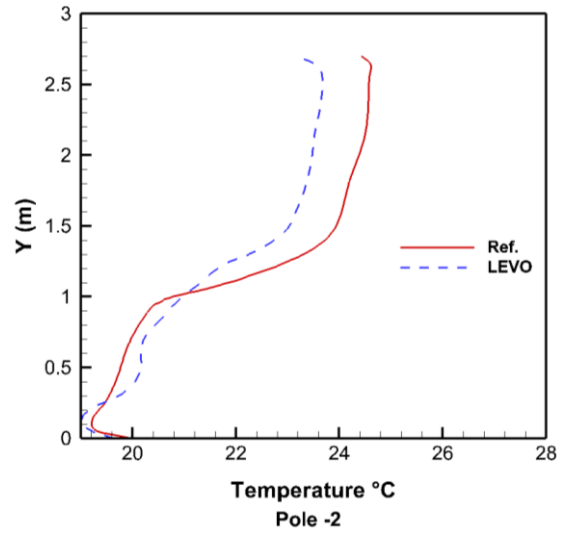
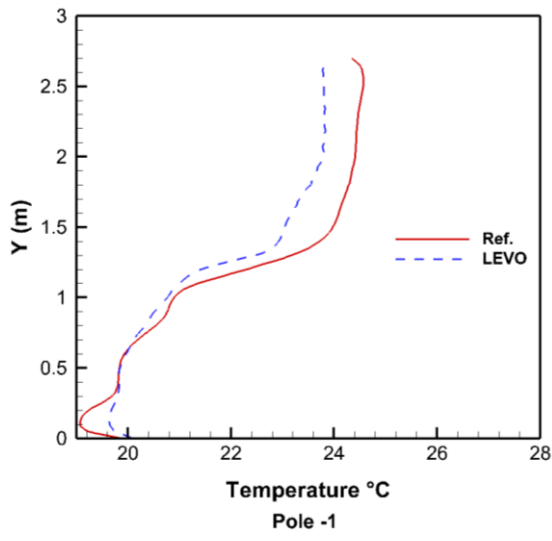
(b)

Case -3

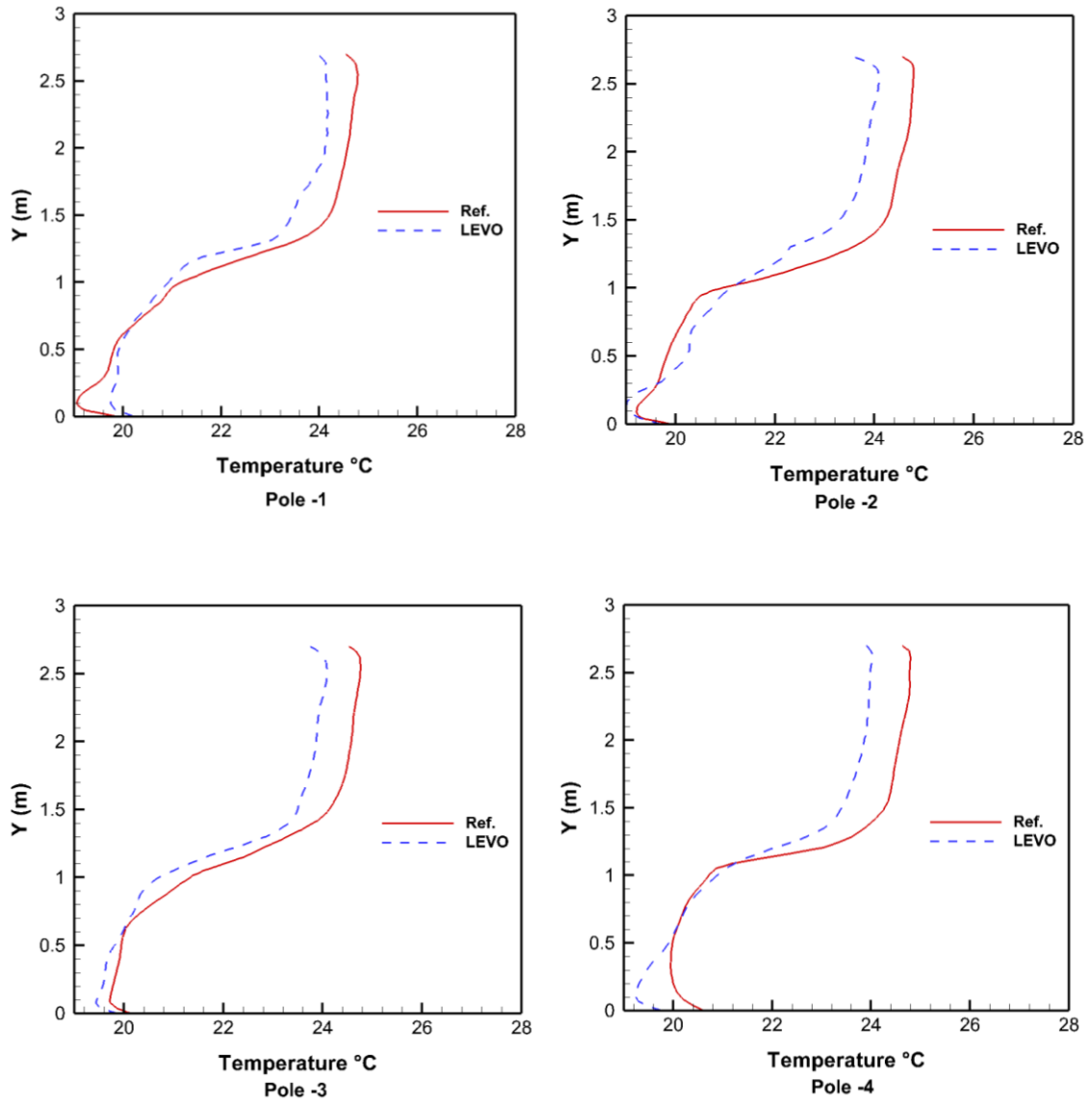
Figure 5-10: Temperature distribution °C and the airflow pattern at the mid plane (x=2m) for each case study (a) with LEVO and (b) without LEVO.



Case -1



Case -2



Case -3

Figure 5-11: Temperature gradients in the vertical direction for each case study at four different locations, pole 1, 2, 3 and 4 respectively.

5.4.3 Energy saving evaluation

The energy savings were evaluated in this study to show the impact of using the LEVO system on the energy consumption. As presented in Chapter 4, Cheng et al. [39] developed a method to evaluate the energy saving in a room using a STRAD system by calculating the reduction in the cooling coil load based on the CFD simulation results.

Table 5-4 shows the reduction in the cooling coil load for each case study. From this table it is clear to see that the amount of energy saving are proportional to the exhaust temperature (T_e) and the exhaust mass flow rate (\dot{m}_e). In cases 1, 2 and 3, a significant improvement in the energy saving was obtained in the office room using the LEVO system compared with the reference case for each case study. The enhancement in the energy saving in cases 1, 2 and 3 was calculated by comparing to the reference case (see Table 5-4). This is because the local extraction of the heat generated from the heat sources contributed to an increase in the exhaust air temperature, consequently enhancing the potential for energy saving.

As illustrated in Table 5-4, the energy saving was improved by decreasing the exhaust mass flow rate (\dot{m}_e) for cases 1, 2 and 3. Correspondingly, the energy saving increased by reducing the exhaust mass flow rate in the room with the LEVO system from 22.56 % in case 1 to 26.6% in case 2 and to 30.4 % in case 3. This is due to the fact that by increasing the exhaust mass flow-rate a small amount of fresh air may be extracted directly by the LEVO system which reduces the exhaust air temperature and subsequently reduces the energy saving. From these results, it can be concluded that the energy saving depends on the exhaust temperature and on the exhaust mass flow-rate; i.e. extra energy saving can be achieved by increasing the exhaust air temperature and decreasing the amount of the exhaust mass flow rate. In energy saving evaluation, other factors, such as the thermal comfort indices, the temperature gradient in the vertical direction, and the contaminant concentration distribution should also be considered carefully.

Table 5-4: Energy saving for cooling coil for each case study.

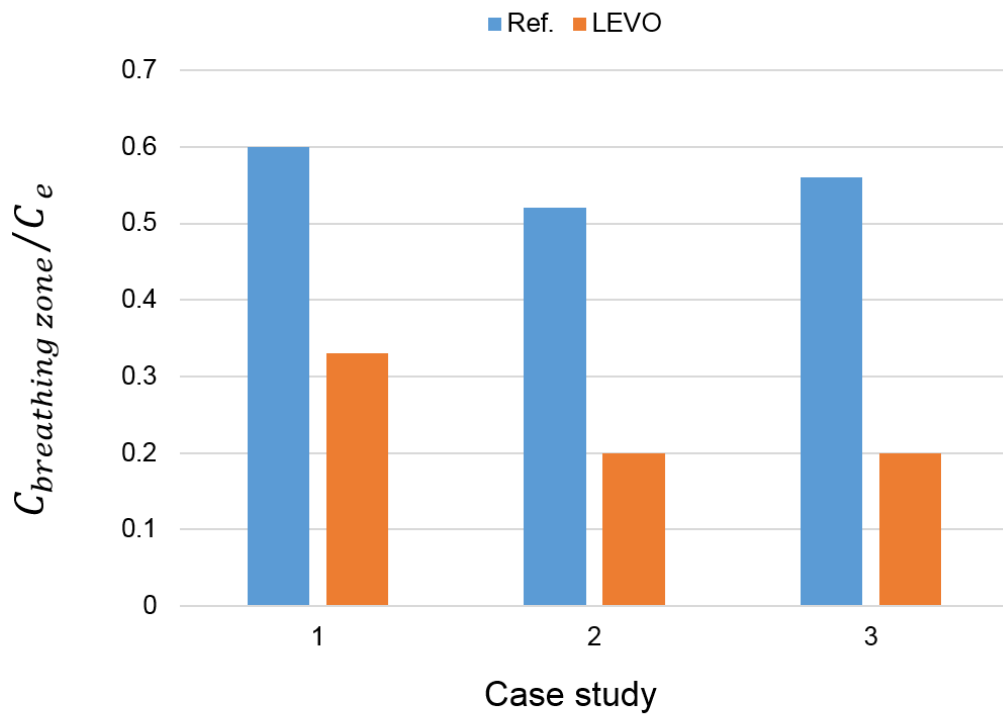
	Case_1		Case_2		Case_3	
	Ref.	LEVO	Ref.	LEVO	Ref.	LEVO
Exhaust air temperature T_{exhaust} (°C)	24.3	25.4	24.4	26.2	24.6	27.6
Return air temperature T_{return} (°C)	23.1	22.3	23.3	22.6	23.4	22.8
ΔQ_{coil} (W)	21.7	96.5	20.6	113.7	21.7	130.2
$\Delta Q_{\text{coil}}/\Delta Q_{\text{space}}$ (%)	5.07	22.56	4.8	26.6	5.0	30.4

5.4.4 The quality of the indoor air in the breathing and in the inhaled zones.

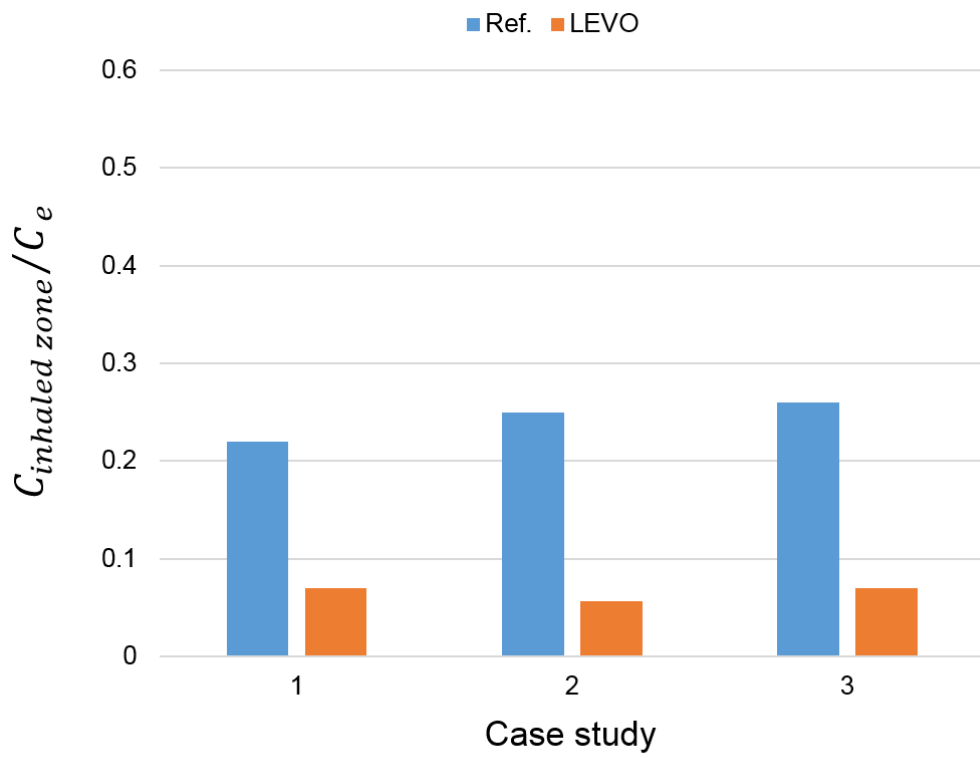
The performance of the LEVO system in terms of the quality of the air in the inhaled and in the breathing zones are discussed in this section. The quality of the occupants' inhaled air was evaluated as in Chapter 4. The air quality in the breathing zone was also evaluated. For this study, the contaminant concentration was normalised according to equation (4-14). Figure 5-12 b, c and d compare the normalised particle concentration for each case in the breathing level and in the inhaled zone respectively. From these figures, it can be noted that the quality of the indoor air was improved significantly in the room using the LEVO system in both the breathing and the inhaled zones. Figure 5-12 b shows the quality of the indoor air at the breathing level for the room with and without the LEVO system for each case study. Cases 1, 2 and 3 show that no noticeable change in the contaminant concentration with changing the return air velocity without LEVO. However, using the LEVO system enhanced the quality of the indoor air significantly (see Figure 5-12 b). This was because a large amount of the generated contaminants was extracted directly from the LEVO system before it could disperse into the breathing or the inhaled zones. In addition, the thermal plumes generated by the heat sources which are located near the LEVO system aid the extraction of contaminants in system [51].

This improved the quality of the indoor air in both the breathing and the inhalation zones (see Figure 5-12 b, c and d). In case 1, the concentration of the contaminant in the breathing level was larger than that in cases 2 and 3. The reason for this was that the mass flow rate of the exhaust in case 1 was low and this led to a reduction in the amount of extracted contaminant at the breathing level and consequently increased the contaminant concentration, compared to cases 2 and 3.

For the inhaled zone, Figure 5-12 shows that the predicted inhaled air quality for occupant 1 was better than that for occupant 2 in all cases. The reason for this is that the position of occupant 1 was located close to the DV supply. The velocity of the supply air was therefore able to drive the contaminant away from the inhaled zone of occupant 1, which helped improve the air quality in this zone compared to occupant 2. This is consistent with the findings reported by Sadrizadeh and Holmberg [163]. From these results it can be concluded that by using the LEVO system the quality of the indoor air in the breathing zone is improved compared to the reference case (see Figure 5-12 a). Furthermore, compared with the reference case, the use of the LEVO system contributes to reducing the contaminant concentration in the inhaled zone for both occupants (see Figure 5-12 b and c).



(a)



(b)

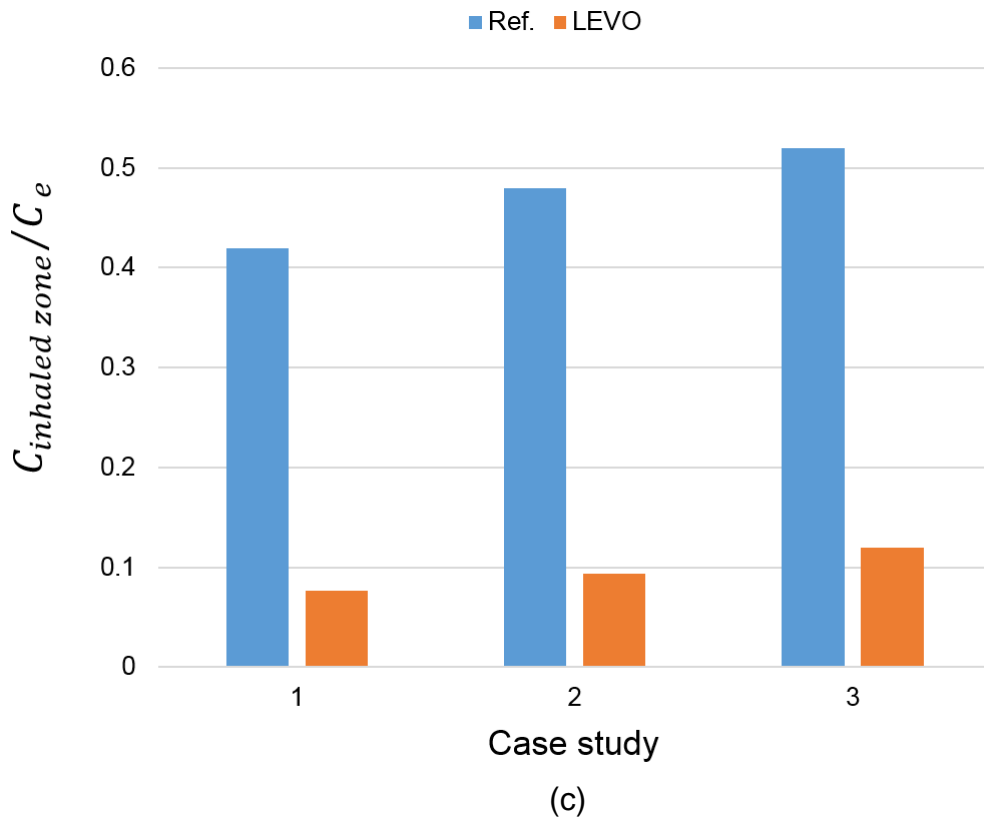


Figure 5-12: Comparison of the quality of indoor air for each case study; (a) contaminant concentration at breathing level; (b) and (c) the inhaled air quality for occupant_1 and occupant_2 respectively.

Chapter 6 Height Impact of the New Local Exhaust System

6.1 Introduction

Chapters 4 and 5, have shown that the exhaust opening location has a significant impact on the thermal environment indoors and on the energy saving. In order to evaluate the performance of any new ventilation system, the exhaust outlet location should be considered carefully. In Chapter 5, the local exhaust ventilation system concept was adopted and developed for use in an office spaces, where the exhaust opening was combined with the office workstation in a single unit, and it's called LEVO system. This new system, the LEVO system, helped to extract the warmed and contaminated air locally before it can disperse to the rest of the room and provides a localised but comfortable environment for any occupants whilst realising a lower energy consumption than conventional DV system. Further investigation is required to select the best height of the exhaust opening for the LEVO system, which may have a significant impact on the local thermal comfort and on the energy savings provided by the proposed system. Therefore, in this chapter, the performance of the new system was assessed using three different heights for the exhaust opening (1.4 m, 1.6 m and 2.0 m from the floor level), the results of which are compared against a conventional DV system. The background to the investigated case is presented in the first part of this chapter. The validated CFD model, which was used in the previous chapters, Chapter 5 and 4, are also used in this investigation. Thereafter, mesh independence tests are performed and presented. Finally, the impact of the LEVO system heights on both the indoor environment and on the energy savings is discussed.

6.2 Background to the investigated case

As presented in the previous chapter, Chapter 5, the new LEVO air distribution system aims to generate energy savings while improving the local thermal environment in the regions around the occupants by removing from these regions the heat emitted from the room heat sources and the contaminants. The concept of combining the heat sources of the office workstation with an exhaust opening was investigated in Chapter 5.

In this chapter, a further investigation is conducted to study the effect of the height of the combined system on the local thermal environment, specifically on the thermal comfort, the inhaled air quality and on the energy consumption. Therefore, a comparative study was performed to analyse the effect on the energy consumption and on the indoor thermal comfort with and without the LEVO system. In the LEV system concept, the exhaust opening should be close to the contaminant sources [49, 50, 64, 84]. Since this investigation aims to provide a local and comfortable thermal environment for the occupants by a LEVO system, the exhaust opening locations in relation to the room heat sources should be considered carefully. Therefore, three different heights of the combined system, 1.4 m, 1.6 m and 2.0 m from the floor level, are investigated (see Table 6-1). The same room geometry of Chapter 5 is used in this investigation. Figure 6-1 shows schematically the change in the height of the proposed LEVO.

Table 6-1: Case studies

Case study	Heights of the combined system from floor level
Case 1	Reference case (without LEVO system)
Case 2	1.4 m
Case 3	1.6 m
Case 4	2.0 m

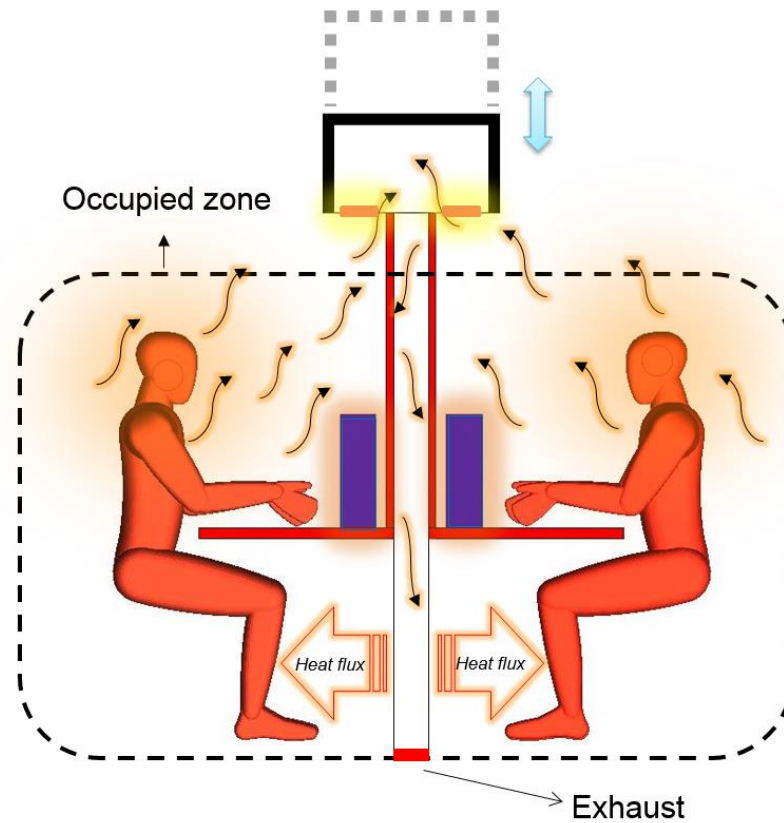


Figure 6-1: The LEVO system operation and flow direction at three investigated heights.

6.3 Mesh generation and independence test

The same tetrahedral unstructured mesh approach of Chapter 5 is used to discretize the computational domain, as shown in Figure 6-2. As a result of the similar geometry and boundary conditions, the meshes used in this study are similar to the meshes used in Chapter 5. All other detailed information can be found in Chapter 5. A grid independence test was also performed in this chapter to select an appropriate mesh size and to make sure that the selected mesh was fine enough to adequately resolve the mass and heat convection without introducing mesh artefacts. Based on the grid test, the total number of cells was set at 2,753,932, which would remain the mesh size for all further simulations.

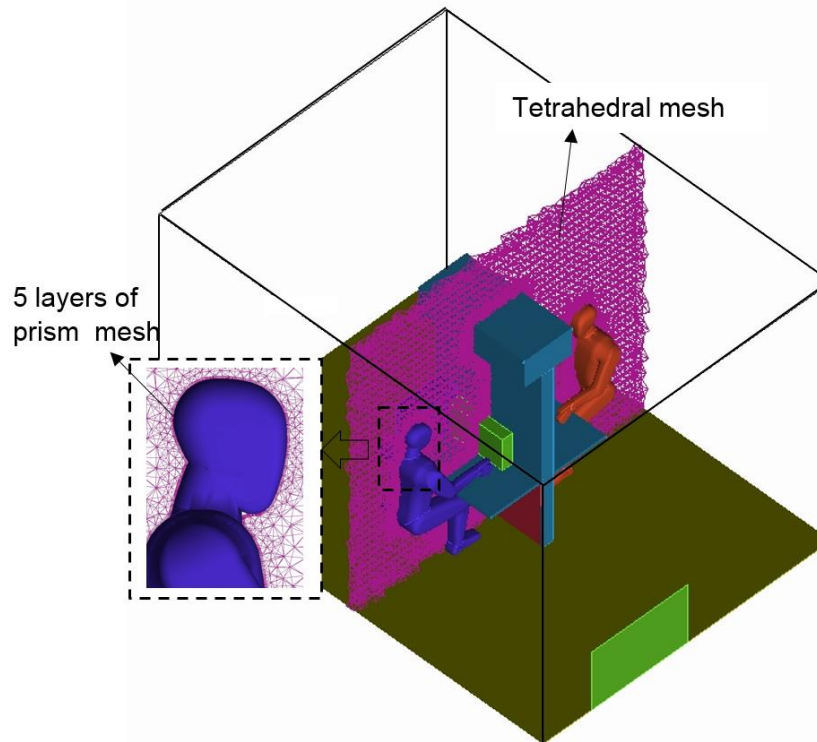
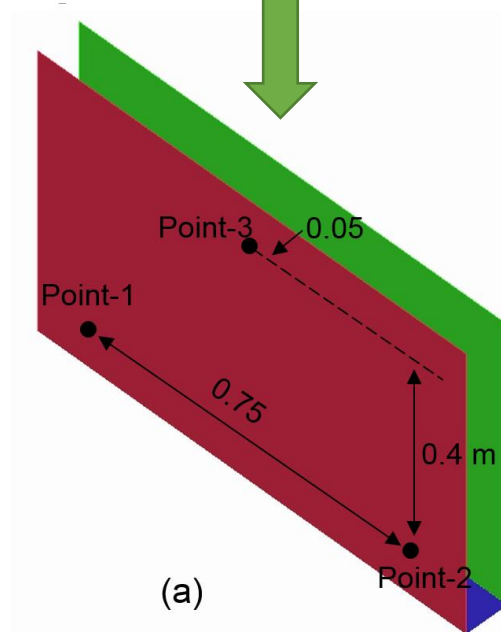
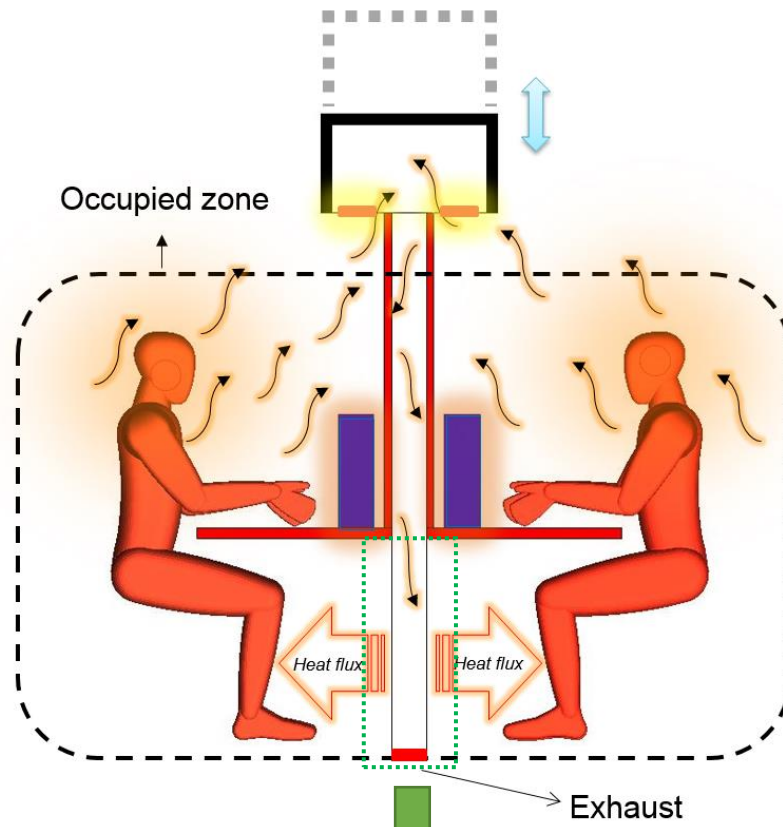


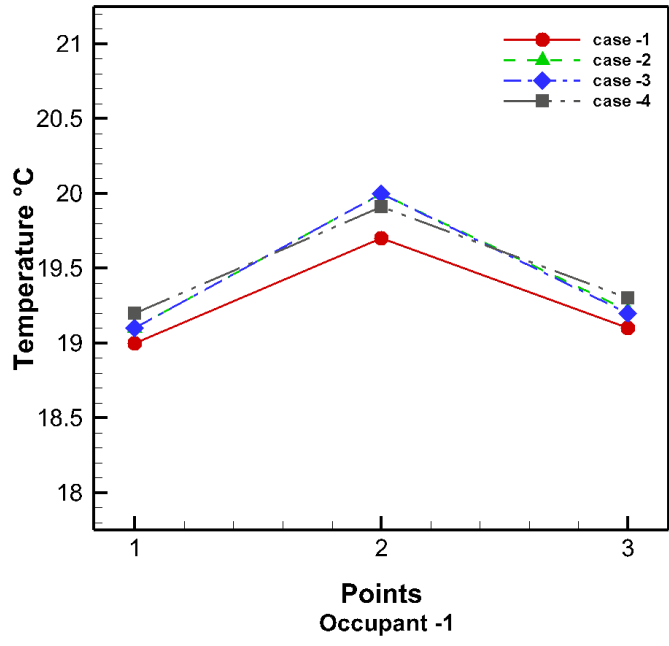
Figure 6-2: Inflation boundary layer around the human body.

6.4 Results and discussion

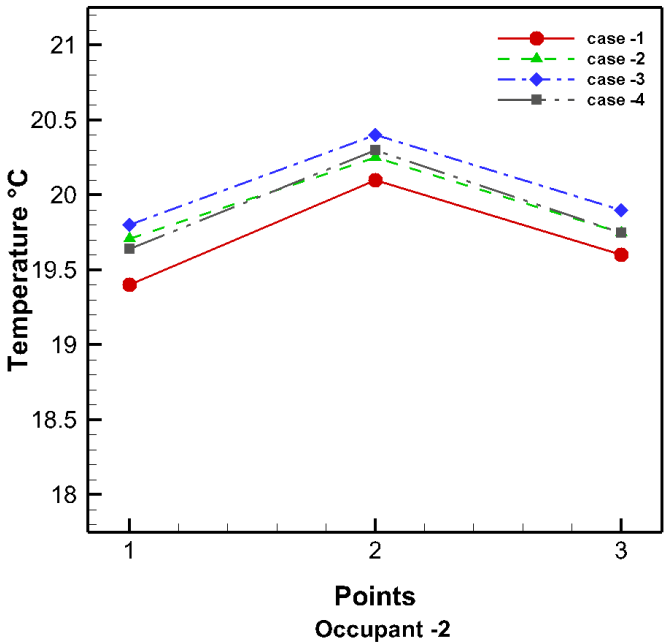
6.4.1 Temperature distribution near the foot zone

As shown in Figure 6-3 a, three monitoring points, points 1, 2 and 3, in the foot zone are used to evaluate the air temperature in various regions for each case study listed in Table 6-1 and for occupant_1 and occupant_2. Figure 6-3 b and c show the calculated air temperatures for all three monitoring points. These figures show that by changing the height of the exhaust opening, there is no noticeable difference in the air temperature values for case 2, 3 and 4 for occupant-1, though for occupant-2, the air temperature in case-3 is slightly higher than in the other case studies. This is due to the position of occupant 2 being slightly further away from the inlet opening.





(b)

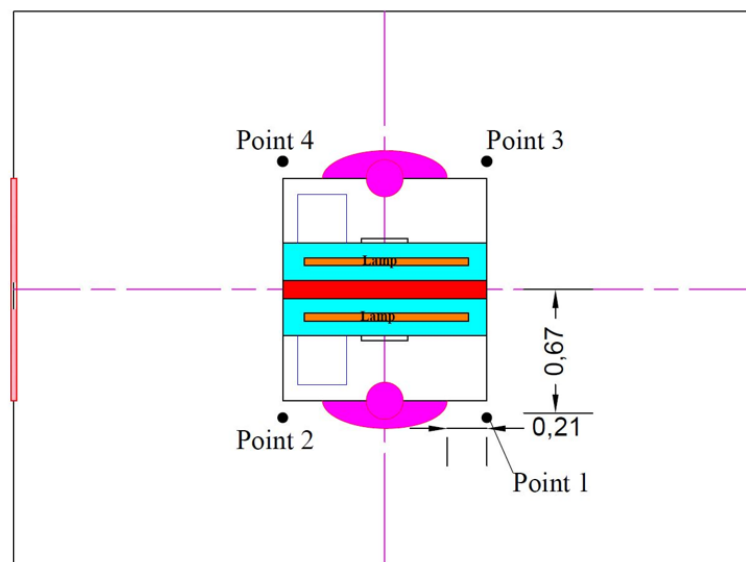


(c)

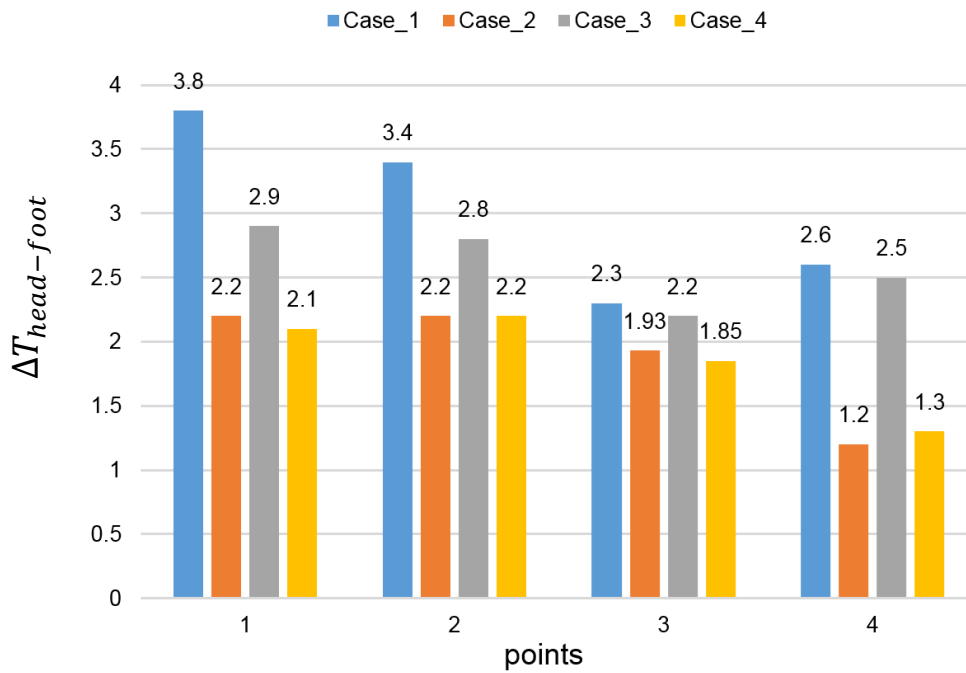
Figure 6-3: (a) Three monitoring points, points 1, 2 and 3, for each case study and (b) and (c) temperature distribution (°C) of the near foot zone for occupant_1 and occupant_2 respectively.

6.4.2 Occupants thermal discomfort evaluation

As explained previously, the temperature difference between the head and foot level should not be more than 3 °C [21]. In this chapter, the human thermal discomfort is evaluated for all case studies. Figure 6-4 a shows the locations of four poles through points 1, 2, 3 and 4, two being near each occupant. Figure 6-4 b shows the predicted vertical temperature difference at $\Delta T_{head-foot}$ for all case studies. Cases 2 and 4, are predicted to give the lowest $\Delta T_{head-foot}$ at all four poles. Although the thermal comfort was satisfactory, with $\Delta T_{head-foot} < 3^{\circ}\text{C}$ in all cases when the new LEVO system was used, case 3, which uses an exhaust opening at 1.6 m above the floor level, shows a higher temperature difference ($\Delta T_{head-foot}$) compared to cases 2 and 4. This was because by placing the extractor at 1.6 m high, the greatest amount of the warmed air generated by the office workstation is directly extracted before it disperses to the rest of the room, and it is directed towards the foot zone. This amount of extracted heat from the region around the head level is large enough to cause a larger $\Delta T_{head-foot}$ compared with cases 2 and 4.



(a)

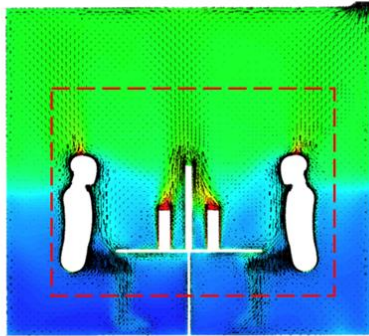
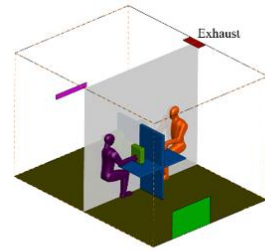
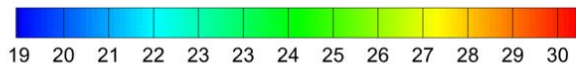


(b)

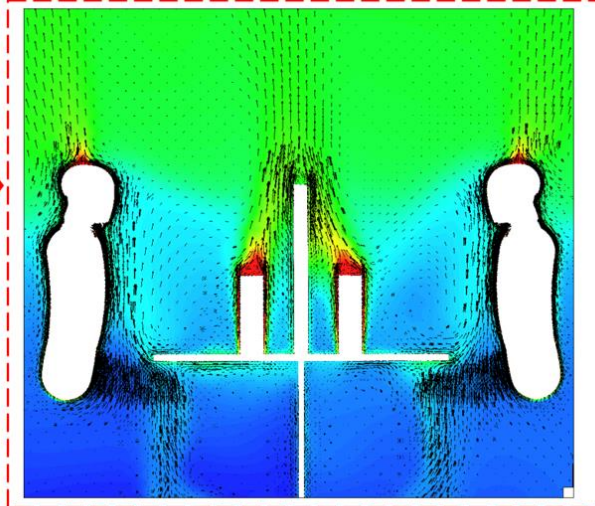
Figure 6-4: (a) Monitoring points; (b) Temperature difference in the vertical direction for each case study at four poles.

Figure 6-5 shows the temperature distributions and the airflow pattern for all case studies. In case 2, where the exhaust of the combined system is 1.4 m above the floor level, the temperature distributions and the airflow pattern are more homogeneous than in cases 3 and 4. By increasing the height of the combined exhaust to 1.6 and then to 2.0 m, as in cases 3 and 4, the temperature distributions and the airflow pattern are predicted to become less homogeneous than in case 1. This was due to the fact that case 1 did not allow the generated thermal plumes to keep developing and thus disturb the flow in the rest of the room domain. The LEVO system decreased the temperature in the upper part of the room by extracting most of the generated heat. This will create a different air stratification for each case. In case 4, the more of the heat generated in the occupied zone may escape before it is extracted by the LEVO system, compared to the heat that is extracted from the upper part of the room in case 3. For this reason, the combined system in case 4 seems slightly less warm than in cases 2 and 3 (see Figure 6-5).

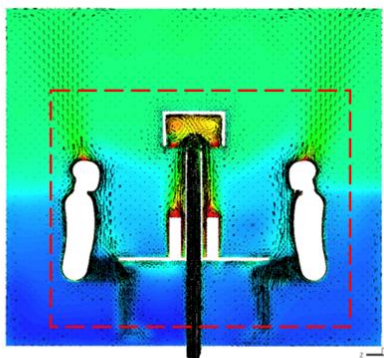
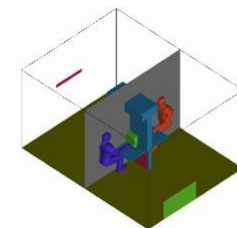
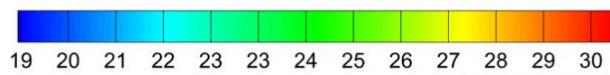
Temperature °C



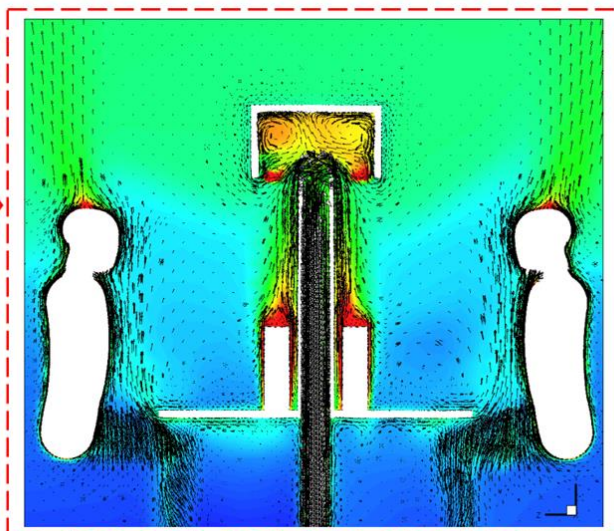
Case-1



Temperature °C



Case-2



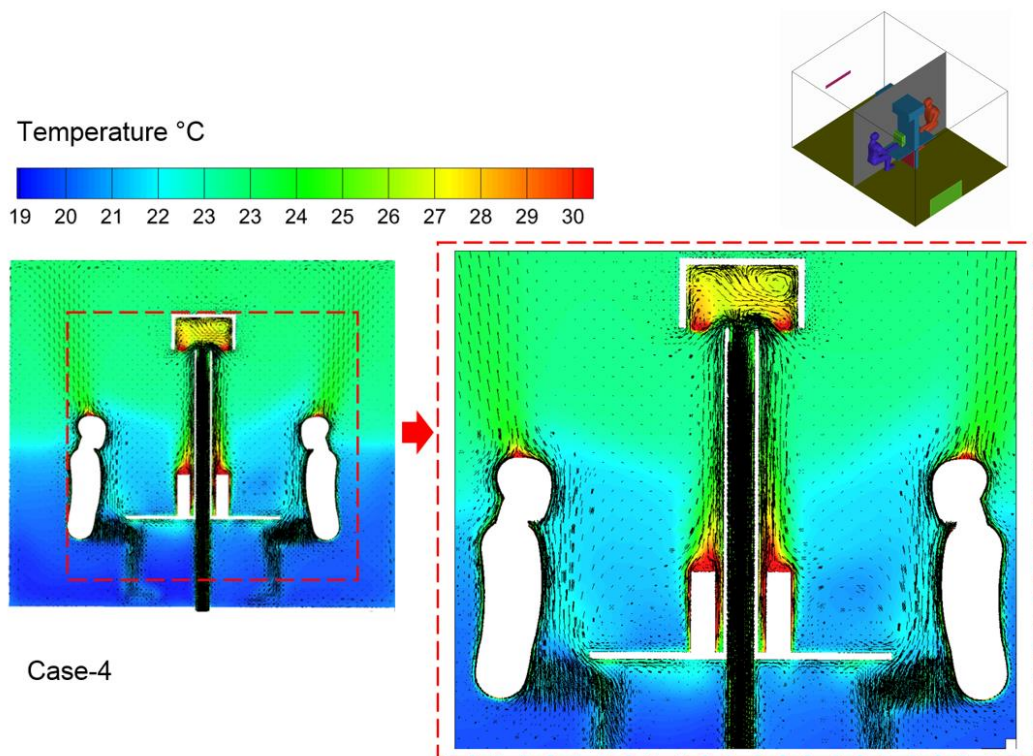
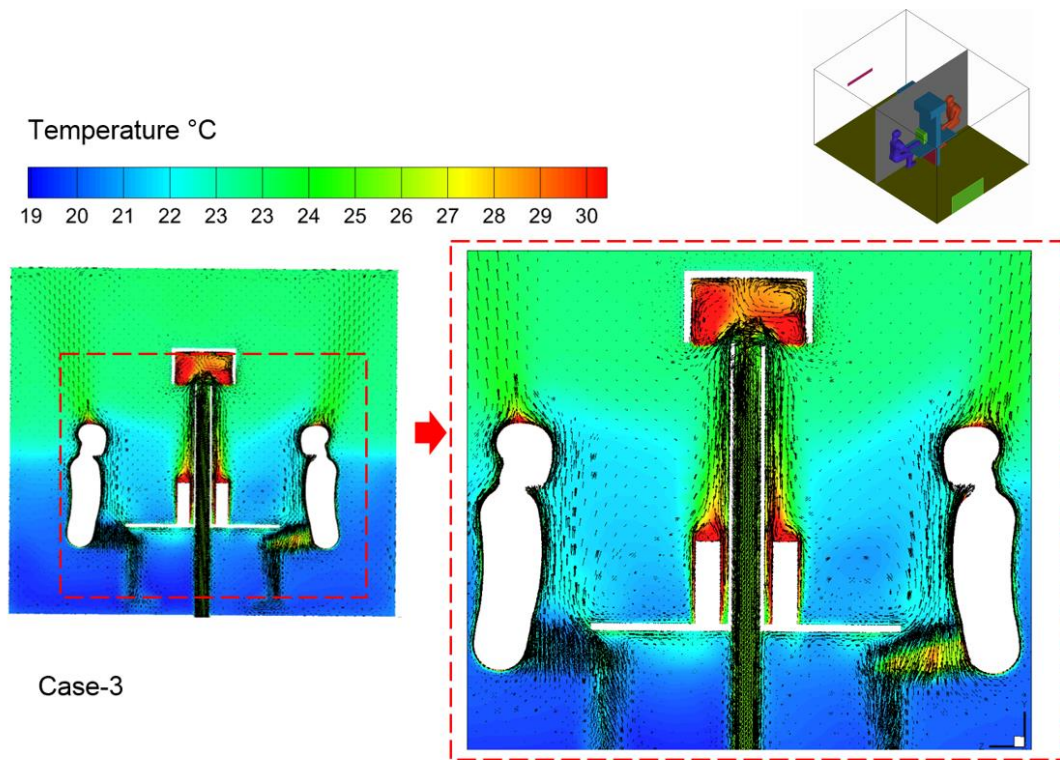


Figure 6-5: Temperature distributions and the airflow pattern in the middle plane ($x = 2$ m) for each case study.

6.4.3 Draught risk evaluation

Draught is an undesired local overcooling of the occupants caused by the airflow [164] and it is considered as one of the most common and significant problems in indoor spaces. This problem can occur when the fresh and cool air is supplied directly to the occupied zone at the floor level, as in DV systems [165]. In any ventilation system, the risk of draught is a major issue that needs to be evaluated to ensure of the ventilation system is able to provide an acceptable thermal comfort. Draught risk can be measured by the percentage of dissatisfied people due to the draught (PD), which should ideally not exceed 20 % (the maximum allowable value) [166]. Therefore, in any ventilation system, the PD values, particularly in the occupied zone, should be considered carefully. In this study, the PD analysis was carried out for all case studies for each occupant. The PD evaluation was performed at the ankle level (0.1 m from the floor). This level 'contains' the most important parts of the occupants' bodies in terms of feeling the sensation of draught, and consequently, the highest draught risk has been identified as being at this level [167-169].

In this study, PD was evaluated by using Fanger's equation [164]:

$$PD = (34 - T)(u - 0.05)^{0.62} (3.14 + 0.37 u TU) \quad (6-1)$$

for $u < 0.05$, use $u = 0.05$ m/sec

for $PD > 100\%$, use $PD = 100\%$

where T and u are the air temperature and the low-averaged air speed, respectively.

TU is the air turbulent intensity, which is determined by:

$$T_u = 100 \frac{(2k)^{0.5}}{u} \quad (6-2)$$

where k is the turbulent kinetic energy, which itself is defined as:

$$k = 1.5 (u T_u)^2 \quad (6-3)$$

Figure 6-6 shows the results of the PD evaluation in all case studies. These results indicate that there is no significant difference in the PD for either occupant

in all case studies. However, the draught risk was slightly increased when using the proposed LEVO system, as in case 2, 3 and 4 when compared with case 1 (No LEVO system was used). This was because the local extraction of air can increase the air movement in the occupant zone, consequently increasing the draught risk. Furthermore, for all case studies, the PD values for occupant -1 were higher than those for occupant -2. This was because the location of occupant -1 was directly in front of the DV supply diffuser. This can result in direct 'contact' between occupant -1 and the supply air (supply velocity and temperature). All in all, the draught risk in all case studies fell within the acceptance range, and did not exceed the maximum allowable value of 20% [166].

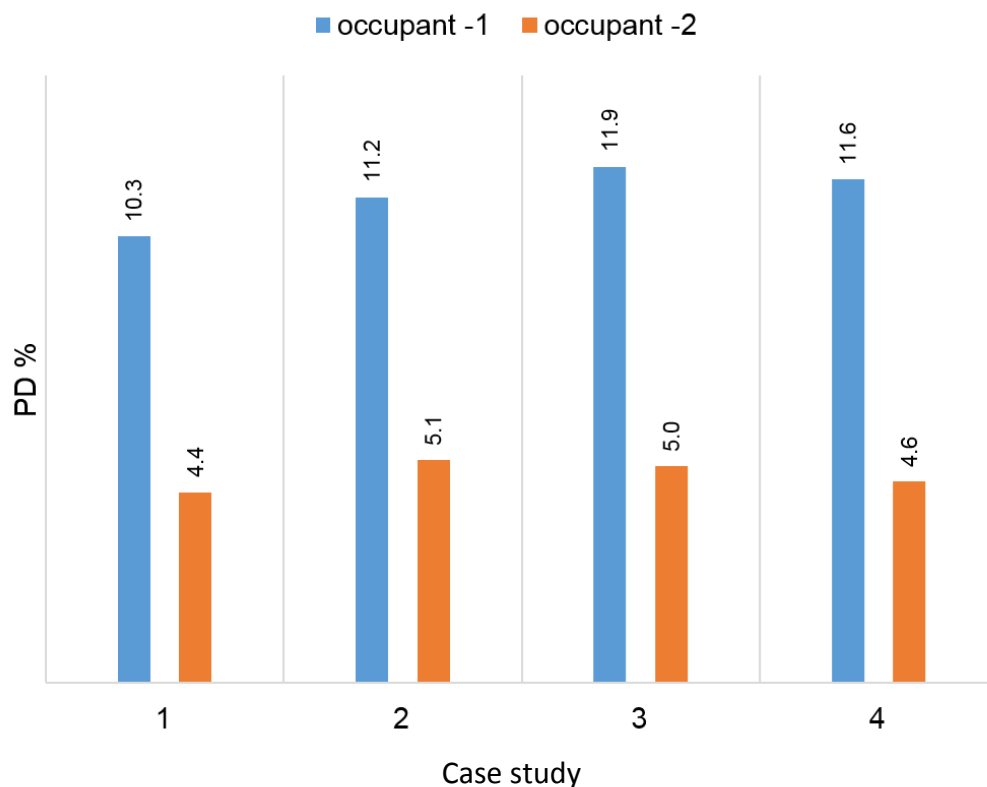


Figure 6-6: Comparison of the PD values for both occupants in each case study.

6.4.4 Energy saving evaluation

For any ventilation system, the energy consumption evaluation is considered one of the principle evaluation indices. The reduction in the cooling coil load and the associated energy savings which are explained and used in Chapters 5 and 6 are also used in this chapter to evaluate the effect of the LEVO height on the energy saving [161, 170, 171]. The energy saving for the cooling coil for each case study is presented in Table 6-2.

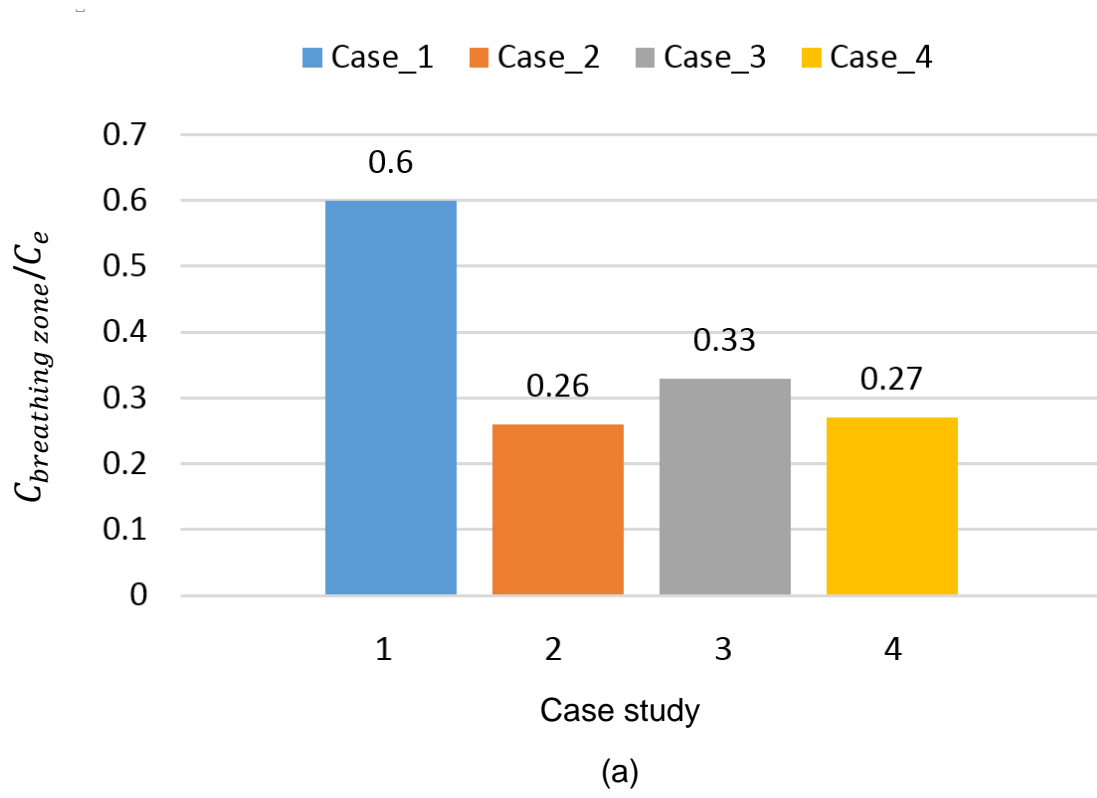
Table 6-2: Energy saving for the cooling coil for each case study.

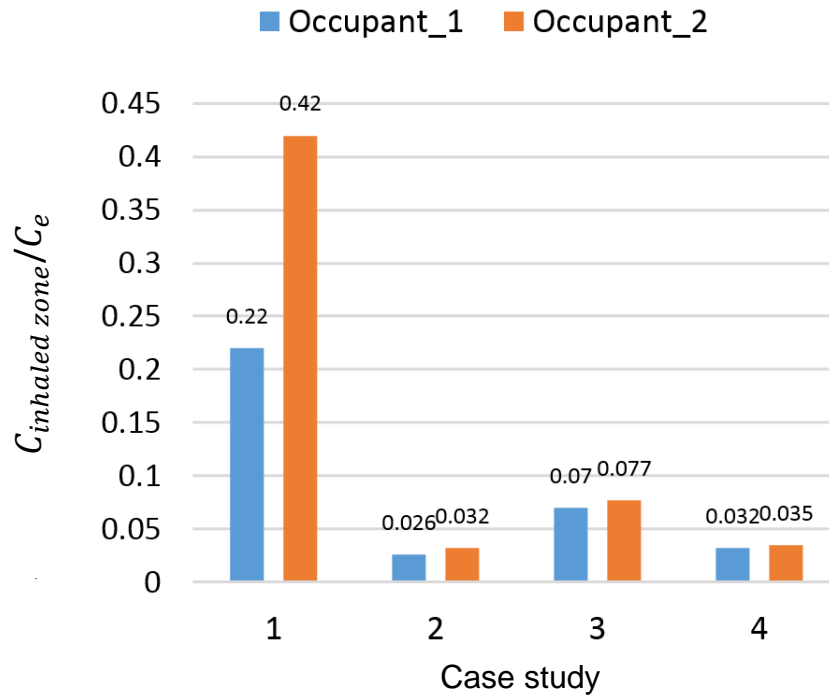
	Case_1	Case_2	Case_3	Case_4
Exhaust air temperature T_{exhaust} (°C)	24.3	25	25.4	25.1
Return air temperature T_{return} (°C)	23.1	22.35	22.3	22.35
ΔQ_{coil} (W)	21.7	70	96.5	75.84
$\Delta Q_{\text{coil}}/\Delta Q_{\text{space}}$ (%)	5.07	16.1	22.56	17.8

These results indicate that the energy saving $\Delta Q_{\text{coil}}/\Delta Q_{\text{space}}$ improves significantly in the room using the LEVO system for cases 2, 3 and 4, as compared with the reference case for which the results from Chapter 5 are used. As shown in Table 6-2, case 3 was the best in terms of saving energy with a 22.56% coil load reduction, compared with 5.07% in case 1, 16.1% in case 2, and 17.8 % in case 4. The reason is that, that compared with cases 1, 2 and 4, case 3 extracted the largest amount of generated heat as the 1.6 m height of the LEVO extractor did not allow a large amount of warmed air to diffuse to the rest of the room. Thus, to improve the energy saving, an appropriate height for the LEVO system needs to be carefully selected. In the assessment of energy saving, other factors, such as the temperature profile distribution in the vertical direction and the air quality in the occupied zone, should also be considered carefully.

6.4.5 The quality of the indoor air in the breathing and inhaled zones

In this section, the quality of the inhaled air is evaluated as in Chapter 5, in a 0.5 m cube region around each occupant's head. By the same procedure used in Chapters 4 and 5, the quality of the indoor air in the breathing zone was also evaluated. Figure 6-7 a and b show the normalised particle concentration in the breathing and the inhaled zones, respectively, for each case study. These figures, indicate an improvement in the quality of the indoor air in both the inhaled and the breathing zones using the LEVO system for cases 2, 3 and 4, compared with the reference case 1. This was because more than 50% of the contaminants generated by the equipment and by the occupants' activities was extracted locally and directly via the LEVO system before it could disperse into the occupied zone, which is the same influence stated in Chapter 5. By comparing case 3 with cases 2 and 4, it is clear that in case 3, when the combined exhaust was located at the height of 1.6 m, a higher contaminant concentration was observed compared with cases 2 and 4. This was because at this height, a certain amount of contaminant escaped and was dispersed directly into the inhaled air, which consequently increased the contaminant distribution concentration in the inhaled zone. In addition, the contaminants are probably not neutrally buoyant and therefore may take different path than that of the warmed air, which is best extracted with a 1.6 m exhaust. However, in this case, case 3, the room air quality is still in the acceptance range. From these results, it can be concluded that by using the LEVO system, the quality of the indoor air in the breathing zone was enhanced significantly compared to the reference case. Also, the quality of the indoor air was influenced by the height of the combined exhaust opening in the room that used the LEVO system.





(b)

Figure 6-7: Comparison of the quality of indoor air for each case study; (a) contaminant concentration at the breathing level; (b) the inhaled air quality for both occupants.

Chapter 7 The Air Turbulence and Flow Behaviours for the Combined System Using RANS Modelling and LES

7.1 Introduction

The incorporation of exhaust openings into ceiling lamps in a combined system was modelled in Chapter 4. For such systems, detailed modelling of the airflow and of the temperature distribution is required for a better understanding of how these develop with time. Therefore, in this chapter, the LES method is employed and its results are compared with the RANS model which was presented in Chapter 4. The background to the investigated case is presented in the first part of this chapter. A brief description of the LES method is then presented in this chapter. The mesh design for the LES method is then described. After that, in order to ensure the validity of the prediction model (LES), the simulation results for the temperature and velocity distributions derived from the LES and RANS predictions are compared with the previous experimental results. In the last part of this chapter, the turbulent flow predictions and its temperature distribution in the investigated room are discussed to demonstrate the advantages of using LES for modelling.

7.2 Background to the investigated case

As in Chapter 4, a numerical study is performed to investigate the influence of the location of exhaust diffusers in relation to the internal heat sources on the indoor thermal environment and the energy saving. Five different locations for the exhaust diffusers are tested in an office served by a DV system. The room geometry, dimensions, the internal heat sources and the room arrangement are the same as the ones in section 4.2.1 of Chapter 4. The configuration of the simulated room and the arrangement of the equipment within the simulated office are presented in Figure 7-1. In this investigation, the flow behaviour around the occupants in zones 1 and 2 (see Figure 7-1) has a significant impact on the comfort of the local environment. For this reason, zones 1 and 2 will be considered carefully in this chapter.

Overall, as stated in Chapter 4, in the combined system an improvement in both the indoor thermal environment and in the energy savings was achieved in the instance of combining the ceiling lamps with the exhaust diffusers at ceiling level [161]. In order to understand the airflow and temperature development indoors and how the flow behaviour was altered near the heat sources, the instantaneous velocity and temperature distributions, as well as the turbulent flow characteristics, are considered to be of particular importance. The RANS model of Chapter 4 does not resolve the instantaneous flow field inside and is inadequate to analyse the two dependent flow behaviour. For these reasons, a further investigation is performed using LES in the current chapter.

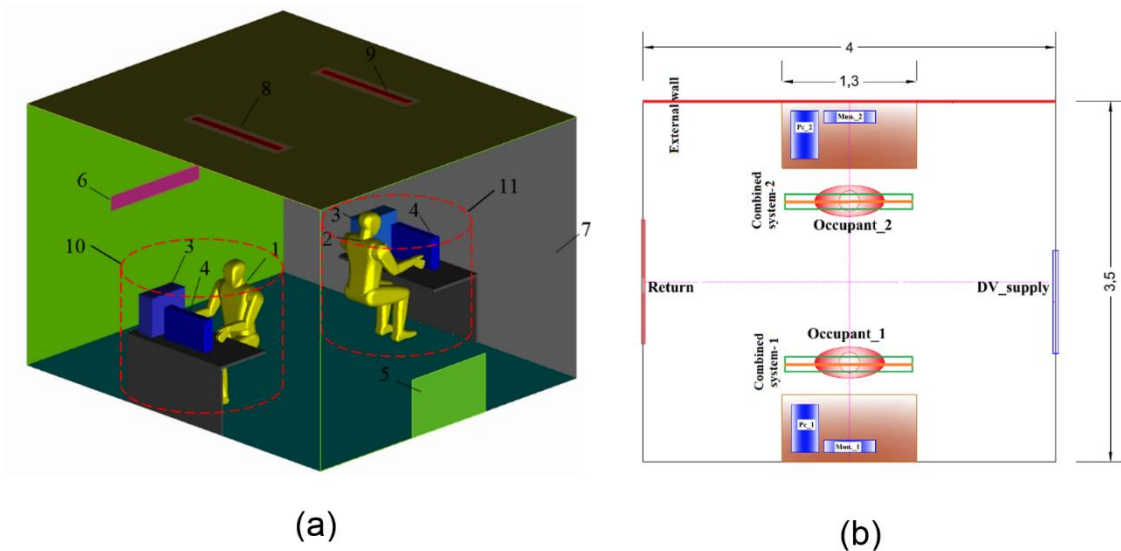


Figure 7-1: (a) The configuration of the simulated room: 1 – occupant_1; 2 – occupant_2; 3 – PC case; 4 – PC monitor; 5 – displacement ventilation (DV) inlet; 6 – return inlet; 7 – external wall; 8 – combined system-1 (exhaust inlet and ceiling lamps); 9 – combined system-2; 10 – zone-1; 11 – zone-2; and (b) the arrangement of the equipment within the simulated office.

7.3 Mesh design for the LES method

The prediction efficiency and the numerical error with the LES method are highly influenced by the mesh design strategies, by the mesh quality and by the mesh density in the computational domain. In LES, avoiding the sudden coarsening of the mesh is highly recommended to prevent an energy “pile-up” at the smallest scale in the coarser grid area [172]. The small flow structures in the regions around rigid bodies play a significant role in turbulent boundary layers and need to be considered carefully. The thermal plumes that are generated by the heat sources inside the room are considered to be the main source of stochastic flow perturbations. Thus, the mesh refinement and the mesh density around such sources are very important to achieve accurate predictions and stable simulations. As a result of the complexity of the investigated room and equipment, a tetrahedral unstructured mesh was generated using the ANSYS ICEM CFD software as in chapter 4.

The number of cells used in the current study was 10 million. This could not be further increased due to the limitations of the computational resources available at the University of Leicester. Therefore, the mesh density was varied to increase the accuracy in the areas of interest, with a high mesh density being generated in regions expected to have high temperature and velocity gradients, such as the areas around the occupants, computers, in the regions close to the combined system and in areas near the external walls (see Figure 7-2). For this mesh design strategy, 10 layers of prism mesh were generated around the room heat sources to resolve the boundary layer in these regions as fully as possible. The initial height and growth rate of the prism mesh were 0.8 mm and 1.13, respectively. This was defined by the requirement for the y^+ value, which is bounded in the range of $0.2 < y^+ < 1$ (see Figure 7-3). y^+ is a dimensionless number representing the distance from the wall.

$$y^+ = \frac{u_{\tau air} y}{V_{air}} \quad (7-1)$$

where V_{air} is the kinematic viscosity which can be defined as:

$$u_{\tau air} = \sqrt{\frac{\tau_w}{\rho}} \quad (7-2)$$

where τ_w and ρ are the wall shear stress and fluid density, respectively and y is the distance from the boundary (m).

Many factors affect the accuracy of the results in a numerical situation. Turbulence model, the discretization schemes, the near wall treatments and the setting of convergence criteria. For the complicated human body geometry, Gao and Niu [63] suggested the application of a very small scale unstructured grid (4 - 8 mm) to predict the flow field with reasonable accuracy in the microenvironment areas around the occupants. Thus, in this study, the maximum and the minimum mesh sizes were 6 and 2 mm, respectively, around the occupants.

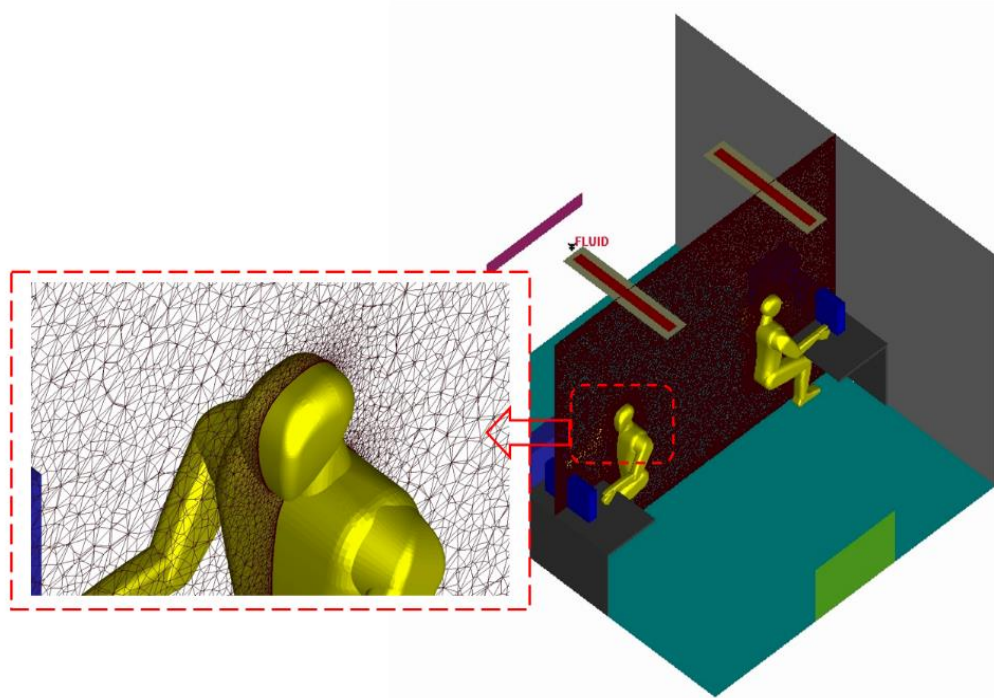


Figure 7-2: Mesh distribution in the investigated room domain.

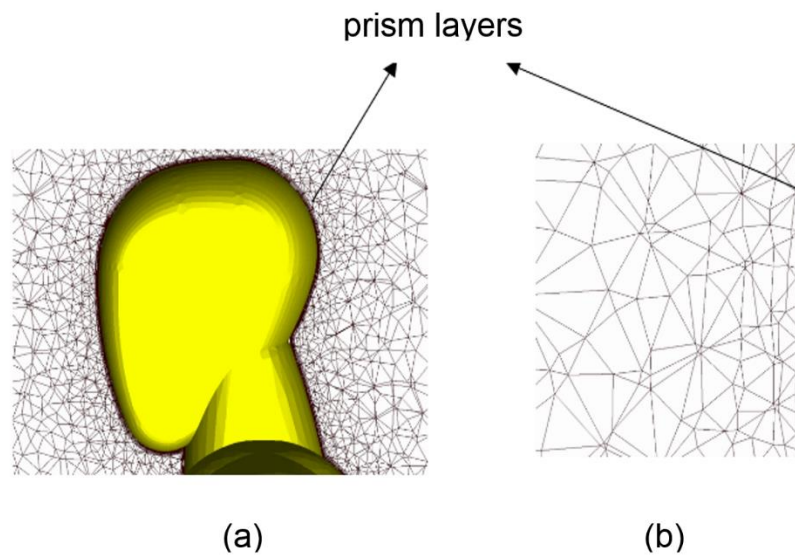


Figure 7-3: Boundary layers inflation (a) around the occupants, and (b) near the external wall.

7.4 Validation work for the LES method

In order to evaluate the performance and the validity of the LES method, the experimental data of Xu et al. [69] was compared against the results of the LES for this chapter and of the RANS model from Chapter 4, are also compared with the LES simulation results. The room layout and the measurement locations used by [69] were presented in Chapter 4 and shown in Figure 4-2 and Figure 4-3. Poles 3 and 4 of Figure 4-3 were chosen to compare the temperature and velocity distributions from the LES and RANS model predictions with the experimental results. For the LES, the instantaneous data for temperature and velocity were collected at different intervals after the simulation reached a statistic steady state; then, the average velocity and temperature were compared with the experimental results. As shown in Figure 7-4 and Figure 7-5, both the RANS model and the LES appear fair agreement for the velocity distributions and in good agreement for the temperature distribution for both poles. However, the LES method also gives time dependent information about the thermal environment indoors, which is presented in this chapter.

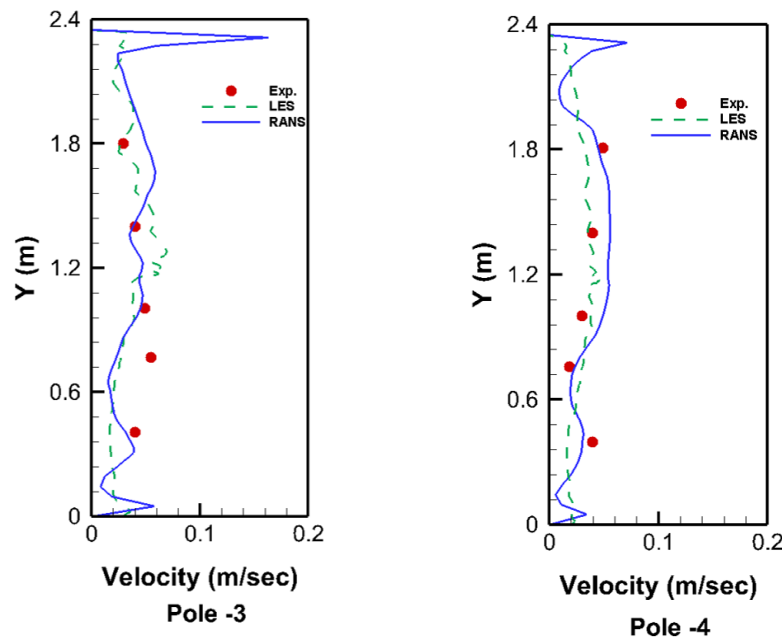


Figure 7-4: Comparison of measured and simulated air velocity magnitude (m/sec) at poles 3 and 4.

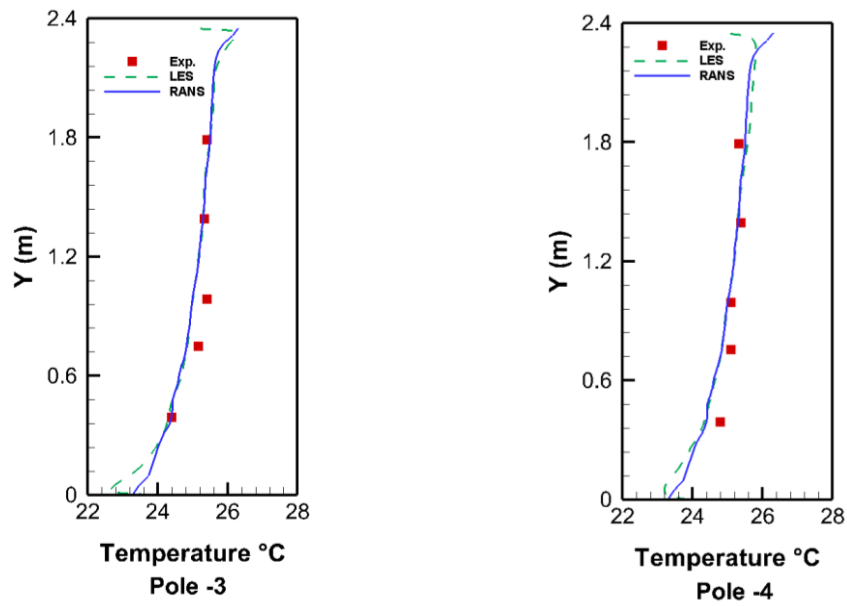


Figure 7-5: Comparison of measured and simulated air temperature (°C) at poles 3 and 4.

7.5 Convergence evaluation of the LES method

In the LES, the solution was considered converged when the air flow and the temperature reached the statistically steady state. In this study, for all the simulation period, the time step Δt was 0.003 sec and the CFL value was taken as 0.4. For each time step, the maximum number of iterations was 50. The convergence solution with time at each time step will accrue with flow simulation time, and the maximum number of iterations will decreased significantly. The starting flow condition of the LES was the converged flow field of the RNG $k - \epsilon$ simulation and the air velocity inlet was assumed to be a “no perturbation”.

The solution convergence was judged using the Root Mean Square (RMS) value for the velocity profile. A pole located at the room centre is used to show the RMS velocity profile at different times. Figure 7-6 shows the RMS profile from the starting time 0.45 s to the simulation end time of 100 s. This figure, indicates it is clear that the airflow is unstable and that velocity fluctuations develop over time, particularly during the starting period between 0.45 and 50.4 s. In the period between 50.4 to 80.2 s, the flow started to become more statistically stationary compared to the starting period, with subsequent variations in the RMS profile tending to be small. In the period between 80.2 and 100 s, the flow finally tended

to reach a statistically steady state and no significant change in RMS velocity profile was subsequently observed (see dashed lines in Figure 7-6). Additionally, however, one should carefully consider other factors in the assessment of convergence; scaled residuals should be less than 10^{-6} for the energy and a minimum value of 10^{-4} for all other variables, whilst the net heat flux should be below 1%.

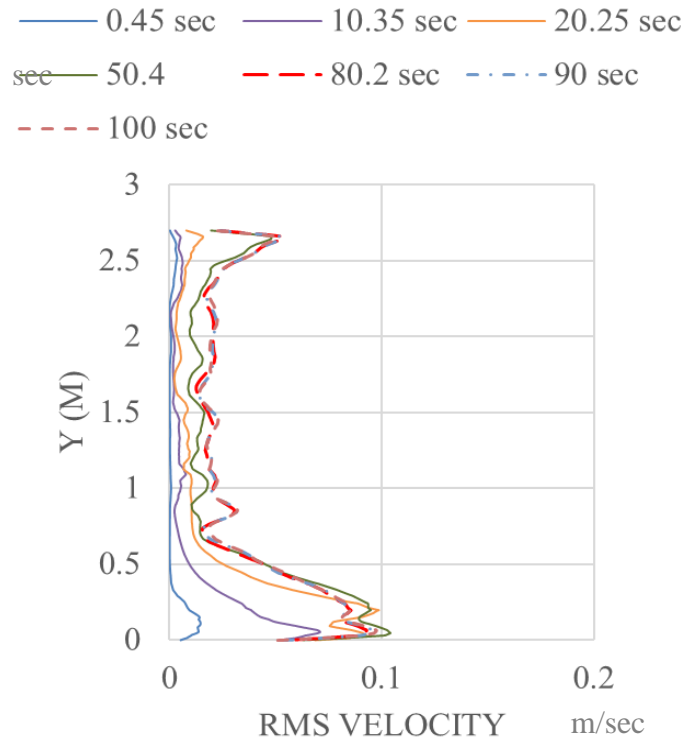
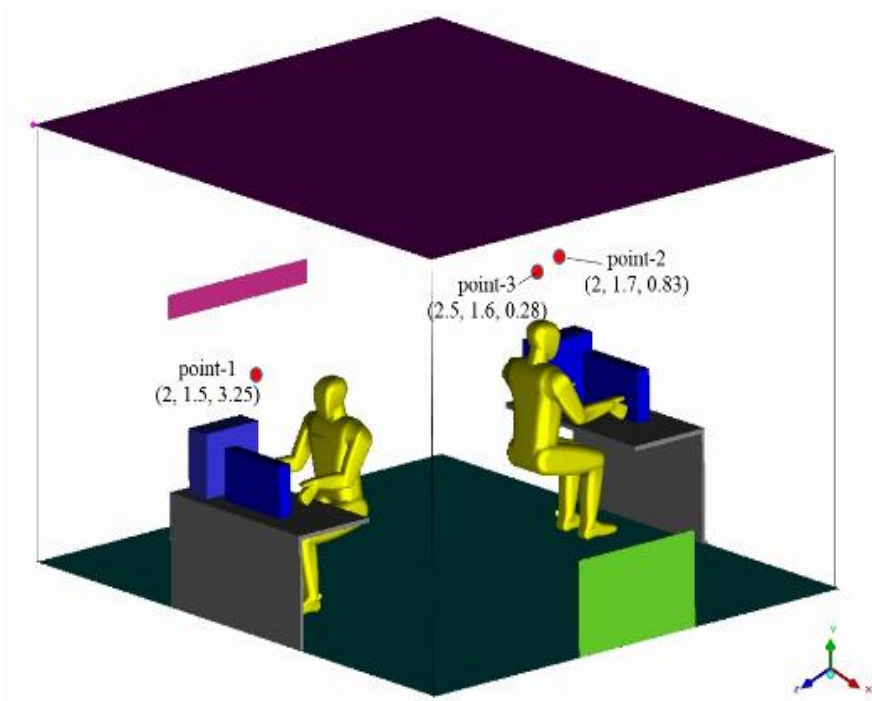


Figure 7-6: RMS convergence test (m/s) for different flow times at the pole located in the room centre.

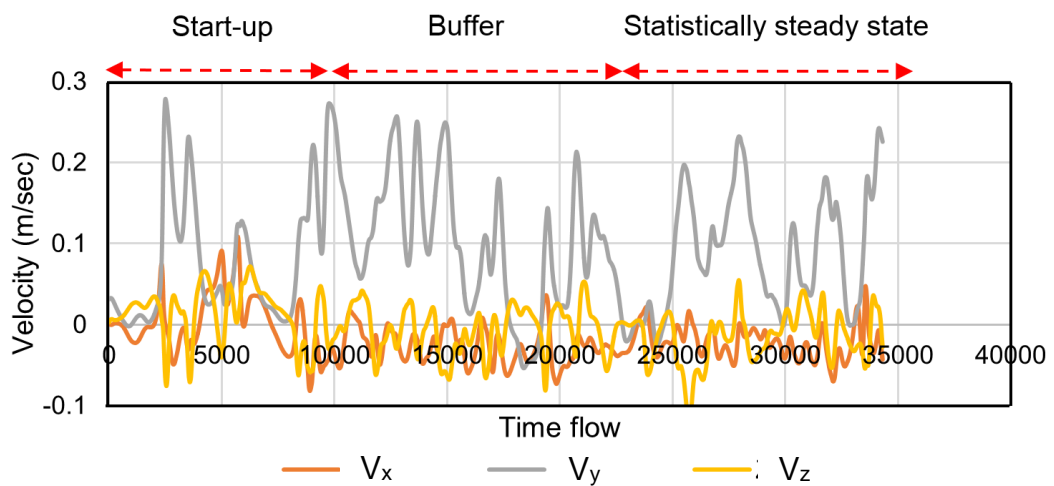
7.5.1 Monitoring points

As shown in Figure 7-7 a, three monitoring points, points 1, 2 and 3, located in regions of interest in the room domain, are used to illustrate the time dependence of the instantaneous velocity components. Figure 7-7 b, c and d show the instantaneous air velocity components, v_x , v_y and v_z , at points 1, 2 and 3, respectively, over the entire simulation period. These figures show that for all the monitoring points the v_y component of air velocity fluctuates more than the air velocity components in the x and z directions. This was due to the fact that the generated thermal plumes will warm the air in these regions and accelerate the air towards the ceiling level. As shown in Figure 7-7 b, c and d, the start-up, the

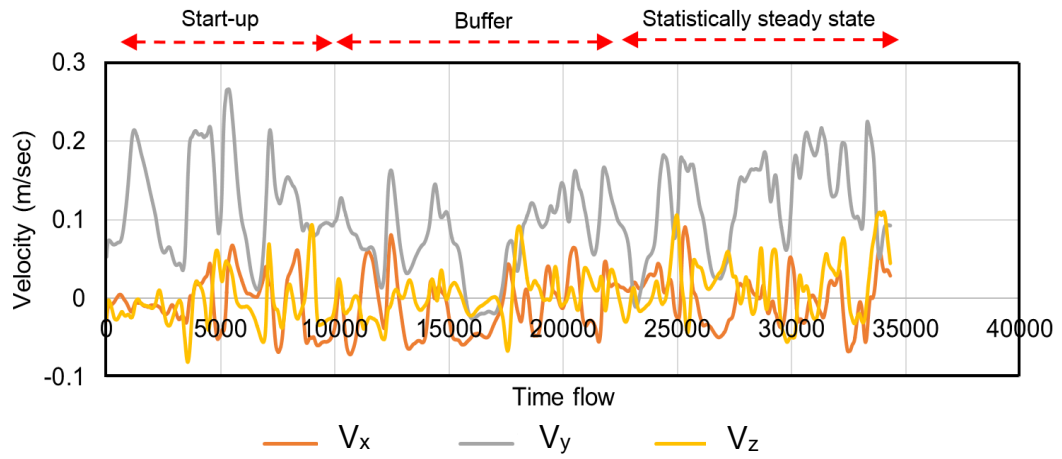
buffer and the statistically steady state period are determined according to the changes to the RMS velocity profiles (see Figure 7-6).



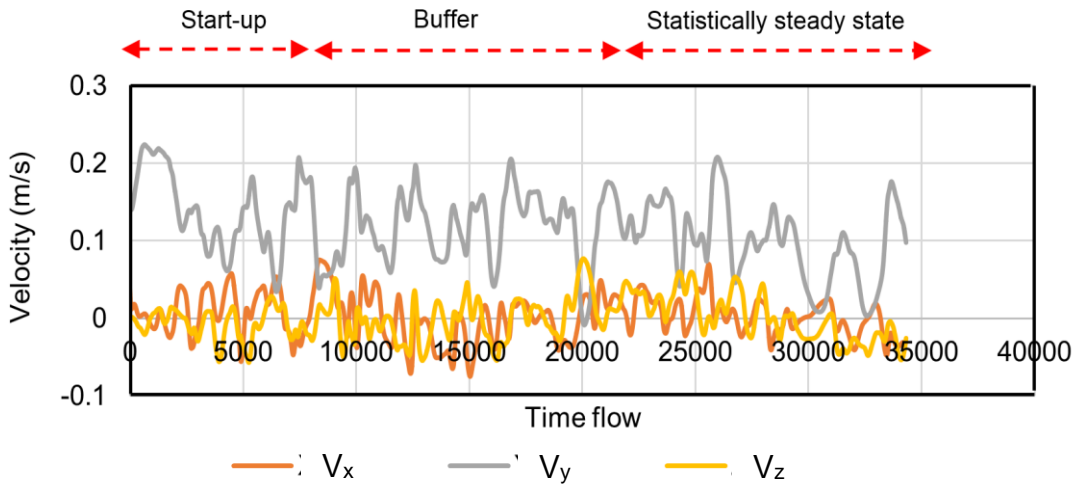
(a)



(b)



(c)



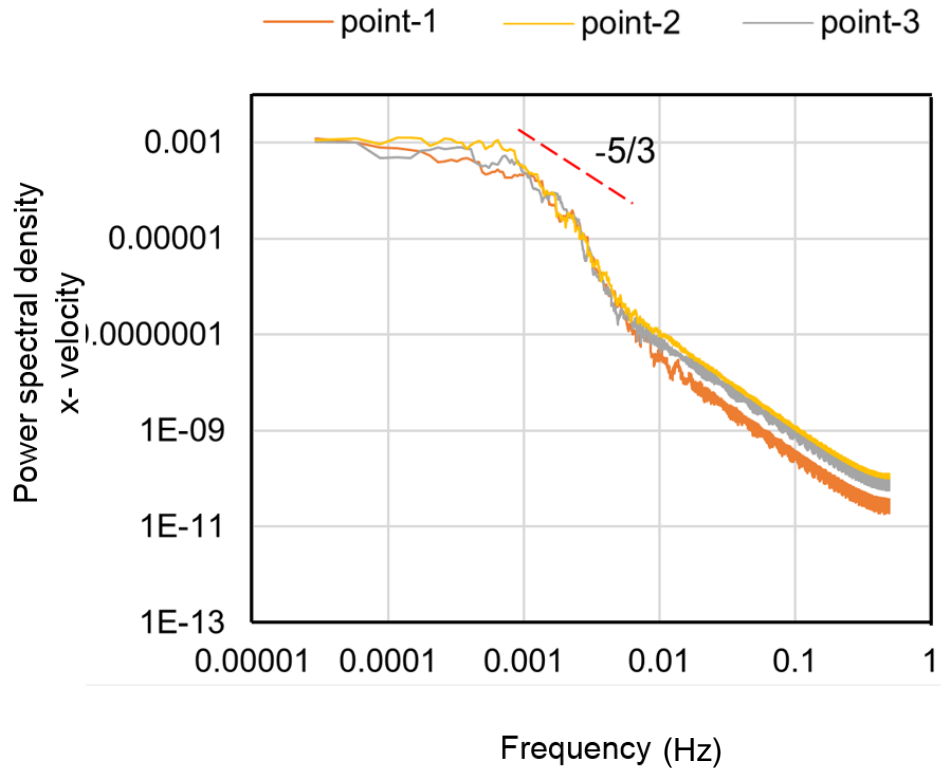
(d)

Figure 7-7: (a) Monitoring points; (b), (c) and (d) instantaneous velocity components at monitoring points 1, 2 and 3, respectively.

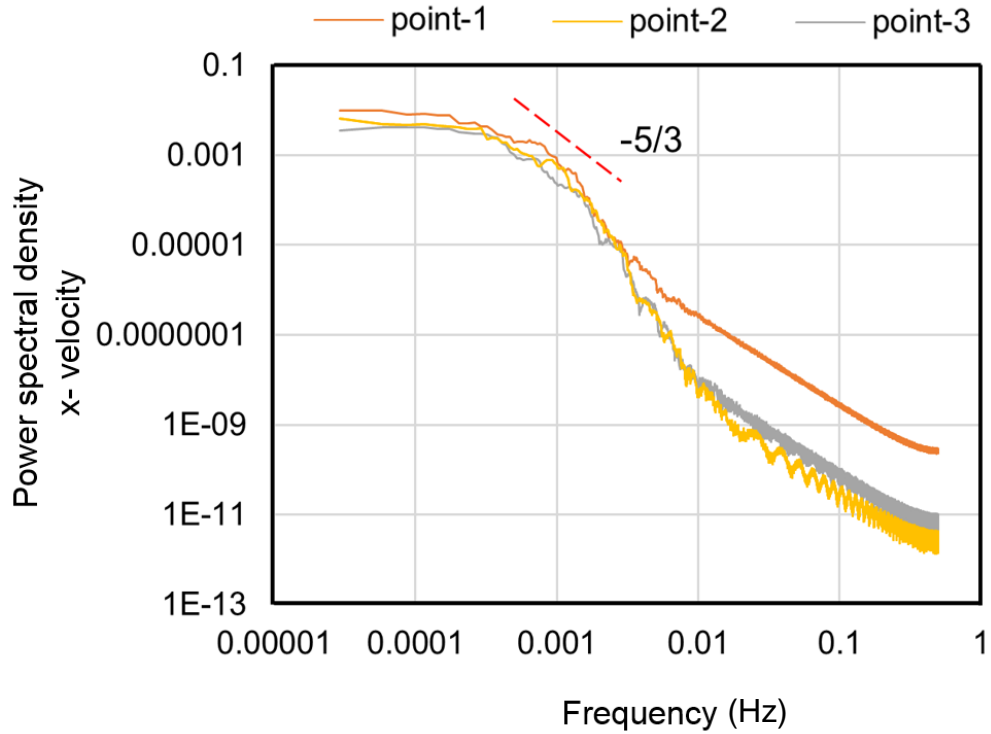
7.5.2 Discrete Fourier Transform

The frequency content of the resolved velocity fluctuations is studied by performing a discrete Fourier Transform of each velocity time history. In a fully turbulent flow, the low frequency energy content of the large scales cascade to the small scales as high frequency energy content, where it is dissipated by viscosity as heat. The Discrete Fourier analysis is used to assess whether the resolved velocities fluctuations display the trends of a fully developed turbulent flow.

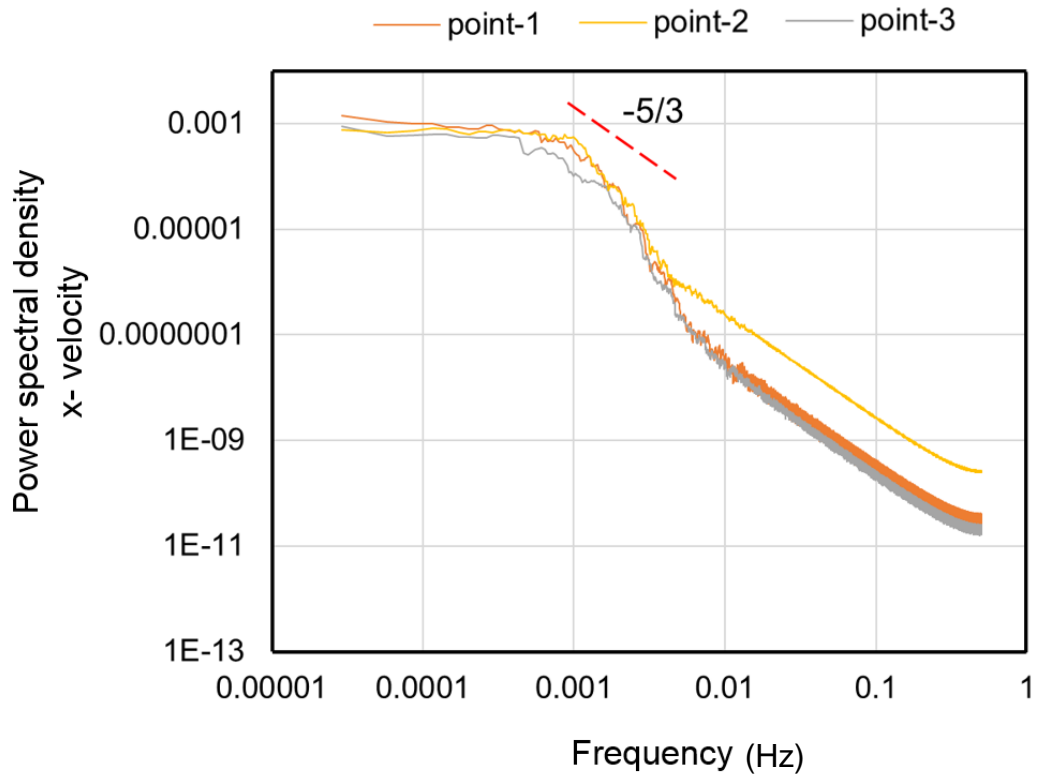
In LES, it is very important to make sure that the simulations are performed with an adequate spatial and temporal resolution. Consequently, the Fourier analysis undertaken during this study was used to examine different point locations – three monitoring points – in the room domain. The velocity spectra can be used to interpret the physics of the energy transfer between different scales of motion and the turbulent energy dissipation due to fluid viscosity. Figure 7-8 a, b and c show the power spectral density of the resolved velocity components v_x , v_y and v_z at the monitoring points 1, 2 and 3, respectively. In general, a slope of $-5/3$ has been found to be representative of the generic features of a fully developed turbulent flow. This slope is shown in Figure 7-8 a, b and c, and indicates that the flow observed in the current study exhibits some of the characteristics of a fully turbulent flow.



(a)



(b)



(c)

Figure 7-8: Graphs (a), (b) and (c) show the FFT analyses for velocity components v_x , v_y and v_z , respectively, at three monitoring points.

7.6 Results and discussion

7.6.1 Temperature distribution

In this chapter, the mid plane crossing the occupants at $z = 2$ m was used to compare the temperature distributions predicted by the RANS model and by LES. Figure 7-9 shows the simulated average temperature distribution using the RANS model. This is the same distribution shown in Figure 4-9 case 3. Steady thermal plumes rise from the occupants and other heat sources towards the ceiling level and the temperature is distributed smoothly across most of the room domain.

The steady RANS model does not resolve the airflow development over time within the domain. Instantaneous air temperature predictions, from LES are able to show how the temperature varied with time from the supply opening to the exhaust opening when passing through the room's heat sources. Figure 7-10 a - k show the snapshots of the instantaneous temperature contours of the LES predictions taken at different times. During the start-up period (5 - 35 sec.), thermal plumes from the occupants and from other heat sources begin to form, and the predicted temperature distribution is similar to that from the RANS model (see Figure 7-10 a - e). After 35 sec., small flow structures can be observed forming from these heat sources start to penetrate in the room, particularly in the regions around the occupants and near the external wall.

This finding was similar to that of Durrani et al. [173]. These structures carried on growing in size up to the simulation time of 50 sec. The location of the structures in Figure 7-10 f suggests that heat generated by the occupants and the heat sources located near the external wall moved towards the ceiling and is extracted with the lamp generated heat via the exhaust opening. Lastly, after 80 sec. the simulation reached the statistically steady state. The thermal plumes are varied and develop gradually with time, resulting in a significant number of eddies. These eddies have a significant impact on the thermal environment around the occupants and near the combined system, all of which are resolved by the LES method. The RANS simulation results for the temperature distribution in Figure 7-10 were also compared with the mean temperature distributions taken from the LES predictions, which is shown in Figure 7-11. From these figures, both the RANS and LES methods show similar predictions for the temperature distribution in the computational domain.

It can also be observed that the air temperature near the combined system-1 is not identical to that around the combined system-2. This is because the heat generated by the external wall adds to the heat generated by the heat sources near occupant -2, and moves towards the ceiling level to be extracted from the combined system-2. This makes the air temperature near the combined system-2 warmer and more prone to developing an active thermal plume than the air around the combined system-1. Thus, the thermal environments around the occupants are affected by the occupants' location relative to the room's heat

sources. All these details can be seen more clearly in the LES predictions than the RANS predictions.

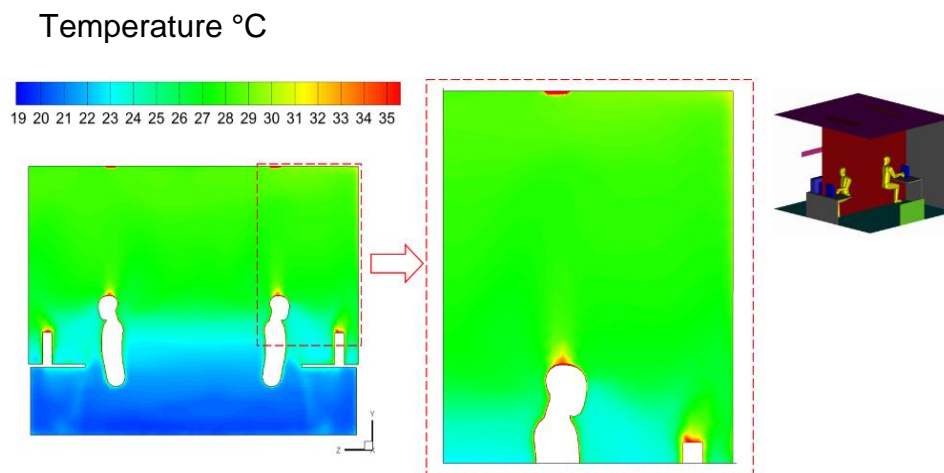
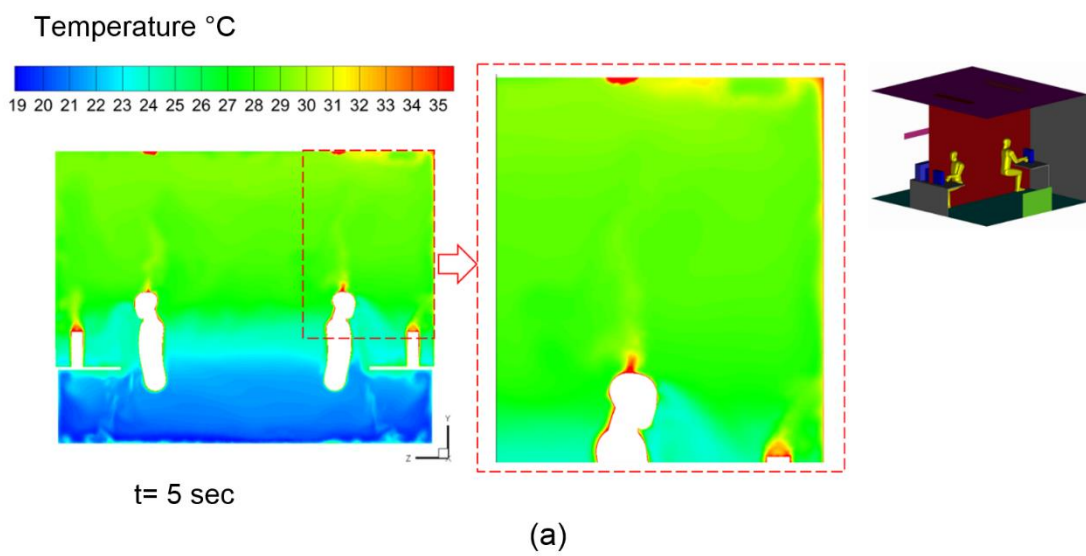
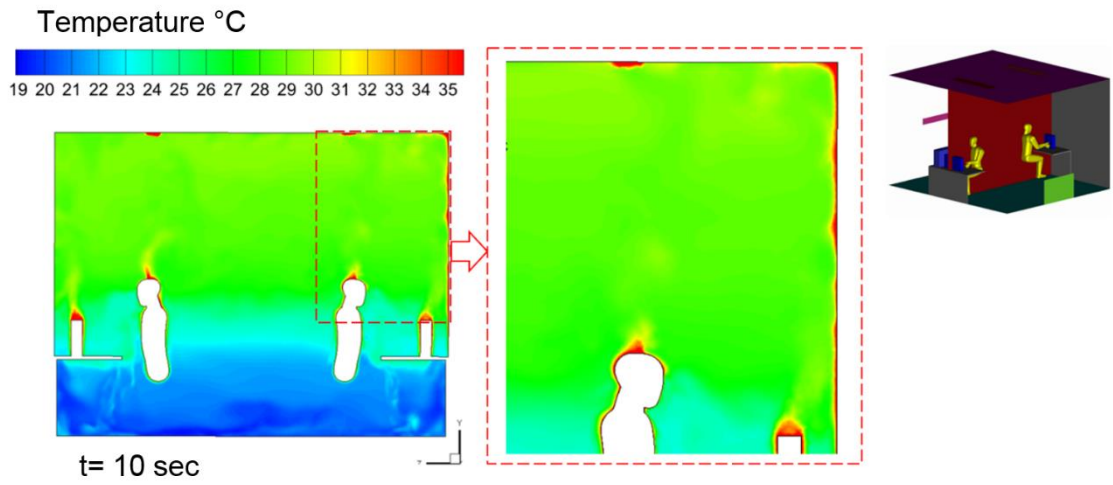
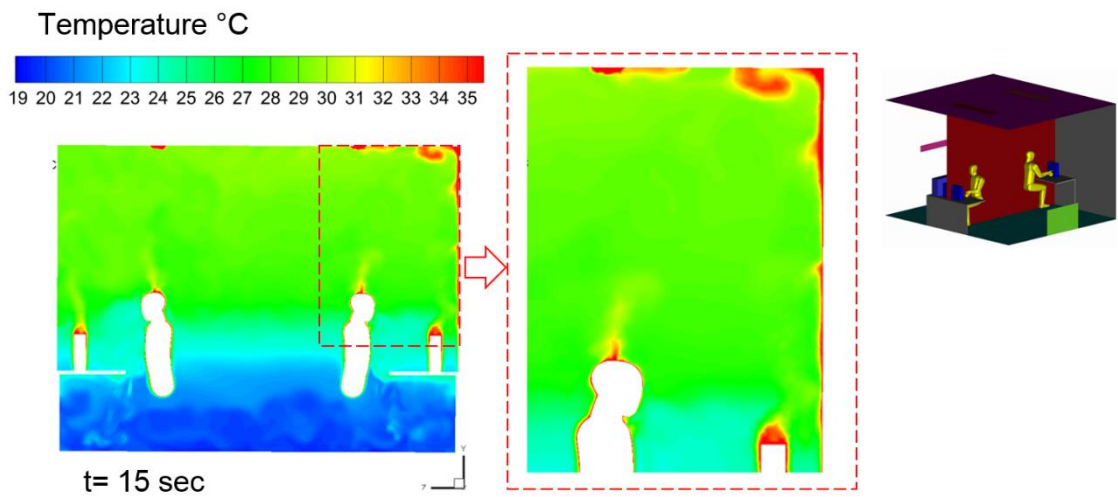


Figure 7-9: The RANS predictions of the temperature distribution.

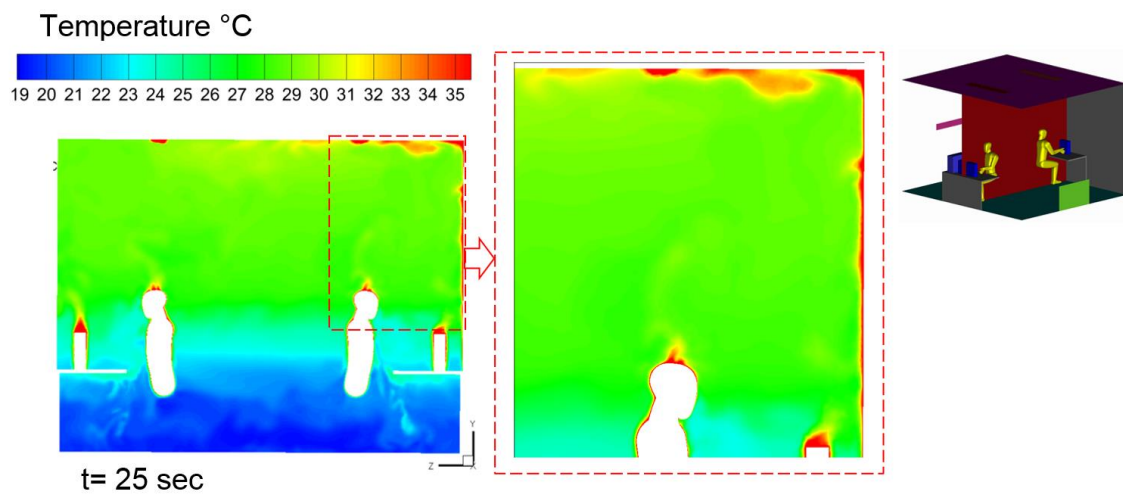




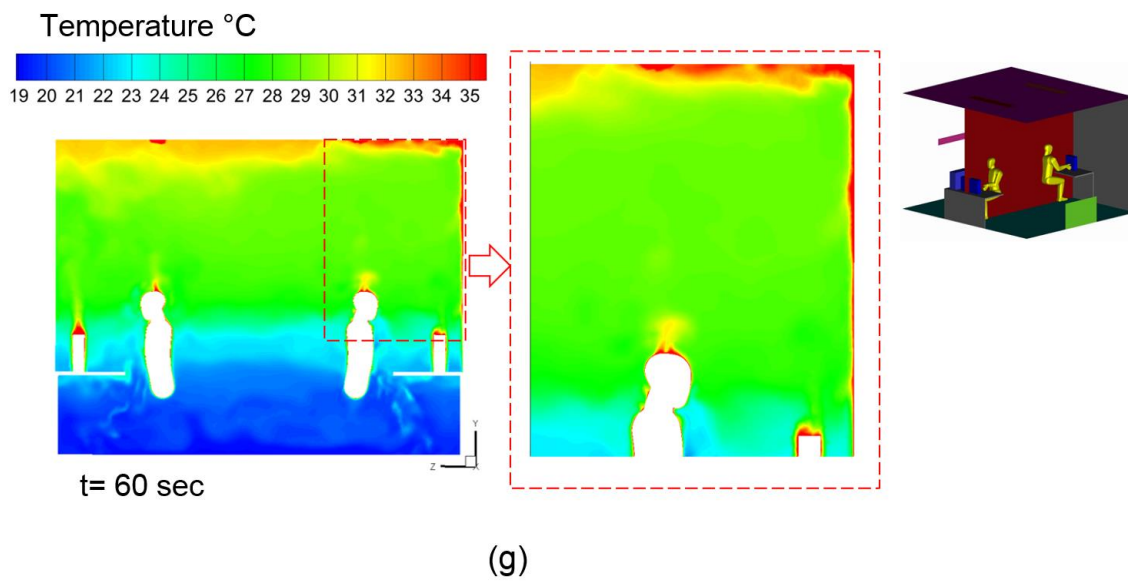
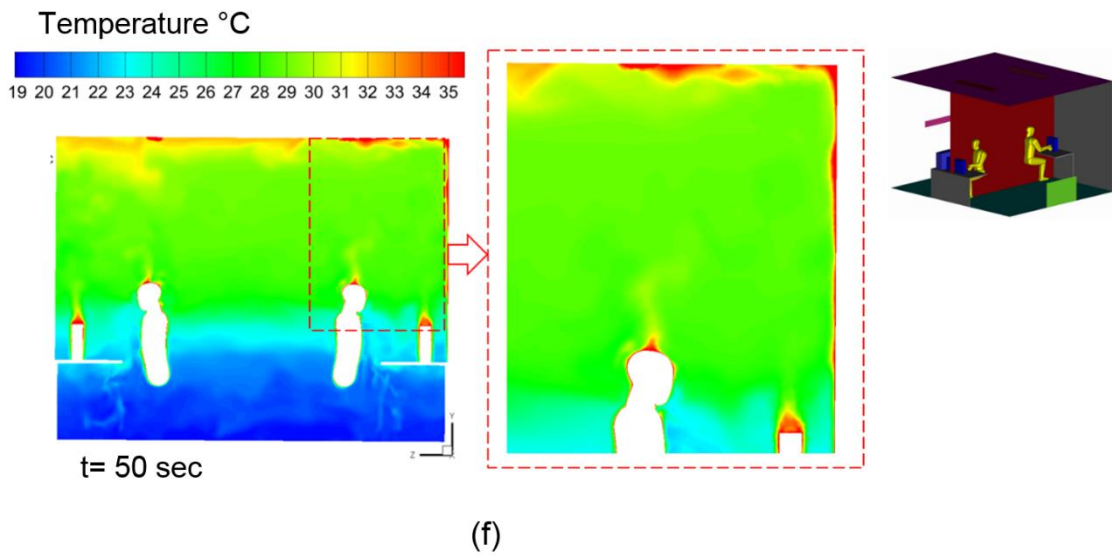
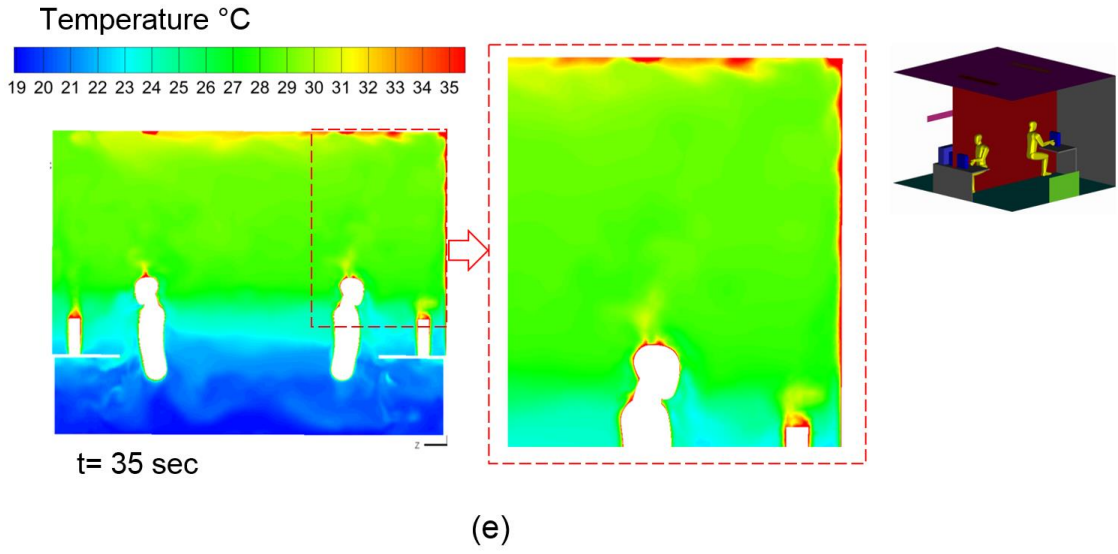
(b)

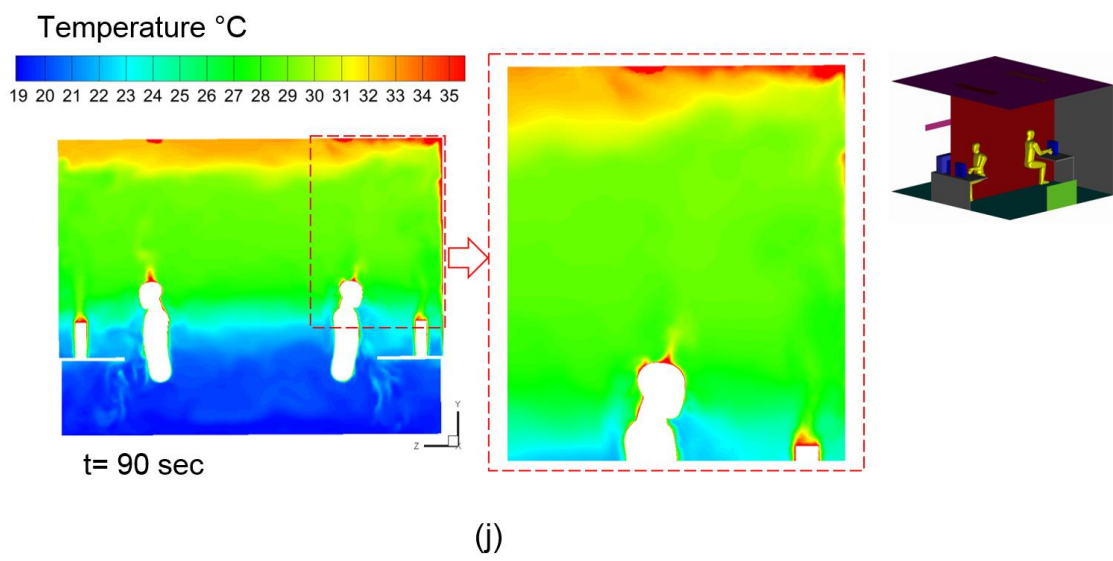
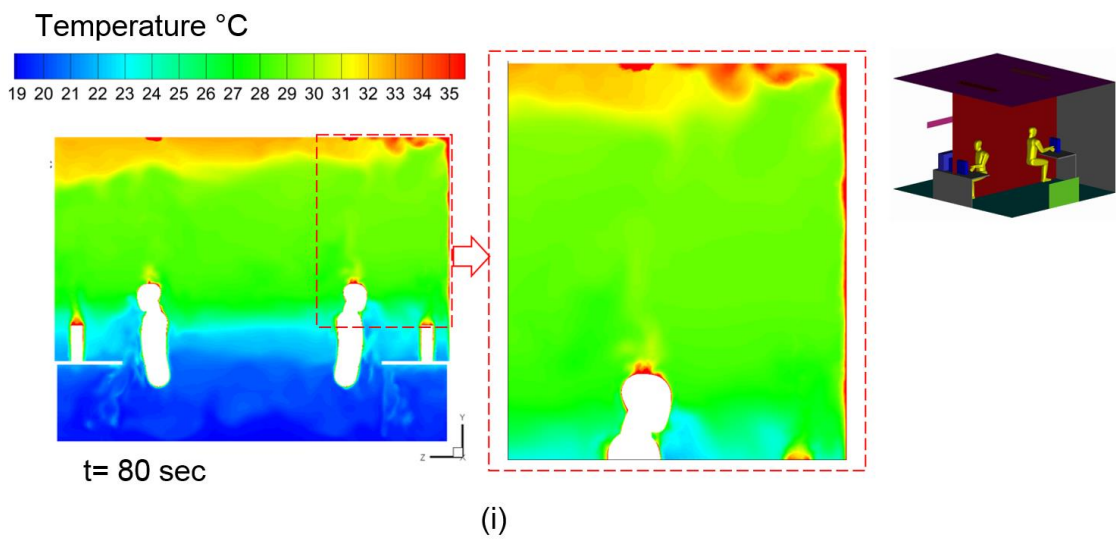
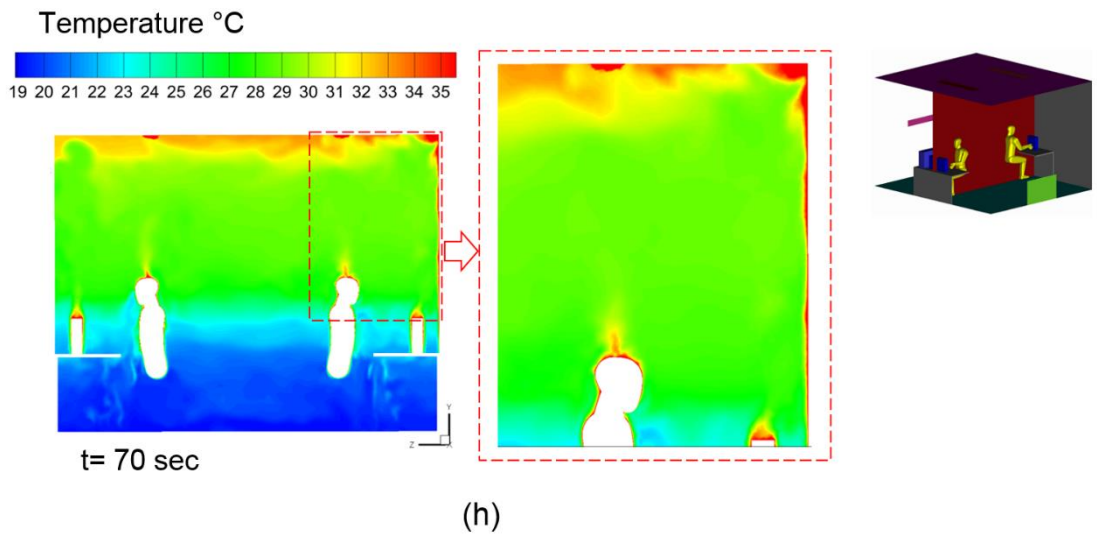


(c)



(d)





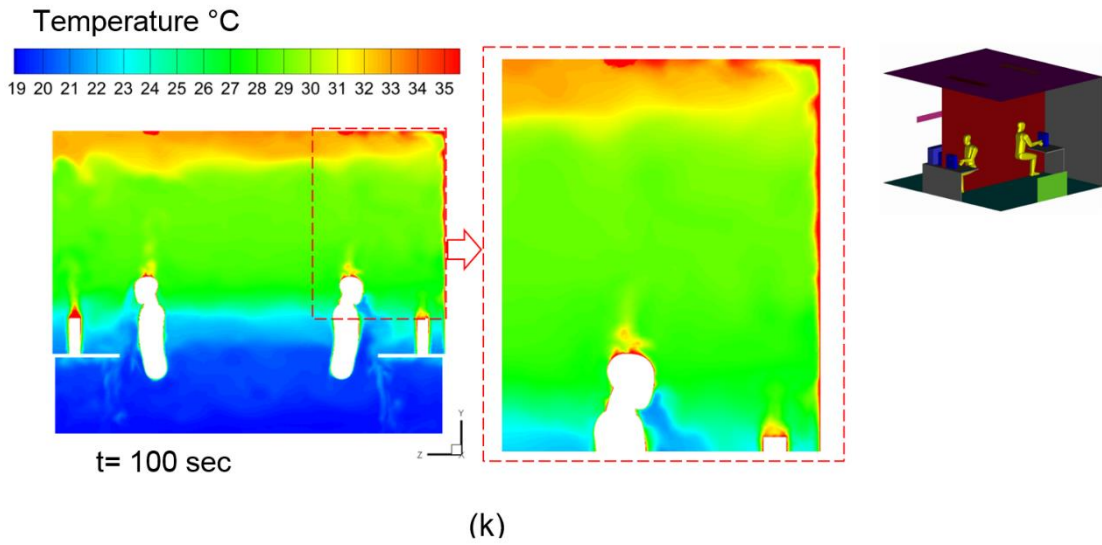


Figure 7-10: The instantaneous temperature contours derived from the LES.

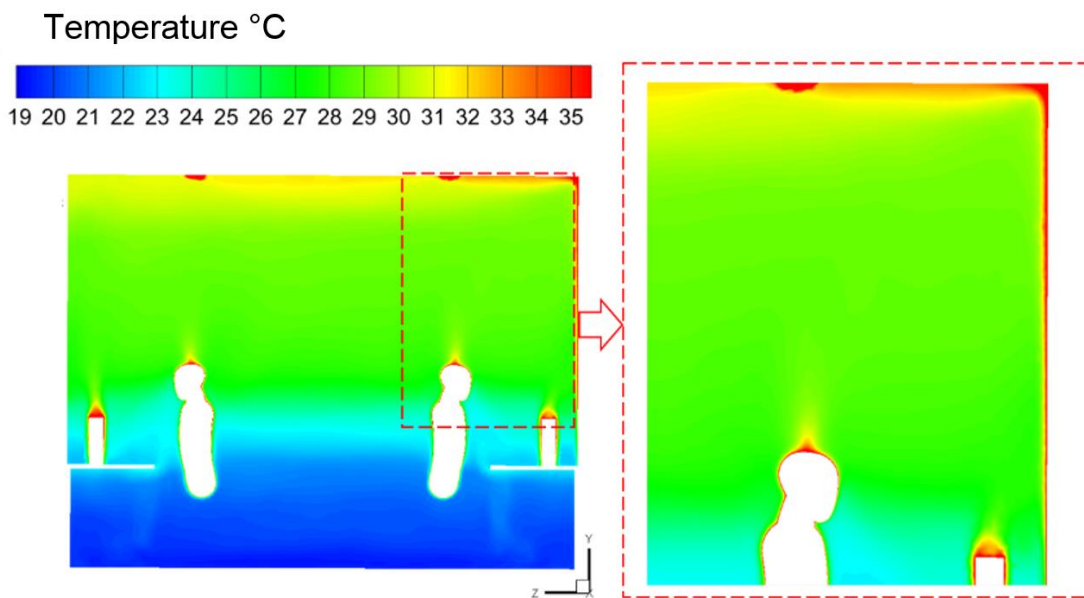


Figure 7-11: The mean temperature distribution contour derived from the LES.

7.6.2 Velocity distribution

Figure 7-12 shows the velocity magnitude distribution predicted by the steady RANS model. By contrast, as presented in Figure 7-13 a - k, the velocity magnitude distributions predicted by LES show considerable time dependence, particularly in the occupied zone around both occupants and in the region near the external wall, where the buoyancy effect are expected to be at their greatest. The instantaneous distributions of velocity magnitude are shown in Figure 7-13 at different simulation times. Figure 7-13 a - e show the flow field during the start-up period between 5 and 35 sec., the circulation in the flow field seems low and there are no large scale eddies within the computational domain. After 35 sec. of the simulation time, the flow appears to become more unsteady and large-scale eddies can be observed, especially in the thermal plumes regions and the area near the external wall (see Figure 7-13 f - i). The flow tended towards a statistically steady state around 80 and 100 sec of the simulation time (see Figure 7-13 i- k). The flow at this region is shown by Figure 7-13 f - i to be unsteady and detailed eddy structures can be seen in the regions around the occupants systems. This was due to the fact that the heat generated by the lamps and by the external wall warms the air in these regions and decreases the air density, resulting in relatively high local natural convection effect.

A closer examination of Figure 7-13 suggests that the air in the occupant zone-2 fluctuates more and has a slightly greater air velocity than that in the occupied zone-1. This is attributed to the local thermal environment around the occupied zone-2 which was influenced by the heated external wall.

From these results, it is fair to say that LES provides more detailed information about the flow behaviour that can help designers to understand the airflow in a complex room geometry and gives the designers an opportunity to develop and improve the ventilation system.

Figure 7-14 shows the mean velocity magnitude distribution predicted by the LES. The comparison of this figure with Figure 7-12 from the RANS model indicates that a faster thermal plume is predicted by LES above the occupant and along the heated external wall. These are in the regions where the buoyancy effects are most active.

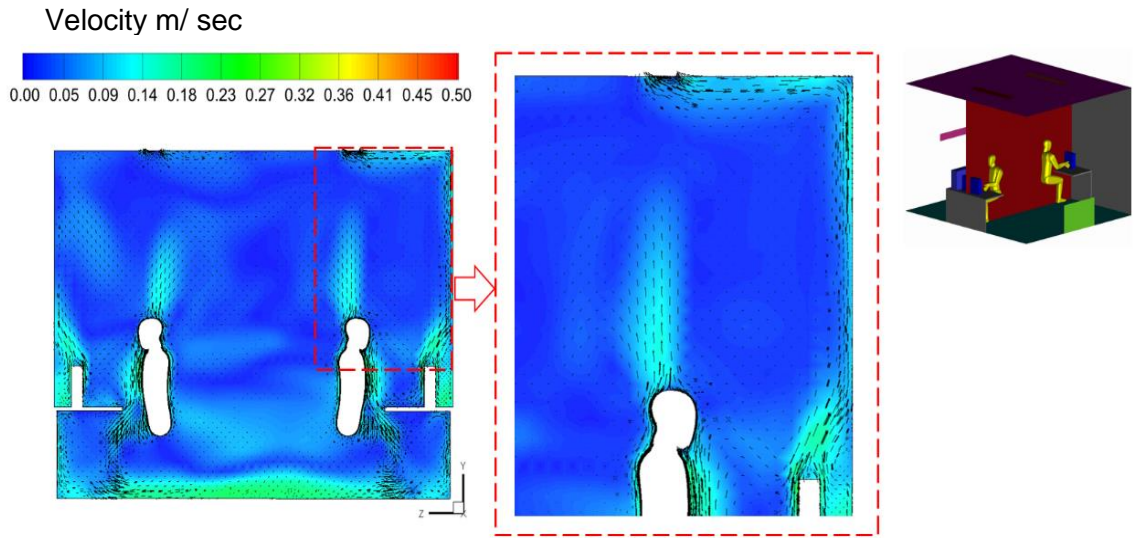
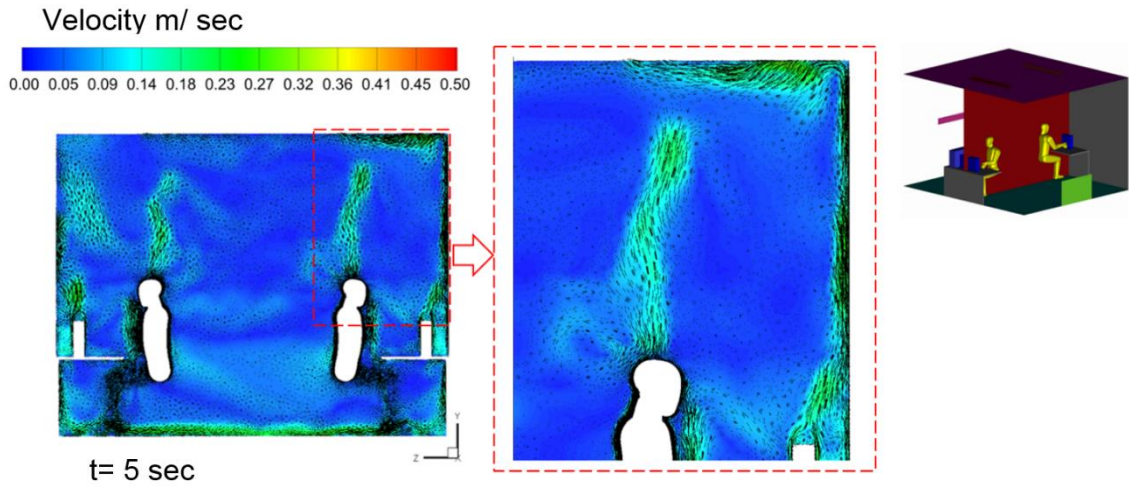
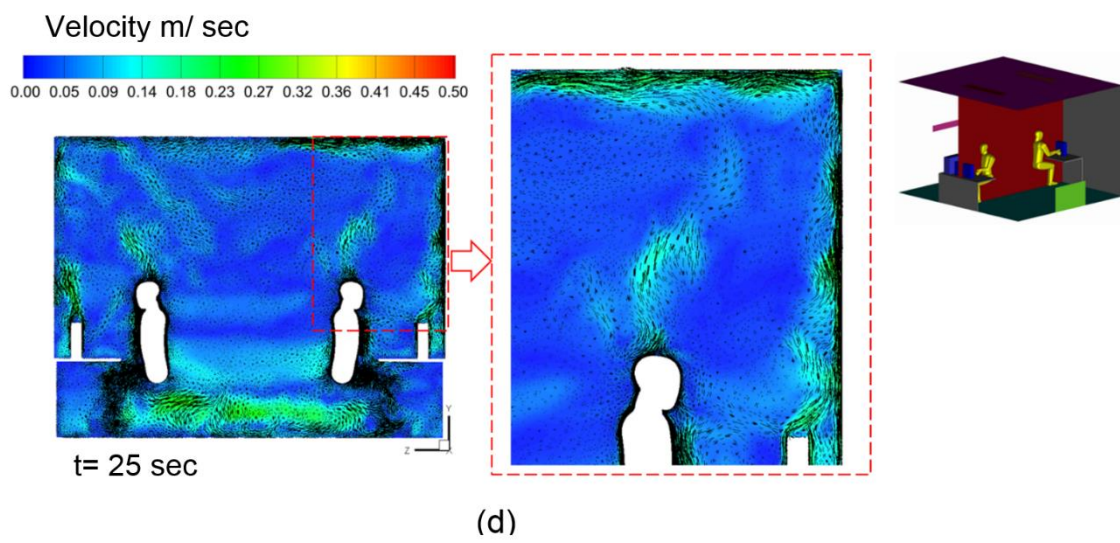
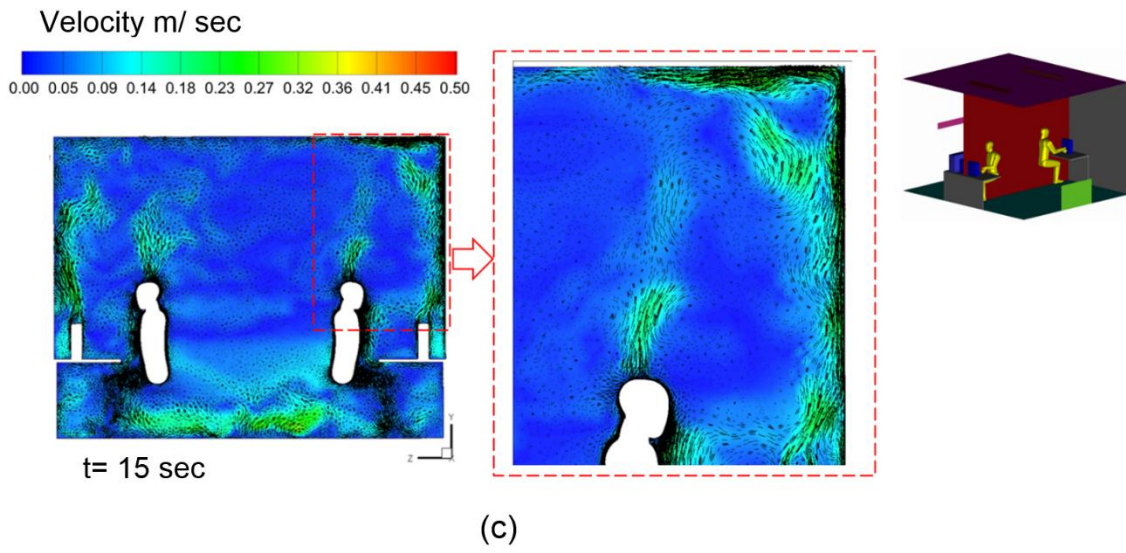
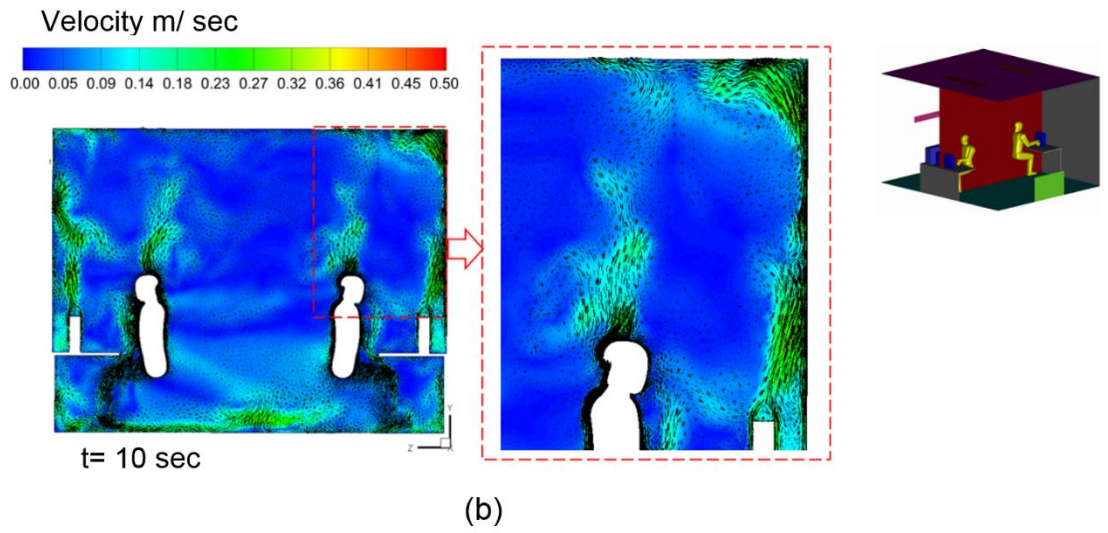
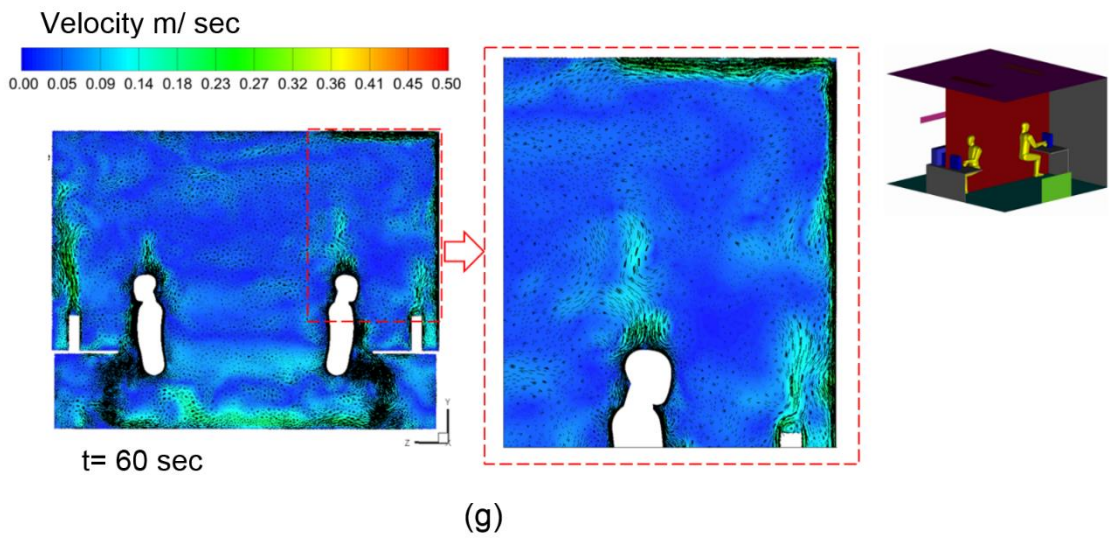
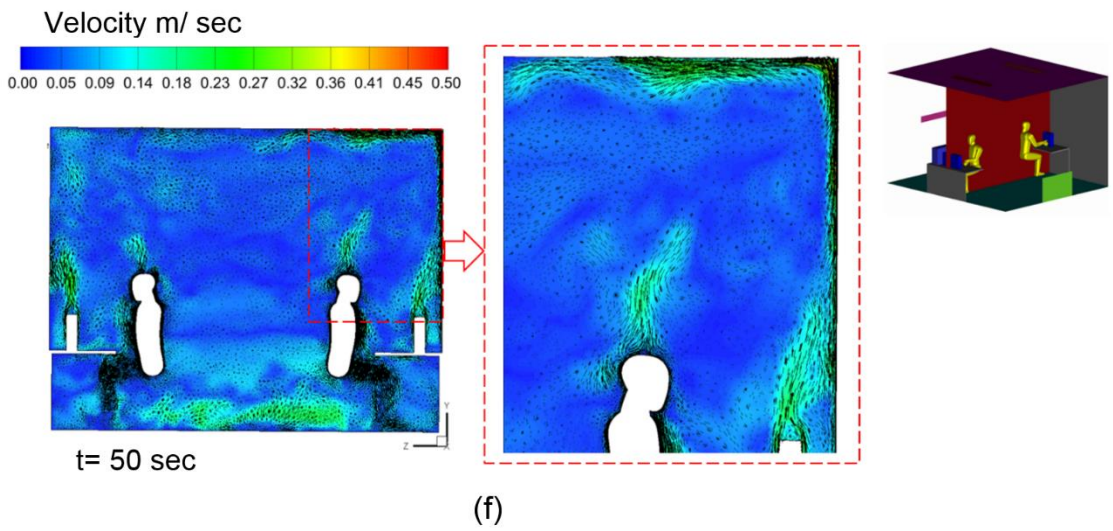
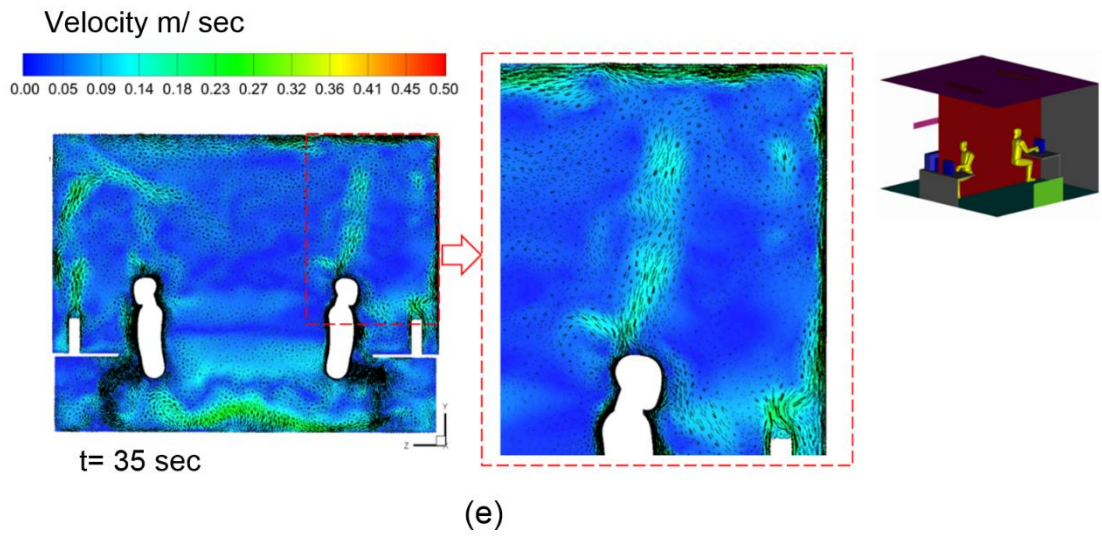


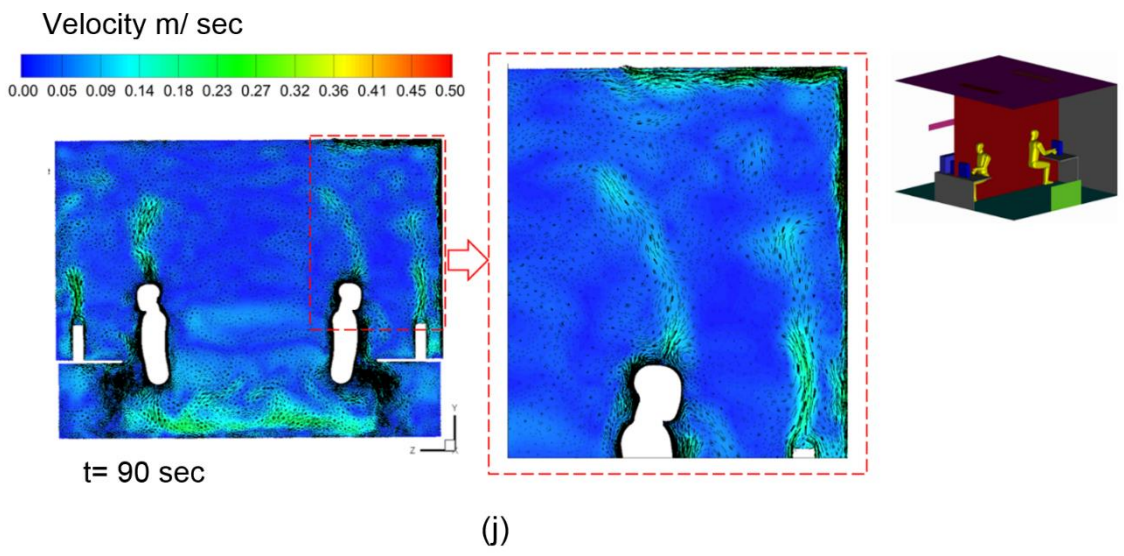
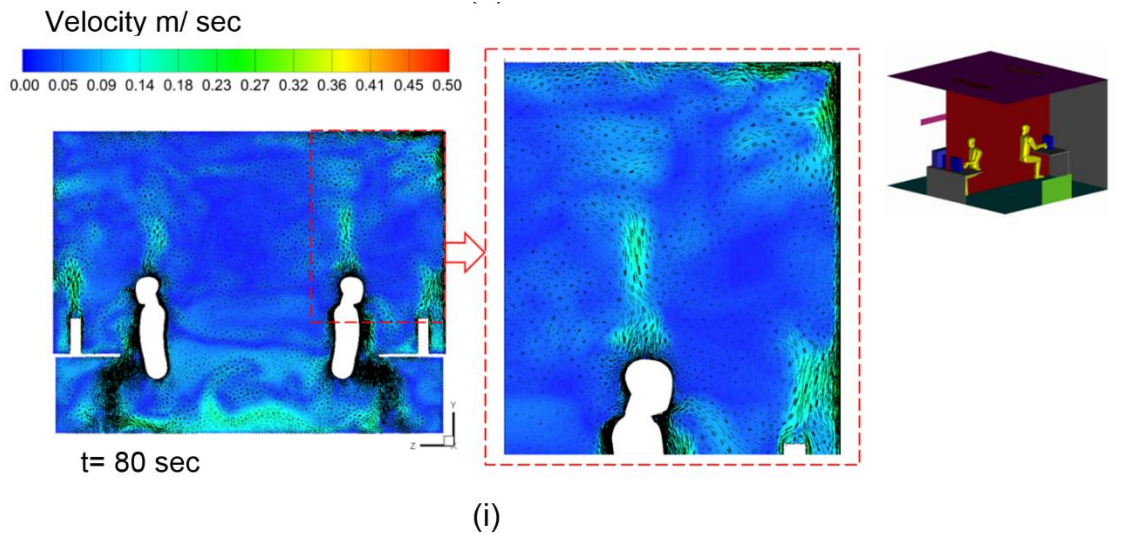
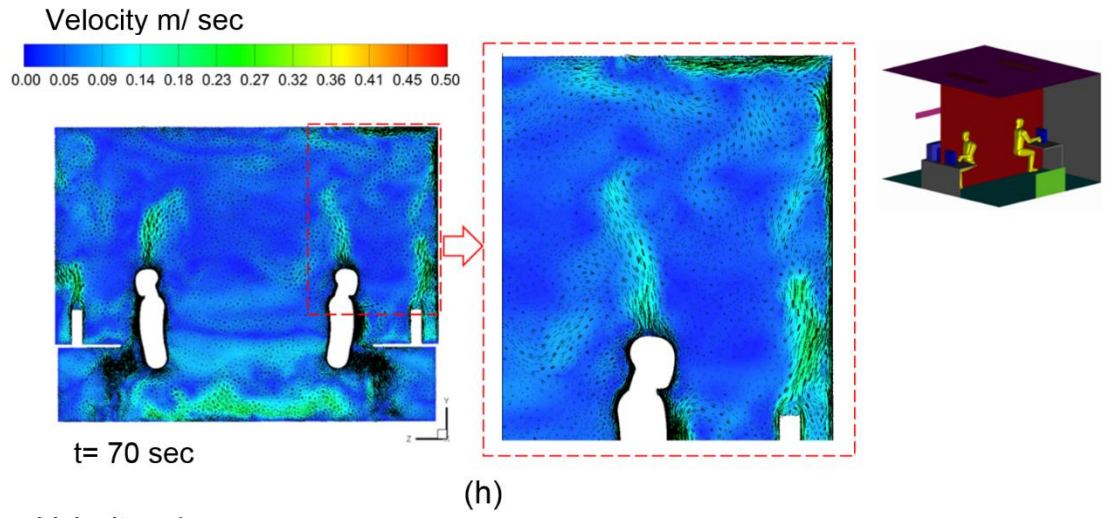
Figure 7-12: RANS predictions of velocity magnitude (m/s).



(a)







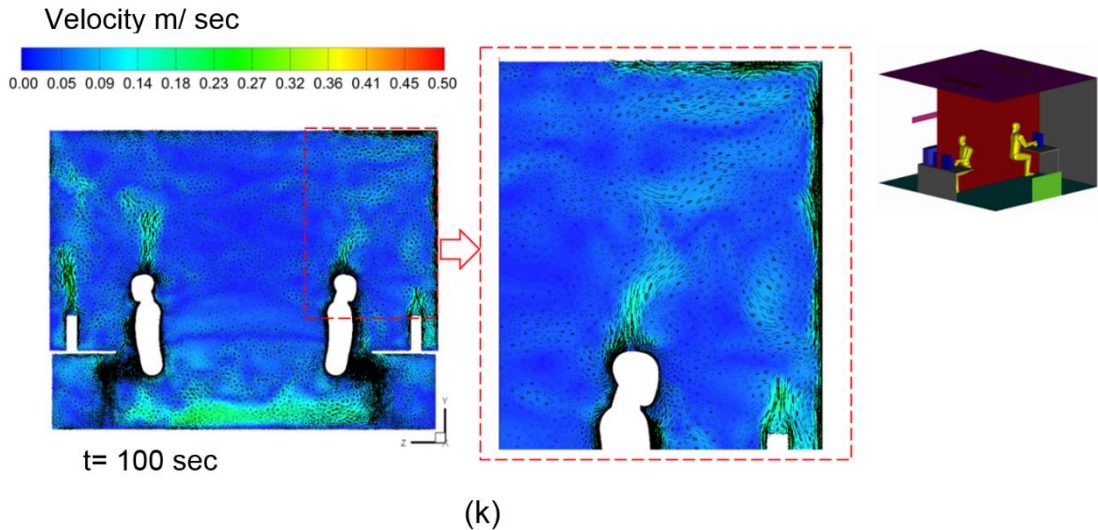


Figure 7-13: Instantaneous velocity magnitude colour iso-levels from the LES predictions.

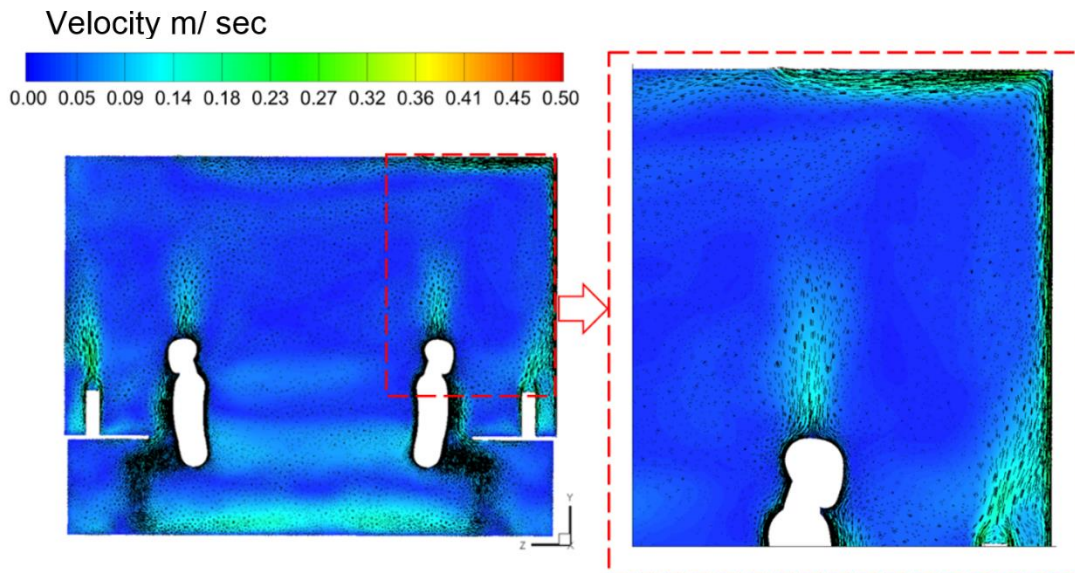


Figure 7-14: Mean velocity magnitude colour iso-levels from the LES.

The instantaneous iso-surfaces of the velocity magnitude at $t = 100$ sec are shown in Figure 7-15. This indicates the unsteady nature of the indoor airflow. As shown in this figure, the flow becomes more unsteady and a turbulent behaviour becomes clearer closer to the room's heat sources. As the main ventilation system is a DV system that supplies air at low velocity, the turbulent structures are not very numerous in the lower part of the room. However, when the supply air reaches the room heated wall and the heat sources, more turbulent structures are generated, particularly in the occupied zone-2. In the occupied zone-2 and

around the combined system-2, the external wall played an important role in the flow development. As shown in Figure 7-15, the flow started with small fluctuations at the foot of the external wall. As the flow rises to the upper part of the room, the number and the velocity magnitude of the eddies increase, due to the local buoyancy effect. In conclusion, the LES method gives detailed information on the time-dependent flow behaviour of the indoor thermal environment, especially in the region of interest.

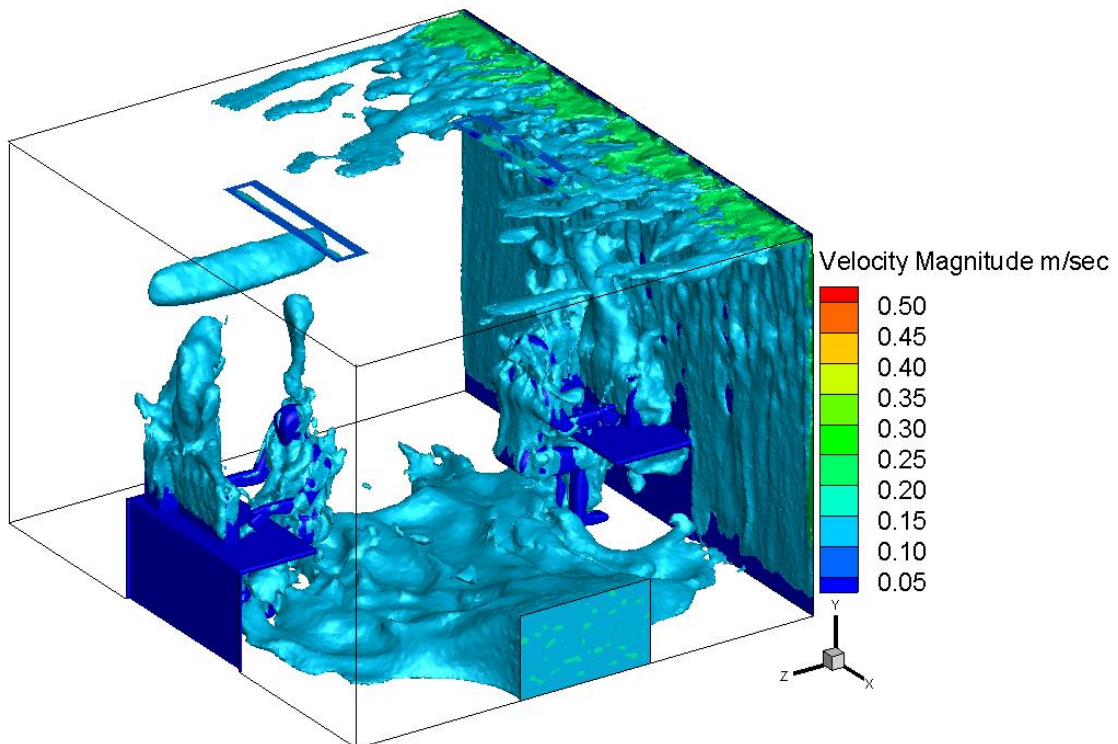


Figure 7-15: The instantaneous iso-surfaces of the velocity magnitude at $t = 100$ sec.

Chapter 8 Conclusion and Future Work

8.1 Conclusion

Ventilation plays a significant role in air conditioning systems in buildings. The current study has employed some strategies to enhance the indoor thermal comfort, the quality of the indoor air and the energy savings. The targeted objectives of this study have been met as described below:

1. Objective (1) has been achieved through the investigation outlined in Chapter 4. In this investigation, the effects of the locations of the exhaust air vent on the indoor thermal comfort, vertical temperature difference, contaminant concentration in the occupied zone, quality of the inhaled air and energy savings in an office were investigated. The results of this study concluded as follows:
 - A significant improvement on energy savings and quality of the inhaled air was made when the exhaust was combined with the room heat sources, such as in case 1 where the exhaust is located between the two heat sources, and in cases 2 and 3 where the exhaust is combined with the external walls and with the ceiling lamps, respectively.
 - In case 3, a 25.0 % cooling coil load reduction was achieved by combining the exhaust diffuser with ceiling lamps. Furthermore, locating the exhaust diffuser near the heat sources, cases 1 and 2, also reduced the cooling coil load by 13.8 % and 12.65 % respectively. In case 5, where the exhaust and return outlets were combined in one unit at the occupied boundary area, the risk of thermal discomfort and of poor air quality in the occupied zone, as well as the energy consumption, was clearly increased.

- An enhancement of the IAQ in the breathing zone and the quality of the inhaled air was obtained by separating the exhaust from the return opening, and by combining it with the heat sources, as shown in case 3.
 - Overall, a better indoor thermal environment in terms of the thermal comfort, the temperature distribution, the quality of indoor air, the inhaled air and of the energy savings was achieved by combining the indoor heat sources with the exhaust outlet vent at the ceiling level.
2. Objective (2) has been achieved through the study presented in Chapter 5. In this study, the effect of using a novel LEVO system on the thermal comfort, the quality of the room air in the inhaled zone and in the breathing zone and on the energy savings was numerically investigated in a typical office room served by a DV system. The performance of the LEVO system was evaluated for different amounts of return air. Contaminants generated by the office workstation equipment and occupant activity were simulated. The results from this study concluded that:
- Using the new LEVO system can provide a healthy and comfortable environment for the occupants compared with a room which does not use this system. The air quality in the breathing zone was significantly improved by using the LEVO system, mainly by reducing the contaminant concentration in the inhaled zone for both occupants. This was due to the fact that most of the generated contaminant at the office workstation was extracted locally via the LEVO system before it diffused to the surroundings in the occupied zone.
 - Directing the extracted warm air towards the foot level slightly improved the temperature distribution in the vertical direction and by this contributed to improving the human thermal comfort in terms of the temperature differences between the head and foot levels.

- Using the LEVO system contributed to reducing the amount of energy consumption of the cooling coil by up to 30% compared with the reference case. This was due to the fact that most of the room heat flux generated by the office work equipment and by the occupants was extracted directly before it could mix with the rest of the room air. This increased the exhaust air temperature and significantly reduced the energy consumption of the cooling coil. In this system, the energy saving efficiency was increased by reducing the exhaust mass flow rate. In case 3, up to 30% of energy savings was achieved compared to 22.5% and 26.6% for cases 1 and 2 respectively.
 - Using the concept of the LEV system in an office application provided a better indoor thermal environment mainly in terms the quality of the indoor air, the quality of the inhaled air and of the energy consumption.
3. Objective (3) has been achieved by the investigations performed in Chapter 6. The investigation of the height impact for the proposed LEVO system was performed numerically in this study. Three different heights (1.4 m, 1.6 m and 2.0 m) for the combined system were used to evaluate the performance of the LEVO system in the modelled office spaces. From the results of this investigation, it can be concluded that:
- Four configurations have been modelled using the general purpose CFD code Fluent with the RNG k- ϵ turbulence model and the Lagrangian discrete phase tracking model.
 - The model predicted that the performance of the LEVO system is highly influenced by its exhaust height.
 - Among the modelled LEVO configurations, the thermal comfort and the indoor air quality in cases 2 (1.4 m) and 4 (2.0 m) were slightly better than those in case 3 (1.6 m). However, a significant amount of energy savings of 22.56% and an acceptable air quality with a good thermal comfort were predicted by case 3. Since the aim of this study was to improve energy savings and provide an acceptable quality of the inhaled air and good thermal comfort, case 3 was considered to be the

best height at which optimal performance is predicted from the LEVO system.

- The draught risk evaluation was conducted for all three cases and the relevant PD values fell comfortably within the required range, which further supported the selected LEVO system configuration.

4. Objective (4) has been achieved through the study presented in Chapter 7. In this investigation, a numerical investigation was undertaken by LES to gain time-resolved predictions of the flow in a realistic office environment where the exhaust opening was combined with the ceiling lamps. The LES results were also compared with the RANS model predictions. The following conclusions can be drawn from these investigations:

- Good predictions for the indoor thermal environment were achieved for the investigated domain using the RANS model. However, this method can only produce the average velocity and temperature distributions, but cannot give any information as to the instantaneous flow field and on the instantaneous temperature distribution.
- LES provided more realistic predictions of the airflow and of the temperature distribution in the investigated domain, because this method has the ability to capture time-dependent flow features.
- The buoyancy effect played a significant role in the LES simulations, particularly in the occupants' zones and in the regions around the external wall and combined systems. This was due to the thermal plumes generated by the room heat sources causing considerable flow perturbations, which can potentially influence the thermal microenvironment around the occupants and in the regions near the combined systems.
- Compared to RANS modelling, LES can help improve the designers' understanding of the flow and of the temperature characteristics in the office rooms using the combined systems, which will lead to better designs of the office ventilation systems.

8.2 Future work

The concept of the combination system, where the exhaust opening and room heat sources were combined, needs further investigation and development to be more efficient regarding the extraction of a large amount of the generated heat flux. This will help improve the amount of energy savings. In addition, the results of the energy savings and of the indoor thermal environment that were presented in Chapter 4 were valid for equipped office rooms served by the DV system for the cooling mode set to be appropriate to summer conditions. In general, the DV system can also be effectively combined with heating systems such as floor heating or ceiling heating. Therefore, further investigation can be useful to study the impact of using the combination concept under winter condition heating modes on the internal thermal environment and energy savings.

In this research, all the variables studied (velocity distribution, temperature distribution and contaminant concentration distribution) were validated by comparing the CFD results against the available experimental results from previous published work. The validation papers were selected carefully to be suitable for this research. However it would be desirable that further related experiments could be performed to support for this investigation.

Appendices

Appendix 1 Publication List

Chapter 4, 5, 6 and part of Chapter 7 have been published in journals and proceedings.

Journal papers:

Paper I: Ahmed AQ, Gao S, Kareem AK. A numerical study on the effects of exhaust locations on energy consumption and thermal environment in an office room served by displacement ventilation. *Energy Conversion and Management.* 2016;117:74-85.

Paper II: Ahmed AQ, Gao S, Kareem AK. Energy saving and indoor thermal comfort evaluation using a novel local exhaust ventilation system for office rooms. *Applied Thermal Engineering.* 2017;110:821-34.

Paper III: Ahmed AQ, Gao S. Numerical investigation of height impact of local exhaust combined with an office work station on energy saving and indoor environment. *Building and Environment.* 2017;122:94-205.

Paper IIII: Ahmed AQ, Gao S. Thermal comfort and energy saving evaluation of a combined system in an office room using displacement ventilation. *World Academy of Science, Engineering and Technology, International Journal of Mechanical, Aerospace, Industrial, Mechatronic and Manufacturing Engineering.* 2015;9:1101-6.

Paper V: Ahmed AQ, Gao S. Numerical study of the indoor environment for an office room with a combined system using the RANS and LES methods. "Under Review".

Conference papers

Paper VI: Ahmed AQ, Gao S., Ali K. Kareem, Evaluation of thermal comfort, indoor air quality and energy saving of a Local Exhaust Ventilation system in an Office room (LEVO), The 14 th International conference of indoor air quality and climate, Ghent-Belgium, 2017.

Paper VII: Ahmed AQ, Gao S., Large Eddy Simulation of Air Flow and Temperature Distributions in an Office Room Served by a Displacement Ventilation System, 7th Annual International Conference on Civil Engineering, Athens- Greece. 2017.

References

- [1] Harrison R, Thornton C, Lawrence R, Mark D, Kinnersley R, Ayres J. Personal exposure monitoring of particulate matter, nitrogen dioxide, and carbon monoxide, including susceptible groups. *Occupational and environmental medicine*. 2002;59:671-9.
- [2] D&R International L. 2011 Buildings Energy Data Book. 2012.
- [3] Butler D. Air conditioning using displacement ventilation to maximise free cooling. *CIBSE Conference2002*. p. 1-20.
- [4] Lim TS, Schaefer L, Kim JT, Kim G. Energy benefit of the underfloor air distribution system for reducing air-conditioning and heating loads in buildings. *Indoor and Built Environment*. 2012; 21:62-70.
- [5] Xu H, Niu J. Numerical procedure for predicting annual energy consumption of the under-floor air distribution system. *Energy and buildings*. 2006; 38:641-7.
- [6] Yuan X, Chen Q, LR. G. A critical review of displacement ventilation. *ASHRAE Transactions*. 1998; 104(1A).
- [7] Riffat S, Zhao X, Doherty P. Review of research into and application of chilled ceilings and displacement ventilation systems in Europe. *International Journal of Energy Research*. 2004;28:257-86.
- [8] Livchak A, Nall D. Displacement ventilation—application for hot and humid climate. *Proceedings of Clima 2000*.
- [9] Rees S J, Haves P. A nodal model for displacement ventilation and chilled ceiling systems in office spaces. *Building and Environment*. 2001; 36:753-62.
- [10] Cao G, Awbi H, Yao R, Fan Y, Siren K, Kosonen R et al. A review of the performance of different ventilation and airflow distribution systems in buildings. *Building and Environment*. 2014; 73:171-86.

- [11] Fanger PO. Provide good air quality for people and improve their productivity. Air Distribution in Rooms, (ROOMVENT 2000, Editor: HB Awbi). 2000; 1:1-5.
- [12] Niu J, Gao N, Phoebe M, Huigang Z. Experimental study on a chair-based personalized ventilation system. Building and environment. 2007;42:913-25.
- [13] Makhoul A, Ghali K, Ghaddar N. Desk fans for the control of the convection flow around occupants using ceiling mounted personalized ventilation. Building and Environment. 2013; 59:336-48.
- [14] Makhoul A, Ghali K, Ghaddar N. Thermal comfort and energy performance of a low-mixing ceiling-mounted personalized ventilator system. Building and Environment. 2013; 60:126-36.
- [15] Melikov AK, Cermak R, Majer M. Personalized ventilation: evaluation of different air terminal devices. Energy and buildings. 2002; 34:829-36.
- [16] Dygert RK, Dang TQ. Mitigation of cross-contamination in an aircraft cabin via localized exhaust. Building and Environment. 2010; 45:2015-26.
- [17] Dygert RK, Dang TQ. Experimental validation of local exhaust strategies for improved IAQ in aircraft cabins. Building and Environment. 2012; 47:76-88.
- [18] Melikov AK, Bolashikov ZD, Brand M. Experimental investigation of performance of a novel ventilation method for hospital patient rooms. 21st Congress of International Federation of Hospital Engineering (IFHE) 2010.
- [19] Zítek P, Vyhlídal T, Simeunović G, Nováková L, Čížek J. Novel personalized and humidified air supply for airliner passengers. Building and Environment. 2010; 45:2345-53.
- [20] Awbi HB. Energy efficient ventilation for retrofit buildings. Proceedings of 48th AiCARR international conference on energy performance of existing buildings 2011. p. e23.

- [21] ASHRAE A. Standard 55-2004, Thermal Environmental Conditions for Human Occupancy, Atlanta: American Society of Heating, Refrigerating, and Air-conditioning Engineers. Inc, USA. 2004.
- [22] Fanger PO. Thermal comfort. Analysis and applications in environmental engineering. Thermal comfort Analysis and applications in environmental engineering.1970.
- [23] He G, Yang X, Srebric J. Removal of contaminants released from room surfaces by displacement and mixing ventilation: modeling and validation. Indoor air. 2005; 15:367-80.
- [24] Budaiwi I, Abdou A. HVAC system operational strategies for reduced energy consumption in buildings with intermittent occupancy: the case of mosques. Energy Conversion and Management. 2013; 73:37-50.
- [25] Schiavon S, Melikov AK, Sekhar C. Energy analysis of the personalized ventilation system in hot and humid climates. Energy and Buildings. 2010; 42:699-707.
- [26] Fong M, Hanby V, Greenough R, Lin Z, Cheng Y. Acceptance of thermal conditions and energy use of three ventilation strategies with six exhaust configurations for the classroom. Building and Environment. 2015; 94:606-19.
- [27] Salvalai G, Pfafferott J, Sesana MM. Assessing energy and thermal comfort of different low-energy cooling concepts for non-residential buildings. Energy Conversion and Management. 2013; 76:332-41.
- [28] Wong L, Mui K. An energy performance assessment for indoor environmental quality (IEQ) acceptance in air-conditioned offices. Energy Conversion and Management. 2009; 50:1362-7.

- [29] Kharseh M, Altorkmany L, Al-Khawaj M, Hassani F. Warming impact on energy use of HVAC system in buildings of different thermal qualities and in different climates. *Energy Conversion and Management*. 2014; 81:106-11.
- [30] Chu C-M, Jong T-L. Enthalpy estimation for thermal comfort and energy saving in air conditioning system. *Energy Conversion and Management*. 2008; 49:1620-8.
- [31] Kanaan M, Ghaddar N, Ghali K, Araj G. New airborne pathogen transport model for upper-room UVGI spaces conditioned by chilled ceiling and mixed displacement ventilation: Enhancing air quality and energy performance. *Energy Conversion and Management*. 2014; 85:50-61.
- [32] Gao C, Lee W, Chen H. Locating room air-conditioners at floor level for energy saving in residential buildings. *Energy Conversion and Management*. 2009;50.
- [33] Bagheri H, Gorton R. Performance characteristics of a system designed for stratified cooling operating during the heating season. *ASHRAE Trans;(United States)*.1987;93.
- [34] Filler M. Best practices for underfloor air systems. *ASHRAE journal*. 2004; 46:39-46.
- [35] Hongtao X, Naiping G, Jianlei N. A method to generate effective cooling load factors for stratified air distribution systems using a floor-level air supply. *HVAC&R Research*. 2009;15:915-30.
- [36] Awad A, Calay R, Badran O, Holdo A. An experimental study of stratified flow in enclosures. *Applied Thermal Engineering*. 2008; 28:2150-8.

- [37] Awad A, Badran O, Hold A, Calay R. The effect of ventilation aperture location of input airflow rates on the stratified flow. *Energy conversion and management*. 2008; 49:3253-8.
- [38] Cheng Y, Niu J, Du Z, Lei Y. Investigation on the thermal comfort and energy efficiency of stratified air distribution systems. *Energy for Sustainable Development*. 2015; 28:1-9.
- [39] Cheng Y, Niu J, Liu X, Gao N. Experimental and numerical investigations on stratified air distribution systems with special configuration: Thermal comfort and energy saving. *Energy and Buildings*. 2013; 64:154-61.
- [40] Kuo J-Y, Chung K-C. The effect of diffuser's location on thermal comfort analysis with different air distribution strategies. *Journal of Building Physics*. 1999;22:208-29.
- [41] Lin Z, Chow T, Tsang C, Fong K, Chan L. CFD study on effect of the air supply location on the performance of the displacement ventilation system. *Building and environment*. 2005; 40:1051-67.
- [42] Espinosa FD, Glicksman LR. Determining thermal stratification in rooms with high supply momentum. *Building and Environment*. 2017;112:99-114.
- [43] Heidarinejad G, Fathollahzadeh MH, Pasdarsahri H. Effects of return air vent height on energy consumption, thermal comfort conditions and indoor air quality in an under floor air distribution system. *Energy and Buildings*. 2015; 97:155-61.
- [44] Fitzgerald SD, Woods AW. Natural ventilation of a room with vents at multiple levels. *Building and Environment*. 2004;39:505-21.

- [45] Thool SB, Sinha SL. Numerical Simulation and Comparison of Two Conventional Ventilation Systems of Operating Room in the View of Contamination Control. *International Journal of Computer Applications*. 2014;85.
- [46] Khan J, Feigley C, Lee E, Ahmed M, Tamanna S. Effects of inlet and exhaust locations and emitted gas density on indoor air contaminant concentrations. *Building and Environment*. 2006;41:851-63.
- [47] Cheong K, Phua S. Development of ventilation design strategy for effective removal of pollutant in the isolation room of a hospital. *Building and Environment*. 2006;41:1161-70.
- [48] Nielsen PV, Li Y, Buus M, Winther FV. Risk of cross-infection in a hospital ward with downward ventilation. *Building and Environment*. 2010;45:2008-14.
- [49] Ho SH, Rosario L, Rahman MM. Three-dimensional analysis for hospital operating room thermal comfort and contaminant removal. *Applied Thermal Engineering*. 2009;29:2080-92.
- [50] Qian H, Li Y, Nielsen PV, Hyltdgaard CE. Dispersion of exhalation pollutants in a two-bed hospital ward with a downward ventilation system. *Building and Environment*. 2008; 43:344-54.
- [51] Zhang T, Chen QY. Novel air distribution systems for commercial aircraft cabins. *Building and Environment*. 2007;42:1675-84.
- [52] Rim D, Novoselac A. Transport of particulate and gaseous pollutants in the vicinity of a human body. *Building and Environment*. 2009; 44:1840-9.
- [53] Deng Q-H, Zhou J, Mei C, Shen Y-M. Fluid, heat and contaminant transport structures of laminar double-diffusive mixed convection in a two-dimensional ventilated enclosure. *International Journal of Heat and Mass Transfer*. 2004; 47:5257-69.

- [54] Park H-J, Holland D. The effect of location of a convective heat source on displacement ventilation: CFD study. *Building and environment*. 2001;36:883-9.
- [55] Gan G. Numerical investigation of local thermal discomfort in offices with displacement ventilation. *Energy and buildings*. 1995;23:73-81.
- [56] Kobayashi N, Chen Q. Floor-supply displacement ventilation in a small office. *Indoor and built environment*. 2003;12:281-91.
- [57] Ho SH, Rosario L, Rahman MM. Comparison of underfloor and overhead air distribution systems in an office environment. *Building and Environment*. 2011;46:1415-27.
- [58] Calay RK, Wang WC. A hybrid energy efficient building ventilation system. *Applied Thermal Engineering*. 2013;57:7-13.
- [59] Chemisana D, López-Villada J, Coronas A, Rosell JI, Lodi C. Building integration of concentrating systems for solar cooling applications. *Applied Thermal Engineering*. 2013;50:1472-9.
- [60] Fong K, Chow TT, Li C, Lin Z, Chan L. Effect of neutral temperature on energy saving of centralized air-conditioning systems in subtropical Hong Kong. *Applied Thermal Engineering*. 2010;30:1659-65.
- [61] Guo Y, Zhang G, Zhou J, Wu J, Shen W. A techno-economic comparison of a direct expansion ground-source and a secondary loop ground-coupled heat pump system for cooling in a residential building. *Applied Thermal Engineering*. 2012;35:29-39.
- [62] Faulkner D, Fisk WJ, Sullivan DP, Lee SM. Ventilation efficiencies and thermal comfort results of a desk-edge-mounted task ventilation system. *Indoor air*. 2004;14:92-7.

- [63] Gao N, Niu J. CFD study on micro-environment around human body and personalized ventilation. *Building and Environment*. 2004; 39:795-805.
- [64] Li X, Niu J, Gao N. Co-occupant's exposure to exhaled pollutants with two types of personalized ventilation strategies under mixing and displacement ventilation systems. *Indoor air*. 2013; 23:162-71.
- [65] Kong M, Dang TQ, Zhang J, Khalifa HE. Micro-environmental control for efficient local cooling. *Building and Environment*. 2017.
- [66] Habchi C, Ghali K, Ghaddar N, Chakroun W, Alotaibi S. Ceiling personalized ventilation combined with desk fans for reduced direct and indirect cross-contamination and efficient use of office space. *Energy Conversion and Management*. 2016;111:158-73.
- [67] Bivolarova MP, Melikov AK, Mizutani C, Kajiwara K, Bolashikov ZD. Bed-integrated local exhaust ventilation system combined with local air cleaning for improved IAQ in hospital patient rooms. *Building and Environment*. 2016;100:10-8.
- [68] Halvoňová B, Melikov AK. Performance of “ductless” personalized ventilation in conjunction with displacement ventilation: Impact of disturbances due to walking person (s). *Building and Environment*. 2010; 45:427-36.
- [69] Xu Y, Yang X, Yang C, Srebric J. Contaminant dispersion with personal displacement ventilation, Part I: Base case study. *Building and Environment*. 2009; 44:2121-8.
- [70] Conceição EZ, Lúcio MMJ, Rosa SP, Custódio AL, Andrade RL, Meira MJ. Evaluation of comfort level in desks equipped with two personalized ventilation systems in slightly warm environments. *Building and Environment*. 2010; 45:601-9.

- [71] Tham KW, Pantelic J. Performance evaluation of the coupling of a desktop personalized ventilation air terminal device and desk mounted fans. *Building and Environment*. 2010; 45:1941-50.
- [72] Halvonová B, Melikov AK. Performance of ductless personalized ventilation in conjunction with displacement ventilation: impact of workstations layout and partitions. *HVAC&R Research*. 2010;16:75-94.
- [73] Schiavon S, Melikov AK. Energy-saving strategies with personalized ventilation in cold climates. *Energy and Buildings*. 2009; 41:543-50.
- [74] Li R, Sekhar S, Melikov AK. Thermal comfort and IAQ assessment of under-floor air distribution system integrated with personalized ventilation in hot and humid climate. *Building and Environment*. 2010; 45:1906-13.
- [75] Kanaan M, Ghaddar N, Ghali K. Quality of inhaled air in displacement ventilation systems assisted by personalized ventilation. *HVAC&R Research*. 2012;18:500-14.
- [76] Yang B, Sekhar C, Melikov AK. Ceiling mounted personalized ventilation system in hot and humid climate—An energy analysis. *Energy and Buildings*. 2010; 42:2304-8.
- [77] Metzger ZJZID. Taguchi-method-based CFD study and optimisation of personalised ventilation systems. *Indoor and Built Environment*. 2012;21:690-702.
- [78] Makhoul A, Ghali K, Ghaddar N. The Energy Saving Potential and the Associated Thermal Comfort of Displacement Ventilation Systems Assisted by Personalised Ventilation. *Indoor and Built Environment*. 2013; 22;3:508–519.

- [79] Makhoul A, Ghali K, Ghaddar N, Chakroun W. Investigation of particle transport in offices equipped with ceiling-mounted personalized ventilators. *Building and Environment*. 2013; 63:97-107.
- [80] Magnier L, Zmeureanu R, Derome D. Experimental assessment of the velocity and temperature distribution in an indoor displacement ventilation jet. *Building and Environment*. 2012; 47:150-60.
- [81] Zhou J, Kim CN. Effect of the personalized ventilation on indoor air quality for an indoor occupant with VOCs emission from carpet. *Journal of mechanical science and technology*. 2012; 26:481-8.
- [82] Yang C, Yang X, Xu Y, Srebric J. Contaminant Dispersion in personal displacement ventilation. *Proceedings of the IBPSA Building Simulation 2007*. 2007:818-24.
- [83] Yang J, Sekhar C, Wai DCK, Raphael B. Computational fluid dynamics study and evaluation of different personalized exhaust devices. *HVAC&R Research*. 2013;19:934-46.
- [84] Junjing Y, Sekhar C, Cheong D, Raphael B. Performance evaluation of an integrated Personalized Ventilation–Personalized Exhaust system in conjunction with two background ventilation systems. *Building and Environment*. 2014; 78:103-10.
- [85] Melikov A, Bolashikov ZD, Georgiev E. Novel ventilation strategy for reducing the risk of airborne cross infection in hospital rooms. *Proceedings of Indoor Air 2011*. 2011:1037.
- [86] Bolashikov Z, Melikov A, Krenek M. Control of the free convective flow around the human body for enhanced inhaled air quality: Application to a seat-incorporated personalized ventilation unit. *HVAC&R Research*. 2010;16:161-88.

- [87] Taghinia J, Rahman MM, Siikonen T. Numerical simulation of airflow and temperature fields around an occupant in indoor environment. *Energy and Buildings*. 2015;104:199-207.
- [88] Posner J, Buchanan C, Dunn-Rankin D. Measurement and prediction of indoor air flow in a model room. *Energy and buildings*. 2003;35:515-26.
- [89] Tavakoli E, Hosseini R. Large eddy simulation of turbulent flow and mass transfer in far-field of swirl diffusers. *Energy and Buildings*. 2013;59:194-202.
- [90] Deevy M, Sinai Y, Everitt P, Voigt L, Gobeau N. Modelling the effect of an occupant on displacement ventilation with computational fluid dynamics. *Energy and Buildings*. 2008;40:255-64.
- [91] Kuznik F, Rusaouën G, Hohotă R. Experimental and numerical study of a mechanically ventilated enclosure with thermal effects. *Energy and buildings*. 2006;38:931-8.
- [92] Naumov AL, Kapko DV, Brodach MM. Ventilation systems with local recirculation diffusers. *Energy and Buildings*. 2014;85:560-3.
- [93] Spitz C, Mora L, Wurtz E, Jay A. Practical application of uncertainty analysis and sensitivity analysis on an experimental house. *Energy and Buildings*. 2012;55:459-70.
- [94] Chafi FZ, Hallé S. Three dimensional study for evaluating of air flow movements and thermal comfort in a model room: Experimental validation. *Energy and Buildings*. 2011;43:2156-66.
- [95] Gaitonde U, Laurence D, Revell A. *Quality Criteria for Large Eddy Simulation*: Citeseer; 2006.
- [96] Zhai ZJ, Zhang Z, Zhang W, Chen QY. Evaluation of various turbulence models in predicting airflow and turbulence in enclosed environments by CFD:

Part 1—Summary of prevalent turbulence models. *Hvac&R Research*. 2007;13:853-70.

[97] Zhang X, Su G, Yu J, Yao Z, He F. PIV measurement and simulation of turbulent thermal free convection over a small heat source in a large enclosed cavity. *Building and Environment*. 2015;90:105-13.

[98] Zhang Z, Chen X, Mazumdar S, Zhang T, Chen Q. Experimental and numerical investigation of airflow and contaminant transport in an airliner cabin mockup. *Building and Environment*. 2009;44:85-94.

[99] Zhang Z, Zhang W, Zhai ZJ, Chen QY. Evaluation of various turbulence models in predicting airflow and turbulence in enclosed environments by CFD: Part 2—Comparison with experimental data from literature. *Hvac&R Research*. 2007;13:871-86.

[100] Cao X, Liu J, Pei J, Zhang Y, Li J, Zhu X. 2D-PIV measurement of aircraft cabin air distribution with a high spatial resolution. *Building and Environment*. 2014;82:9-19.

[101] Liu W, Wen J, Chao J, Yin W, Shen C, Lai D et al. Accurate and high-resolution boundary conditions and flow fields in the first-class cabin of an MD-82 commercial airliner. *Atmospheric Environment*. 2012;56:33-44.

[102] Chen WZ, Qingyan. Large eddy simulation of natural and mixed convection airflow indoors with two simple filtered dynamic subgrid scale models. *Numerical Heat Transfer: Part A: Applications*. 2000;37:447-63.

[103] Lin C, Horstman R, Ahlers M, Sedgwick L, Dunn K, Topmiller J et al. Numerical simulation of airflow and airborne pathogen transport in aircraft cabins—Part I: Numerical simulation of the flow field. *ASHRAE Transactions*. 2005;111:755-63.

- [104] Lin C, Wu T, Horstman R, Lebbin P, Hosni M, Jones B et al. Comparison of large eddy simulation predictions with particle image velocimetry data for the airflow in a generic cabin model. HVAC&R Research. 2006;12:935-51.
- [105] Liu W, Wen J, Lin C-H, Liu J, Long Z, Chen Q. Evaluation of various categories of turbulence models for predicting air distribution in an airliner cabin. Building and Environment. 2013;65:118-31.
- [106] Wang M, Chen Q. Assessment of various turbulence models for transitional flows in an enclosed environment (RP-1271). HVAC&R Research. 2009;15:1099-119.
- [107] EBRAHIMI K. Numerical simulation of turbulent airflow, tracer gas diffusion, and particle dispersion in a mockup aircraft cabin: Kansas State University; 2012.
- [108] Zhu Y, Luo M, Ouyang Q, Huang L, Cao B. Dynamic characteristics and comfort assessment of airflows in indoor environments: A review. Building and Environment. 2015.
- [109] Zhang W, Chen Q. Large eddy simulation of indoor airflow with a filtered dynamic subgrid scale model. International Journal of Heat and Mass Transfer. 2000;43:3219-31.
- [110] Emmerich SJ, McGrattan KB. Application of a large eddy simulation model to study room airflow. TRANSACTIONS-AMERICAN SOCIETY OF HEATING REFRIGERATING AND AIR CONDITIONING ENGINEERS. 1998;104:1128-40.
- [111] Musser A, McGrattan K. Evaluation of a fast large-eddy-simulation model for indoor airflows. Journal of architectural engineering. 2002;8:10-8.
- [112] Jiang Y, Chen Q. Study of natural ventilation in buildings by large eddy simulation. Journal of wind engineering and industrial aerodynamics. 2001;89:1155-78.

- [113] Karadimou D, Markatos N. Modelling of two-phase, transient airflow and particles distribution in the indoor environment by Large Eddy Simulation. *Journal of Turbulence*. 2016;17:216-36.
- [114] Davidson L, Nielsen PV. Large eddy simulations of the flow in a three-dimensional ventilated room. Dept. of Building Technology and Structural Engineering; 1996.
- [115] Emmerich SJ, McGrattan KB, Kato S, Baker A. Application of a large eddy simulation model to study room airflow. *Ashrae Transactions*. 1998;104:1128.
- [116] Tian Z, Tu J, Yeoh G, Yuen R. On the numerical study of contaminant particle concentration in indoor airflow. *Building and Environment*. 2006;41:1504-14.
- [117] Caciolo M, Stabat P, Marchio D. Numerical simulation of single-sided ventilation using RANS and LES and comparison with full-scale experiments. *Building and Environment*. 2012;50:202-13.
- [118] Gousseau P, Blocken B, Stathopoulos T, Van Heijst G. CFD simulation of near-field pollutant dispersion on a high-resolution grid: a case study by LES and RANS for a building group in downtown Montreal. *Atmospheric Environment*. 2011;45:428-38.
- [119] Rodi W. Comparison of LES and RANS calculations of the flow around bluff bodies. *Journal of Wind Engineering and Industrial Aerodynamics*. 1997;69:55-75.
- [120] Salim SM, Buccolieri R, Chan A, Di Sabatino S. Numerical simulation of atmospheric pollutant dispersion in an urban street canyon: comparison between RANS and LES. *Journal of Wind Engineering and Industrial Aerodynamics*. 2011;99:103-13.

- [121] Tominaga Y, Stathopoulos T. Numerical simulation of dispersion around an isolated cubic building: model evaluation of RANS and LES. *Building and Environment*. 2010;45:2231-9.
- [122] Tominaga Y, Stathopoulos T. CFD modeling of pollution dispersion in a street canyon: Comparison between LES and RANS. *Journal of Wind Engineering and Industrial Aerodynamics*. 2011;99:340-8.
- [123] Yang C, Zhang X, Yao Z, Cao X, Liu J, He F. Numerical study of the instantaneous flow fields by large eddy simulation and stability analysis in a single aisle cabin model. *Building and Environment*. 2016;96:1-11.
- [124] Gerhart PM, Gross RJ. *Fundamentals of fluid mechanics*: Addison-Wesley; 1985.
- [125] Okiishi MY, Munson B, Young D. *Fundamentals of Fluid Mechanics*. John Wiley & Sons, Inc. 2006.
- [126] Versteeg HK, Malalasekera W. *An introduction to computational fluid dynamics: the finite volume method*: Pearson Education; 2007.
- [127] Horikiri K, Yao Y, Yao J. Numerical study of unsteady airflow phenomena in a ventilated room. *ICHMT DIGITAL LIBRARY ONLINE*. 2012.
- [128] Horikiri K, Yao Y, Yao J. Modelling conjugate flow and heat transfer in a ventilated room for indoor thermal comfort assessment. *Building and Environment*. 2014;77:135-47.
- [129] Srebric J, Chen Q. Simplified numerical models for complex air supply diffusers. *HVAC&R Research*. 2002;8:277-94.
- [130] Yuan X, Chen Q, Glicksman LR, Hu Y, Yang X. Measurements and computations of room airflow with displacement ventilation. *Ashrae Transactions*. 1999;105:340.

- [131] Yakhot V, Orszag S, Thangam S, Gatski T, Speziale C. Development of turbulence models for shear flows by a double expansion technique. *Physics of Fluids A: Fluid Dynamics* (1989-1993). 1992;4:1510-20.
- [132] Lilly DK. A proposed modification of the Germano subgrid-scale closure method. *Physics of Fluids A: Fluid Dynamics* (1989-1993). 1992;4:633-5.
- [133] Germano M, Piomelli U, Moin P, Cabot WH. A dynamic subgrid-scale eddy viscosity model. *Physics of Fluids A: Fluid Dynamics* (1989-1993). 1991;3:1760-5.
- [134] Durrani F. Using large eddy simulation to model buoyancy-driven natural ventilation: © Faisal Durrani; 2013.
- [135] FLUENT A. Theory Guide. 2011.
- [136] Fluent A. ANSYS fluent user's guide, release 14.0. PA: ANSYS Fluent. 2011.
- [137] Patankar SV, Spalding DB. A calculation procedure for heat, mass and momentum transfer in three-dimensional parabolic flows. *International journal of heat and mass transfer*. 1972;15:1787-806.
- [138] Wargocki P, Wyon DP, Sundell J, Clausen G, Fanger P. The effects of outdoor air supply rate in an office on perceived air quality, sick building syndrome (SBS) symptoms and productivity. *Indoor air*. 2000;10:222-36.
- [139] Chandrasekhar S. Radiative heat transfer 1960.
- [140] Zhang Z, Chen Q. Comparison of the Eulerian and Lagrangian methods for predicting particle transport in enclosed spaces. *Atmospheric Environment*. 2007;41:5236-48.
- [141] Fluent A. Fluent theory guide. Ansys Inc. 2012.
- [142] Nazaroff WW. Indoor particle dynamics. *Indoor air*. 2004;14:175-83.

- [143] Wang M, Lin C-H, Chen Q. Advanced turbulence models for predicting particle transport in enclosed environments. *Building and Environment*. 2012;47:40-9.
- [144] Zhao B, Zhang Y, Li X, Yang X, Huang D. Comparison of indoor aerosol particle concentration and deposition in different ventilated rooms by numerical method. *Building and Environment*. 2004;39:1-8.
- [145] Li A, Ahmadi G. Dispersion and deposition of spherical particles from point sources in a turbulent channel flow. *Aerosol Science and Technology*. 1992;16:209-26.
- [146] McLaughlin JB. Aerosol particle deposition in numerically simulated channel flow. *Physics of Fluids A: Fluid Dynamics (1989-1993)*. 1989;1:1211-24.
- [147] Nazaroff WW, Cass GR. Mathematical modeling of indoor aerosol dynamics. *Environmental Science & Technology*. 1989;23:157-66.
- [148] Rizk M, Elghobashi S. The motion of a spherical particle suspended in a turbulent flow near a plane wall. *Physics of Fluids (1958-1988)*. 1985;28:806-17.
- [149] Romano F, Marocco L, Gustén J, Joppolo CM. Numerical and experimental analysis of airborne particles control in an operating theater. *Building and Environment*. 2015;89:369-79.
- [150] Hinds WC. *Aerosol technology: properties, behavior, and measurement of airborne particles*. New York, Wiley-Interscience, 1982 442 p. 1982;1.
- [151] Chen F, Simon C, Lai AC. Modeling particle distribution and deposition in indoor environments with a new drift-flux model. *Atmospheric Environment*. 2006;40:357-67.
- [152] ISO7730. Moderate thermal environments-determination of the PMV-PDD indices and specification of the conditions for thermal comfort. 1994.

- [153] Horikiri K, Yao Y, Yao J. Numerical optimisation of thermal comfort improvement for indoor environment with occupants and furniture. *Energy and Buildings*. 2015;88:303-15.
- [154] Lian Z, Wang H. Experimental study of factors that affect thermal comfort in an upward-displacement air-conditioned room. *HVAC&R Research*. 2002;8:191-200.
- [155] Rees S, McGuirk J, Haves P. Numerical investigation of transient buoyant flow in a room with a displacement ventilation and chilled ceiling system. *International Journal of Heat and Mass transfer*. 2001;44:3067-80.
- [156] Fathollahzadeh MH, Heidarinejad G, Pasdarsahri H. Prediction of thermal comfort, IAQ, and energy consumption in a dense occupancy environment with the under floor air distribution system. *Building and Environment*. 2015;90:96-104.
- [157] Wang H, Lu S, Cheng J, Zhai ZJ. Inverse modeling of indoor instantaneous airborne contaminant source location with adjoint probability-based method under dynamic airflow field. *Building and Environment*. 2017.
- [158] Licina D, Melikov A, Pantelic J, Sekhar C, Tham KW. Human convection flow in spaces with and without ventilation: personal exposure to floor-released particles and cough-released droplets. *Indoor air*. 2015.
- [159] Serrano-Arellano J, Xamán J, Álvarez G. Optimum ventilation based on the ventilation effectiveness for temperature and CO₂ distribution in ventilated cavities. *International Journal of Heat and Mass Transfer*. 2013;62:9-21.
- [160] Tuan N, Huang K. Airflow circulation cell study of an air-conditioning energy-saving mechanism. *Applied Thermal Engineering*. 2011;31:3956-3962.

- [161] Ahmed AQ, Gao S, Kareem AK. A numerical study on the effects of exhaust locations on energy consumption and thermal environment in an office room served by displacement ventilation. *Energy Conversion and Management*. 2016;117:74-85.
- [162] Hussain S, Oosthuizen PH. Numerical investigations of buoyancy-driven natural ventilation in a simple atrium building and its effect on the thermal comfort conditions. *Applied Thermal Engineering*. 2012;40:358-72.
- [163] Sadrizadeh S, Holmberg S. Effect of a portable ultra-clean exponential airflow unit on the particle distribution in an operating room. *Particuology*. 2015;18:170-8.
- [164] Fanger PO, Melikov AK, Hanzawa H, Ring J. Air turbulence and sensation of draught. *Energy and buildings*. 1988;12:21-39.
- [165] Melikov AK, Langkilde G, Derbiszewski B. Airflow characteristics in the occupied zone of rooms with displacement ventilation. *ASHRAE Transactions*. 1990.
- [166] Standard I. 7730. Ergonomics of the thermal environment—Analytical determination and interpretation of thermal comfort using calculation of the PMV and PPD indices and local thermal comfort criteria. International Organization for Standardization: Geneva, Switzerland 2005.
- [167] Chen H, Moshfegh B, Cehlin M. Computational investigation on the factors influencing thermal comfort for impinging jet ventilation. *Building and Environment*. 2013;66:29-41.
- [168] Chen H, Moshfegh B, Cehlin M. Investigation on the flow and thermal behavior of impinging jet ventilation systems in an office with different heat loads. *Building and Environment*. 2013;59:127-44.

- [169] Melikov A, Pitchurov G, Naydenov K, Langkilde G. Field study on occupant comfort and the office thermal environment in rooms with displacement ventilation. *Indoor air*. 2005;15:205-14.
- [170] Ahmed AQ, Gao S, Kareem AK. Energy saving and indoor thermal comfort evaluation using a novel local exhaust ventilation system for office rooms. *Applied Thermal Engineering*. 2017;110:821-34.
- [171] Ahmed Q, Ahmed SG, Ali K, Kareem. Evaluation of thermal comfort, indoor air quality and energy saving of a Local Exhaust Ventilation system in an Office room (LEVO). *The 14 th International conference of indoor air quality and climate Ghent-Belgium: ISIAQ*; 2016.
- [172] Van Driest ER. On turbulent flow near a wall. *Journal of the Aeronautical Sciences (Institute of the Aeronautical Sciences)*. 2012;23.
- [173] Durrani F, Cook MJ, McGuirk JJ. Evaluation of LES and RANS CFD modelling of multiple steady states in natural ventilation. *Building and Environment*. 2015;92:167-81.